LIBERATION-LIMITED GRADE/RECOVERY CURVES FOR AURIFEROUS PYRITE ORES AS DETERMINED BY HIGH RESOLUTION X-RAY MICROTOMOGRAPHY

by

Juan Francisco Medina

A dissertation submitted to the faculty of
The University of Utah
in partial fulfillment of the requirements for the degree of

Doctor of Philosophy

Department of Metallurgical Engineering

The University of Utah

August 2012

The University of Utah Graduate School

STATEMENT OF DISSERTATION APPROVAL

The dissertation of **Juan Francisco Medina**

has been approved by the following supervisory committee members:

Jan D. Miller	, Chair	**5/3/2012** Date Approved
Chen-Lu Lin	, Member	**5/3/2012** Date Approved
Raj K. Rajamani	, Member	**5/3/2012** Date Approved
Michael S. Moats	, Member	**5/3/2012** Date Approved
Erich Petersen	, Member	**5/3/2012** Date Approved

and by **Jan D. Miller**, Chair of the Department of **Metallurgical Engineering**

and by Charles A. Wight, Dean of The Graduate School.

ABSTRACT

As in all flotation separations, the separation efficiency for the flotation of pyrite from auriferous pyrite ores depends on the flotation conditions and the particle properties of the feed ore. Liberation and texture are particle properties that refer to release of valuable minerals from gangue waste minerals during size reduction and the arrangement of these mineral phases within the particles. Separation efficiency may be impacted significantly by variation in liberation and the texture of locked particles, even with locked particles having the same overall composition. Not all locked particles of the same composition will have the same flotation response. Their flotation response will also depend on their texture. Now, analysis of liberation and texture is possible using High Resolution X-ray Microtomography (HRXMT). This analytical technique can provide quantitative information on liberation and exposure (texture) for each particle in a given particle population.

Products from the flotation of two types of auriferous pyrite ores, both batch scale experiments and plant operations, were analyzed by HRXMT. In this way, the degree of liberation of the pyrite grains was determined. The liberation-limited grade/recovery curves were calculated for each ore. The liberation-limited grade/recovery curves are used to determine the limits of the separation efficiency. Also, the characteristic texture

of particles in each flotation product was determined and the effect of these textural features on the flotation separation efficiency discussed.

It was found that the separation efficiency of auriferous pyrite was controlled principally by factors other than liberation. In general the texture analysis revealed that the pyrite-containing particles with a high exposure of pyrite grains at the particle surface have a better possibility of being recovered in the concentrate during flotation.

TABLE OF CONTENTS

ABSTRACT iii

LIST OF ABBREVIATIONS vii

ACKNOWLEDGMENTS xiii

1. INTRODUCTION 1

1.1 Liberation 1
1.2 Texture 4
1.3 Liberation Measurements from Polished Sections 5
1.4 High Resolution X-ray Microtomography (HRXMT) 12
1.5 Gold Ores 14
1.6 Sampling 17
1.7 Research Objectives and Thesis Organization 19

2. MATERIALS AND METHODS 22

2.1 High Resolution X-ray Microtomography Analysis and Data Processing 22
2.2 Laboratory Flotation Experiments 36
2.3 Flotation Plant Operation 51
2.4 Liberation-Limited Grade/Recovery Curves 53
2.5 Minimum Sample Weight 55
2.6 HRXMT Analysis 59

3. PRODUCTS FROM LABORATORY FLOTATION EXPERIMENTS, RESULTS, ANALYSIS AND DISCUSSION 66

3.1 Liberation-Limited Grade/Recovery Curves from HRXMT Analysis 67
3.2 Comparison of Volumetric Grade Analysis with Area Grade Analysis of Feed 68
3.3 Correlation of HRXMT Data and Chemical Analysis 71
3.4 Flotation Results for Complete Feed Size Distribution 72
3.5 Results for Separate Flotation of Individual Size Classes 104

3.6 Discussion 108

4. PRODUCTS FROM FLOTATION PLANT OPERATIONS, RESULTS, ANALYSIS AND DISCUSSION 139

4.1 Chemical Analysis and Particle Size Distributions of Flotation Products 140
4.2 HRXMT Analysis of Flotation Products 143
4.3 Correlation of HRXMT Data and Chemical Analysis 145
4.4 Mass Balance of Flotation Circuit from Chemical Analysis 146
4.5 Liberation-Limited Grade/Recovery Curves for Flotation Products 149
4.6 Discussion of Results from HRXMT Analysis for Flotation Products 151
4.7 Exposure Analysis of Flotation Products 156
4.8 Comparison of Pyrite Grade from MLA and HRXMT Analyses 161

5. SUMMARY AND CONCLUSIONS 164

5.1 Batch Flotation Experiments 164
5.2 Flotation Plant Operation 168

Appendices

A. EXAMPLE OF CALCULATION OF LIBERATION-LIMITED GRADE/RECOVERY CURVES 171

B. DETERMINATION OF MINIMUM SAMPLE WEIGHT 176

C. EXPOSURE ANALYSIS OF INDIVIDUAL PARTICLES OF FEED AND FLOTATION PRODUCTS 180

D. MASS BALANCE OF PLANT FLOTATION CIRCUIT 215

E. EXPOSURE ANALYSIS OF INDIVIDUAL PARTICLES OF SAMPLES FROM PLANT FLOTATION CIRCUIT 217

F. PYRITE GRADE OF MLA AND HRXMT ANALYSIS OF FLOTATION CIRCUIT SAMPLES 226

REFERENCES 232

LIST OF ABBREVIATIONS

a	Variable with small dependence on energy
$(Ag,Au)Te_2$	Sylvanite
Au_2Bi	Maldonite
$AuSb_2$	Aurostibite
$AuTe_2$	Calaverite
b	Constant
BMA	Bulk Mineralogical Analysis
BSE	Back Scattered Electron
C	Flow rate of concentrate
CANMET	Mining and Mineral Sciences Laboratories (Canada)
cm^3	Cubic centimeter
CT	x-ray computed tomography
CT_{number}	CTnumber
C_S	Sampling constant for the material to be sampled
Cu_3AsS_4	Enargite
$Cu_{12}As_4S_{13}$	Tennantile
Cv_F	Calculated pyrite volume grade of feed
Cv_{Py}	Calculated pyrite volume grade of feed

d	Size the largest pieces in the material to be sampled
d’	Size smaller than 95% in the material to be samled
d_{max}	Maximum size of the size class
d_{min}	Minimum size of the size class
E	Energy
EDS	Energy Dispersive Spectroscopy
F	Flow rate of feed
f_S	Shape factor
f	Pyrite grade of concentrate
FeAs2	Loellingite
FeS2	Pyrite
fi	Fraction of the total number of electrons contributed by element i
g	Grams
GXMAP	Grain-based X-ray Mapping
h	H-Extreme parameter
hr	Hour
HRXMT	High Resolution X-ray Microtomography
HU	Hounsfield units
I	Final intensity of emerging beam
i	Size class
Io	Initial intensity of emerging beam
j	Flotation product
kg	Kilograms

kV	Kilovolts
L	Liter
L_S	Particle size at the mineral is essentially liberated
ℓ	Liberation factor
LLGR	Liberation- Limited Grade/Recovery Curve
M	Minimum weight of sample required
MBT	Mercaptobenzothazole
MFP	Mass of flotation product
m^3	Cubic meter
MLA	Mineral Liberation Analyzer
mm	Millimeters
mm^2	Square millimeters
mm^3	Cubic millimeters
m_{Py}	Pyrite mass grade
nm	Nanometer
PAX	Potassium amil xanthate
PGM	Platinum group metals
pH	Hydrogen ion concentration
PMA	Particle mineral analysis
PSD	Particle size distribution
R	Pyrite recovery from flotation circuit
$R_{Concentrate}$	Pyrite recovery of concentrate
Ro	Overall recovery

RPM	Revolutions per minute
RPS	Rare Phase Search
R_{Py}	Pyrite recovery
Rv	Scanning voxel resolution
s	relative standar desviation
SD	Standard deviation
SDC	Silicon Drift Chamber
SEM	Scanning electron microscope
SIP	Species identification protocol
SMA	Specific mineral analysis
SPL	Sparse phase liberation analysis
SXBSE	Super extended BSE liberation analysis
T	Flow rate of tailings
t	Pyrite grade of tailings
TMS	Trace mineral search
ton	metric tons
V_C	Volume of concentrate
v_C	Pyrite volume grade of concentrate
V_{C1}	Volume of concentrate 1
V_{C2}	Volume of concentrate 2
V_{C3}	Volume of concentrate 3
v_{C1}	Pyrite volume grade for concentrate 1
v_{C2}	Pyrite volume grade for concentrate 2

v_{C3}	Pyrite volume grade for concentrate 3
$v_{Concentrate}$	Pyrite volume grade of concentrate
V_F	Volume of feed
V_{FP}	Particle volume of flotation product
v_{FPPy}	Mean pyrite volume grade of flotation product
v_{Py}	Pyrite volume grade
v_{PyO}	Pyrite volume grade of overall concentrate
WDS	Wavelength- dispersive spectroscopy
X	Percent solids of concentrate
XBSE	Extended BSE liberation analysis
XMOD	X-ray modal analysis
XRD	X-ray Diffraction
y	Water fraction in the concentrate slurry
Z	Atomic number
Z_e	Effective atomic number
Z_i	Atomic number of element i
α	Fractional average mineral content
β	Mineralogical composition factor
ε	Factor dependent on the particle size
μ	Attenuation coefficient
μm	Micrometers
$\mu_{Material}$	Attenuation coefficient of material
μ_{Water}	Attenuation coefficient of water

ρ	Density of the absorber
ρ_C	Density of concentrate
ρ_{FP}	Density of flotation product
ρ_G	Density of gangue minerals
ρ_{Py}	Density of pyrite
$\rho_{SlurryC}$	Density of concentrate slurry
ρ_{Water}	Density of water
σ	Relative variance
τ	Mean density of gangue minerals
ω	Mean density of valuable minerals
%	Percentage
<	Smaller than
>	Greater than

ACKNOWLEDGEMENTS

I would like to thank my advisor, Professor Jan D. Miller, for his support, advice and knowledge during my time at the University of Utah. Thanks to Professor Chen-Luh Lin for his advice, knowledge and patience.

Support and confidence from Lic. Jose Cerrillo Chowel and Santa Maria de la Paz are gratefully acknowledged. Also, financial support provided by Newmont Mining Corporation is gratefully acknowledged. Thanks to Ronel Kappes for the helpful support to complete this thesis.

A special recognition to my parents, Juan Francisco Medina Castilleja and Martha Mendoza de Medina; they taught me the basic principles for success in this life.

Finally, I would like to give special thanks to Jessica, my wife, for her invaluable support and patience.

CHAPTER 1

INTRODUCTION

1.1 Liberation

Liberation is a fundamental issue in mineral processing technology. Basically liberation is the release of valuable minerals from waste gangue minerals during comminution and is desired at the coarsest possible particle size. Liberation occurs in the comminution processes of crushing and grinding during size reduction of multiphase ore particles. Liberation is the natural link between comminution operations and mineral recovery operations. In practice, complete liberation is seldom achieved, even if the ore is ground to the desired particle size. Of course, some degree of liberation is necessary if separation and concentration is to be achieved in mineral processing operations.

Comminution generally requires a lot of energy. In the mineral processing plant operations, up to 50% of the energy consumed is used for crushing and grinding. In order to obtain a high grade concentrate it is frequently necessary to grind the ore to small particle sizes. This increases the cost of operation and, further, the presence of fine particles can compromise recovery, because fine particles are difficult to recover and frequently are lost in the tailings. If the grains of valuable minerals are finely disseminated, the cost for size reduction increases and the fine particles may be lost in the

tailings. In the comminution process a balance between costs and benefits (recovery) must be found (Wills 2006).

The prediction of mineral liberation is difficult to model due to the variation in ore texture and the complexity of fracture processes during comminution. Models to determine the extent of liberation generally have unrealistic assumptions with respect to the geometric features of grain structure, the fracture pattern (random or preferential grain boundary breakage), and the breakage characteristics (breakage function and selection function) of the mineral components.

The foundation for liberation prediction models is the Andrews-Mika diagram which describes what type of progeny particles will be generated when a single particle breaks during comminution (King 2001). The diagrams are useful because the graphical representation is fairly easy to interpret and the diagrams explicitly include a number of essential constraints that must be applied to the breakage process in population balance models. An example of an Andrews-Mika diagram is shown in Figure 1.1.

In the diagram consider a parent particle at point A (see Figure 1.1). When this particle is broken, the progeny particles can not appear at every point in the phase space. They are restricted by definite physical constraints. Clearly progeny particles can appear only below point A because every progeny particle must be smaller than the parent particle. In addition the progeny particles must satisfy the law of conservation of phase volume. This means that no progeny particle can contain a greater volume of mineral than the volume of mineral in the parent particle. The region R, called the attainable region, shows where progeny particles can appear after fracture of a parent particle A. In particular the liberated edges of the region, represented by BF and CG in the diagram, are

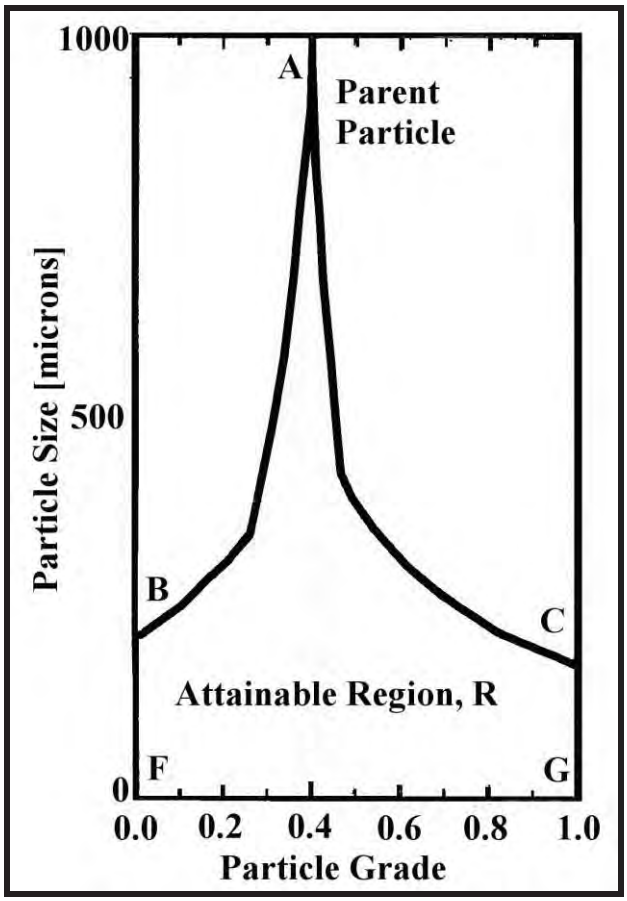

Figure 1.1 Andrews-Mika diagram.

included in the attainable region because an unliberated particle can generate completely liberated particles (King 2001, Xu 2010).

Models for liberation prediction developed by Gaudin (Gaudin 1939), King (King et al. 1982; King and Schneider 1998), Schneider (Scheider et al. 2003), Davy (Davy 1984), Wiegel (Wiegel 1976), Barbery (Barbery 1991) and Gay (Gay 2004b) are based on mineral composition and texture analysis. Basically these models were developed for binary systems and they may not apply for multimineral ores. Gay developed a model using a probability method to simulate liberation for binary systems and also for particles with many minerals (Gay 1999; 2004a). This method is essentially a random breakage

model. All these liberation prediction models rely on 2D polished section measurements which has limited their utility.

Now it is possible to make 3D X-ray microtomography measurements of liberation and such measurements and analysis are presented in this thesis. The extent to which preferential grain boundary fracture contributes to liberation can be established by examination of interfacial area using high resolution x-ray microtomography (Garcia et al. 2009).

So when liberation is considered, the problem of liberation prediction during the particle breakage should be distinguished from the problem of liberation measurement. It should be noted that prediction models cannot be validated without accurate measurement of the liberation state for feed to and product from comminution operations.

In this thesis research prediction models are reviewed but the instruments and methods utilized are focused on the measurement of liberation.

1.2 Texture

The texture of the ore is defined as size, dissemination, association and shape of the mineral grains within the ore. Knowledge of the mineralogical assembly must be considered in the design of grinding and concentration operations. Texture analysis has been used to predict liberation during comminution (Gay 2004b).

Typically the description of texture is achieved by image analysis of polished sections. The images can be obtained by optical microscopy. This technique is very tedious, time consuming, and depends on the experience of the microscopist.

Presently the SEM-based automated image analysis systems such as QEMSCAN and Mineral Liberation Analyzer (MLA) have been used for 2D texture analysis. New techniques have been developed for texture analysis; these techniques include the incorporation of new software and methods. In the work presented by Donskoi (Donskoi et al. 2007) and Pirard (Pirard et al. 2007) new software and new methods of 2D image analysis are utilized for classification of particles based on texture analysis.

Until recently it has not been possible to accomplish mineral exposure analysis by traditional mineralogical techniques due to stereological limitations. It is important to note that exposed grains can be identified accurately only through 3D analysis of multiphase particles. Now such analysis is possible using high-resolution x-ray microtomography (HRXMT). High-resolution x-ray microtomography can be used for the direct determination of the grain size distribution and the extent of grain exposure for individual multiphase particles, the particle texture.

1.3 Liberation Measurements from Polished Sections

Analysis of concentrate and tailings products in 2D by optical microscopy reveals the extent to which the separation efficiency is limited by liberation. However, this technique is very tedious and time consuming for the microscopist. More important, the extent of liberation is always overestimated.

In 1977 Peter King developed one of the early automated mineral liberation analyzer for polished sections. This system measured liner intercept lengths using an optical microscope and mini computer that controlled a motorized stage and photometer circuit (Fandrich et al. 2007).

In 1982 the IBAS II image analyzer was manufactured by Carl Zeiss. The image of the particles was captured from optical microscope and displayed in a monitor. The images were processed by computer software. The measurements obtained by this system were: area percent, count, linear analysis and mean distance between objects (Lin 1986).

In 1984 a system based on an electron microprobe with wavelength-dispersive spectroscopy (WDS) detectors was developed by Jones at Imperial College, London, United Kingdom. The system identified the minerals using linear scans at a pixel size of ~2 μm and the elemental X-ray signal from the WDS detectors. The identification of a single mineral required acquiring and processing information from 10 to 30 pixels spot (Smart et al. 2007).

In 1993 an image analysis based on the Scanning Electron Microscope (SEM) was developed at University of Utah. The system was developed by King and Schneider (Schneider 1995). The mineral phases were discriminated in the SME images and the system provided a precise measurement of linear grade intercepts through cross sections of multiphase particles. At the end of analysis the linear grade distribution of the particles in the sample was obtained from the image analysis.

Now automated SEM instruments are available for polished section analyses and include the Mineral Liberation Analyzer (MLA) and the QEMSCAN, photos of these instruments, supplied by FEI, are shown in Figure 1.2. These modern instruments are routinely used to quantify liberation in 2D. Companies are routinely using these instruments for 2D liberation analysis of feed and products from their plant operations. In February 2011 it was reported from FEI that 60 QEMSCAN and 68 MLA instruments had been installed globally.

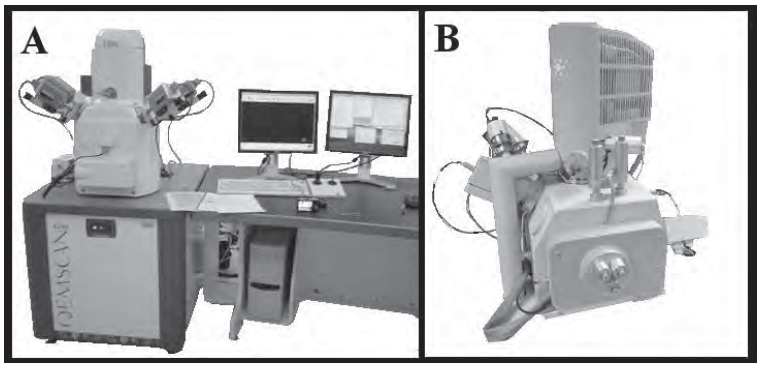

Figure 1.2 A) QEMSCAN system, B) MLA System

CANMET Mining and Mineral Sciences Laboratories (Canada) developed a liberation analysis system in 1984. However, this system is not available commercially. This system has three types of x-ray detectors: one energy dispersive spectroscopy detector (EDS), four wavelength dispersive spectroscopy detectors (WDS) and one silicon drift chamber detector (SDC).

The SDC detector can be considered to be equivalent to ~8 conventional energy dispersive spectroscopy (EDS) detectors. The SDC detector is capable of a high x-ray count rate of up to ~400,000 counts per second.

The discrimination of minerals is determined from back scattered electron (BSE) images and it complements the mineral information from x-ray detectors. The system at CANMET can process between 20,000 - 100,000 particles per hour depending on the mode of analysis such as BSE and X-ray configuration analysis. The image analysis is performed using a Zeiss KS400 image analyzer (Lastra 2007).

1.3.1 QEMSCAN

QEM*SEM system (Old configuration of QEMSCAN) was developed by CSIRO in Australia. It was first described by Grant in 1976 (Grant et al. 1976). At the present time

FEI develops and commercializes the new optimized QEMSCAN. In the actual configuration of QEMSCAN the geometry of particles and grains are described in 2D by back scattered electron spectroscopy (BSE) and the minerals are identified from elemental analysis by energy dispersive spectroscopy. The QEMSCAN system has four energy dispersive detectors (EDS) to increase the acquisition rate for fast analysis. A low fixed count rate of 1000 counts is used for fast data acquisition. Images are generated and each pixel is classified by mineral species according to the characteristic elemental peaks in the x-ray spectrum. The data obtained from each pixel are compared to a known mineral database called Species Identification Protocol (SIP), the database contains the x-ray spectrum for each element that is present in the mineral species. When the minerals have similar x-ray spectra, they are distinguished by back scattered electron brightness. If minerals in the same ore have similar x-ray spectra and back scattered electron brightness such as chalcopyrite ($CuFeS_2$) and cubanite ($CuFe_2S_3$), the identification occurs by elemental ratios.

The principal measurement modes are bulk mineralogical analysis (BMA), particle mineral analysis (PMA), specific mineral analysis (SMA), trace mineral search (TMS) and field image analysis. In the bulk mineralogical analysis (BMA) the system records the number of intercepts of all the minerals. With this analysis the modal abundance, particle and mineral surface areas, mineral associations, mineral grain size, and particle size are determined in 2D. Particle mineralogical analysis (PMA) is used for liberation analysis, the data collected is the same as bulk mineralogical analysis but the data is recorded on a particle-by-particle basis. In the specific mineral particle analysis (SMA) and trace mineral analysis (TMS) the system creates images only for the particles

containing the mineral of interest. The same data for PMA are collected for each particle. In the field image analysis, the analysis is performed in pixel-by-pixel basis. A map of the sample surface is created with mineralogy and textural information. The size resolution limitation for QEMSCAN is about 1 μm to 2 μm. The scanning of particles less than 5 μm in size may compromise the reliability of the analysis. When one sample is scanned the operator must consider both spatial resolution and chemical resolution. The spatial resolution refers to the resolution at which two phases can be separately recognized and the chemical resolution is the ability to identify two phases with different chemical composition (Gottlieb et al. 2000; Goodall et al. 2008; Azenkeng 2010).

1.3.2 Mineral Liberation Analyzer (MLA)

The Mineral Liberation Analyzer (MLA) was developed by JKMRC/FEI and was presented by Gu in 1997 (Gu and Nappier-Munn 1997). MLA combines back scattering electron (BSE) image with x-ray mineral identification to characterize the mineral liberation. Typically the particle size range for the particles is between 10 μm and 1 mm, and the particles are scanned in narrow size classes. The particles are identified from the BSE image. Once the particles are defined the different phases in each particle are classified according to the average atomic number. An average atomic number is assigned to each region in the BSE image, this average atomic number is proportional to the gray level registered in the BSE image. In a typical analysis each mineral is identified by collecting the x-ray spectrum from the center of the gray level region to avoid contamination with other phases. There are two other modes of x-ray analysis: area x-ray analysis and x-ray mapping. In the area x-ray analysis, the spectra is collected from the

BSE region, the perimeter is not scanned to avoid contamination in the boundaries. For the x-ray mapping, a grid is imposed over each particle and the x-ray spectrum is collected at each grid point to determine the mineral identity. This mode requires a lot of time in comparison with the other two modes of x-ray analysis. A mineralogy map is created for each particle.

A library of mineral standards is available for the mineral identification by x-ray analysis. The spectra identification process involves an error-based search for the measured spectrum in the standards library to find the most probable fit.

MLA offers different measurement modes. The mode implemented for each sample depends on the mineralogical information required. The seven modes of measurement for MLA are: standard BSE liberation analysis (BSE), extended BSE liberation analysis (XBSE), grain-based x-ray mapping (GXMAP), sparse phase liberation analysis (SPL), x-ray modal analysis (XMOD), rare phase search (RPS) and super extended BSE liberation analysis (SXBSE or Latti analysis). Each measurement mode is reviewed in detail in the literature (Gu 2003; Fandrich 2007).

The 2D mineralogical information produced from MLA analysis includes modal mineralogy, calculated assay, elemental distributions, elemental and mineral grade recoveries, particle and grain size distributions, particle density distributions, mineral associations and locking, phase specific surface area and mineral liberation by particle composition and free surface analysis.

In the future the combination of MLA with the beam ion milling and deposition capability of a dual beam SEM system (QUANTA 3D system offered by FEI) will be

able to provide the quantitative mineral liberation in 3D (Fandrich 2007). Such analysis will require considerable time.

1.3.3 Limitations of Polished Section Analysis

Optical microscopy, automated image analyses using SEM-based techniques (QEMSCAN and MLA), and other techniques for liberation analysis are based on the examination of polished particle sections (Wills 2006).

In general the particles are classified into narrow size fractions, then the particles are sampled and placed into a mold with epoxy resin to form a hardened disk (typically 30 mm in diameter and 20 mm in height). Next the surface of the disk is polished and the surface is coated with carbon for the QEMSCAN and MLA analysis (Fandrich 2007).

The liberation analysis of polished sections overestimates the extent of liberation because the sectioned particles can appear to be fully liberated in the polished section as is shown in Figure 1.3. In order to estimate the volumetric liberation from polished section analysis, stereological models are applied. However the stereological models are not satisfactory because model parameters depend on the ore texture which is unique for each ore type (Miller and Lin 1988).

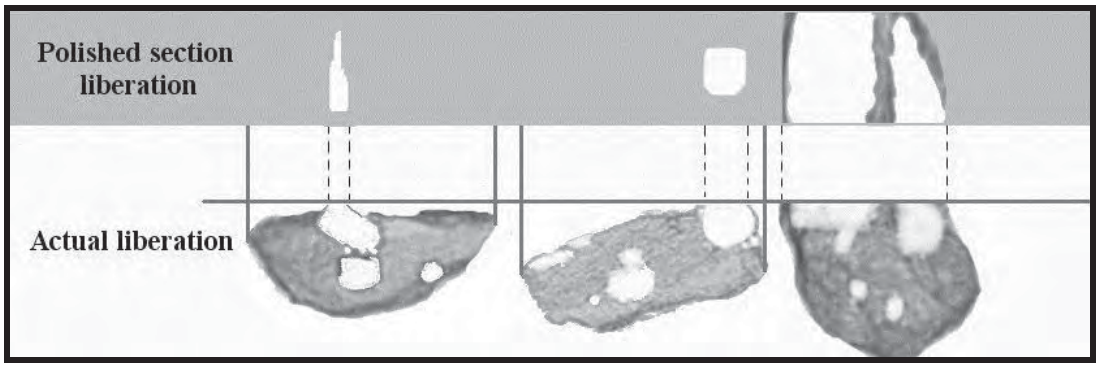

Figure 1.3. Overestimation of liberation from polished sections analysis.

1.4 High Resolution X-ray Microtomography (HRXMT)

High Resolution X-ray Microtomography (HRXMT) is a powerful tool for the 3D characterization of multiphase particles at a voxel resolution as small as 1-2 μm. This HRXMT scan and subsequent analysis with special software generates a three-dimensional reconstruction of packed particle beds and the quantitative composition of individual particles in the particle bed. The volume grade of the valuable minerals in each particle is measured from reconstructed images generated by HRXMT. The High Resolution X-ray Microtomography is a non-destructive technique that has the capability to scan particles with a density of up to 8 g/cm^3 (Miller and Lin 2004).

The particles do not require any special preparation. The sized particles from the sample are placed inside a plastic cylinder of up to 40 mm in diameter. The sample is placed between the x-ray source and the detector, photons pass through the sample and the projected image is collected by the detector. The sample is rotated and projections at different angles are collected. For example, at a voxel resolution of 5 μm 208x106 μm sample containing particles is scanned for 4 hours during which time 1000 projections are recorded. A schematic diagram of the data acquisition process is shown in Figure 1.4.

In a previous research (Miller and Lin 2004) HRXMT applications have been reported for 3D analysis of coal washability, mineral exposure/liberation, the pore network structure of packed particle beds and geometric features of the particles including size, shape, and texture. Coal washability curves constructed from HRXMT analysis were in good agreement with the data generated in the lab from sink-float analysis.

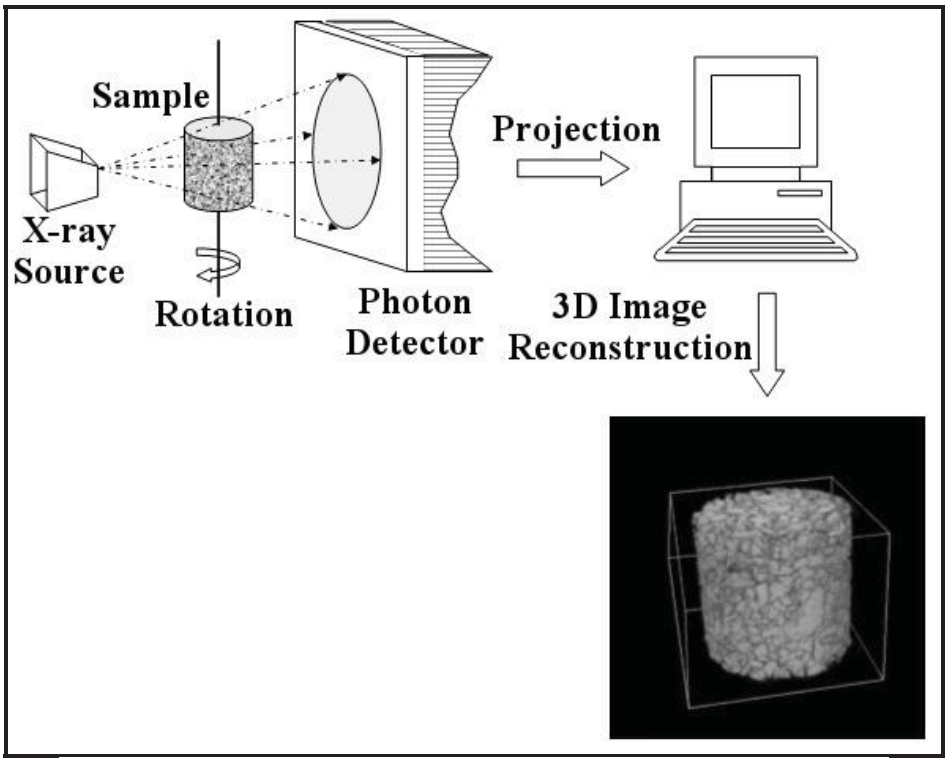

Figure 1.4 Process for HRXMT analysis of packed particle beds.

The copper recovery in heap-leaching was predicted successfully from the 3D exposure/liberation data obtained by HRXMT. Particle shape and texture has been described by HRXMT analysis. Also parameters that describe these features have been established (Lin and Miller 2005). Pore network structure in a packed particle bed as determined from HRXMT analysis and the 3Dimensional reconstruction was used for fluid flow simulation through the particle bed. A similar analysis has been used to predict fluid flow in filtration cake. Finally microtomography has been used to describe particle damage during crushing by measuring the specific crack surface area in mm^2/mm^3 (Miller 2010) and the extent of preferential grain boundary fracture as a function of energy dissipation rate (Miller 2010).

1.5 Gold Ores

1.5.1 Gold Minerals and Alloys

Gold is found as native gold, gold alloys and gold minerals in gold ore. Native gold is frequently alloyed with silver, when the silver content exceeds 20% the alloy is called electrum. Gold also forms alloys with copper and platinum group metals (PGM). The principal gold minerals are maldonite (Au_2Bi), Calaverite ($AuTe_2$), sylvanite ((Ag, Au)Te_2) and aurostibite ($AuSb_2$) (Adams 2005).

1.5.2 Submicroscopic Gold Occurrences

There are three important submicroscopic gold occurrences: solid-solution gold, colloidal gold and surface gold. Solid-solution gold refers to gold that is atomically distributed in the crystal structure of sulfide minerals such as pyrite and arsenopyrite. Solid-solution gold tends to concentrate preferentially in arsenopyrite and gold is enriched in the finer sulfide mineral grains (< 20 μm). In these cases it is difficult to liberate gold from arsenopyrite. Pyrite, especially arsenious pyrite, is the most common sulfide mineral that incorporates a significant amount of gold in its crystal structure. Typically gold is hosted mostly by the coarser (> 50 μm) pyrite grains. There is a positive correlation between arsenic and gold concentration in pyrite, this correlation is shown schematically in Figure 1.5 (Adams 2005). Other minerals that may contain significant concentrations of solid-solution gold are loellingite ($FeAs_2$), enargite (Cu_3AsS_4) and tennantite ($Cu_{12}As_4S_{13}$).

The term colloidal gold describes submicron gold inclusions in sulfide minerals, invisible by optical and conventional scanning electron microscopy (SEM). Colloidal

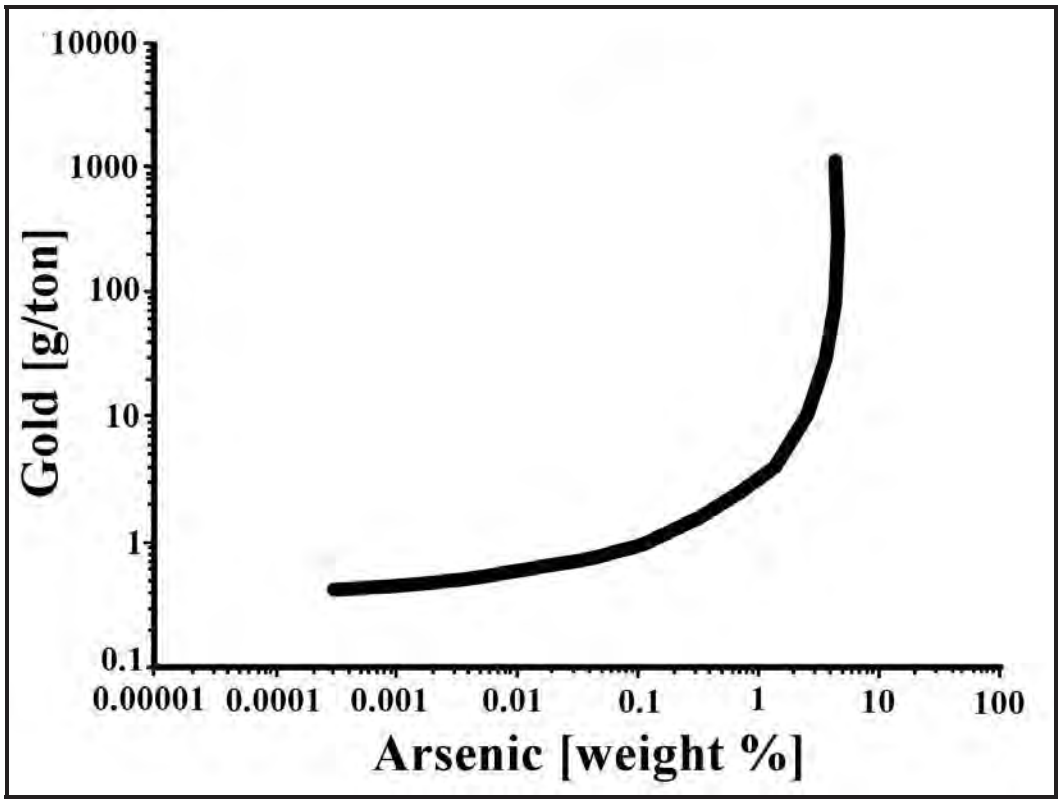

Figure 1.5 Correlation between arsenic and gold in pyrite.

gold ranges in the size between 5 and 500 nm, which is also the range of gold in colloidal solutions.

Colloidal gold is mostly spherical and is not always confined to the sulfide matrix, it has been observed in surrounding clay minerals. The preferential host of colloidal gold is pyrite and to a lesser extent arsenopyrite.

Surface gold refers to the gold found at the surface of the mineral particles, the most classic example is the gold observed on the surface of naturally occurring carbonaceous material. Surface gold is the result of sorption, reductive deposition, precipitation and ion-exchange deposition from gold-bearing solutions (Adams 2005).

1.5.3 Forms and Carriers of Gold

In the flotation of gold-bearing minerals, two terms are introduced: form and carrier. Form refers to the state of gold such as gold minerals as well as gold occurrences such: solid-solution gold, colloidal gold and surface gold. Carrier refers to the minerals which host one or more forms of gold therefore the flotation is designed for the carrier minerals, for example auriferous pyrite.

Gold particles may be present in the ore from large nuggets to fine grains locked in crystals of sulfide minerals. These sulfide minerals are gold carriers and the flotation of the sulfide minerals such as auriferous pyrite is required.

1.5.4 Flotation of gold and gold-bearing ores

It is generally accepted that surface of pure clean gold is hydrophilic (Adams 2005). Gold particles below 150 μm float readily with most collectors and in particular with xanthate and dithiophosphate. Copper sulfate is used to enhance the flotation of pyrite, pyrrhotite, arsenopyrite and it increases the rate of sulfide minerals flotation, providing an overall increase in gold recovery because of the gold associated with the sulfide minerals, such as auriferous pyrite. The adsorption of copper onto pyrite and pyrrhotite is pH dependent, smaller quantities are adsorbed under alkaline conditions. For some ores the presence of copper at values of pH between 7 and10 may be harmful and may reduce the flotation response of pyrite (Adams 2005).

When the pyrite is clean and free of oxidation, its surface is naturally hydrophobic however, on exposure to the atmosphere, oxidation occurs and the surface becomes hydrophilic under these circumstances. Collector is necessary for pyrite flotation. Pyrite

can be floated in either acidic or alkaline conditions. Xanthates are the primary collectors on the alkaline side and mercaptobenzothazole (MBT) on the acidic side. Dithiophosphates are usually used as secondary collectors and are particularly effective for pyrite recovery. Pyrite and arsenopyrite float well in the pH range 3-5. Pyrite depression occurs at high pH but recovery can be achieved by the addition of more collector, use of a stronger collector, and activation with copper sulfate (Adams 2005).

1.6 Sampling

Particulate sampling is the process of selecting a part from the whole; if done properly this part should have the same characteristics as the whole, the original population. If sampling is not carried out correctly, the entire measurement chain is corrupted at the outset and no amount of analysis can fix this problem.

For example, segregation is typical of particles suspended in slurry with a greater proportion of the coarser and denser particles occurring near the bottom of the tank. Hence, it is impossible to take a representative sample of slurry by taking a dip sample at a fixed depth.

The sampling error can be eliminated by correct design of sampling and sample processing systems include sample spillage, sample contamination and incorrect extraction such as taking a grab sample. The sampling error that can be minimized but not completely eliminated includes change in moisture content, size degradation and dust loss (Adams 2005).

Sampling error can be classified into different types of errors: the fundamental error, the grouping and segregation error, the delimitation error, the extraction error, the

preparation error and the weighting error (Pitard 2002). The first two errors types are largely random errors and are related to differences between individual fragments or group of fragments in the immediate neighborhood of sample collection. Segregation is the other error that has a random behavior.

The delimitation error refers to the incorrect geometrical definition of the sample taken. For example all the parts of a stream cross-section most be diverted by the sample cutter, the same length of time. The extraction error occurs when the sample is taken but the material is rebounding or being lost from the cutter.

The preparation errors occur when the sample is processed by crushing, grinding, pulverizing, drying, screening and packaging. The preparation error can introduce a loss, contamination or an alteration of the physical or chemical integrity of the sample.

The weighting error refers to the variation in the flow rate of the stream, so that individual samples do not carry with them the correct weighting information when they are combined into partial samples and gross samples, particularly for the time-basis sampling.

After the samples are collected from a process unit, they are crushed, dried and divided as necessary in a number of smaller scale sampling stages to produce test samples. Suitable methods for sample division include rotary sample division, riffle division, strip division and manual sample division. Of these, rotary sample division is the most reliable method (Adams 2005).

Sampling nugget effect is related to errors induced by inadequate sample size and preparation of analytical procedures and is particularly problematic with coarse gold-bearing ores. Gold deposits display a high nugget effect as a result of sparsely distributed

grains of gold. Sampling of the gold material produces a relatively wide range of gold grain abundance. For example, a sample of several kilograms that contains five large gold grains per kilogram has good sample properties. If a subsample of 10 kilograms is taken, it would have 50 grains of gold and provide what was for all practical proposes a normal sampling distribution. Much smaller sample weights, however would have a high probability of undersampling sparse coarse grains, resulting in a extremely misrepresentative sampling distribution and significant error (Dominy et al. 2001).

Some methods have been developed by Taggart (Kelly 1982), Pitard (Adams 2005) and Gy (Wills 2006) to determine the minimum weight of sample to give a required degree of accuracy. Taggart method is based on the particle size and a plot is used to determine the minimum weight of sample required. Pitard method is based principally on the particle size and the average grade of the particles. The method developed by Gy is based on maximum particle size, liberation, ore grade, particle size distribution, particle shape and confidence in the results of the sampling method. Gy's method is used in this research work to estimate the minimum weight of sample required for HRXMT analysis for certain accuracy.

1.7 Research Objectives and Thesis Organization

In this thesis high resolution x-ray microtomography (HRXMT) was used to determine the liberation characteristics and textural features of two auriferous pyrite ores, pyrite ore from a mine site and from plant operations.

The principal objectives of this thesis research include:

- Demonstrate the utility of High Resolution X-ray Microtomography for 3D liberation analysis for selected auriferous ores including the construction of liberation-limited grade/recovery curves.
- Determine the particle size limit for High Resolution X-ray Microtomography 3Dimensional liberation analysis.
- Evaluate the flotation separation efficiency using liberation-limited grade/recovery curves for bench scale experiments and for samples from an industrial flotation circuit.
- Determinate the influence of texture in the analysis of flotation separation efficiency.

Samples from the mine site were provided for this research. Bench scale flotation experiments were completed, the products from each flotation experiment were dried, classified into different size classes, and scanned by HRXMT. The pyrite grade and recovery were calculated for each particle size class from HRXMT data.

Samples were collected from flotation plant operations in central Nevada for HRXMT analysis. Samples from feed, concentrate and tailings were collected from the flotation circuit. The samples were dried and separated into different size classes for HRXMT analysis. Based on the HRXMT data the pyrite grade and recovery were calculated.

For both ores, mine site and plat operations, the liberation-limited grade/recovery (LLGR) curves were constructed from the HRXMT analysis of feed samples. The pyrite grade and recovery from bench scale flotation experiments for the mine site ore and from the plant flotation circuit were plotted on their respective liberation-limited

grade/recovery curves to determine if factors other that liberation affect the separation efficiency in the flotation process.

A textural analysis was done to determine the percentage of external and internal grains for each particle in all products both from batch scale flotation experiments and from flotation plant samples. The textural analysis provided information to understand the behavior of the particles in the flotation process according to the exposure of the pyrite grains at the particle surface.

The thesis is organized in the following way:

In Chapter 1 the research is introduced with discussion of liberation, high resolution x-ray mictotomography, gold ores, and sampling.

The characteristics of the mine site and plant operation ore are discussed in Chapter 2 including sampling, sample preparation for HRXMT analysis, procedure for HRXMT analysis and data processing.

Experimental results from bench scale flotation experiments of the mine site ore are presented in Chapter 3 as well as a discussion of these results with respect to flotation efficiency.

In the Chapter 4 results from HRXMT analysis of feed and products from the plant flotation circuit are presented and discussed.

Finally, Chapter 5 presents a summary and general conclusions regarding the use of HRXMT for liberation analysis. The significance of HRXMT textural features on the analysis of flotation separation efficiency is summarized.

CHAPTER 2

MATERIALS AND METHODS

2.1 High Resolution X-ray Microtomography

Analysis and Data Processing

The X-ray computed tomography (CT) procedure was developed as a radiological 3D imaging technique for medical diagnosis in 1972. CT techniques have found other practical applications in other areas including material science, oil and gas industries, as well as other applications (Videla 2006).

Recently researchers at University of Utah have been using X-ray microtomography as an analytical tool. This type of analysis has revealed interesting applications in the characterization of coal and mineral resources (Miller and Lin 2004). The microtomography technique offers a unique capability for the quantitative analysis of multi phase systems through the acquisition of high resolution 3D images.

One area of application for X-ray microtomography is mineral liberation analysis. Typically, liberation is measured from polished sections of mineral particles where just one section of a particle is revealed. The analysis from polished sections requires stereological transformations for estimation of 3D characteristics; however even with stereological transformation the liberation state of the particle population is only a rough estimate because of textural issues. In addition, the cost and time taken by the

microtomography liberation analysis can be dramatically reduced by the examination of packed particle beds (Miller and Lin 2004).

The extent of liberation is a dominant factor in mineral processing operations. A suitable degree of liberation of mineral phases is the objective in crushing and grinding circuits. Another application of microtomography in the mineral processing area is exposure analysis. In this type of analysis of multiphase particles the exposure of mineral grains is quantified.

Recently High Resolution X-ray Microtomography (HRXMT) systems have been developed. These new systems employ an x-ray detector with a submicron resolution, combined with advanced x-ray optics and a microfocus x-ray source.

2.1.1 Review of X-ray Computed Tomography Principles

The general principle of x-ray microtomography was described in Chapter 1. See Figure 1.4. The number of photons received by the detector depends on the density of the mineral, the higher the density the less the number of photons passing through the sample. Each image projection is a map created by the number of photons counted at a particular angle. The attenuation coefficient is the ratio of photons counted by the detector to the initial number of photons from the x-ray source. The attenuation coefficient depends on the energy of the photons, density and atomic number of the minerals (Videla 2006, Videla et al. 2006, Videla et al. 2007). The photon density that emerges when a narrow beam of mono-energetic photons with energy E and intensity I_0 passes through a homogeneous absorber of thickness x can be expressed by Beer's law:

$$I = I_0 \exp\left[-\mu(\rho, Z, E)\, x\right] \tag{2.1}$$

where,

I_0 = Initial intensity of emerging beam

I = Final intensity of emerging beam

μ = Attenuation coefficient

ρ = Density of the absorber

Z = Atomic number

E = Energy

If the absorber is not homogeneous, the attenuation coefficient is a space-variant function dependent on the distribution of material in the sample being interrogated. Beer's law can be modified and expressed by the simple integration that the intensity between successive blocks of different material can be written as:

$$I = I_0(x) \exp\left[-\int \mu(\rho, Z, E_0)\, dx\right] \tag{2.2}$$

Once the projections at different angles are acquired the three-dimensional (3D) reconstruction is done using computational algorithms. The three-dimensional reconstruction is the spatial reconstruction of the attenuation coefficients values. The 3D reconstructed image is represented by a matrix of voxels. A voxel is the minimum volume element (cube) in the three-dimensional reconstructed image. Each voxel has an intensity established by the composition in that region and given by the corresponding attenuation coefficient value. The 3Dimension reconstruction not only provides the

multiphase composition of particles, but other features can be characterized such as grain size, interfacial area, exposure/liberation, shape, texture and the pore structure of packed particle beds (Videla et al. 2007).

A high resolution x-ray microtomography system from Xradia was been installed in the Department of Metallurgical Engineering at the University of Utah. The model number of the system is MicroXCT-400 which has a mechanism that generates x-rays from 40 to 150 kV to image samples. Lenses are mounted in a rotary turret for different resolution analysis. The magnification level of the lenses are 4X, 10X, 20X and 40X corresponding to a voxel resolution of 5 µm, 2 µm, 1.5 µm and 1 µm, respectively. A macro lens is mounted beside the rotary turret. The macro lens has a magnification level of 0.5X with a voxel resolution of 40 µm. The detector has a pixel resolution of 2048x2048 for imaging the projections of the sample. The x-ray microtomography equipment installed at the University of Utah and principal components of the acquisition system are shown in Figure 2.1.

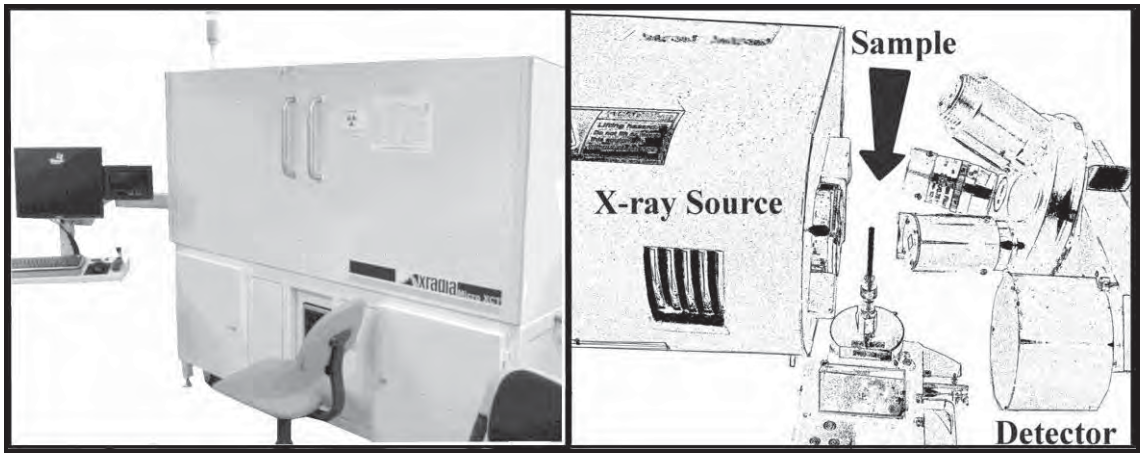

Figure 2.1 High Resolution X-ray Microtomography equipment and acquisition system.

2.1.2 Source of Errors from Reconstruction Process

There are certain errors that are unavoidably associated with the interaction of object heterogeneities and the x-ray energy used. In the following section the unavoidable errors are explained briefly.

2.1.2.1 Polychromaticity

In the 3D reconstruction algorithm it is assumed that beams are monochromatic. Since attenuation coefficients are strongly energy dependent, any energy spread leads to the averaging of attenuation coefficients and degrades the resolution in transmission tomography. In practice the x-ray sources in microtomography scanning are polychromatic and the attenuation coefficient is energy dependent. Thus the characteristic information reconstructed from the x-ray microtomography is the measured attenuation coefficient at a particular energy. The effective energy is defined as the monochromatic energy at which a given material will exhibit the same attenuation coefficient as is measured by the scanner. Therefore, the intensity value assigned to a voxel is only an approximation of the true property value of the material in the voxel and corrections must be made during the mathematical reconstruction in order to be sure that the value assigned to a voxel does not depend on the location of the voxel. In order to reduce the range of photon energy spectrum, the x-ray beam is passed through an aluminum, glass or copper filter. In this way the beam is more monochromatic before being passed through the sample (Videla 2006).

2.1.2.2 Photon statistics

One basic limitation in the accuracy of the microtomography scanning is the fundamental statistical nature of the x-ray photon production, photon interaction with the sample, and photon detection. A certain amount of error is unavoidable, however some aspects in design and operation can be modified to reduce this effect. For example, to prevent scattering of the photons leading to projection errors it is necessary to use a collimated detector. This way, the x-rays that are not traveling in a straight line between the source and the detector are rejected (Videla 2006).

2.1.2.3 Partial volume effect

The value of each voxel represents an average of the attenuation coefficients of the total material inside the voxel. When the voxel is near a boundary of two or more phases the data acquisition process will combine the attenuation coefficients and the voxel value will represent an average. This is illustrated in Figure 2.2 where the 2D pixels are shown over phases A and B. By analogy, it is clear that in three dimensions for the boundary voxels between phases A and B, the attenuation coefficient of such voxels will be a linear combination of the attenuation coefficient of each phase based on the volume occupied by each phase in the voxel. Therefore an attenuation value of a nonexistent material is obtained. This error will depend on the resolution or size of the voxels, phase dissemination in the material and particle geometry. The partial volume effect can have an important influence in the quantitative and qualitative analysis of the images (Videla 2006).

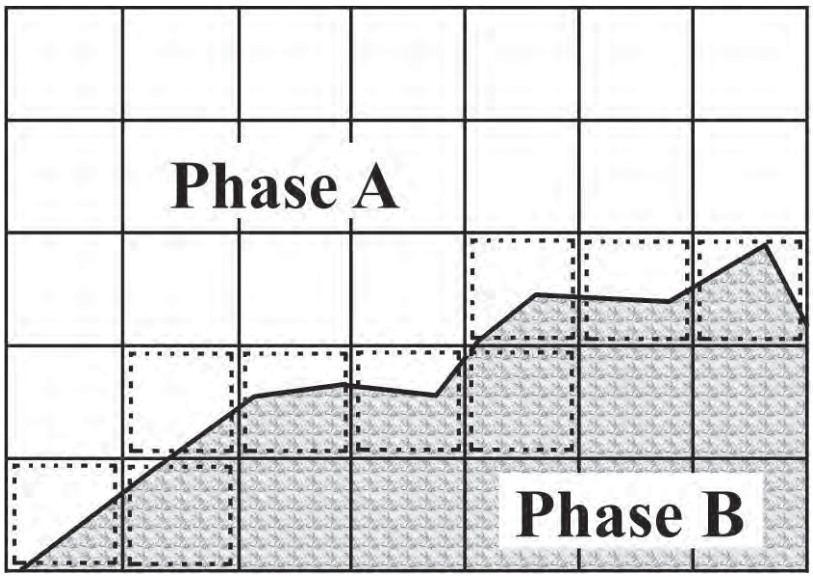

Figure 2.2 Partial volume effect; phase A and phase B are combined in voxels at the phase boundary.

2.1.3 Watershed Segmentation Process

The data acquired are a map of the material analyzed. The particles are not distinguished in a packed particle bed and the image of individual particles requires particle segmentation using computer algorithms. The segmentation process consists of the following sequential steps: noise removal, thresholding, distance transformation, H-extrema transformation, semivariogram process, labeling and flooding process. Further details of each step in the 3D watershed segmentation process have been explained previously (Videla 2006). In this thesis a brief description of each step in the segmentation process is given.

In the first step the noise from errors of the reconstruction is removed using a mean filtering algorithm. The mean filter consists of replacing the intensity of each voxel by the average intensity of the voxel itself and the voxels of a defined neighborhood region.

The separation between the particles and the air occurs in the thresholding step. The threshold value is the attenuation coefficient that separates background (air) and foreground (particles). Usually the histogram of the image has a bi-modal distribution of the attenuation coefficient values and the threshold value is established by the user. In this step a binary image is generated with the assigned threshold value.

In the distance transformation step, the binary image is replaced by an image where each voxel value has a value that approximates to the Euclidean distance to the nearest background voxel. The result is that each particle has in the center at least one local maxima value.

In the H-extrema transformation step, the local maxima values established in the previous step are used as markers for the position of a particular particle in the image, the markers are unique regions of space for particle locations. The markers definition is the key step to get a good result in the segmentation process since the number of particles detected in an image will be equivalent to the number of markers defined.

The number of markers in one particle depends on the particle shape, for example if the particle is spherical then it will have just one maxima point in the center; if the particle is a non-convex polygon then the particle will have more than one maxima point along the medial axis or plane of the polygon. The maxima points that are connected must be merged into just one marker. The region of maxima connected points will be used as markers and it is called regional maxima. The regional maxima are obtained using the H-extrema transform. The H-extrema transform requires the definition of a user-defined parameter *h*. The H-extrema transform suppresses all regional maxima with a length smaller that the given threshold value *h*. Those particles with a radius smaller

than *h* will not be considered in the segmentation process because they do not have a marker. Therefore, the value of *h* must be selected carefully because it could eliminate small particles from further processing. Oversegmentation may occur due to noise, minor structures in the particles and irregular shape of the 3D particles in the image. In some cases the oversegmentation can be corrected manually when oversegmentation can be detected by the user. When the size of the particles is very small it is difficult to identify the oversegmentation.

In the semivariogram process the average size of the particles is estimated and the correlation between markers is established. The semivariogram operator solves the problem of particles that have two or more local maxima values due to the irregular particle shapes. In the ideal case each particle has a local maximum, but that only happens when the object of interest is a sphere.

In the labeling process each regional maxima (marker) is labeled with a unique number. In this way, each particle that will emerge form those markers will be differentiated from the rest of the particles by its identification number.

Finally, once the markers are defined the flooding process method is used. This method can be understood as the process of valley flooding where the voxel values are considered similar to topography of a surface with valleys and peaks. In the flooding process the valleys are flooded with water at a constant rate, and dams are formed when the two different valleys merge. The point at which the water of two flooded valleys merge a line will be formed and this line is the boundary between the different objects. An example of this concept for one-dimensional (1D) image is shown in Figure 2.3. At the end of the flooding process an identification number is assigned to each particle.

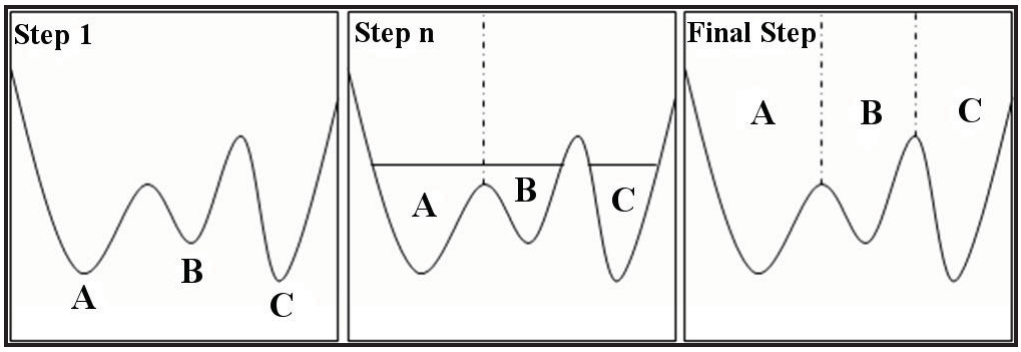

Figure 2.3 The region growing method in one dimension. The valleys A, B and C are identified. Then the level water is raised to sequentially cover peaks which separate valleys, when the water in the two flooded valleys (A and B) merges a barrier (dash line) is formed to separate the valleys. The process continues until all the boundaries are established and the image is segmented.

2.1.4 Identification of Sulfide Mineral Phases

As previously explained, the attenuation coefficient (μ) is directly related to the material density (ρ), atomic number (Z) and the level of energy (E) applied during the scanning. The Equation 2.3 illustrates an approximate relationship between these quantities. When a mixture of atomic species is present the effective atomic number (Z_e) is used and it is defined by Equation 2.4 (Miller et al. 2003).

$$\mu = \rho\left(a + \frac{bZ_e^{3.8}}{E^{3.2}}\right) \tag{2.3}$$

$$Z_e^{3.8} = \sum_i \left(f_i [Z_i]^{3.8}\right) \tag{2.4}$$

where,

μ = Attenuation coefficient

ρ = Material density

a = Variable with small dependence on energy

b = Constant

E = Energy

Z_e = Effective atomic number

Z_i = atomic number of element i

f_i = fraction of the total number of electrons contributed by element i

A higher level leads to a larger number of photons passing through the sample and hitting the detector. On the other hand, a lower level leads to a smaller number of photons hitting the detector reducing the reliability of the measurements. In fact there is a direct relationship between exposure time, energy level, material density, atomic number and the resolution that has to be balanced in order to achieve satisfactory CT imaging.

In the medical field the CT number is defined by Equation 2.5. The CT number is expressed in Hounsfield Units (HU). By definition, vacuum has a value of -1000 HU and water has a value of 0 HU, thus providing two energy-independent calibration points. Substances other than water have energy-dependent CT numbers (Bryant et al. 2012).

$$CT_{number} = \frac{\mu_{Material} - \mu_{Water}}{\mu_{Water}} 1000 \tag{2.5}$$

where,

μ_{Water} = Attenuation coefficient of water

$\mu_{Material}$ = Attenuation coefficient of material

CT_{number} = CT number [HU]

When raw data collected from the HRXMT analysis are processed to generate the three-dimensional reconstruction of the sample the attenuation coefficient values in each voxel can be translated to scaled CT number values. Scaled CT number values were used in the classification process for identification of the different minerals. The HRXMT equipment is calibrated using standard pure mineral samples. A scaled CT number range is assigned to each pure mineral. In this way, the identification of the different mineral phases is accomplished in the scanned samples according to the scaled CT numbers. The spectrum of scaled CT numbers from sulfide minerals at a resolution of 5 µm (4X) and 80 kV is shown in Figure 2.4. The values below the scaled CT number range for pyrite (see Figure 2.4) correspond to gangue minerals and the values higher than the scaled CT value range for pyrite correspond to high density minerals. These data were used to characterize the samples analyzed in this study. A similar calibration process was done for a voxel resolution of 2 µm (10X).

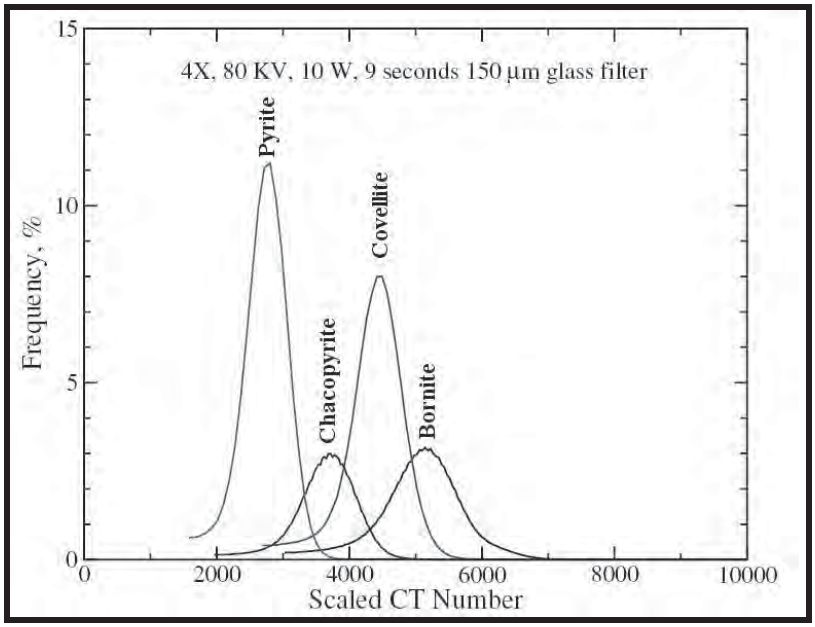

Figure 2.4 Scaled CT number spectrum for sulfide mineral phases at a voxel resolution of 5 µm (4X).

2.1.5 Mineral Classification and Quantitative Analysis

Once the segmentation process is completed, codes in C language were utilized to classify the mineral phases in each particle and quantify the number of voxels for each mineral phase. First, the code called "partial_voxel_correction_new.c" minimized the partial volume effect in the 3D reconstruction of the segmented particles. Then, the code called "histogram_cygwin_u8.c" classified the mineral phases in each particle according to the scaled CT number. The mineral phase classification was completed for three types of minerals: gangue, pyrite and high density minerals. Finally, the code called "mu_histogram_classificaiton_cuore_double.c" determined the number of voxels that correspond to each mineral type for the segmented particles. A data file called "mu_cuore_class_hist.dat" was created. This data file contains a list with the number of particles in the sample and the number of voxels of each mineral phase. An example of the results in "mu_cuore_class_hist.dat" file is shown in Table 2.1. The percent volume of each mineral was calculated from the number of voxels since the voxel volume is constant for the 3D reconstruction.

Table 2.1

Example of Data Collected after Segmentation Process and Mineral Classification

	Voxels			
Particle Number	**Gangue**	**Pyrite**	**High Density**	**Total voxels**
1	110189	144731	0	254920
2	11676	8053	0	19729
3	78633	86039	100	164772
4	28043	16467	4	44514
⋮	⋮	⋮	⋮	⋮
6780	5640	5743	0	11383

2.1.6 Exposure Analysis from HRXMT Data

Once the 3D reconstruction image was analyzed by the segmentation procedure, the mineral phases were classified into gangue phase, internal and external grains. The classification was completed using codes in C language developed for exposure analysis from previous microtomography research (Miller et al. 2003). This procedure creates separate 3D images of the gangue phase, internal grains and exposed grains. The new three 3D images are combined to create a new 3D image where the internal and exposed grains can be distinguished from the gangue phase. Cross-sectional images of the 3D reconstructed image (A) and 3D image created from exposure analysis (B) are shown in Figure 2.5. The image from exposure analysis has false colors for easy identification of the gangue phase (gray color), internal grains (red color) and exposed grains (blue color).

The 3D image from exposure analysis was analyzed quantitatively using the same procedure as the mineral quantification method, but in this case the three phases considered were: the gangue phase, internal grains and exposed grains. The codes "histogram_cygwin_u8.c" and "mu_histogram_classificaiton_cuore_double.c" were employed for the quantitative analysis of each particle.

A data file similar to the mineral quantification process was created. This file has a list of individual particles with the number of voxels that corresponds to the gangue phase, internal grains and exposed grains. In this way, the data can be used to calculate the percent volume of internal and exposed grains for each particle. These data will be used to determine percentage of internal pyrite grains and exposed pyrite grains in each sample. The results of internal and exposed internal pyrite grains will be presented in 3D plots.

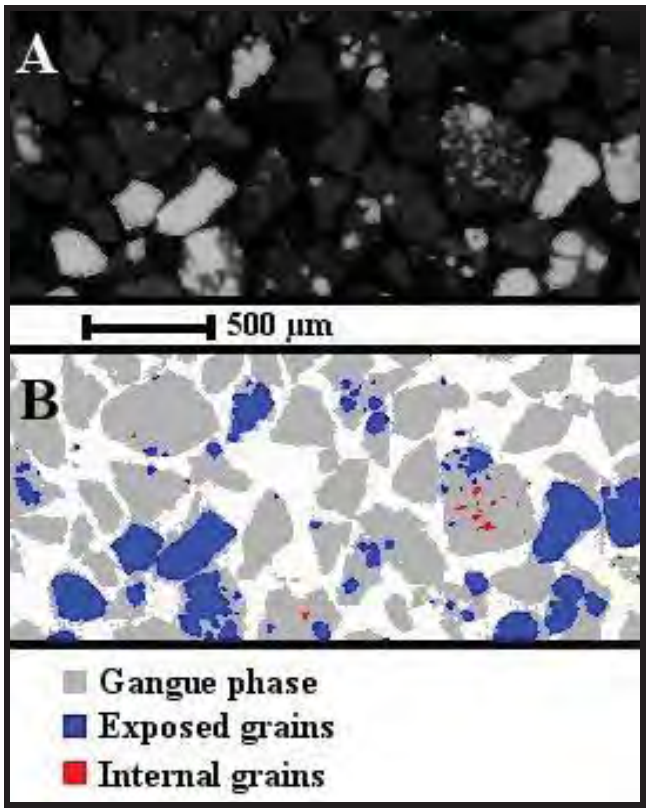

Figure 2.5 Exposure analysis, cross-sectional image of 3D reconstruction (A) and 3D image reconstructed from exposure analysis (B).

2.2 Laboratory Flotation Experiments

2.2.1 Mine Site Ore Sample

The mine site is located in Northern Canada, this mine is still in development with a potential of up to 9 million ounces of gold. The minerals present in this pyrite ore are: quartz, albite, ankerite, siderite, muscovite, chlorite, rutile, pyrite and gold as identified by XRD and chemical analysis, see Table 2.2.

Pyrite ore samples were received from the mine site. The samples had a size of -2 mm (-10 mesh). The ore samples were received in 10 bags, each bag contained 2 kg of the pyrite ore.

Table 2.2

Mineralogy of Hope Ore from XRD Analysis

Mineral	Mass Percentage [%]	Mineral	Mass Percentage [%]
Quartz	20	Albite	18
Ankerite	38	Siderite	5
Muscovite	8	Chlorite	7
Pyrite	2	Rutile	2
Gold	~ 3 g/ton†		

† Determined by atomic absorption spectroscopy

This pyrite ore was selected for study because of its relatively simple composition allowing for easy identification of the different mineral phases by HRXMT. The particle size distribution of the samples received was determined from a 1 kg sample of the pyrite ore. For this purpose a 2 kg bag sample was split into two samples of 1 kg each using a Quantachrome rotary riffler (Figure 2.6) with a capacity of up to 4 kg. The particle size distribution was determined by wet and dry screening and the average for the 80% passing size (P80) was found to be 1260 μm.

Figure 2.6 Quantachrome rotary riffler.

2.2.2 Grinding for Flotation Experiments

In order to obtain an appropriate particle size distribution for flotation experiments and subsequent HRXMT analysis of the flotation products, 1 kg samples of pyrite ore were ground using a ball mill of 7.5 inches in diameter and 8.5 inches in length (Figure 2.7). Mild steel balls were used as grinding media, the rotational speed of the ball mill was 84 rpm (79% of critical speed) and the percent solids in the ball mill charge was 58 %. The diameter and mass distribution of grinding media in the ball mill is shown in Table 2.3.

Figure 2.7 Ball mill for flotation experiments.

Table 2.3

Size and Distribution of Grinding Media in the Ball Mill

Ball diameter [mm]	**Mass Percent [%]**
13	12.48
20	15.26
27	32.18
39	40.08
	100.00

The pyrite ore was ground at three different grinding times, 5, 10 minutes and 16 minutes. The particle size distribution was calculated from wet and dry screening, and the P80 values of 607 µm, 262 µm and 150 µm were determined for 5, 10 and 16 minutes, respectively. The particle size distribution of the sample as received and the particle size distributions for the different grinding times are shown in Figure 2.8. In Figure 2.8 it is clear that when the grinding time was increased the percentage of fine particles is increased considerably.

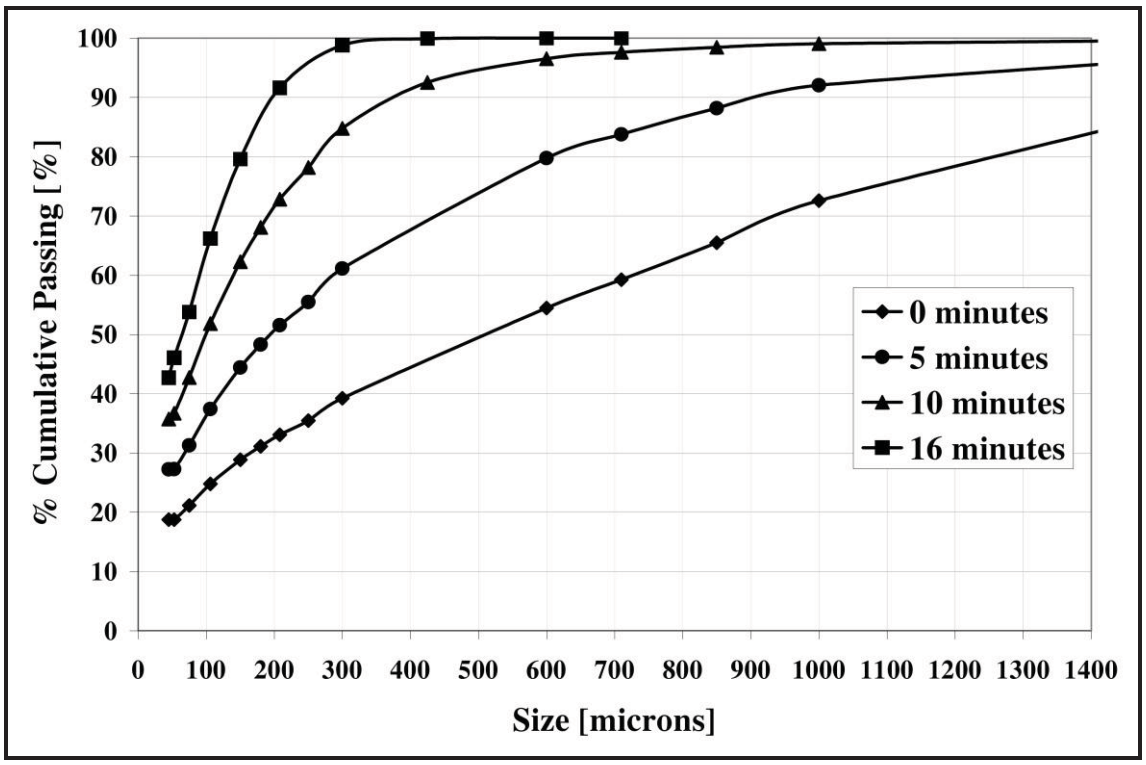

Figure 2.8 Mine site ore particle size distributions for different grinding times.

The size classes selected for the HRXMT analyses were: 2000x425 µm, 425x208 µm, 208x106 µm, 106x45 µm and -45 µm. The particle size distribution obtained at 10 minutes grinding was chosen because it was satisfactory for flotation experiments and the mass in each size class was sufficient for obtaining a representative sample. The mass distributions for different grinding times are shown in Figure 2.9 as well as the mass distribution of the pyrite ore sample as received (0 minutes).

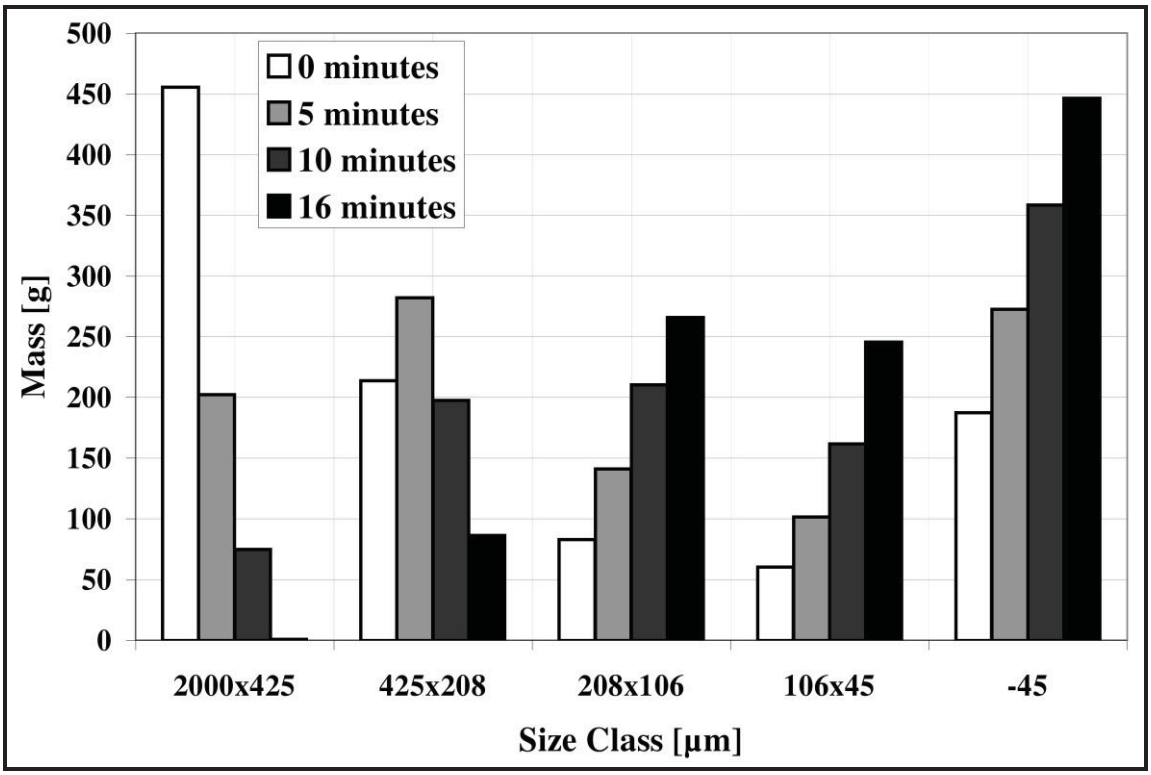

Figure 2.9 Mass distributions for different grinding times of mine site ore.

2.2.3 Bench Scale Flotation Tests

In this study the results from 10 flotation tests were analyzed by HRXMT. For the 10 flotation tests different flotation conditions were explored in order to find preferred conditions for recovery of pyrite. The aim of these flotation tests was to obtain concentrates with a high pyrite grade and high recovery. Samples of 1 kg were obtained from the 2 kg samples received from the mine site using the Quantachrome rotary riffler. Prior to each flotation test a 1 kg sample was ground under the same conditions as previously described. Each 1 kg was ground to the desired particle size distribution. A Denver laboratory flotation machine was used, the model was D-12 FLOAT (Figure 2.10). In this type of flotation machine air is introduced into the cell by the impeller movement. Two sizes of flotation cells were used, one of them had a volume of 1 L and the other one had a volume of 2 L.

In these experiments potassium amyl xanthate (PAX), Cytec 208 and Danafloat 571 were used as collectors and the frother used was Cytec F-533. The principal components in Cytec 208 are sodium diethyl dithiophosphate and sodium disec-butyl dithiophosphate. The principal components in Danafloat 571 are sodium diisobutyl dithiophosphate and sodium 2-mercaptobenzothiazole. Sulfuric acid was used for pH adjusment, a solution of 3% by weight was prepared.

In all the flotation experiments the slurry was conditioned for 5 minutes and 3 rougher concentrates were collected at different times (2 minutes, 3 minutes and 17 minutes). The remaining sample in the cell was collected as tailings. The collectors, frother and modifier were added during the flotation test at different stages: at the beginning of the flotation test (0 minutes), after concentrate 1 (2 minutes) and after

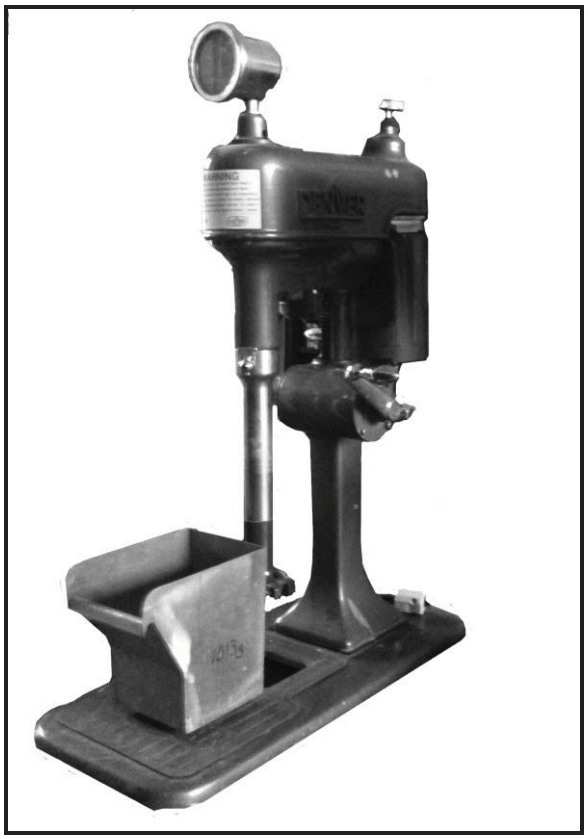

Figure 2.10 Denver laboratory flotation machine D-12 FLOAT.

concentrate 2 (5 minutes) were collected. The addition of frother Cytec F-533 was not recorded. The frother was added according to the aspect and performance of the froth in the flotation experiment.

The flotation products (concentrates and tailings) were split into different size classes: 2000x425 µm, 425x208 µm, 208x106 µm, 106x45 µm and -45 µm for HRXMT analysis. Sized samples from flotation tests # 1, 2, 3 and 4 were submitted for chemical analysis as well. Sulfide sulfur was estimated in all the samples, the sulfide sulfur content was used to calculate the pyrite content in each sample. The pyrite content results from the chemical analysis were compared with the pyrite content from HRXMT analysis.

2.2.3.1 Flotation test with cleaner flotation stage (test # 1)

The 1 kg sample was ground for 10 minutes and the P80 for this flotation test was 262 µm. Concentrate 1 was considered as final product. Concentrate 2 and concentrate 3 were combined and re-floated in a cleaner flotation stage. A cleaner concentrate was collected for 5 minutes and the remaining pulp in the flotation cell was collected as cleaner tailings. The pH value for this flotation test was 8.30 (natural pH). The flotation conditions and reagents dosage is shown in Table 2.4.

Table 2.4

Conditions and Reagent Dosages of Flotation Test with

Cleaner Flotation Stage (Test # 1)

Flotation conditions		
Mine Site Feed = 1000.03 g P80 = 262 µm Volume of flotation cell = 2 L % solids = 33.50 % Impeller speed = 1200 RPM pH = 8.30 (Natural pH)		
Reagent dosages		
Rougher flotation	PAX [g/ton]	Cytec 208 [g/ton]
Beginning of flotation test (0 minute)	40	10
After concentrate 1 (2 minutes)	40	10
After concentrate 2 (5 minutes)	20	10
Total	100	30
Cleaner flotation	PAX [g/ton]	Cytec 208 g/ton]
Beginning of flotation test (0 minute)	20	10

2.2.3.2 Flotation test without cleaner flotation stage (test # 2)

A 1 kg sample of pyrite ore was ground to a P80 of 262 µm. In this flotation experiment 3 rougher concentrates were collected similar to the flotation test # 1. A cleaner flotation stage was not required in this experiment.

The impeller speed was the only difference between flotation test #1 and # 2. In flotation test # 1 the impeller speed was 1200 rpm and for flotation test # 2 the impeller speed was 1000 rpm. The pH value was 8.30 (natural pH). The flotation conditions and reagents dosage are shown in Table 2.5.

Table 2.5

Conditions and Reagent Dosages of Flotation Test without Cleaner Flotation Stage (Test # 2)

Flotation conditions		
Mine Site Feed = 996.98 g P80 = 262 µm Volume of flotation cell = 2 L % solids = 33.50 % Impeller speed = 1000 RPM pH = 8.30 (Natural pH)		
Reagents dosages		
Rougher flotation	PAX [g/ton]	Cytec 208 [g/ton]
Beginning of flotation test (0 minute)	40	10
After concentrate 1 (2 minutes)	40	10
After concentrate 2 (5 minutes)	20	10
Total	100	30

2.2.3.3 Flotation test with increment of collector dosage and low pH (test # 3)

The P80 used in this flotation test was 262 µm. The dosage of the collectors, Cytec 208 and PAX, was increased for an improved flotation of pyrite. The Cytec 208 and PAX dosages were increased to 200 and 50 g/ton, respectively. Also the pH was decreased to a value of 5.6 using sulfuric acid solution. The flotation conditions and dosage of the flotation reagents are shown in Table 2.6.

Table 2.6

Conditions and Reagent Dosages of Flotation Test with an Increment of Collector Dosages and low pH (Test # 3).

Flotation conditions			
Mine Site Feed = 999.98 g P80 = 262 µm Volume of flotation cell = 2 L % solids = 33.50 % Impeller speed = 1000 RPM pH = 5.6			
Reagent dosages			
Rougher flotation	PAX [g/ton]	Cytec 208 [g/ton]	Sulfuric Acid [kg/ton]
Beginning of flotation test (0 minute)	80	20	3
After concentrate 1 (2 minutes)	80	20	0
After concentrate 2 (5 minutes)	40	10	0
Total	200	50	3

2.2.3.4 Flotation test with a new collector and low pH (test # 4)

The sample for this flotation experiment was ground to a P80 of 262 µm. The collector Cytec 208 was replaced by Danafloat 571. Similar collector dosages to the flotation test # 3 were used in this flotation test. The dosages of Danafloat 571 and PAX used in this flotation test were 200 and 50 g/ton, respectively. The pH was decreased to a value of 5.7 using sulfuric acid solution. The flotation conditions and dosage of the flotation reagents are shown in Table 2.7.

Table 2.7

Conditions and Reagent Dosages of Flotation Test with a

New Collector and lower pH (Test # 4).

Flotation conditions			
Mine Site Feed = 997.17 g P80 = 262 µm Volume of flotation cell = 2 L % solids = 33.50 % Impeller speed = 1000 RPM pH = 5.7			
Reagent dosages			
Rougher flotation	PAX [g/ton]	Danafloat 571 [g/ton]	Sulfuric Acid [kg/ton]
Beginning of flotation test (0 minute)	80	20	3
After concentrate 1 (2 minutes)	80	20	0
After concentrate 2 (5 minutes)	40	10	0
Total	200	50	3

2.2.3.5 Flotation test with a reduced particle size distribution (test # 5)

In this flotation test the size reduction to a smaller particle size was explored. The 1 kg sample was ground for 16 minutes therefore the P80 of the ground sample was 150 µm. In the previous flotation tests the samples were ground to p80 of 262 µm. The collectors used were PAX and Cytec 208, the dosages were 200 and 50 g/ton respectively. The pH was reduced to 5.7 using sulfuric acid. The flotation conditions and reagent dosages are shown in Table 2.8.

Table 2.8

Conditions and Reagent Dosages of Flotation Test with a Reduced Particle Size Distribution (Test # 5).

Flotation conditions			
Mine Site Feed = 995.79 g P80 = 150 µm Volume of flotation cell = 2 L % solids = 33.50 % Impeller speed = 1000 RPM pH = 5.7			
Reagent dosages			
Rougher flotation	PAX [g/ton]	Cytec 208 [g/ton]	Sulfuric Acid [kg/ton]
Beginning of flotation test (0 minute)	80	20	3.5
After concentrate 1 (2 minutes)	80	20	0
After concentrate 2 (5 minutes)	40	10	0
Total	200	50	3.5

2.2.3.6 Flotation tests of separate size classes

(Test # 6 –Test # 10)

In order to determine if the fine particles (-45 µm) may affect the pyrite flotation performance, flotation tests for separate size classes were completed. For these flotation tests 2 samples of 1 kg were ground separately and combined after grinding. The samples were ground to a P80 of 262 µm. After grinding the 2 kg sample was separated into 5 size classes by wet screening. The size classes used for the flotation tests were: 2000x425 µm, 425x208 µm, 208x106 µm, 106x45µm and -45 µm. After each size class was separated by wet screening, the sized sample was placed in the flotation cell immediately.

The flotation conditions and reagent dosages of the size classes 2000x425 µm, 425x208 µm, 208x106 µm, 106x45µm and -45 µm are shown in Table 2.9, 2.10, 2.11, 2.12 and 2.13, respectively. The pH value for these flotation tests was between pH 5.0 and 6.0, the pH was reduced using the sulfuric acid solution.

The dosage of the collectors was calculated based on the mass distribution of the size classes for 10 minutes grinding in the ball mill (P80 = 262 µm). The target for the dosage of PAX and Cytec 208 was 50 g/ton and 200 g/ton, respectively. However, the dosages were offset of the target value due to the variation in the weight of each size class.

Flotation test products were analyzed by HRXMT, but samples were not submitted for chemical analysis. Based on the results from the HRXMT analysis the pyrite volume grade will be determined for the concentrates and tailings of each size class. Also, the pyrite recovery will be calculated based on the weight and pyrite volume grade of the flotation products. The results of the flotation tests for separate size classes are presented in Chapter 3.

Table 2.9

Conditions and Reagent Dosages of Flotation

Test for Size Class 2000x425 µm (Test # 6)

Flotation conditions			
Sample weight = 79.61 g Volume of flotation cell = 1 L % solids = 6.38 % Impeller speed = 1000 RPM pH = 5.4			
Reagent dosages			
Rougher flotation	PAX [g/ton]	Cytec 208 [g/ton]	Sulfuric Acid [kg/ton]
Beginning of flotation test (0 minute)	64	14	1.5
After concentrate 1 (2 minutes)	64	14	0
After concentrate 2 (5 minutes)	33	6	0
Total	161	34	1.5

Table 2.10

Conditions and Reagent Dosages of Flotation

Test for Size Class 425x208 µm (Test # 7)

Flotation conditions			
Sample weight = 457.83 g Volume of flotation cell = 2 L % solids = 18.78 % Impeller speed = 1000 RPM pH = 5.4			
Reagent dosages			
Rougher flotation	PAX [g/ton]	Cytec 208 [g/ton]	Sulfuric Acid [kg/ton]
Beginning of flotation test (0 minute)	84	18	1.7
After concentrate 1 (2 minutes)	84	18	0
After concentrate 2 (5 minutes)	42	9	0
Total	210	45	1.7

Table 2.11

Conditions and Reagent Dosages of Flotation

Test for Size Class 208x106 µm (Test # 8)

Flotation conditions			
Sample weight = 429.49 g Volume of flotation cell = 2 L % solids = 15.75 % Impeller speed = 1000 RPM pH = 5.6			
Reagent dosages			
Rougher flotation	PAX [g/ton]	Cytec 208 [g/ton]	Sulfuric Acid [kg/ton]
Beginning of flotation test (0 minute)	97	21	2.0
After concentrate 1 (2 minutes)	97	21	0
After concentrate 2 (5 minutes)	49	10	0
Total	243	52	2.0

Table 2.12

Conditions and Reagent Dosages of Flotation

Test for Size Class 106x45 µm (Test # 9)

Flotation conditions			
Sample weight = 358.41 g Volume of flotation cell = 2 L % solids = 12.80 % Impeller speed = 1000 RPM pH = 5.5			
Reagent dosages			
Rougher flotation	PAX [g/ton]	Cytec 208 [g/ton]	Sulfuric Acid [kg/ton]
Beginning of flotation test (0 minute)	92	20	2.8
After concentrate 1 (2 minutes)	92	20	0
After concentrate 2 (5 minutes)	46	10	0
Total	230	50	2.8

Table 2.13

Conditions and Reagent Dosages of Flotation

Test for Size Class -45 μm (Test # 10)

Flotation conditions			
Sample weight = 633.62 g Volume of flotation cell = 2 L Impeller speed = 1000 RPM pH = 5.7			
Reagent dosages			
Rougher flotation	PAX [g/ton]	Cytec 208 [g/ton]	Sulfuric Acid [kg/ton]
Beginning of flotation test (0 minute)	107	23	6.8
After concentrate 1 (2 minutes)	107	23	0
After concentrate 2 (5 minutes)	54	14	0
Total	268	60	6.8

2.3 Flotation Plant Operation

2.3.1 Samples from Flotation Plant

Samples from an industrial flotation circuit in central Nevada were received at University of Utah. The samples were taken from the feed to the flotation circuit, final concentrate and final tailings. On December 15th, 2010 these samples were taken at plant operations for HRXMT analysis. Auriferous pyrite ore is processed in this flotation plant. The pyrite ore that is mined and sent to the flotation plant varies depending on the geology characteristics of the deposit being mined. Therefore, the mineral content of the feed to the flotation circuit varies with respect to time. Pyrite is the major sulfide mineral in this ore, the mass percent of pyrite varies between 3 and 7%. The principal components of feed and their typical contents are shown in Table 2.14.

Table 2.14

Principal Minerals in Feed to Flotation Circuit at Plant

Sulfide Minerals	Mass percent [%]	Gold and Copper content	
Pyrite	4.0	Au [g/ton]	2
Arsenopyrite	0.3	Cu [g/ton]	80
Arsenian Pyrite	0.2		

Other components:	Trace amounts:
Phosphate	Bismuthinite
Carbonate	Chalcopyrite
Silicate	Sphalerite
Oxide / Hydroxide Minerals	Tennantite

Approximately 1 kg of each product was received. The samples were split into 6 size classes for HRXMT analysis using wet and dry screening. The size classes were: 435-2000 µm, 425x208 µm, 208x106 µm, 106x45 µm, 25-45 µm and -25 µm. Most of these size classes are suitable for HRXMT analysis. The mass percent in each size class and the P80 estimated are presented in the Table 2.15.

Representative samples for each size class of each product were obtained for HRXMT analysis, chemical assay and Mineral Liberation Analysis (MLA). The representative samples were taken using a Quantachrome micro riffler (Figure 2.11). The weight of samples used samples used for HRXMT analysis is very small. The weight may vary between 0.1 and 0.5 depending on the density and size of the particles. The Quantachrome micro riffler is the best method for obtaining representative samples for HRXMT analysis. The Quanchrome micro riffler reduces the sampling error and this device is adequate for very small samples.

Table 2.15

Mass Percent Distribution of Samples Taken in Flotation Circuit

	Mass Percent [%]		
Size Class [µm]	Feed	Final Concentrate	Tailings
2000x425	0.57	0.00	1.05
425x208	5.65	0.13	7.78
106-45	19.30	5.00	21.60
106x45	20.23	18.81	19.99
25-45	5.65	7.59	5.28
-25	48.60	68.47	44.30
P80 [µm]	136	48	161

Figure 2.11 Quantachrome rotary micro riffler.

2.4 Liberation-Limited Grade/Recovery Curves

The liberation-limited grade/recovery curve describes the limits for separation efficiency. The curves are determined by particle composition. Even with the best equipment and operating conditions, ultimately the separation efficiency will be limited by the liberation state of the feed particles.

The liberation-limited grade/recovery curve is constructed from the mineral liberation analysis of the feed sample. Usually the mineral liberation analysis is done on polished

sections by optical microscopy or other automated techniques. However, such two-dimensional (2D) analysis overestimates the extent of liberation.

HRXMT analysis offers a three-dimensional liberation analysis, this type of analysis is more accurate and the liberation-limited grade/recovery grade curve provides a better description of the separation efficiency boundaries (Miller et al. 2009). The liberation-limited grade/recovery curve is calculated from HRXMT analysis of the feed ore; the curve represents the best separation that can be achieved for that particular ore. HRXMT data include the liberation spectrum, the histogram showing the percentage of pyrite-containing particles in each grade class. In our case 16 grade classes containing 0%, 1%, 3%, 5%, 7%, 9%, 15%, 25%, 35%, 45%, 55%, 65%, 75%, 85%, 95% and 100% volume percent pyrite are used.

Cumulative recovery and volume grade in the liberation-limited grade/recovery curve are calculated from the liberation spectrum. First, the pyrite content in each grade class is calculated from the percentage of pyrite-containing particles and grade class value. The addition of the pyrite content in each grade class is equal to the total pyrite content in the sample. Then, the pyrite distribution is calculated dividing the individual pyrite content in each grade class by the total pyrite content in the sample. The cumulative pyrite recovery is equal to the cumulative pyrite content distribution beginning with the richest grade class. The cumulative pyrite volume grade is calculated by dividing the cumulative pyrite content by the cumulative percentage of pyrite-containing particles beginning with the richest grade class. An example of calculation of liberation-limited grade/recovery curve is presented in Appendix A.

The liberation-limited grade/recovery curve represents the boundary for the separation efficiency. The recovery and grade for any separation process can not exceed the limit of this curve. In the best case the actual grade and recovery of the separation process would fall on the curve and under these conditions improved separation can only be achieved by further liberation with size reduction. If the recovery and grade for the separation process falls below the liberation-limited grade/recovery curve the separation efficiency is limited by factors other than liberation (Miller et al. 2009).

In this study the liberation-limited grade/recovery curves were prepared for the laboratory flotation tests and flotation circuit in the plant. In the case of the flotation tests the liberation-limited grade/recovery curves were established for a particle size distribution of the feed with a P80 of 262 µm.

2.5 Minimum Sample Weight

2.5.1 Determination of the Minimum Sample Weight

The determination of the minimum weight of sample necessary for an accurate analysis is based on the simplified Gy's equation (Wills 2006) which is given by Equation 2.6.

$$M = \frac{C_S d^3}{s^2} \tag{2.6}$$

where M is the minimum weight of sample required, C_S is the sampling constant for the material to be sampled, d is the dimension of the largest pieces in the material to be sampled and s is the relative variance of the assays.

The sampling constant C_S is specific to the material to being sampled, taking into account the mineral content, and its degree of liberation. The sampling constant is given by Equation 2.7.

$$C_S = f_S \, \varepsilon \, \ell \, \beta \tag{2.7}$$

where f_S is a shape factor, which is taken as 0.5, except for gold ores, where it is 0.2, ε is a factor which is dependent on the particle size range. If approximately 95 % of the sample weight contains particles of size less than d, and the 95 % of size greater than d', ε is determined based on Table 2.16. ℓ is a liberation factor, which is given by Equation 2.8, where L_S is the size at which, for practical purposes, the mineral is essentially liberated. Finally, β is a mineralogical composition factor that can be calculated from Equation 2.9.

$$\ell = \sqrt{\frac{L_S}{d}} \tag{2.8}$$

Table 2.16

Determination of Particles Size Range Factor ε Based on d and d'

d/d'	ε
d/d' > 4	0.25
d/d' = 2- 4	0.50
d/d' < 2	0.75
d/d' = 1	1.00

$$\beta = \frac{1-\alpha}{\alpha}\left[(1-\alpha)\omega + \alpha\,\tau\right] \tag{2.9}$$

where ω and τ are the mean densities of the valuable mineral and gangue minerals respectively, and α is a fractional average mineral content of the material being sampled. An example of the minimum sample weight calculations for the size class 208x106 µm is presented in Appendix B.

2.5.2 Determination of the Minimum Sample Weight of Feed for HRXMT Analysis

The minimum weight of sample required for an acceptable representation of the original sample was calculated for each size class. Gy's equation (Wills 2006) was used for this purpose. The average liberation size for pyrite was estimated to be 75 µm. The factors determined for feed are shown in Appendix B as well as the values of the parameters in Equations 2.6-2.9.

The mineral of interest is pyrite (FeS_2); the sulfide sulfur percent was determined from chemical assays of the feed samples. The sulfide sulfur present in the samples was considered as pyrite (FeS_2) since this was the only sulfide mineral of significance as established from XRD, see Table 2.2. The pyrite mass percent was calculated from the formula for pyrite (FeS_2). The sulfide sulfur and the calculated pyrite mass percent for each size class are shown in Table 2.17. There was not enough sample from each size class to calculate the relative variance of the chemical assay. Consequently the relative variance of each sample was assumed to be 0.01. The results of minimum sample weight calculations for feed samples are shown in Table 2.18.

Table 2.17

Sulfide Sulfur Mass Percent from Chemical Assay and

Calculated Pyrite Mass Percent for Feed Samples

Size Class	Sulfide Sulfur [% by Mass]	Pyrite [% by Mass]
-45 µm	1.61	3.01
106x45 µm	2.33	4.36
208x106 µm	1.61	3.01
425x208 µm	1.07	2.00
2000x425 µm	1.05	1.96

Table 2.18

Minimum Sample Weight Calculated from Gy's Equation

for Feed Samples of Different Particle Size Classes

Size Class	-45 µm	106x45 µm	208x106 µm	425x208 µm	2000x425 µm
Mass [g]	0.00023	0.00270	0.03224	0.19595	4.79891

The feed sample weight used for HRXMT analysis was between 0.2 and 0.4 g. For the size classes -45 µm, 106x45 µm, 208x106 µm and 425x208 µm the minimum weight calculated from Gy's equation was smaller than the weight of the feed sample used for HRXMT analysis. However, the minimum weight for the size class 2000x425 µm calculated from Gy's equation is greater than the weight of the sample used for HRXMT analysis. With exception of the 2000x425 µm size class, sufficient amounts of each size class were taken to establish statistical significance.

2.6 HRXMT Analysis

2.6.1 Sample Preparation and Analysis

The samples for the flotation tests and samples from the flotation plant were analyzed by HRXMT. First, the samples were sized into different size classes for analyses. A narrow size range in the sample allows a better identification and segmentation of the particles.

In this study the particle size classes selected for HRXMT analysis were: 2000x425 µm, 425x208 µm, 208x106 µm, 106x45 µm, 25-45 µm and -25 µm. For each size class one representative sample between 0.2 – 0.4 g was taken using the Quantachrome rotary micro riffler.

The representative samples for each size class were placed in plastic tubes. The diameter of the tubes for the size classes 2000x425 µm, 425x208 µm and 208x106 µm was 5 mm. The tube diameter for the size classes 106x45 µm, 25-45 µm and -25 µm was 2 mm. The plastic tubes were mounted inside the HRXMT machine for scanning and analysis.

The size classes 2000x425 µm, 425x208 µm and 208x106 µm were analyzed at a resolution of 5 µm (4X lens), the voltage used was 80 kV and each projection was taken for 9 seconds. The size classes 106x45 µm, 25-45 µm and -25 µm were analyzed at a resolution of 2 µm (10X lens), the voltage was 80 kV and the time for each projection was 30 seconds. A glass filter with a thickness of 150 µm was used as the X-ray filter for all the samples.

2.6.1.1 H-Extrema parameter value *h*

The H-extrema parameter *h* is an important parameter in the segmentation process and is defined by the user. In the segmentation process of each size class the value of *h* was calculated based on Equation 2.10.

$$h = \frac{d_{max} - d_{min}}{4 \cdot R_v} \tag{2.10}$$

where,

d_{max} = maximum size of the size class, µm

d_{min} = minimum size of the size class, µm

R_v = scanning voxel resolution, µm/voxel

The *h* values for each size class is shown in Table 2.19. For the size class -25 µm, the minimum size of the size class was considered as 1 µm for practical purposes.

Table 2.19

H-Extrema Parameter Value for each Size Class

Size Class [µm]	Resolution [µm/voxel]	*h* [voxel]
2000x425	5	122
425x208	5	32
208x106	5	16
106-45	2	19
25-45	2	9
-25	2	4

2.6.1.2 Manual correction of oversegmentation

When oversegmentation occurred in some of the samples, it was corrected using the image processing software, MIPAV. The image created after the H-extrema process is opened with MIPAV software. The particles with more than one maxima point are identified and these maxima points are connected manually. The new image is saved and reprocessed in the segmentation procedure. This way, the error due to the oversegmentation problem can be minimized in data analysis.

2.6.2 HRXMT Analysis of Feed Samples

A feed sample of 1 kg was ground to a P80 of 262 µm. The sample was split into the size classes: 2000x425 µm, 425x208 µm, 208x106 µm, 106x45 µm and -45µm. Representative samples for each size class were prepared and analyzed by HRXMT. The feed sample for the size class -45 µm was not scanned because of resolution limitations. Due to the size of the fine particles (few microns), mineral phases of these fine particles can not be spatially distinguished by HRXMT analysis. The major error that comprises the analysis of -45 µm size class is the partial volume effect described in Section 2.1.2. The partial volume effect is more evident for small particles because of the reduced number of voxels used to describe these small particles. Of course particles with a size smaller than 2 µm, the HRXMT resolution limit used, cannot be analyzed.

Different phases were identified in the reconstructed particles of the feed sample, basically the phases were classified as three types of minerals based on scaled CT numbers: gangue minerals, pyrite mineral and high density minerals. The minerals with a

density lower than pyrite were all classified as gangue minerals and the minerals with a density greater than pyrite were classified as high density minerals.

Image sections for HRXMT of the reconstructed feed particles are shown in Figure 2.12 for all size classes. The particles are well defined in the sectioned images. The black color in the images corresponds to the air voids between particles, the dark gray color represents the gangue particles, most of the bright grains are pyrite and only a few of the bright grains correspond to high density minerals.

In Figure 2.12 it is observed that the most of pyrite grains are locked in the size class 2000x425 µm, in the size class 425x208 µm some pyrite particles appear to have a high degree of liberation, but some pyrite grains are still locked. In the size classes 208x106 µm and 106x45 µm most of the pyrite grains appear to have a high degree of liberation and only a few pyrite grains are locked. As expected, a higher degree of liberation of pyrite grains is achieved at smaller particle sizes.

The pyrite volume grade was calculated for the feed samples in each size class from the HRXMT analysis. In order to evaluate the reliability of the sample preparation, the pyrite volume grade from HRXMT analysis was determined for different samples from the size classes 2000x425 µm, 425x208 and 208x106 µm. In the case of the size class 106x45 µm only one sample was scanned because the resolution used for this sample requires more scanning time. The results of pyrite grade, number of particles and scanning resolution (µm/voxel) for the different size classes are shown in Table 2.20.

The pyrite grade is increased as the particle size decreases, for instance the average pyrite grade for the size classes 2000x425 µm and 106x45µm are 1.01% by volume and 3.30% by volume, respectively.

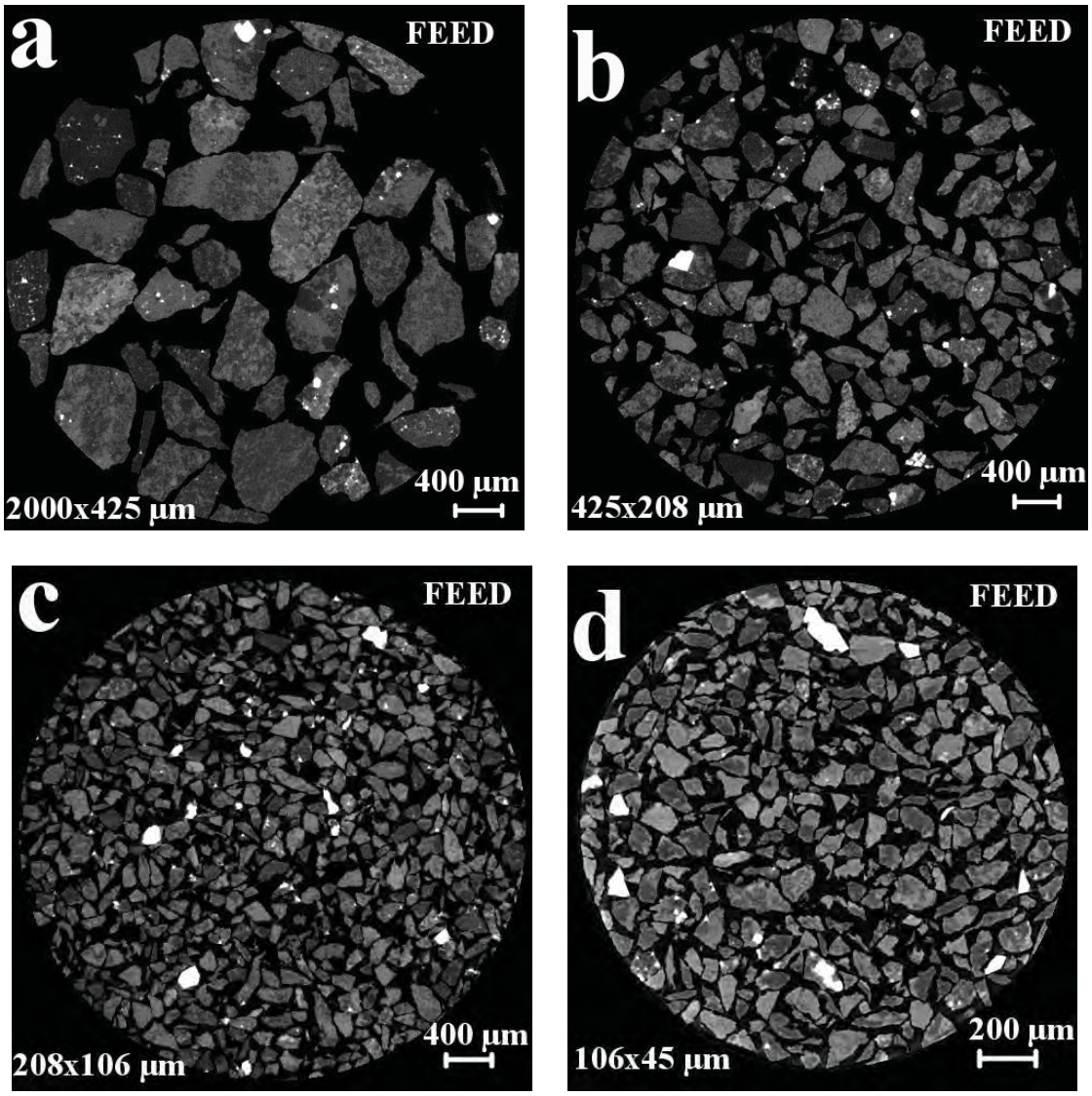

Figure 2.12 Image sections of feed particles from HRXMT analysis. a) 2000x425 µm, b) 425x208 µm, c) 208x106 µm and d) 106x45 µm.

Table 2.20

Volume Grade of Pyrite in Feed (Volume Percent), Number of Particles and Resolution for the Size Classes

2000x425 µm, 425x208 µm, 208x106 µm and 106x45 µm

	2000x425 µm			425x208 µm			208x106 µm			106x45 µm		
Sample	Pyrite Grade	Particles	µm/voxel	Pyrite Grade	Particles	µm/voxel	Pyrite Grade	Particles	µm/voxel	Pyrite Grade	Particles	µm/voxel
1	0.94	389	5	1.61	2030	5	2.18	15432	5	3.30	8365	2
2	0.98	331	5	1.53	1714	5	2.32	18206	5	-	-	-
3	1.14	362	5	1.44	1730	5	2.57	14623	5	-	-	-
4	0.84	299	5	1.01	1811	5	2.10	17195	5	-	-	-
5	1.13	348	5	1.43	1595	5	2.87	16612	5	-		-
6	-	-	-	2.13	1649	5	-	-	-	-	-	-
Mean	1.01	-	-	1.53	-	-	2.41	-	-	3.30	-	-
SD[§]	0.13	-	-	0.36	-	-	0.31	-	-	-	-	-

§ = Standard Deviation

The results for pyrite grade are consistent and variation of the HRXMT analysis is small. The standard deviations for the size classes 2000x425 µm, 425x208 µm and 208x106 µm are 0.13, 0.36 and 0.31, respectively.

2.6.3 Chemical Assays and MLA Analysis for Comparison with HRXMT Analysis

Representative samples from the batch flotation tests and the flotation plant samples were submitted to an external laboratory for chemical assay and MLA analysis. The bench flotation tests that products were submitted for chemical assay are test #1, test # 2, test # 3 and test # 4. All the samples from the flotation plant were submitted for MLA analysis. The MLA analysis was done on polished sections.

CHAPTER 3

PRODUCTS FROM LABORATORY FLOTATION EXPERIMENTS, RESULTS, ANALYSIS AND DISCUSSION

The results of flotation experiments with the auriferous pyrite ore from the mine site are presented in this chapter. The liberation-limited grade/recovery curves from HRXMT analysis of the feed for the different size classes are presented in Section 3.1. The liberation-limited grade/recovery curves were built from volumetric grade analysis and area grade analysis. These curves were determined from HRXMT analysis and they are compared in Section 3.2. The results from chemical analysis of feed and products are compared with quantitative analysis from HRXMT analysis in Section 3.3. The results of the flotation tests for complete size distribution are presented in Section 3.4. The results of the flotation tests for separate size classes are presented in Section 3.5. The results from the flotation tests for complete size distribution and separate size classes are compared and discussed in Section 3.6. The liberation-limited grade/recovery curves were compared with the results from the flotation tests and the results are presented in Section 3.6. Also, the results from HRXMT exposure analysis of feed samples and flotation products are discussed in Section 3.6.

3.1 Liberation-Limited Grade/Recovery Curves from HRXMT Analysis

The liberation spectra obtained from the analysis of feed samples were used to determine the liberation-limited grade/recovery curve for each particle size class. The liberation-limited grade/recovery curves were calculated for 2000x425 µm, 425x208 µm, 208x106 µm and 106x45 µm. The liberation-limited grade/recovery curves represent the boundary for separation efficiency for each feed particle size class. The curves predict the maximum pyrite recovery and concentrate grade for each particle size that can be achieved during flotation considering pyrite liberation as the only limitation. The liberation-limited grade/recovery curves for the feed with a P80 of 262 µm are shown in Figure 3.1. The curves were constructed considering all the samples scanned for each size class. The results of each sample were combined to generate one composite for each size class.

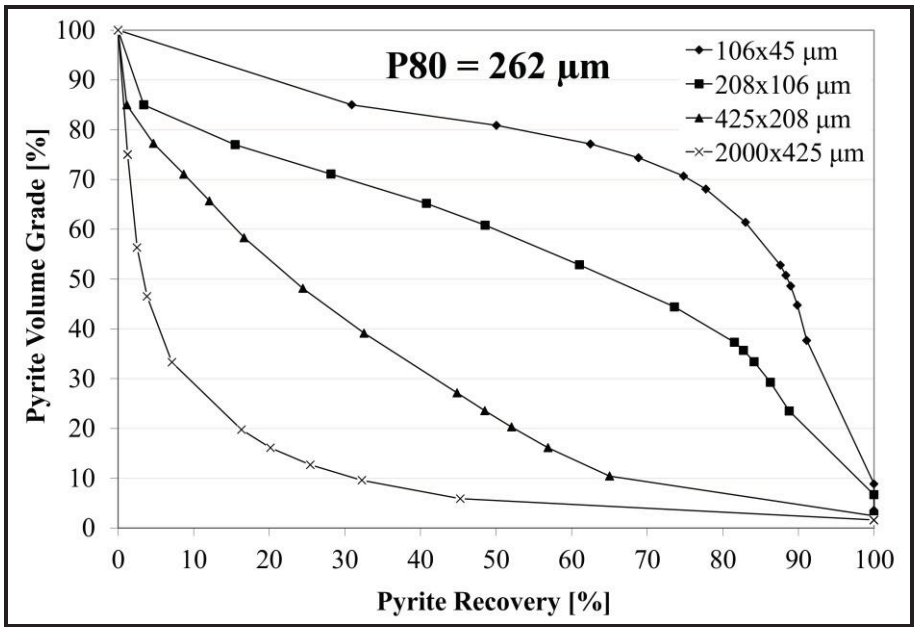

Figure 3.1 Liberation-limited grade/recovery curves from analysis of sized feed by HRXMT for mine site ore with a P80 of 262 µm.

The smaller particle size classes have better pyrite liberation and a higher volume grade can be achieved as evidenced by the displacement of the curves toward higher pyrite recovery and volume grade when the particle size is reduced. For instance, in the case of size class 2000x425 µm at a theoretical pyrite recovery of 80 % the maximum pyrite grade that can be achieved is 8 %. On the other hand, in the case of size class 106x45 µm at a pyrite recovery of 80 % the maximum pyrite grade increases significantly to 35 % by volume.

3.2 Comparison of Volumetric Grade Analysis with Area Grade Analysis of Feed

The two-dimensional (2D) liberation-limited grade/recovery curves were calculated based on data processed from image sections taken from the three-dimensional (3D) reconstruction of the samples. The liberation-limited grade/recovery curves were calculated using the same procedure. The 2D (area) and 3D (volume) curves for the size classes 2000x425 µm, 425x208 µm, 208x106 µm and 106x45 µm are shown in Figure 3.2-Figure 3.5. Overestimation of pyrite liberation was expected for all particle size classes in the 2D analysis. For the size class 208x106 µm (Figure 3.4) the overestimation of pyrite liberation is less evident. The 2D and 3D analysis curves almost overlap. For the size classes 2000x425 µm, 425x208 µm and 106x45 µm the difference between the 2D and 3D analysis is greater. The 2D analysis overestimates pyrite liberation because in the 2D images apparently liberated particles may actually be locked. The information is incomplete. In 3D analysis the whole particle is interrogated.

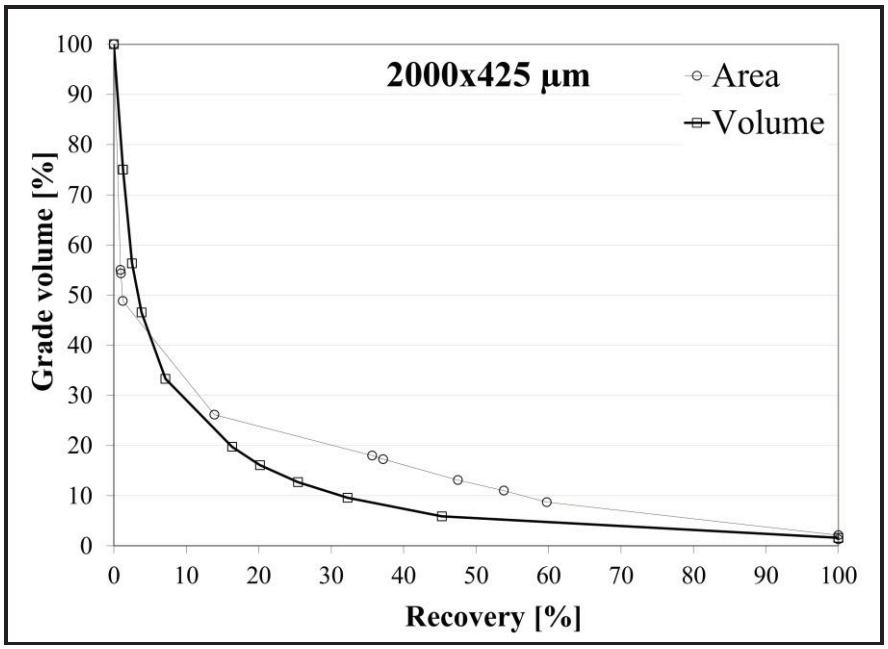

Figure 3.2 Comparison of liberation-limited grade/recovery curves from 2D and 3D analyses by HRXMT for feed 2000x425 µm size class.

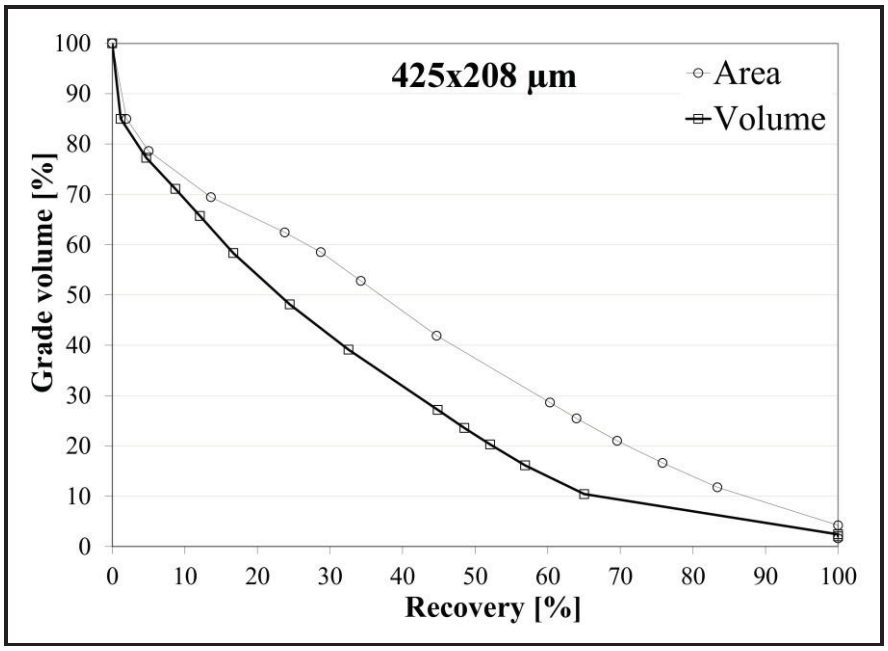

Figure 3.3 Comparison of liberation-limited grade/recovery curves from 2D and 3D analyses by HRXMT for feed 425x208 µm size class.

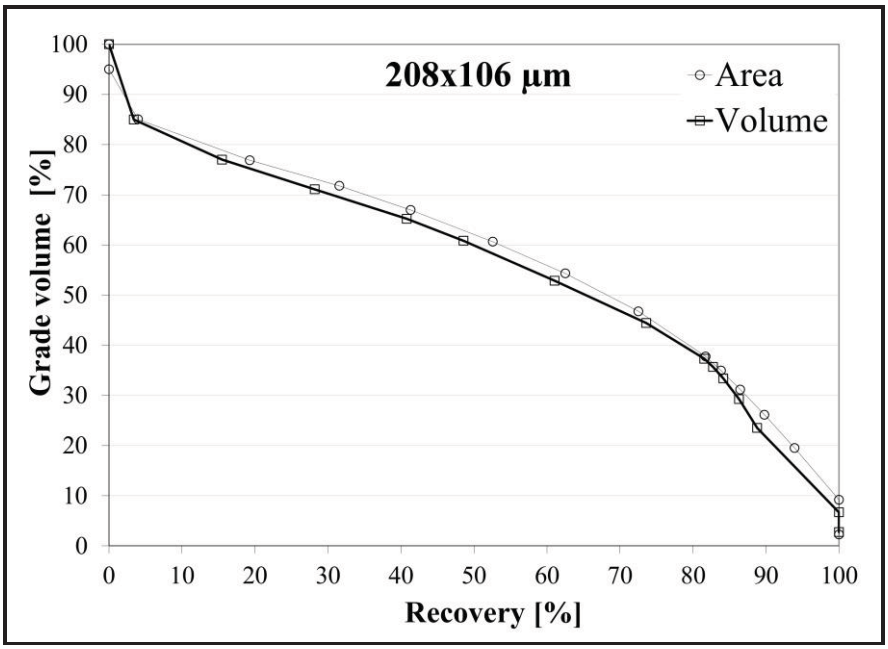

Figure 3.4 Comparison of liberation-limited grade/recovery curves from 2D and 3D analyses by HRXMT for feed 208x106 µm size class.

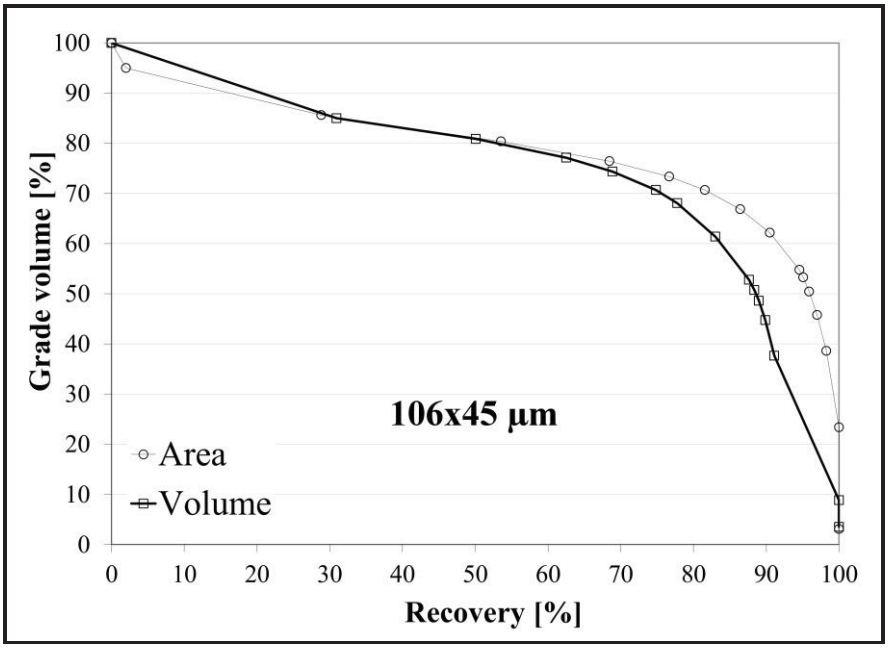

Figure 3.5 Comparison of liberation-limited grade/recovery curves from 2D and 3D analyses by HRXMT for feed 106x45 µm size class.

3.3 Correlation of HRXMT Data and Chemical Analysis

Chemical analyses were done for samples from Test # 1, Test # 2, Test # 3 and Test # 4. The samples were separated into the size classes 2000x425 µm, 425x208 µm, 208x106 µm and 106x45 µm before chemical analysis. Sulfide sulfur was determined for feed, concentrate and tailings from the flotation tests. The feed and flotation product samples were analyzed chemically for sulfide sulfur and assuming that all the sulfide sulfur belongs to pyrite, the pyrite mass grade was calculated from the formula for pyrite (FeS_2).

In total 68 samples were analyzed by chemical assay and HRXMT. The relationship between mass grade and volume grade of each sample can be defined by Equation 3.1, assuming a binary system considering pyrite and gangue minerals.

$$m_{Py} = \frac{v_{Py} \cdot \rho_{Py}}{v_{Py} \cdot \rho_{Py} + (1 - v_{Py}) \cdot \rho_G} \tag{3.1}$$

where:

m_{Py} = pyrite mass grade [%]

v_{Py} = pyrite volume grade [%]

ρ_{Py} = density of pyrite [g/cm^3]

ρ_G = density of gangue minerals [g/cm^3]

In this way, the relationship between mass and volume can be established if the densities of the minerals are known and are constant from one particle to other. The correlation of pyrite volume grade from HRXMT analysis with the pyrite mass grade determined by chemical assay is shown in Figure 3.6.

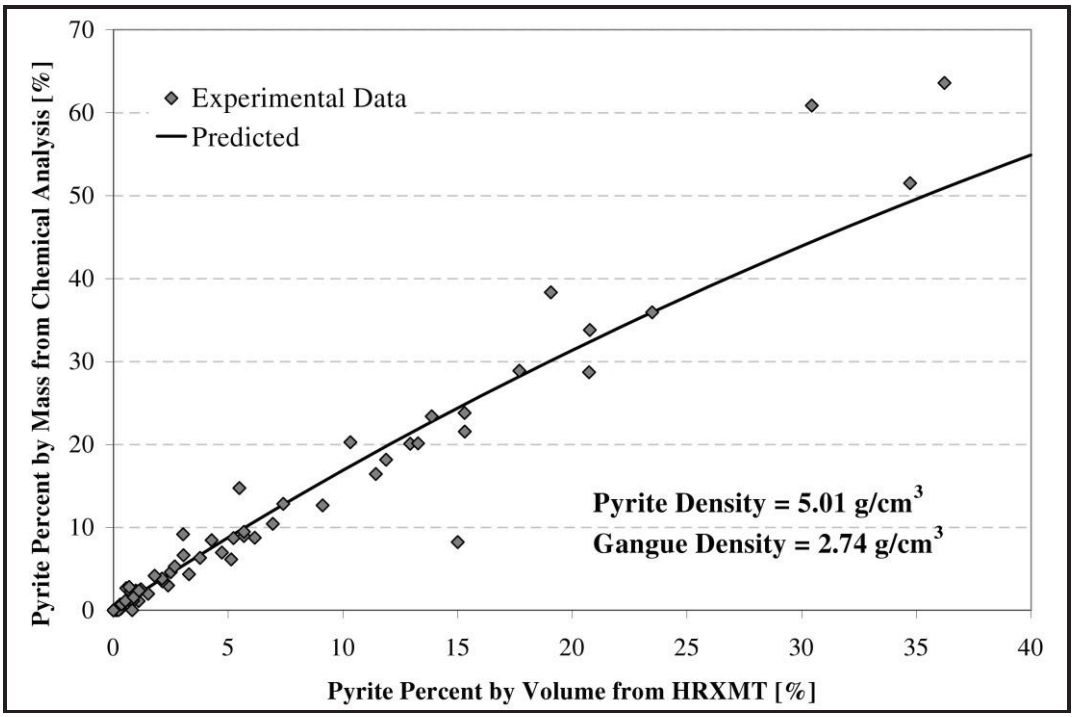

Figure 3.6 Correlation between pyrite volume grade from HRXMT analysis and pyrite mass grade by chemical analysis. The predicted line is calculated from Equation 3.1 with density of gangue minerals = 2.74 g/cm^3 and pyrite density of 5.01 g/cm^3.

The relationship predicted from Equation 3.1 was calculated based on a gangue mineral density of 2.74 g/cm^3 and pyrite density of 5.01 g/cm^3. A good correlation between the quantitative analysis from HRXMT and the chemical analysis was found for feed and products of the four flotation tests. Of course, there are some points that are not close to the predicted line, the difference is due to the experimental error from sample preparation, chemical and HRXMT analysis.

3.4 Flotation Results for Complete Feed Size Distribution

3.4.1 HRXMT Analysis of Flotation Products

The flotation products, concentrates and tailings, were separated into the same size classes used for the feed sample analysis and each size class was analyzed by HRXMT.

The size class -45 µm was not scanned due to the resolution limitation and partial volume effect. A representative sample was taken using the rotary riffler and the micro rotary riffler for the size classes 2000x425 µm, 425x208 µm, 208x106 µm and 106x45 µm. A representative sample of each size class from the flotation products was analyzed by HRXMT. For instance, image sections of the flotation products from flotation test # 2 (without cleaner flotation stage) in the size class 425x208 µm are shown in Figure 3.7.

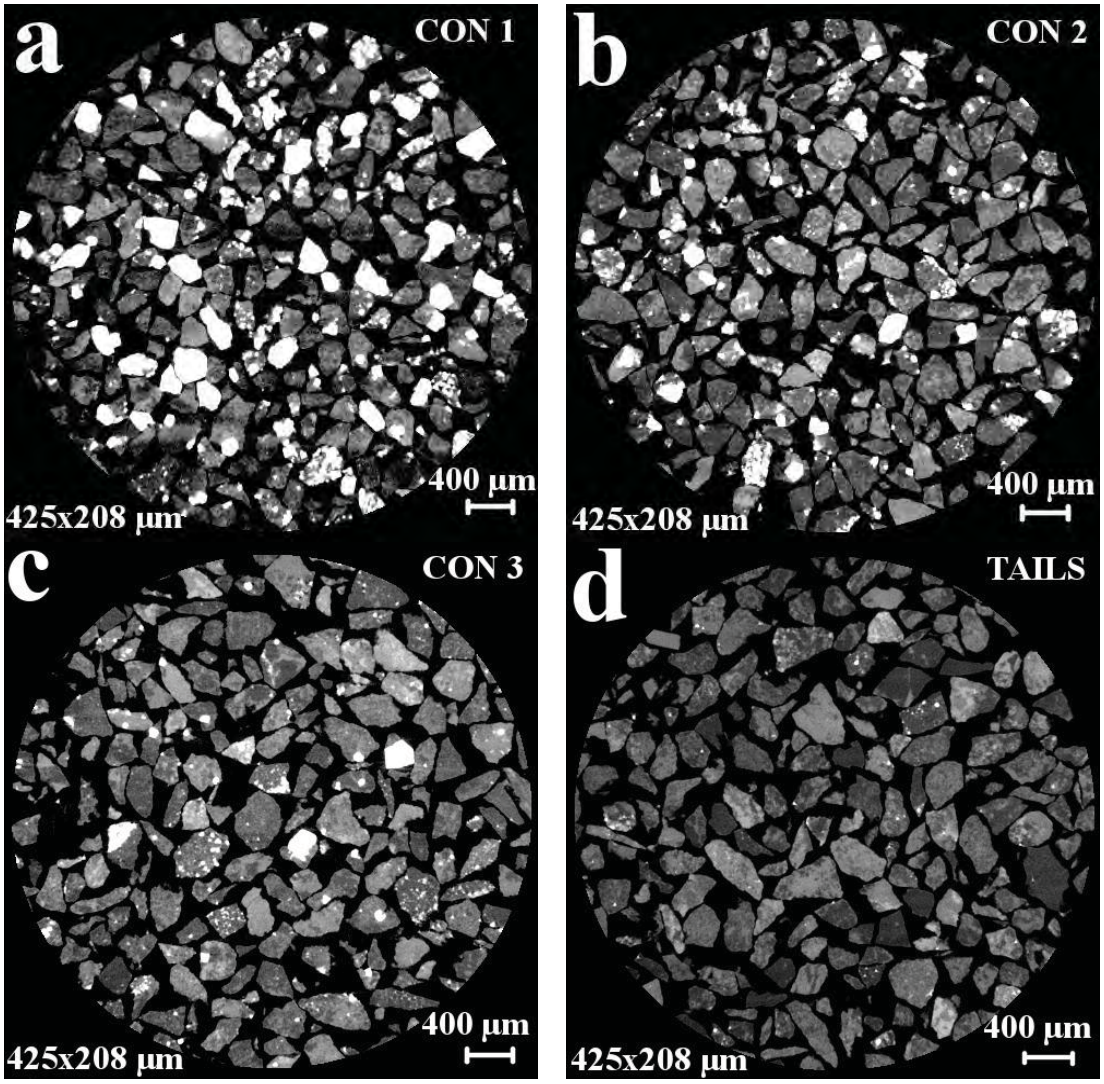

Figure 3.7 Products from flotation test # 2 for size class 425x208 µm. a) concentrate 1, b) concentrate 2, c) concentrate 3 and d) tailings.

It can be observed from image sections that the number of pyrite-containing particles (bright grains) in concentrates (Figure 3.7a-3.7c) is high in comparison with the number of pyrite-containing particles in the tailings (Figure 3.7d). Also, pyrite grains appear to have a higher degree of liberation in the concentrates than pyrite grains in the tailings. In fact, all the pyrite grains in the section image of tailings appear to be locked.

There is an obvious difference between the concentrates (Figure 3.7a-3.7c) from flotation test # 2 with regard to the pyrite-containing particles. Concentrate 1 (Figure 3.7a) has more pyrite-containing particles than concentrate 2 (Figure 3.7b) and concentrate 3 (Figure 3.7c). Also, pyrite grains in concentrate 1 appear to have a high degree of liberation in comparison with pyrite grains present in concentrate 2 and concentrate 3. The products from other flotation tests follow the same tendency in terms of number of pyrite-containing particles and degree of liberation of pyrite grains.

3.4.2 Recovery Calculations

Pyrite grade determination from HRXMT analysis was based on volume. In order to determinate the pyrite recovery in the flotation products for each size class, the particle volume of the flotation products was calculated. The particle volume of feed, concentrates and tailings for each size class was calculated for pyrite and gangue assuming a binary system of pyrite and gangue minerals.

The pyrite mass content of each size class in the flotation products was calculated using the Equation 3.1. The particle density of the products was calculated from Equation 3.2. The particle volume of the flotation products was calculated from Equation 3.3. Pyrite and gangue mineral densities used for volume calculations were 5.01 g/cm^3 and

2.74 g/cm^3, respectively. These density values for pyrite and gangue minerals produced a good correlation between mass and volume of the pyrite ore as demonstrated in Section 3.3.

$$\rho_{FP} = v_{FP\,py} \cdot \rho_{Py} + (100 - v_{FP\,py}) \cdot \rho_G \tag{3.2}$$

$$V_{FP} = \frac{M_{FP}}{\rho_{FP}} \tag{3.3}$$

The pyrite volume grade for the feed and flotation products (concentrates and tailings) was calculated from Equation 3.4. The pyrite volume grade calculated from the products was used to calculate the pyrite recovery in the concentrates for each size class using Equations 3.5 and 3.6.

$$Cv_{Py\,i} = \frac{\sum_j \left(V_{FP\,i} \cdot v_{FP\,Py_i}\right)}{\sum_j V_{FP\,i}} \tag{3.4}$$

$$V_{F\,i} = \sum_j V_{FP\,i} \tag{3.5}$$

$$R_{Py_i} = \frac{V_{FP\,i} \cdot v_{FP\,Py_i}}{Cv_{Py_i} \cdot V_{F\,i}} \cdot 100 \tag{3.6}$$

where:

i = Fraction of size class (2000x425 µm, 425x208 µm, 208x106 µm and 106x45 µm)

j = Flotation product (concentrate 1, concentrate 2, concentrate 3 and tailings)

$v_{FP\,Py}$ = Mean pyrite volume grade of flotation product [%]

ρ_{Py} = Density of pyrite [g/cm^3]

ρ_{G} = Density of gangue minerals [g/cm^3]

V_{FP} = Particle volume of flotation product [cm^3]

M_{FP} = Mass of flotation product [g]

ρ_{FP} = density of flotation product [g/cm^3]

Cv_{Py} = Calculated pyrite volume grade of feed [%]

V_F = Particle volume of feed [%]

R_{Py} = Pyrite recovery [%]

The pyrite volume grade of feed from the HRXMT analysis and the pyrite volume grade of the feed calculated from the flotation products in flotation test #1 - # 4 are presented in Table 3.1. Flotation tests # 1 - # 4 can be classified within one group because the particle size distributions of these tests were similar and the grinding occurred under similar conditions. In the size classes 425x208 µm and 2000x425 µm it can be observed that there is a small difference between the average of the calculated pyrite grade of the feed of the flotation tests # 1 - # 4 and the pyrite grade of the feed from the HRXMT analysis. In the case of the size classes 208x106 µm and 106x45 µm the average of the calculated pyrite grade of feed from flotation tests # 1 - # 4 is lower that the pyrite grade from HRXMT analysis.

Table 3.1

Comparison of Calculated Pyrite Volume Grade of Feed from Flotation Products and Pyrite Volume Grade from HRXMT Analysis of Feed for Flotation Tests # 1 - # 4

Grind size the feed P80 = 262 µm	Pyrite Volume Grade [%]			
	Size Class [µm]			
	2000x425	425x208	208x106	106x45
HRXMT Analysis	**1.01**	**1.53**	**2.41**	**3.30**
Calculated pyrite grade of feed from flotation products				
Test # 1	1.39	1.26	1.82	2.24
Test # 2	1.20	1.16	1.96	2.38
Test # 3	0.88	1.23	1.86	2.17
Test # 4	0.83	1.39	1.93	2.61
Average	**1.08**	**1.26**	**1.89**	**2.35**

The pyrite volume grade of feed calculated from the flotation products in the flotation test # 5 are presented in Table 3.2. In the flotation test # 5 the feed particle size distribution (P80 = 150 µm) is finer than the feed particle size distribution (P80 = 262 µm) analyzed by HRXMT. There is a significant difference between the calculated pyrite grade of the feed for the flotation test # 5 and the pyrite grade of the feed from HRXMT analysis. The calculated pyrite grade of the feed from flotation test # 5 for all the size classes was much lower than the pyrite grade of the feed from HRXMT analysis. Except for the size class 106x45 µm, in this size class the difference between the pyrite grade of feed from HRXMT and calculated pyrite grade is small.

Table 3.2

Comparison of Calculated Pyrite Volume Grade of Feed from Flotation Products and Pyrite Volume Grade from HRXMT Analysis of Feed for Flotation Test # 5

Grind size the feed P80 = 150 µm	Pyrite Volume Grade [%]			
	Size Class [µm]			
	2000x425	425x208	208x106	106x45
HRXMT Analysis	**1.01**	**1.53**	**2.41**	**3.30**
Calculated pyrite grade of feed from flotation products				
Test # 5	0.63	0.49	0.71	2.93

3.4.3 Effect of Flotation Conditions on the Pyrite Recovery and Pyrite grade

The different conditions of the flotation test are compared in this section. The comparison is based on the pyrite recovery and pyrite grade of the overall concentrate. The overall concentrate is produced combining concentrates from each flotation tests. The calculations of pyrite recovery and volume grade for overall concentrate are explained in Section 3.4.6. The flotation tests are compared in pairs in Table 3.3. The flotation conditions, pyrite recovery and pyrite volume grade of the overall concentrate for each flotation test are presented in the Table 3.3. When the impeller speed was decreased and the cleaner flotation stage was not used, the pyrite recovery and grade were increased in the concentrate. The increment of pyrite recovery was from 84.42% to 91.80%, the increment of the pyrite grade was less significant from 11.61% to 11.90%. The cleaner flotation stage did not work well to improve the pyrite grade of the overall concentrate and pyrite was lost in the cleaner tailings reducing the pyrite recovery.

Table 3.3

Flotation Conditions, Pyrite Recovery and Pyrite Volume Grade

of Overall Concentrate

Test #		Test #
Distinct conditions	Similar Conditions	Distinct conditions
Test # 1		**Test # 2**
Impeller = 1200 RPM Cleaner flotation stage	PAX = 100 g/ton Cytec 208 = 30 g/ton pH = 8.30 P80 = 262 µm	Impeller = 1000 RPM No cleaner flotation stage
Pyrite recovery = 84.42% Pyrite grade =11.61%		Pyrite recovery = 91.80% Pyrite grade = 11.90%
Test # 2		**Test # 3**
Cytec 208 = 30 g/ton PAX = 100 g/ton pH = 8.30	Impeller = 1000 RPM No cleaner flotation stage P80 = 262 µm	Cytec 208 = 50 g/ton PAX = 200 g/ton pH = 5.60
Pyrite recovery = 91.80% Pyrite volume grade = 11.90%		Pyrite recovery = 95.35% Pyrite volume grade = 9.27%
Test # 3		**Test # 4**
Cytec 208 = 50 g/ton	Impeller = 1000 RPM No cleaner flotation stage PAX = 200 g/ton pH = 5.60 P80 = 262 µm	Danafloat 571 = 50 g/ton
Pyrite recovery = 95.35% Pyrite volume grade = 9.27%		Pyrite recovery = 84.12% Pyrite volume grade = 8.98%
Test # 3		**Test # 5**
P80 = 262 µm	Impeller = 1000 RPM No cleaner flotation stage PAX = 200 g/ton Cytec 208 = 50 g/ton pH = 5.60	P80 = 150 µm
Pyrite recovery = 84.12% Pyrite volume grade = 8.98%		Pyrite recovery = 97.92% Pyrite volume grade = 10.21%

The impeller speed had a negative effect decreasing the concentrate pyrite grade because gangue particles were transported to the froth phase due to the higher turbulence in the flotation cell.

When the dosage of the collector was increased and the pH was decreased the pyrite recovery increased but the pyrite grade decreased. The pyrite recovery increased from 91.80% to 95.12%, the pyrite grade decreased from 11.90% to 9.27%. The excess of collector and the lower pH value increased the pyrite recovery but at the same time more gangue particles were collected decreasing the pyrite grade of the concentrate.

When the collector Cytec 208 was replaced by the collector Danafloat 571 the pyrite recovery and grade decreased. The pyrite recovery decreased from 95.25% to 84.12% and the pyrite grade decreased slightly from 9.27% to 8.98%. The collector Cytec 208 worked better than collector Danafloat 571 for this type of ore.

When the particle size was reduced there is an improvement of pyrite recovery and grade. The pyrite recovery increased from 95.35% to 97.92% and the pyrite grade improved from 8.98% to 10.21%. When the particle size was reduced the number of particles with a higher degree pyrite liberation is increased. The particles with a high degree of liberation have more opportunity to interact with the collector, increase their hydrophobicity and then they are recovered in the concentrate.

3.4.4 Weight and Mass Distribution of Products from Flotation Tests

The weight of the flotation products (tailings and concentrates) were recorded for each test. The mass percent in different size classes of the flotation products were

determined by wet and dry screening. The size classes used were: 2000x425 µm, 425x208 µm, 208x106 µm, 106x45 µm and -45 µm.

The mass collected of the concentrates in flotation tests # 1 - # 5 are shown in Tables 3.4 – 3.8. The mass distributions of the concentrates and tailings for different size classes are shown in Tables 3.4 – 3.8.

In flotation tests # 2 - # 4 concentrate 3 had the highest mass in comparison with the concentrate 1 and concentrate 2. In the case of flotation test # 1 concentrate 1 had the highest mass. The high impeller speed in flotation test # 1 caused more mass to be collected in concentrate 1.

In flotation tests # 1 - # 4 most of the particles in the concentrate 1 were collected in the size classes 208x106 µm, 106x45 µm and -45 µm. In concentrate 2 most of the particles were collected in the size classes -425x208 µm, 106x45 µm and -45 µm. Finally, most of the particles in the concentrate 3 were collected in size classes 425x208 µm and -45 µm.

In flotation test # 5 most of the mass in the three concentrates were collected in the size classes 106x45 µm and -45 µm due to the reduced particle size (P80 = 150 µm) used for this flotation test.

In flotation tests # 1 - # 5 the mass collected in concentrates for the size class 2000x425 µm was very small because the mass of this size class is low in the feed as well. The mass of size class 2000x425 µm was reduced considerably when the 1 kg sample for these flotation experiments were ground for 10 minutes to a P80 of 262 µm. Also, in the flotation experiments the mass recovered in the concentrates is small in comparison with the mass of feed experiments for the size class 2000x425 µm.

Table 3.4

Weight of Products from Flotation Test with

Cleaner Flotation Stage (Test # 1[§])

	Weight Percent [%]					
	Size Class [µm]					
Product	-45	106x45	208x106	425x208	2000x425	Total Weight [g]
Concentrate 1	58.24	16.61	17.67	7.44	0.04	117.87
Cleaner Concentrate	23.80	10.01	29.72	35.18	1.29	47.84
Cleaner Tailings	86.05	4.15	2.77	5.94	1.09	83.71
Tailings	28.06	19.01	22.87	25.19	4.87	750.61

[§]Impeller = 1200 RPM, Cleaner flotation stage, PAX = 100 g/ton, Cytec 208 = 30 g/ton, pH = 8.30, P80 = 262 µm

Table 3.5

Weight of Products from Flotation Test without

Cleaner Flotation Stage (Test # 2[§])

	Weight Percent [%]					
	Size Class [µm]					
Product	-45	106x45	208x106	425x208	2000x425	Total Weight [g]
Concentrate 1	36.42	19.36	26.86	17.17	0.19	63.67
Concentrate 2	38.96	9.85	23.41	26.64	1.14	50.83
Concentrate 3	65.25	6.28	8.85	16.99	2.63	65.91
Tailings	32.84	17.79	20.83	23.37	5.17	816.57

[§]Impeller = 1000 RPM, No cleaner flotation stage, PAX = 100 g/ton, Cytec 208 = 30 g/ton, pH = 8.30, P80 = 262 µm

Table 3.6

Weight of Products Flotation Test with Increment of Collector Dosage and Low pH (Test # 3[§])

	Weight Percent [%]					
	Size Class [µm]					
Product	-45	106x45	208x106	425x208	2000x425	Total Weight [g]
Concentrate 1	30.04	19.65	31.22	18.90	0.19	63.12
Concentrate 2	39.02	6.72	25.84	27.71	0.71	54.06
Concentrate 3	57.37	5.89	15.16	20.23	1.35	92.93
Tailings	36.85	20.33	23.55	17.33	1.94	789.87

[§]Impeller = 1000 RPM, No cleaner flotation stage, PAX = 200 g/ton, Cytec 208 = 50 g/ton, pH = 5.60, P80 = 262 µm

Table 3.7

Weight of Products from Flotation Test with a New Collector and Low pH (Test # 4[§])

	Weight Percent [%]					
	Size Class [µm]					
Product	-45	106x45	208x106	425x208	2000x425	Total Weight [g]
Concentrate 1	34.26	17.65	28.03	19.88	0.18	71.81
Concentrate 2	42.87	8.63	25.22	22.71	0.57	47.62
Concentrate 3	54.48	6.16	17.08	20.98	1.30	96.77
Tailings	35.97	20.26	23.99	17.80	1.98	780.97

[§]Impeller = 1000 RPM, No cleaner flotation stage, PAX = 200 g/ton, Danafloat 571 = 50 g/ton, pH = 5.60, p80 = 262 µm

Table 3.8

Weight of Products from with a Reduced Particle Size Distribution (Test # 5[§])

	Weight Percent [%]					
	Size Class [µm]					
Product	-45	106x45	208x106	425x208	2000x425	Total Weight [g]
Concentrate 1	45.59	32.54	19.36	2.51	0.00	30.13
Concentrate 2	35.00	18.75	33.92	12.27	0.06	69.83
Concentrate 3	69.54	9.04	14.59	6.76	0.07	115.11
Tailings	41.61	28.74	23.47	6.10	0.08	780.97

[§]Impeller = 1000 RPM, No cleaner flotation stage, PAX = 200 g/ton, Cytec 208 = 50 g/ton, pH = 5.60, p80 = 150 µm

3.4.5 Pyrite Recovery and Pyrite Volume Grade of Concentrates from Flotation Tests

The pyrite recovery was calculated using the Equation 3.6 for each size class in each concentrate of the flotation tests. The pyrite volume grade was obtained from the HRXMT analysis of each sample. The pyrite volume grade was estimated from the number of voxels of each mineral in the sample analyzed as it was explained in Section 2.1.5.

3.4.5.1 Pyrite recovery and volume grade of products from flotation test with cleaner flotation stage (Test # 1)

The recovery and concentrate volume grade for the flotation products for the flotation test # 1 are shown in Table 3.9. Concentrate 1 and cleaner concentrate were combined mathematically to form a final concentrate in each size class.

Table 3.9

Pyrite Recovery and Pyrite Volume Grade for Flotation Test with Cleaner Flotation Stage (Test # 1[§])

Size Class [µm]		Tailings	Concentrate # 1	Concentrate Cleaner	Concentrate Final
2000x425	Recovery %	-	1.67	14.87	16.24
	Grade (volume %)	1.10	16.17	11.44	11.79
425x208	Recovery %	-	48.24	34.78	83.03
	Grade (volume %)	0.32	15.01	5.24	8.42
208x106	Recovery	-	82.73	8.96	91.70
	Grade (volume %)	0.10	17.70	2.50	11.07
106x45	Recovery %	-	86.07	5.29	91.36
	Grade (volume %)	0.22	19.07	4.28	15.78

[§]Impeller = 1200 RPM, Cleaner flotation stage, PAX = 100 g/ton, Cytec 208 = 30 g/ton, pH = 8.30, P80 = 262 µm

In concentrate 1 the recovery increased as the particle size decreased, the pyrite recovery for the size class 2000x425 µm was 1.67% and the pyrite recovery for the size class 106x45 µm was 86.07%.

In the cleaner concentrate the pyrite recovery for the size classes 425x208 µm and 2000x425 µm was greater than the pyrite recovery in the size classes 208x106 µm and 106x45 µm. The highest pyrite recovery corresponded to the size class 425x208 µm (34.78%) and the lowest pyrite recovery corresponded to the size class 106x45 µm (5.29%). The final concentrate followed the trend of the concentrate 1, the smallest the particle size the greater the pyrite recovery.

The highest pyrite recovery (106x45 µm) was 91.36% and the lowest pyrite recovery (2000x425 µm) was 16.24%.

In concentrate 1 the pyrite grade in the size classes 208x106 µm (17.70%) and 106x45 µm (19.07%) was greater than the pyrite grade in the size classes 2000x425 µm (16.17%) and 425x208 µm (15.01%).

In the cleaner concentrate the pyrite grade was greater for the size classes 425x208 µm and 2000x425 µm than the pyrite grade of the size classes 208x106 µm and 106x45 µm. The highest volume grade corresponded to the size class 2000x425 µm (11.44%) and the lowest pyrite grade corresponded to the size class 208x106 µm (2.50%).

In the final concentrate the size classes 2000x425 µm (11.79%), 208x106 µm (11.07%) and 106x45 µm (15.78%) had a greater pyrite volume than the size class 425x208 µm (8.42%).

3.4.5.2 Pyrite recovery and volume grade of products from flotation test without cleaner flotation stage (Test # 2)

The pyrite recovery and pyrite volume grade of the concentrates from the flotation test # 2 are shown in Table 3.10. The three concentrates were combined to form a final concentrate for each size class.

The pyrite recovery in concentrate 1 increased as the particle size decreased, the pyrite recovery varied from 3.10% to 84.25%. In concentrate 2 the size classes 425x208 µm and 208x106 µm had a greater pyrite recovery than the size classes 2000x425 µm and 106x45 µm. The highest pyrite recovery corresponded to the size class 425x208 µm

Table 3.10

Pyrite Recovery and Concentrate Grade for Flotation Test without Cleaner Flotation Stage (Test # 2[§])

Size Class [µm]		Tailings	Concentrate # 1	Concentrate # 2	Concentrate # 3	Concentrate Final
2000x425	Recovery %	-	3.10	11.63	17.41	32.14
	Grade (volume %)	0.86	15.49	11.89	5.69	7.59
425x208	Recovery %	-	51.59	27.90	8.85	88.34
	Grade (volume %)	0.16	13.88	5.69	2.12	6.91
208x106	Recovery %	-	75.44	19.50	1.73	96.67
	Grade (volume %)	0.08	20.74	6.95	1.20	12.27
106x45	Recovery %	-	84.25	12.08	1.02	97.35
	Grade (volume %)	0.07	34.73	10.33	0.98	21.00

[§]Impeller = 1000 RPM, No cleaner flotation stage, PAX = 100 g/ton, Cytec 208 = 30 g/ton, pH = 8.30, P80 = 262 µm

(27.90%) and the lowest pyrite recovery corresponded to the size class 2000x425 µm (11.63%). In concentrate 3 the pyrite recovery decreased as the particle size decreased, the highest pyrite recovery was 17.41% for the size class 2000x425 µm and the lowest pyrite recovery was found for size class 106x45 µm with a value of 1.02%.

In the final concentrate the pyrite recovery was increased as the particle size was decreased. The highest pyrite recovery was 97.35% for the size class 106x45 µm and the lowest pyrite recovery corresponded to the size class 2000x425 µm (32.14%).

In concentrate 1 the size classes 208x106 µm and 106x45 µm had a greater pyrite grade than the pyrite grade in the size classes 2000x425 µm and 425x208 µm. The

highest pyrite grade corresponded to the size class 106x45 µm with a value of 34.73% and the lowest pyrite grade corresponded to the size class 425x208 µm (15.49%).

In concentrate 2 the size classes 2000x425 µm and 106x45 µm had a greater pyrite grade than the size classes 425x208 µm and 208x106 µm. The size class 2000x425 µm had the highest pyrite grade with a pyrite grade of 11.89% and the lowest pyrite grade corresponded to the size class 425x208 µm (5.69%). In concentrate 3 the pyrite grade decreased as the particle size decreased. The highest pyrite grade was 5.59% that corresponded to the size class 2000x425 µm and the lowest pyrite grade corresponded to the size class 106x45 µm with a value of 0.98%. In fact, the pyrite grade in concentrate 3 for the size classes 208x106 µm and 106x45 µm was lower than the calculated pyrite grade of the feed in this flotation test. The calculated pyrite grade of feed in the size classes 208x106 µm and 106x45 µm were 1.96% and 2.38%, respectively. In the final concentrate the size classes 208x106 µm and 106x45 µm had a greater pyrite grade than the pyrite grade for the size classes 2000x425 µm and 425x208 µm. The highest pyrite volume corresponded to the size class 106x45 µm (21.00%) and the lowest pyrite grade corresponded to the size class 425x208 µm (6.91%).

3.4.5.3 Pyrite recovery and volume grade of products from flotation test with increment of collector dosage and low pH (Test # 3)

The pyrite recovery and pyrite volume grade for the products of the flotation test # 3 are shown in Table 3.11. The three concentrates were combined to form a final concentrate for each size class.

Table 3.11

Pyrite Recovery and Concentrate Grade for Flotation Test with Increment of Collector Dosage and Low pH (Test # 3[§])

			Concentrate			
Size Class [µm]		Tailings	# 1	# 2	# 3	Final
2000x425	Recovery %	-	11.03	17.93	41.49	70.55
	Grade (volume %)	0.29	15.32	7.41	5.14	6.28
425x208	Recovery %	-	73.02	17.67	6.33	97.03
	Grade (volume %)	0.05	15.31	2.68	0.75	6.90
208x106	Recovery %	-	90.45	5.78	1.69	97.92
	Grade (volume %)	0.05	23.49	1.80	0.52	9.47
106x45	Recovery %	-	88.86	2.77	0.78	92.42
	Grade (volume %)	0.18	36.23	3.04	0.56	19.40

[§]Impeller = 1000 RPM, No cleaner flotation stage, PAX = 200 g/ton, Cytec 208 = 50 g/ton, pH = 5.60, P80 = 262 µm

In concentrate 1 the size classes 106x45 µm and 208x106 µm had a greater pyrite recovery than the pyrite recovery in the size classes 2000x425 µm and 425x208 µm. The highest pyrite recovery corresponded to the size class 208x106 µm (90.45%) and the lowest pyrite recovery corresponded to the size class 2000x425 µm (11.03%).

In concentrate 2 the pyrite recovery decreased as the particle size decreased. The highest pyrite recovery corresponded to the size class 2000x425 µm (17.93%) and the lowest pyrite recovery corresponded to the size class 106x45 µm (2.77%).

In the concentrate 3 the pyrite recovery decreased as the particle size decreased. The highest pyrite recovery for the size class 2000x425 µm was 41.49% and the lowest pyrite recovery corresponded to the size class 106x45 µm (0.78%).

In the final concentrate the pyrite recovery varied between 92.42% and 97.92% for the size classes 425x208 µm, 208x106 µm and 106x45 µm. The highest pyrite recovery corresponded to the size class 208x106 µm. The size class 2000x425 µm had a pyrite recovery of 70.55%.

In concentrate 1 the pyrite grade for the size classes 208x106 µm and 106x45 µm were greater than the pyrite grade of the size classes 2000x425 µm and 425x208 µm. The highest pyrite volume corresponded to the size class 106x45 µm (36.23%) and the lowest pyrite grade corresponded to the size classes 2000x425 µm and 425x208 µm (~15%).

In concentrate 2 the pyrite grade for the size classes 2000x425 µm and 106x45 µm was greater than the pyrite grade in the size classes 425x208 µm and 208x106 µm. The pyrite grade in the size class 2000x425 µm (7.41%) was much greater than the other size classes which had a pyrite recovery lower than 3.10 %.

In concentrate 3 the size class 2000x425 µm had a pyrite grade greater than the other size classes. The pyrite grade of the size class 2000x425 µm was 5.14% and the pyrite grade for the other size classes varied between 0.52% and 0.75%. The pyrite grade of the size classes 425x208 µm, 208x106 µm and 106x45 µm was lower than the calculated pyrite grade of the feed for the flotation test.

The calculated pyrite grade in the feed varied from 1.23% to 2.17% for the size classes 425x208 µm, 208x106 µm and 106x45 µm. In the final concentrate the pyrite grade increased as the particle size decreased. The pyrite grade for the size class 106x45 µm was 19.40%. The pyrite grade for the size class 2000x425 µm was 6.28%.

3.4.5.4 Pyrite recovery and volume grade of products from flotation test with a new collector and low pH (Test # 4)

The pyrite recovery and pyrite volume grade of the products from the flotation test # 4 are shown in Table 3.12. The three concentrates were combined to form a final concentrate for each size class.

In concentrate 1 the pyrite recovery in the size class 208x106 µm (79.74%) was greater than the pyrite recovery in the size classes 2000x425 µm (11.15%), 425x208 µm (66.03%) and 106x45 µm (66.60%). In concentrate 2 the pyrite recovery decreased as the particle size decreased. The pyrite recovery in the size class 2000x425 µm was 16.37% and the pyrite recovery in the size class 106x45 µm was 4.66%. In concentrate 3 the pyrite recovery decreased as the particle size decreased. The pyrite recovery in the size class 2000x425 µm was 32.69% and the pyrite recovery in the size class 106x45 µm was 0.89%.

In the final concentrate the pyrite recovery in the size classes 425x208 µm and 208x106 µm was greater than the pyrite recovery in the size classes 2000x425 µm and 106x45 µm. The highest pyrite recovery corresponded to the size class 208x106 µm (95.21%) and the lowest pyrite recovery corresponded to the size class 2000x425 µm (60.20%).

In concentrate 1 the pyrite grade in the size classes 208x106 µm and 106x45 µm was greater than the pyrite grade in the size classes 2000x425 µm and 425x208 µm. The size class 106x45 µm had the highest pyrite grade with a value of 30.45%. The lowest pyrite grade corresponded to the size class 425x208 µm (12.94%).

Table 3.12

Pyrite Recovery and Concentrate Grade for Flotation Test with a New Collector and Low pH (Test # 4[§])

Size Class [µm]		Tailings	Concentrate # 1	Concentrate # 2	Concentrate # 3	Concentrate Final
2000x425	Recovery %	-	11.15	16.37	32.69	60.20
	Grade (volume %)	0.36	13.38	9.12	3.78	5.34
425x208	Recovery %	-	66.03	12.75	8.94	87.73
	Grade (volume %)	0.22	12.94	3.06	1.12	5.09
208x106	Recovery %	-	79.74	12.22	3.26	95.21
	Grade (volume %)	0.11	20.77	4.73	0.89	9.44
106x45	Recovery %	-	66.60	4.66	0.89	72.14
	Grade (volume %)	0.82	30.45	5.49	0.69	16.71

[§]Impeller = 1000 RPM, No cleaner flotation stage, PAX = 200 g/ton, Danafloat 571 = 50 g/ton, pH = 5.60, p80 = 262 µm

In concentrate 2 the pyrite grade in the size classes 2000x425 µm and 106x45 µm was greater than the pyrite grade in the size classes 425x208 µm and 208x106 µm. The size class 2000x425 µm had a pyrite grade of 9.12%. The lowest pyrite grade corresponded to the size class 425x208 µm (3.06%).

In concentrate 3 the pyrite grade decreased as the particle size decreased. The pyrite grade for the size class 2000x425 µm was 3.78% and the pyrite grade of the size class 106x45 µm was 0.69%. The pyrite grade of the size classes 425x208 µm, 208x106 µm and 106x45 µm was lower than the calculated pyrite grade in the feed for the same size classes.

The calculated pyrite grade of the feed for the size classes 425x208 µm, 208x106 µm and 106x45 µm was 1.39%, 1.93% and 2.61% respectively. In fact the pyrite grade of the size class 106x45 µm in concentrate 3 was lower than the pyrite grade in the tailings for the same size class.

In the final concentrate the size classes 208x106 µm and 106x45 µm had a pyrite grade greater than the size classes 2000x425 µm and 425x208 µm. The pyrite grade of the size classes 208x106 µm and 106x45 µm was 9.44% and 16.71%, respectively. The pyrite grade of the size classes 2000x425 µm and 425x208 µm was ~5%.

3.4.5.5 Pyrite recovery and volume grade of products from flotation test with a reduced particle size distribution (Test # 5)

The pyrite recovery and pyrite grade of the products from the flotation test # 5 are shown in Table 3.13. The three concentrates were combined to form a final concentrate for each size class.

In concentrate 1 the pyrite recovery in the size class 208x106 µm (62.72%) was greater than the pyrite recovery in the size classes 425x208 µm (35.49%) and 106x45 µm (46.25%). The pyrite recovery in the size class 2000x425 µm was 0% because no particles were found in this size class.

In concentrate 2, the pyrite recovery in the size classes 425x208 µm (50.94%) and 106x45 µm (50.85%) was greater than the pyrite recovery in the size classes 2000x425 µm (30.22%) and 208x106 µm (33.03%).

Table 3.13

Pyrite Recovery and Concentrate Grade for Flotation Test with a Reduced Particle Size Distribution (Test # 5)

Size Class [µm]		Tailings	Concentrate			
			# 1	# 2	# 3	Final
2000x425	Recovery %	-	0.00	30.22	29.18	59.60
	Grade (volume %)	0.30	0.00	3.76	1.79	2.44
425x208	Recovery %	-	35.49	50.94	8.76	95.14
	Grade (volume %)	0.03	17.03	1.92	0.36	1.80
208x106	Recovery %	-	62.72	33.03	2.28	98.04
	Grade (volume %)	0.02	20.32	2.30	0.22	3.52
106x45	Recovery %	-	46.25	50.85	0.94	98.04
	Grade (volume %)	0.06	48.83	37.51	0.67	26.45

[§]Impeller = 1000 RPM, No cleaner flotation stage, PAX = 200 g/ton, Cytec 208 = 50 g/ton, pH = 5.60, p80 = 150 µm

In concentrate 3 the greater the particle size the greater the pyrite recovery. The pyrite recovery for the size class 2000x425 µm was 29.18% and the pyrite recovery for the size class 106x45 µm was 0.94%.

In the final concentrate the smaller the particle size the greater the pyrite recovery. The size classes 208x106 µm and 106x45 µm had a pyrite recovery of 98.04%. The pyrite recovery of the size classes 425x208 µm and 2000x425 µm was 95.14% and 59.60%, respectively.

For concentrate 1 the smaller the particle size the greater the pyrite grade. The highest pyrite grade corresponded to the size class 106x45 µm (48.83%). The lowest pyrite grade

corresponded to the size class 425x208 µm (17.03%). No particles were found in the size class 2000x425 µm.

In concentrate 2 the pyrite grade is much greater in the size class 106x45 µm (37.51%) than the pyrite grade in the other size classes which had a pyrite grade below 4%. The lowest pyrite grade corresponded to the size class 425x208 µm (1.92%).

In concentrate 3 the size classes 2000x425 µm (1.79%) and 106x45 µm (0.67%) had a greater pyrite grade than the size classes 425x208 µm (0.36%) and 208x106 µm (0.22%).

In the final concentrate the size class 106x45 µm had the highest pyrite grade (26.45%), the pyrite grade in this size class was much greater than the pyrite grade in the other size classes. The pyrite grade in the size classes 2000x425 µm, 425x208 µm and 208x106 µm was 2.44%, 1.80% and 3.52%, respectively.

3.4.6 Comparison of Flotation Tests

The pyrite recovery and pyrite volume grade for concentrate 1, concentrate 2 and concentrate 3 were calculated for each flotation test. The calculations are based on the volume and the pyrite volume grade of each size class in the concentrates. The pyrite contents in the size classes for each concentrate were combined mathematically. In flotation test # 1 the pyrite recovery and pyrite volume grade were calculated for concentrate 1 and the cleaner concentrate.

The Equations 3.7 and 3.8 were used to calculate the pyrite recovery and pyrite volume grade for each concentrate, respectively.

$$R_{Concentrate} = \frac{\sum_j \left(V_{Ci} \cdot v_{Ci}\right)}{\sum_j \left(V_{Fi} \cdot Cv_{Fi}\right)} x100 \quad (3.7)$$

$$v_{Concentrate} = \frac{\sum_j \left(V_{Ci} \cdot v_{Ci}\right)}{\sum_j V_{Ci}} x100 \quad (3.8)$$

where:

i = size class (2000x425 µm, 425x208 µm, 208x106 µm and 106x45 µm)

j = concentrate 1, concentrate 2 and concentrate 3

$R_{Concentrate}$ = Pyrite recovery of concentrate [%]

$v_{Concentrate}$ = Pyrite volume grade of concentrate [%]

V_C = Volume of concentrate [cm^3]

V_F = Volume of feed [cm^3]

v_C = Pyrite volume grade of concentrate [%]

Cv_F = Calculated pyrite volume grade of feed [%]

The pyrite recovery and the volume pyrite grade for concentrate 1, concentrate 2 and concentrate 3 from each test are shown in Table 3.14.

The overall pyrite recovery and the pyrite volume grade of the overall concentrate were calculated combining the three concentrates of each flotation test. In the case of flotation test # 1, concentrate 1 and the cleaner concentrate were combined to form the overall concentrate.

Table 3.14

Pyrite Recovery and Pyrite Volume Grade of Individual Concentrates for each Flotation Test

Test #		Concentrate		
		1	2	3
1	Recovery %	70.88	13.54†	-
	Grade (volume %)	17.75	4.13†	-
2	Recovery %	69.40	18.48	3.93
	Grade (volume %)	22.68	7.02	1.94
3	Recovery %	85.07	7.35	2.90
	Grade (volume %)	24.42	2.40	0.78
4	Recovery %	70.81	9.41	3.90
	Grade (volume %)	20.67	4.21	1.05
5	Recovery %	48.72	47.75	1.46
	Grade (volume %)	35.89	10.66	0.39

† Results of cleaner concentrate

The Equations 3.9 and 3.10 were used to determine the overall pyrite recovery and pyrite volume grade of overall concentrate.

$$R_O = \frac{V_{C1} \cdot v_{C1} + V_{C2} \cdot v_{C2} + V_{C3} \cdot v_{C3}}{V_F \cdot Cv_{Py}} x100 \tag{3.9}$$

$$v_{PyO} = \frac{V_{C1} \cdot v_{C1} + V_{C2} \cdot v_{C2} + V_{C3} \cdot v_{C3}}{V_{C1} + V_{C2} + V_{C3}} x100 \tag{3.10}$$

where:

R_O = Overall recovery [%]

v_{PyO} = Pyrite volume grade of overall concentrate [%]

V_{C1} = Volume of concentrate 1 [cm^3]

V_{C2} = Volume of concentrate 2 [cm^3]

V_{C3} = Volume of concentrate 3 [cm^3]

V_F = Volume of feed [%]

Cv_{Py}= Calculated pyrite volume grade of feed [%]

v_{C1} = Pyrite volume grade for concentrate 1 [%]

v_{C2} = Pyrite volume grade for concentrate 2 [%]

v_{C3} = Pyrite volume grade for concentrate 3 [%]

The pyrite recovery and the volume pyrite grade of the overall concentrate for the flotation tests # 1 - #5 are shown in Table 3.15.

Table 3.15

Pyrite Recovery and Pyrite Volume Grade of Overall Concentrate

Test #	Recovery [%]	Volume Grade [%]
1	84.42	11.61
2	91.80	11.90
3	95.32	9.27
4	84.12	8.98
5	97.92	10.21

3.4.6.1 Comparison of results for concentrate 1

The pyrite recovery and pyrite volume grade of the concentrate for flotation tests #1 - # 5 are shown in Figure 3.8. The concentrate 1 had highest pyrite recovery and pyrite of all the flotation tests. The range for the pyrite recovery was 48-85% and the range for the pyrite volume grade was 17%-36%. The best recovery and pyrite volume grade were obtained for the test # 3 (high dosage of collectors and low pH) with a recovery of 85.07 % and pyrite grade of 24.42%. The concentrate 1 in flotation test #1 and #2 was floated under the same conditions, and the results for the concentrate 1 in both tests were similar. The pyrite recovery of test # 1 was 70.88% and the pyrite recovery of the test # 2 was 69.40%. The pyrite volume grade of the test # 1 was 17.75% and the pyrite volume grade of the test # 2 was 22.68%. The concentrate 1 in flotation test # 4 (Danafloat collector and low pH) had a pyrite recovery and pyrite grade of 70.81% and 20.67%, respectively. The pyrite recovery and pyrite volume grade decreased when the Cytec collector was

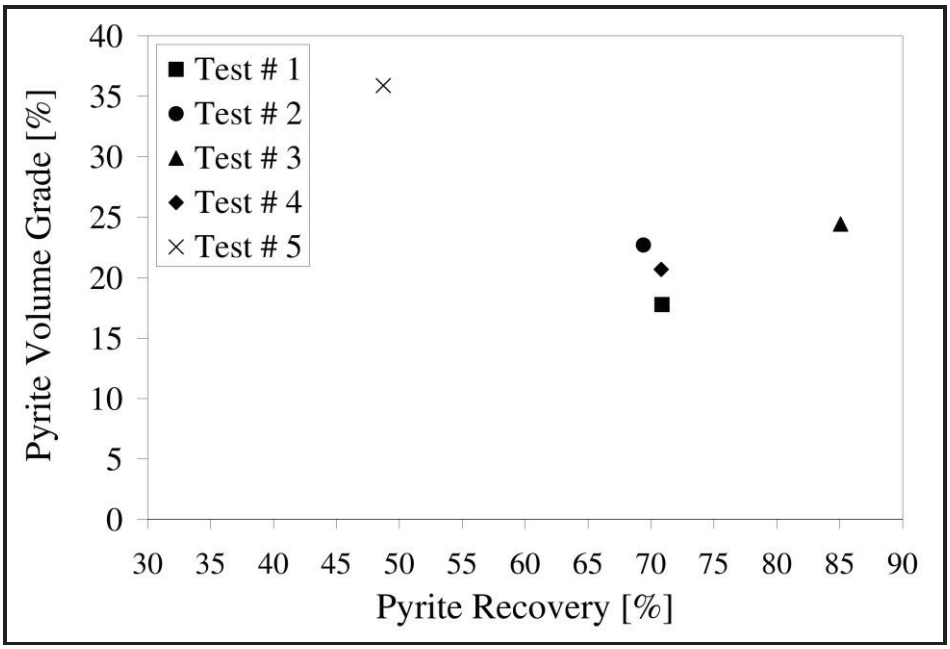

Figure 3.8 Pyrite recovery and volume grade of concentrate 1 for flotation tests #1 - #5.

replaced by the Danafloat collector. The concentrate 1 in flotation test # 5 had a high pyrite grade (35.89%) but the pyrite recovery was the lowest in all the flotation tests, the recovery was 48.72%. The reduction of the particle size increased the pyrite grade but the pyrite recovery decreased significantly.

3.4.6.2 Comparison of results for concentrate 2

The pyrite recovery and pyrite volume grade of the concentrate 2 for flotation tests # 1 - # 5 are shown in Figure 3.9. The concentrate 2 of flotation test # 1 (with cleaner flotation stage) was refloated together with concentrate 3 in the cleaner flotation stage. The cleaner concentrate from the cleaner flotation was compared with the concentrate 2 of the other flotation tests. The flotation test # 5 (reduced particle size distribution) had the best results in the concentrate 2. The pyrite recovery was 47.75% and the pyrite volume grade 10.66%. The pyrite recovery for the other flotation tests varied between 9% and 19% and the pyrite volume grade varied between 2% and 7%. The second best values were obtained for the flotation test # 2 (without cleaner flotation stage). The pyrite recovery was 18.48% and the pyrite volume grade was 7.02%. The flotation test # 4 (Danafloat collector and low pH) and the flotation test # 1 (with cleaner flotation stage) had similar pyrite grade with a value of ~4% but the test # 1 had a better pyrite recovery. The pyrite recovery of the test # 4 was 9.41% and the pyrite recovery of the test # 1 was 13.54%. The pyrite recovery and pyrite grade of the flotation test # 1 correspond to the cleaner concentrate, but it can be compared with the concentrate 2 of the other flotation tests. The flotation test # 3 (high dosage of collectors and low pH) had the lowest values in the concentrate 2. The pyrite recovery was 7.35% and the pyrite grade was 2.40%.

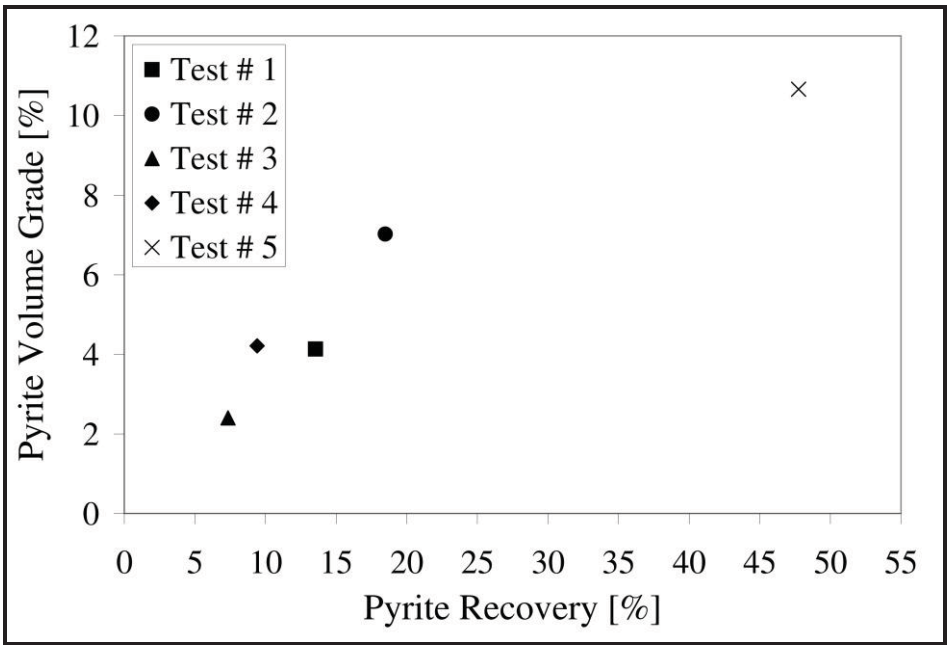

Figure 3.9 Pyrite recovery and volume grade of concentrate 2 for flotation tests #1 - #5.

3.4.6.3 Comparison of results for concentrate 3

The pyrite recovery and pyrite volume grade of the concentrate 2 for flotation tests # 2 - # 5 are shown in Figure 3.10. The concentrate 3 of the flotation test # 1 was floated together with the concentrate 2, therefore no concentrate 3 was collected for this flotation test. The concentrate 3 in all the flotation the pyrite recovery and pyrite volume grade were very low. The range of the pyrite recovery was between 1.5% and 4% and the pyrite volume grade varied between 0.4% and 2%. The flotation test # 2 (without cleaner flotation stage) and the flotation test # 4 (Danafloat collector and low pH) had similar pyrite recovery value (~4%). However, the pyrite volume grade of the flotation test # 2 was greater than the pyrite grade of the flotation test # 4. The pyrite grade of the test # 2 was 1.94% and the pyrite grade of the flotation test # 4 was 1.05%. The concentrate 3 in the flotation test # 3 (high dosage of collector and low pH) had a pyrite recovery of

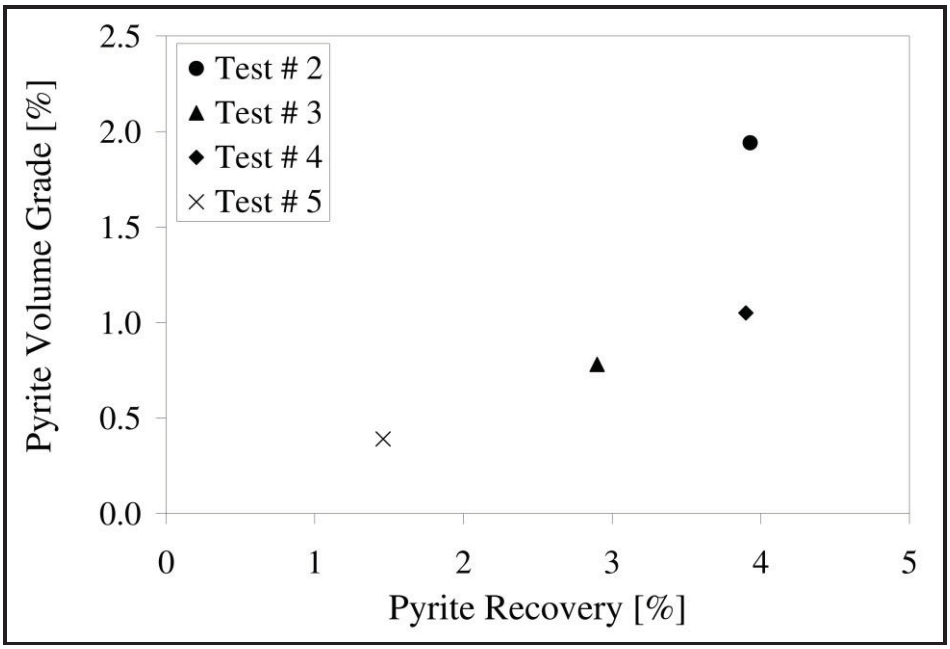

Figure 3.10 Pyrite recovery and volume grade of concentrate 3 for flotation tests #2 - #5.

2.90% and the pyrite grade was 0.78%. The lowest pyrite recovery and pyrite volume grade in concentrate 3 was found for flotation test # 5 (reduced particle size distribution). The pyrite recovery was 1.46% and the pyrite volume grade was 0.39%.

3.4.7 Summary

In general for the flotation tests # 1 - # 5 the highest pyrite recovery and pyrite grade for concentrate 1 are obtained in the fine size classes (208x106 µm and 106x45 µm). The highest pyrite recovery and pyrite grade for concentrate 2 and concentrate 3 are obtained in the coarse size classes (2000x425 µm and 425x208 µm). The fine particles are floated faster and they are collected in the concentrate 1. On the other hand the coarse particles are collected slowly in the concentrate 2 and concentrate 3. It seems that the degree of liberation is playing an important role in the flotation kinetics. The fine particles with

high degree of liberation are floated faster because more pyrite surface is exposed. The pyrite surface exposure is important because the collectors can be attached to the pyrite surface and increase the particle hydrophobicity. On the other hand, the coarse particles with a low degree of liberation are floated slowly, also the size of the particles may influence in the recovery of this particles because it is more difficult to carry the heavy particles to the top of the cell.

In general concentrate 1 had the best pyrite recovery and pyrite grade were obtained for all the flotation tests. The concentrate 2 of all the flotation tests had a lower pyrite recovery and pyrite grade than concentrate 1. Finally, the pyrite recovery and pyrite grade were very low for concentrate 3. In concentrate 1 and 2 good results are obtained because the fines particles with a higher degree of liberation are recovered. This high degree of liberation enhances the high pyrite recovery and pyrite grade in these concentrates. In concentrate 3 the coarse particles with a lower degree of liberation were recovered, this decreases the pyrite recovery and pyrite grade. Also, concentrate 3 was collected for 17 minutes and during this period of time more gangue particles were collected affecting the pyrite grade.

In flotation test # 5 was ~~an~~a special case, concentrate 1 had the worst pyrite recovery of all flotation tests but it had the best pyrite grade. In the concentrate 2 flotation test # 5 had the best pyrite recovery and pyrite grade. The reason is due to the amount of fine particles in the feed was not collected totally in concentrate 1, they need more time and they were collected in concentrate 2. Also, the concentrate 3 of this flotation test had the worst pyrite recovery and pyrite grade.

3.5 Results for Separate Flotation of Individual Size Classes

3.5.1 Weight and Mass Distribution of Products from Flotation Tests

The mass collected of the concentrates in flotation tests # 6 - # 10 are shown in Table 3.16. In flotation test # 6 (2000x425 µm), flotation test # 7 (425x208 µm) and flotation test # 10 (-45 µm) the concentrate with the greatest mass was the concentrate 3. In the case of the flotation test # 8 (208x106 µm) and flotation test # 9 (106x45 µm) the concentrate with the greatest mass was the concentrate 1. In all the flotation tests the concentrate 2 had the lowest mass.

In general the fine particles (208x106 µm, 106x45 µm and -45 µm) are collected faster (in concentrate 1) and the coarse particles (2000x425 µm and 425x208 µm) are collected slower (in the concentrate 2 and concentrate 3). The pyrite liberation is better in the fine particles than in the coarse particles. It seems that the particles with a better liberation have a better probability of being recovered faster due to the exposure of the pyrite grains. The collector interacts with the surface of pyrite. The higher the pyrite exposure, the greater the hydrophobic surface state of the particles.

Table 3.16

Weight of Products from Flotation Tests of Separate Size Classes (Test # 6 – Test # 10)

		Mass [g]				
Size Class [µm]	Test #	Concentrate			Tailings	Total Weight
		1	2	3		
2000x425	6	0.34	0.21	1.97	77.09	79.61
425x208	7	21.05	11.95	28.65	396.18	457.83
208x106	8	43.65	16.30	21.68	347.86	429.49
106x45	9	25.36	8.50	10.41	314.14	358.41
-45	10	22.34	19.38	54.22	537.68	633.62

3.5.2 Feed Pyrite Grade from Flotation Products

The pyrite volume grade of feed calculated from the flotation products in the flotation tests # 6 - # 10 are presented in Table 3.17.

Particle size classes were floated separately in flotation tests # 6 – # 10. The calculated pyrite grade of feed was calculated for each size class. The calculated pyrite grade of feed in each size class is lower than the pyrite grade from the HRXMT analysis.

In the calculations of the pyrite grade of the feed for each size class (Tests # 6 - # 10) the errors from sample manipulation, sample preparation and HRXMT analysis are incorporated. This may have increased the difference between the pyrite grade of feed from the HRXMT analysis and the calculated pyrite grade from the flotation products. Other error that should be considered is the error from sampling. When the 1-kg samples were obtained from the 2-kg sample bags, there is a difference in terms of pyrite content between samples of 1-kg that were used for the HRXMT analysis of the feed and the samples used for the flotation tests. It can be observed that in most size classes the pyrite grade from the HRXMT analysis of the feed was greater than the calculated pyrite grade of feed from flotation products. In the case of the size classes 2000x425 µm, 425x208 µm and 208x106 µm the pyrite grade calculated from HRXMT analysis is almost two times the values of the pyrite grade of feed from flotation products. In the size class 106x45 µm the difference between the pyrite grade from HRXMT analysis and the pyrite grade of the feed from flotation products is smaller.

The results of pyrite grade from the flotation products show that the greater the particles size the smaller the pyrite grade of the feed. Similar trend was found for the results from HRXMT analysis.

Table 3.17

Comparison of Calculated Pyrite Volume Grade of Feed from Flotation Products and Pyrite Volume Grade from HRXMT Analysis of Feed for Flotation Tests # 6 - # 9.

Grind size the feed P80 = 262 µm	Pyrite Volume Grade [%]			
	Size Class [µm]			
	2000x425	425x208	208x106	106x45
HRXMT Analysis	**1.01**	**1.53**	**2.41**	**3.30**
Calculated pyrite grade of feed from flotation products				
Test # 6	0.64	-	-	-
Test # 7	-	0.87	-	-
Test # 8	-	-	1.39	-
Test # 9	-	-	-	2.20

3.5.3 Pyrite Recovery and Pyrite Volume Grade of Concentrates from Flotation Tests

The three concentrates of each flotation test were combined to form a final concentrate for each size class. The pyrite recovery and pyrite grade of the final concentrate in the flotation test # 6 - # 10 are presented in Table 3.18. In Flotation test # 6 (size class 2000x425 µm) the pyrite recovery in concentrate 1 was lower than the pyrite recovery in concentrate 2. The pyrite recovery in concentrate 3 was greater than the pyrite recovery in the concentrate 1 and concentrate 2. In contrast, the pyrite grade in concentrate 1 was greater than the pyrite grade in concentrate 2 and concentrate 3. The concentrate 2 had a higher pyrite grade than concentrate 3.

In the flotation tests #7, #8, #9 and # 10 (size classes 425x208 µm, 208x106 µm, 106-45 µm and -45 µm) the pyrite recovery in the concentrate 1 was greater than the pyrite in

Table 3.18

Pyrite Recovery and Products Grade for Flotation Tests of

Separate Size Classes (Test # 6 - Test # 10)

		Size Class [µm]				
		2000x 425	425x 208	208x 106	106x 45	-45
		Test # 6	Test # 7	Test # 8	Test # 9	Test # 10
Tailings	Grade (volume %)	0.54	0.09	0.02	0.05	0.03
Concentrate 1 2 minutes	Recovery %	4.16	61.04	89.93	94.84	67.14
	Grade (volume %)	6.56	12.75	13.52	38.10	10.17
Concentrate 2 3 minutes	Recovery %	5.22	17.77	6.29	2.54	18.83
	Grade (volume %)	2.61	6.22	2.32	2.36	3.11
Concentrate 3 17 minutes	Recovery %	13.63	12.22	2.34	0.53	8.66
	Grade (volume %)	3.62	1.72	0.64	0.40	0.50
Final Concentrate	Recovery %	18.85	91.02	98.56	97.89	94.62
	Grade (volume %)	3.93	6.17	7.57	19.96	3.16

concentrate 2 and concentrate 3. The pyrite recovery in concentrate 2 was greater than the pyrite recovery in concentrate 3.

Similar behavior was found for the pyrite volume grade in the flotation test #7 - #10. The pyrite grade in concentrate 1 was greater than the pyrite grade in the concentrate 2 and concentrate 3. The pyrite grade in the concentrate 2 was greater than the pyrite grade in concentrate 3. Based on the pyrite recovery and pyrite volume grade of the final concentrate the size class 106x45 µm (Test # 9) had the best results. The pyrite recovery was 97.89% and the pyrite grade was 19.96%. For the flotation tests # 7, #8 and #10 the pyrite recovery was greater than 90% but the pyrite volume grade was lower than 8%.

3.5.4 Summary

When the size classes were floated separately the highest pyrite recovery and pyrite grade for concentrate 1 are obtained in the fine size classes (208x106 µm and 106x45 µm). The highest pyrite recovery and pyrite grade for concentrate 2 and concentrate 3 are obtained in the coarse size classes (2000x425 µm and 425x208 µm).

Concentrate 1 of flotation tests for size classes below 425 µm had a better pyrite recovery and pyrite grade than concentrate 2 and concentrate 3. And the concentrate 2 had a better pyrite recovery and grade than concentrate 3. On the other hand, concentrate 3 of flotation test with the size class 2000x425 µm had a better recovery and pyrite grade than concentrate 2 and concentrate 1. Concentrate 2 had a better pyrite recovery than concentrate 1.

3.6 Discussion

The pyrite recovery and pyrite volume grade of the final concentrate in the size class 2000x425 µm for flotation tests # 1 - # 6 are shown in Figure 3.11. In flotation test # 6 the particle size 2000x425 µm was floated individually to determine the effect of the fine particles (-45 µm) on the performance of the flotation experiments.

In flotation test # 1 (with cleaner flotation stage) the pyrite recovery and the pyrite volume grade was 16.24% and 11.79%, respectively. The best pyrite volume grade was obtained in this flotation test for the size class 2000x425 µm.

The pyrite recovery increased in this size class when the cleaner flotation stage was not used (flotation test # 2), however the pyrite grade decreased. The pyrite recovery was 32.14% and the pyrite grade was 7.59%.

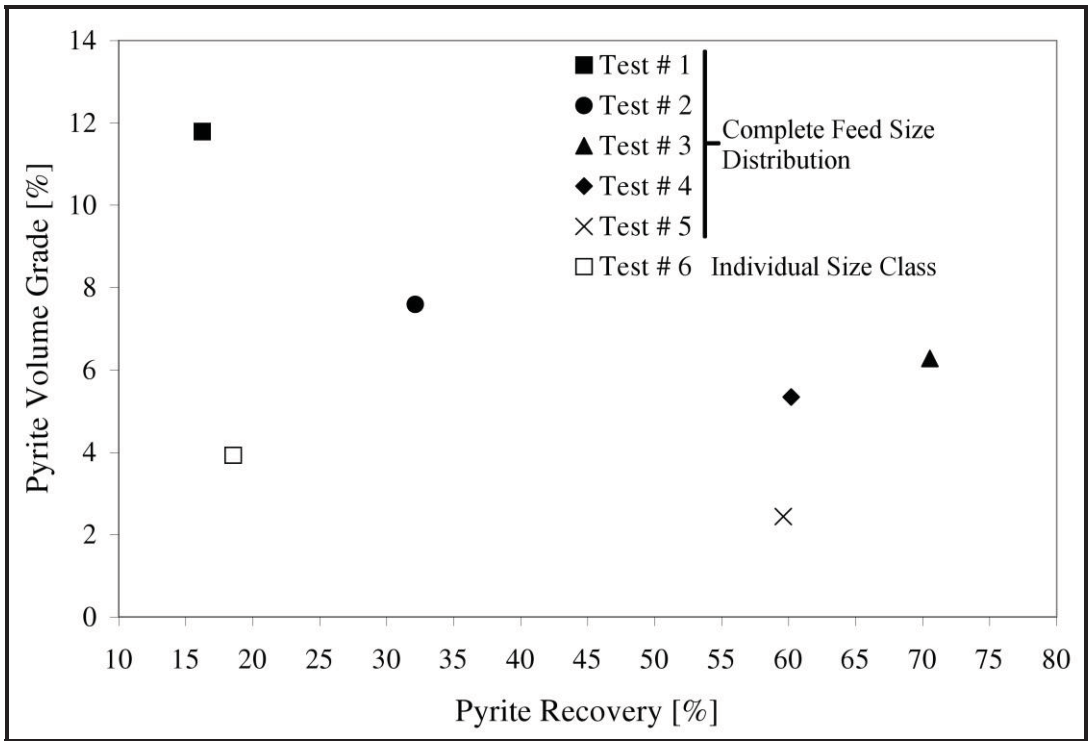

Figure 3.11 Pyrite recovery and volume grade of size class 2000x425 µm for flotation tests # 1 - # 6.

With the dosage increment of the collectors and a low pH (flotation test # 3), there is a significant increment in the pyrite recovery to 70.55%, but the pyrite grade decreased to a value of 6.28%.

The pyrite recovery and the pyrite grade decreased when the new collector (Danafloat) was used in the flotation test # 4. The pyrite recovery decreased to 60.20% and the pyrite grade decreased to 5.34%.

In flotation test # 5 (reduced particle size distribution) the pyrite volume grade was lower than the other flotation tests. The pyrite grade was 2.44% and the pyrite recovery of this test was 59.60%.

When the particles in the size class 2000x425 µm were floated separately the pyrite recovery and the pyrite grade were 18.55% and 3.93%, respectively. There is not a negative effect of the fines (-45 µm particles) on this size class, most of the flotation tests had better results than the flotation test # 6.

The pyrite recovery and pyrite volume grade of the size class 425x208 µm in the final concentrate for flotation tests # 1-# 5 and flotation test # 7 are shown in Figure 3.12. In flotation test #7 the size class 425x208 was floated separately.

The flotation test # 1 (with cleaner flotation stage) had a pyrite recovery and pyrite volume grade of 83.03% and 8.42%, respectively.

In flotation test without the cleaner flotation stage (flotation test # 2), there is a decrement in the pyrite volume grade but the pyrite recovery was increased. The pyrite volume grade was 6.91% and the pyrite recovery increased to a value of 88.34%.

When the dosage of the collector was increased and the pH was decreased (flotation test # 3) the pyrite recovery increased significantly and the pyrite volume grade did not change in relation to flotation test # 2. In flotation test # 3 the pyrite recovery was 97.03% and the pyrite volume grade was 6.90%.

The pyrite recovery and the pyrite volume grade decreased with the use of the Danafloat collector (flotation test # 4) in comparison with flotation test # 3. The pyrite recovery decreased to 87.73% and the pyrite decreased to 5.09%.

The lowest pyrite volume grade was found in the flotation test # 5 (reduced particle size distribution), however the second best pyrite recovery was obtained in this flotation test. The pyrite volume grade was 1.80% and the pyrite recovery was 95.14%.

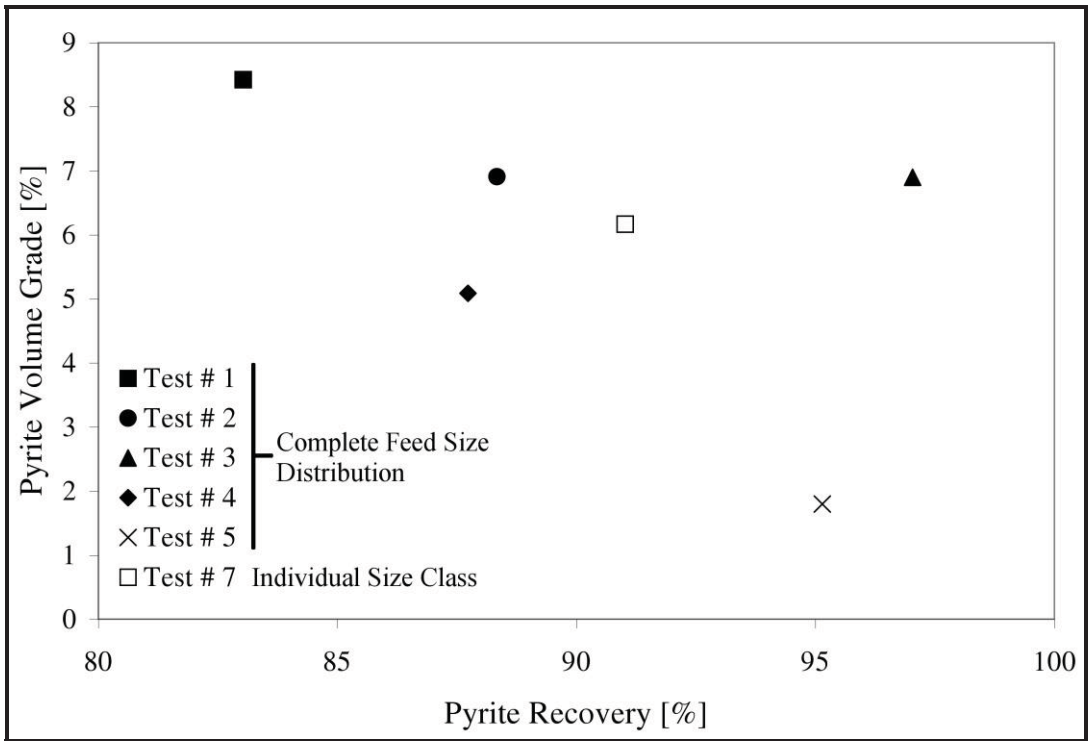

Figure 3.12 Pyrite recovery and volume grade of size class 425x208 µm for flotation tests # 1 - # 5 and flotation test # 7.

In individual flotation of the size class 425x208 µm (flotation test # 7) the pyrite recovery was 91.02% and the pyrite volume grade was 6.17%. These results are lower than the pyrite recovery and pyrite grade of the flotation test # 3 (high dosage of collectors and low pH). There is not a negative effect of the fine particles (-45 µm) when the collectors (Cytec and PAX) are added in excess.

The pyrite recovery and pyrite volume grade of the size class 208x106 µm in the final concentrate for flotation tests # 1- # 5 and flotation test # 8 are shown in Figure 3.13. In flotation test # 8 the size class 425x208 was floated separately.

In flotation test # 1 (with cleaner flotation stage) the pyrite recovery and the pyrite volume grade was 91.70% and 11.07%, respectively.

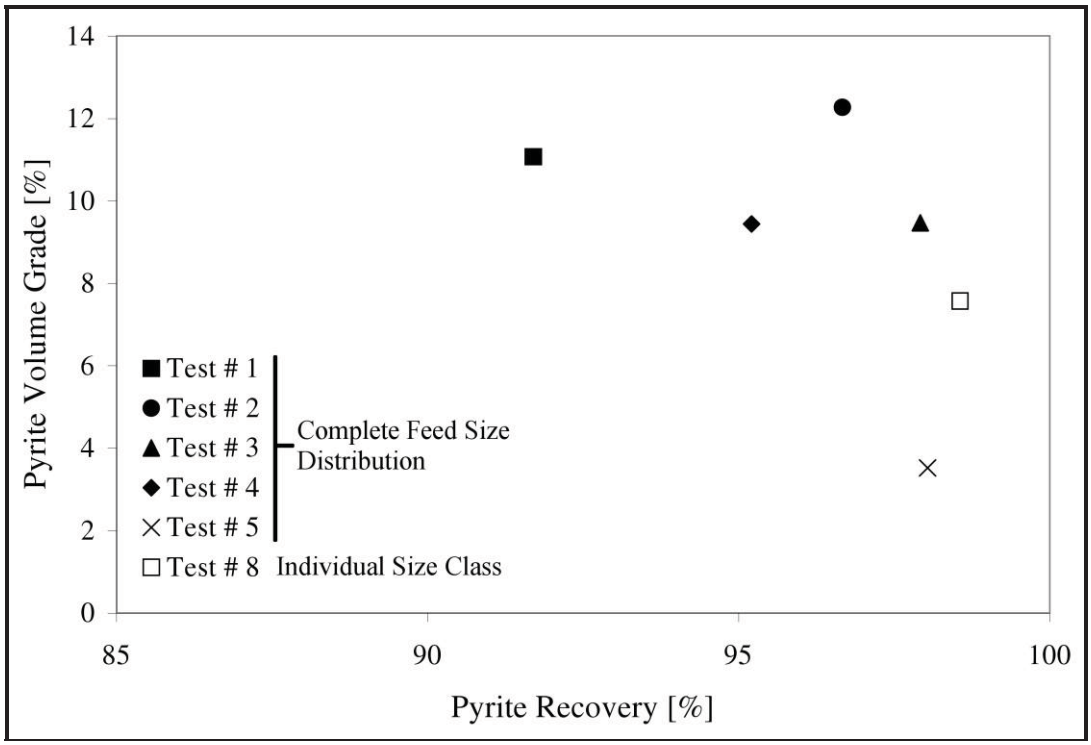

Figure 3.13 Pyrite recovery and volume grade of size class 208x106 µm for flotation tests #1 - #5 and flotation test # 8.

In flotation test # 2 (without cleaner flotation stage) better results were obtained in comparison with flotation test # 1, the pyrite recovery and the pyrite volume grade were increased. The pyrite recovery and pyrite grade were increased to 96.67% and 12.27%, respectively.

When the dosage of the collector was increased and the pH was decreased (flotation test # 3), the pyrite recovery was increased slightly to 97.92% but the pyrite was decreased to 9.47%.

In flotation test # 4 (Danafloat collector and low pH), the pyrite grade remained similar to flotation test # 3, the pyrite volume grade was 9.44%. However, the pyrite recovery decreased to 95.21%.

In flotation test # 5 (reduced particle size), the pyrite recovery was 98.04%, this pyrite recovery is one of the highest recoveries for this size class, but in this flotation test the lowest pyrite grade was obtained, 3.52%.

When particles of the size class 208x106 µm were floated separately, the highest pyrite recovery was found, 98.56%. The pyrite grade in this flotation test was lower than the pyrite grade in flotation tests # 1 - # 5. Comparing flotation test # 5 (high dosage of collectors and low pH) with flotation test # 3 (high dosage of collectors and low pH), the pyrite recovery was similar in both tests but flotation test # 3 had a higher pyrite grade. The fine particles (-45 µm) did not make a significant difference when an excess of collectors Cytec and PAX are used for the flotation of this size class.

The pyrite recovery and pyrite volume grade of the size class 106x45 µm of the final concentrate in flotation tests # 1 - # 5 and flotation test # 9 are shown in Figure 3.14. In flotation test # 9 the size class 106x45 µm was floated separately.

The flotation test # 1 (with cleaner flotation stage) had a pyrite recovery and a volume grade of 91.36% and 15.78%, respectively.

In flotation test without the cleaner flotation stage (flotation test # 2) there is an increment in the pyrite recovery and pyrite volume grade in comparison with flotation test # 1. The pyrite recovery of this test was 97.35% and the pyrite volume grade was 21.00%.

The increment in the dosage of the collectors and and low pH (flotation test # 3) did not improve the flotation performance in this size class, in the fact the pyrite recovery and the pyrite grade decreased. The pyrite recovery and the pyrite volume grade in the flotation test # 3 was 92.42% and 19.40%, respectively.

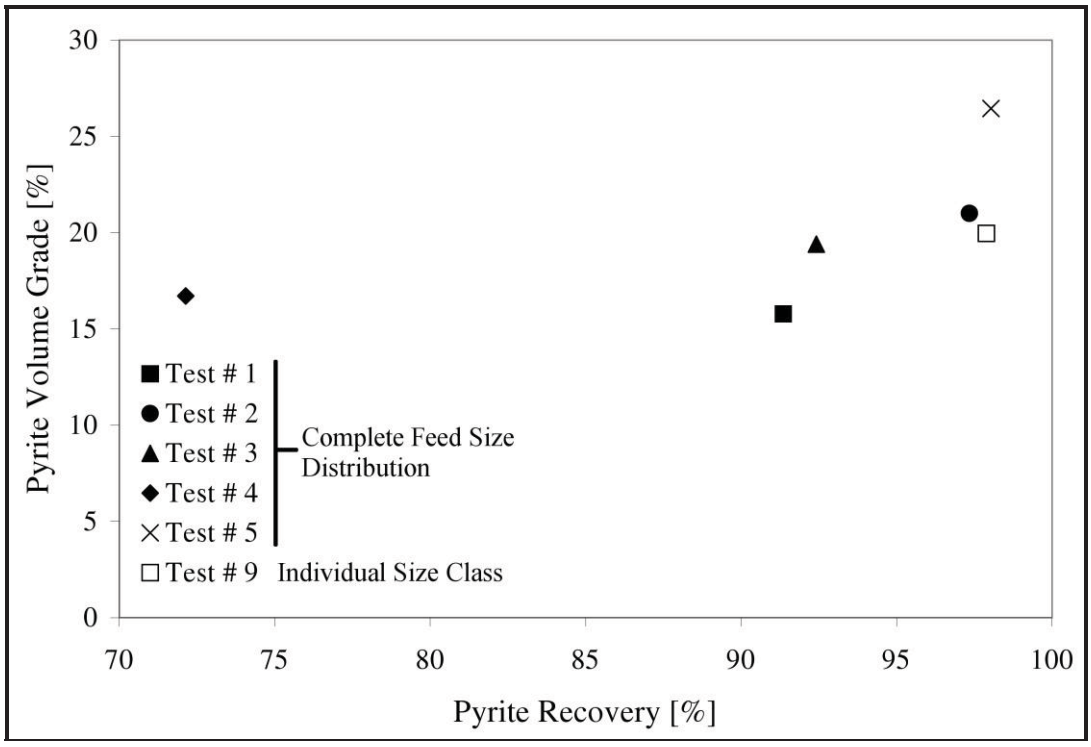

Figure 3.14 Pyrite recovery and volume grade of size class 106x45 µm for flotation tests # 1 - # 5 and flotation test # 9.

When the Cytec collector was replaced by the Danafloat collector (flotation test # 4) the pyrite recovery and pyrite volume grade decreased in comparison with flotation test # 3. The pyrite recovery decreased significantly to a value of 72.14%. The pyrite volume grade decreased to a value of 16.71%.

The best pyrite recovery and pyrite volume grade was found for flotation test # 5 (reduced particle size), the pyrite recovery was 98.04% and the pyrite grade was 26.45%. With size reduction of the feed sample there is an improvement of the recovery and grade in the flotation of the size class 106x45 µm.

In flotation test # 9 (separate flotation of size class 106x45 µm), the pyrite recovery and the pyrite volume grade were 97.89% and 19.96%. These results are similar to flotation test # 2 (without cleaner flotation stage) and slightly higher than the results from

flotation test # 1, # 3 and # 4. The negative effect of the fine particles (size class -45 µm) in the flotation was not evident in the size class 106x45 µm.

In summary when the collectors were used in excess with a low pH (test # 3, test # 4 and test # 5) the best results were obtained for the size classes 2000x425 µm in terms of pyrite recovery. However, the pyrite grade was not favored under these conditions.

The best pyrite recovery and grade for the size class 425x208 µm were obtained in flotation test # 3. In the other flotation tests the pyrite recovery or pyrite grade are compromised.

In the size classes 208x106 µm the pyrite recovery of the flotation test varied between 91% and 98%. The best pyrite grade was obtained for flotation test # 2 and # 3.

In the size class 106x45 µm the pyrite recovery of most of the flotation tests varied between 91% and 98%, the only exception was the flotation test # 4 which had pyrite recovery of 72%. The collector Danafloat 571 did not work well in this size class. The best pyrite recovery was obtained in the flotation test # 2.

The flotation test # 5 had a high pyrite recovery in the size classes 2000x425 µm, 425x208 µm and 208x106 µm. However the pyrite grade was the lowest of all the flotation tests. In the size class 106x45 µm flotation test # 5 had the best pyrite recovery and pyrite grade. This size class has the highest mass percent in concentrate 1 and his contribution to the overall concentrate is significant. This is the reason why the overall concentrate of this flotation test has the best pyrite recovery and one the best pyrite grades.

It seems that the negative effect of fine particles (-45 µm) on the flotation performance only may occur in the size class 106x45 µm, but the negative effect is not

significant. Apparently the fine particles (-45 µm) enhance the flotation of coarse particles. Possibly the fine particles help to form agglomerations of particles and these agglomerations are trapped by the bubbles to the surface of the cell.

3.6.1 Liberation-limited Grade/Recovery Curves and Discussion

The overall pyrite recovery and pyrite concentrate grade were compared with the liberation-limited grade/recovery curves for each size class. The recovery and grade for any separation process can not exceed the limit of this curve. In the best case the actual grade and recovery of the separation process would fall on the curve and under these conditions improved separation can only be achieved by further liberation with size reduction. If the recovery and grade for the separation process falls below the liberation-limited grade/recovery curve the separation efficiency is limited by factors other than liberation (Miller et al. 2009).

3.6.1.1 Size class 2000x425 µm

The liberation-limited grade/recovery curve for the size class 2000x425 µm was plotted with the corresponding pyrite recovery and pyrite grade of the final concentrates for flotation tests # 1 - # 4 (Figure 3.15).

The pyrite recovery and pyrite grade of the final concentrate in flotation tests # 1 (with cleaner flotation stage) and flotation test # 2 (with cleaner flotation stage) are below the liberation-limited grade/recovery curve. The pyrite recovery and grade of this flotation tests can be improved by changing the flotation conditions.

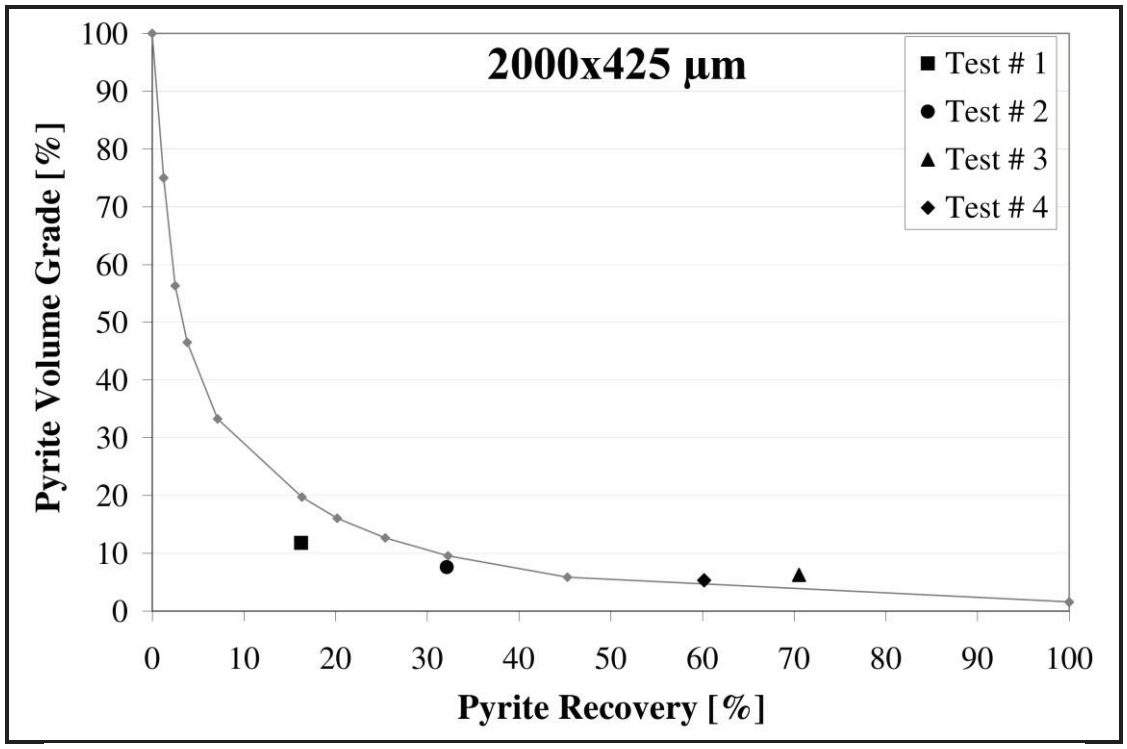

Figure 3.15 Pyrite recovery and grade of final concentrates and liberation-limited grade/recovery curves for the size class 2000x425 µm.

The pyrite recovery and pyrite grade for the 208x106 µm size class in flotation test # 3 (high dosage of collectors and low pH) and flotation test # 4 (Danadfloat collector and low pH) were above the liberation-limited grade/recovery curve. The pyrite recovery and grade can not exceed the liberation-limited grade/recovery curve. However due to the error in the flotation test and HRXMT analysis, the pyrite recovery and grade were above the liberation-limited grade recovery curve. The pyrite recovery and grade of flotation test # 3 and flotation test # 4 should fall on the liberation-limited grade/recovery curve, which is the limit for the grinding conditions of the flotation tests. The results of flotation tests # 3 and flotation test # 4 can be improved only by a further size reduction of the feed sample.

3.6.1.2 Size class 425x208 µm

The pyrite recovery and pyrite grade of the final concentrate for flotation tests # 1 - # 4 and corresponding liberation-limited grade/recovery curve for the size class 425x208 µm are shown in the Figure 3.16. The pyrite recovery and pyrite grade of flotation tests #1 - #3 are above the liberation-limited grade/recovery curve. The pyrite recovery and grade can not exceed the liberation-limited grade/recovery curve. The pyrite recovery and grade of flotation test #1 - #3 should fall on the liberation-limited grade/recovery curve, which is the limit for the grinding conditions of the flotation tests. The pyrite recovery and pyrite grade of the flotation test # 4 fell on the liberation-limited grade/recovery curve. The results of flotation tests #1 - #4 can be improved only by a further size reduction of the feed sample.

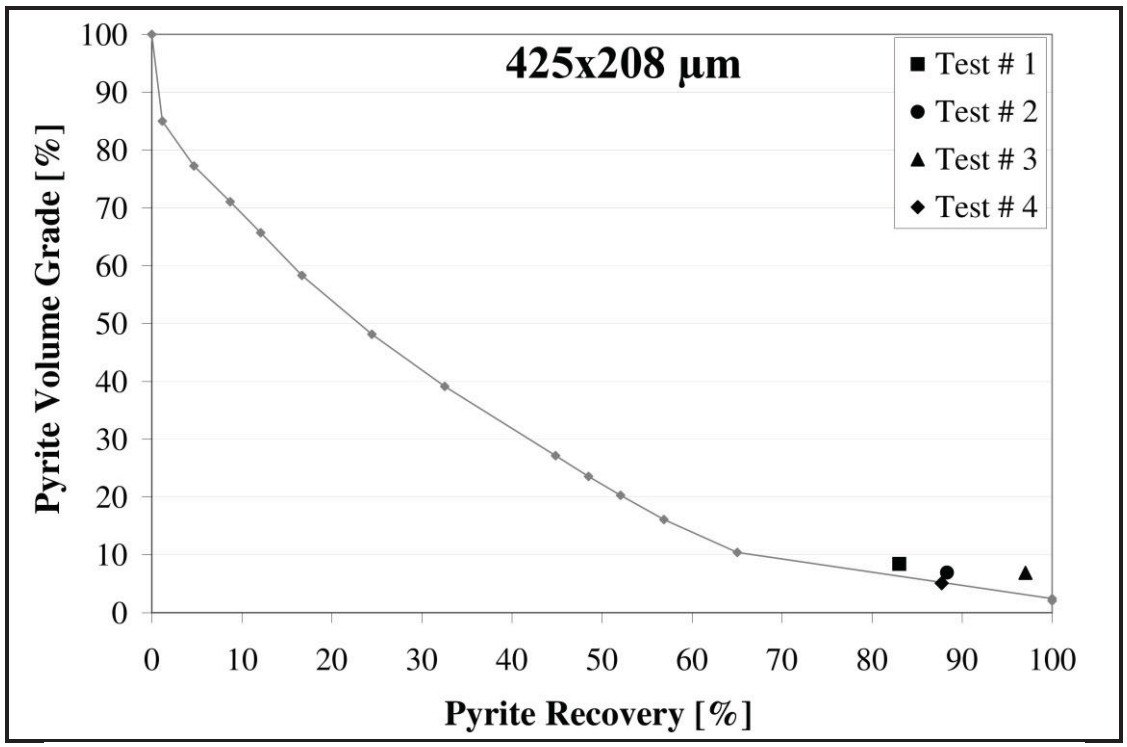

Figure 3.16 Pyrite recovery and grade of final concentrates and liberation-limited grade/recovery curves for the size class 425x208 µm.

3.6.1.3 Size class 208x106 µm

The pyrite recovery and pyrite grade of the final concentrate for flotation tests # 1 - # 4 and corresponding liberation-limited grade/recovery curve for the size class 208x106 µm are shown in Figure 3.17.

The pyrite recovery and pyrite grade of the final concentrate in flotation tests # 1 (with cleaner flotation stage) and flotation test # 4 (Danafloat collector and low pH) are below the liberation-limited grade/recovery curve. The pyrite recovery and grade of this flotation tests can be improved by changing the flotation conditions.

The pyrite recovery and pyrite grade for the 208x106 µm size class in flotation test # 3 (high dosage of collectors and low pH) the pyrite recovery was close to the liberation-limited grade/recovery curve.

The pyrite recovery and pyrite grade for the 208x106 µm size class in flotation test # 2 (without cleaner flotation stage) were slightly above the liberation-limited grade/recovery curve. The pyrite recovery and grade can not exceed the liberation-limited grade/recovery curve.

However due to the error in the flotation test and HRXMT analysis, the pyrite recovery and grade were above the liberation-limited grade recovery curve. The pyrite recovery and grade of flotation test # 2 should fall on the liberation-limited grade/recovery curve, which is the limit for the grinding conditions of the flotation tests. The results of flotation tests # 2 and flotation test # 3 can be improved only by a further size reduction of the feed sample. A reduction of the particle size distribution is recommended for the flotation test # 2 and flotation test # 3.

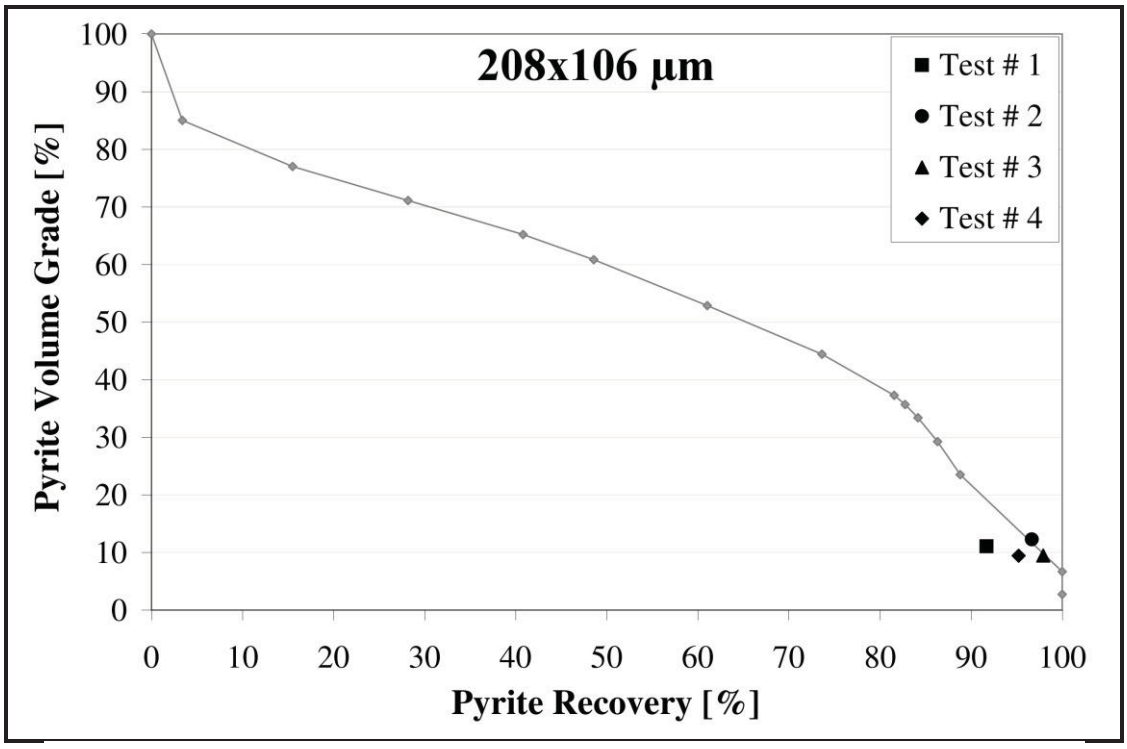

Figure 3.17 Pyrite recovery and grade of final concentrates and liberation-limited grade/recovery curves for the size class 208x106 µm.

3.6.1.4 Size class 106x45 µm

The pyrite recovery and pyrite grade of the final concentrates for flotation tests # 1 - # 4 and the corresponding liberation-limited grade/recovery curve for the size class 106x45 µm are shown in the Figure 3.18.

The pyrite recovery and pyrite grade of flotation test # 1 (with cleaner flotation test), test # 3 (high dosage of collectors and low pH) and flotation test # 4 (Danafloat and low pH) were below the liberation-limited grade/recovery curve. The pyrite recovery and grade of these flotation tests can be improved by changing the flotation conditions. The flotation conditions of the flotation test # 1 and flotation test # 3 are not the optimum.

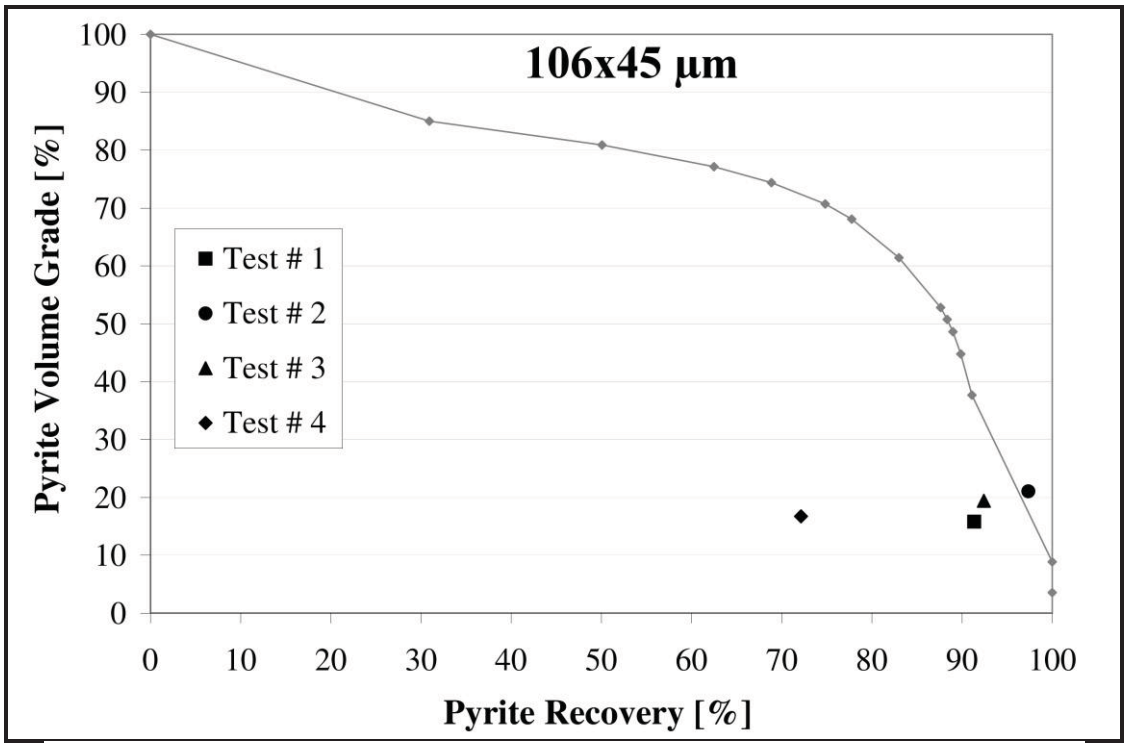

Figure 3.18 Pyrite recovery and grade of final concentrates and liberation-limited grade/recovery curves for the size class 106x45 µm.

The pyrite recovery and volume grade of flotation test # 2 (without cleaner flotation stage) exceeded the liberation-limited grade/recovery curve, this is not possible because the liberation-limited grade/recovery curve is the limit of the recovery and grade of the concentrate.

However, due to the error from the flotation test and HRXMT analysis, the pyrite recovery and grade was above the curve. The pyrite recovery and grade of this flotation should be on the liberation-limited grade/recovery curve.

The results of flotation tests # 2 can be improved only by decreasing the particle size of the feed for the flotation tests.

3.6.2 Exposure Analysis of Feed and Flotation Products

The valuable minerals have some unknown grain size distribution, texture/exposure, and spatial distribution in the ore particles. The procedure is to crush the ore so that the valuable mineral grains are exposed and provide the desired mineral surface for bubble attachment and subsequent concentration of valuable mineral particles during the flotation process. If the relationship between mineral exposure and particle size can be established, then the ultimate separate efficiency in the flotation process can be predicted for a specific particle size distribution. It is therefore extremely important to determine the percentage of exposed valuable mineral grains in the ore as a function of particle size. However, the percentage of exposed valuable grains in the ore can not be determined using conventional polished section analysis such as typically practiced in the mining industry. The exposure analysis was done from the data generated from the HRXMT analysis. In the exposure analysis the voxels corresponding to the internal and exposed pyrite grains were determined. The exposure analysis was completed for the entire sample and for individual particles in the sample.

The exposure analysis was done for the feed samples and the products of flotation tests # 1 - # 4. The analysis was completed for each size class of the different samples, the size classes used were: 106x45 µm, 208x106 µm, 425x208 µm and 2000x425 µm. The results are discussed based on internal and external pyrite grains.

3.6.2.1 Internal and exposed grains of entire samples

In the exposure analysis of feed samples by HRXMT the number of voxels corresponding to internal and exposed grains in the entire sample was determined. With

the number of voxels of internal and exposed grains in the pyrite-containing particles, the percentages of internal and exposed grain voxels were calculated for the feed in each size class. The percentages of internal and exposed grain voxels in the feed samples are shown in Figure 3.19.

As it was expected there is a direct relationship between the external grains and the particle size of the feed samples. The percentage of external grain voxels decreased as the particles size increased. The percentage of external grain voxels in the size class 106x45 µm was 99.76%. The percentage of external grain voxels for the size class 2000x425 µm was 74.07%. In the size class 106x45 µm practically all the pyrite grains are exposed, in the size classes 208x106 µm and 425x208 µm most of the pyrite grains are exposed but there are still some internal grains. In the size class 2000x425 µm most of grains are exposed but there are a significant number of internal grains. The percentages of internal and exposed grain voxels were determined for the flotation products of flotation test # 1 - # 4. The results of flotation test # 1 (with cleaner flotation stage) are shown in Figure 3.20.

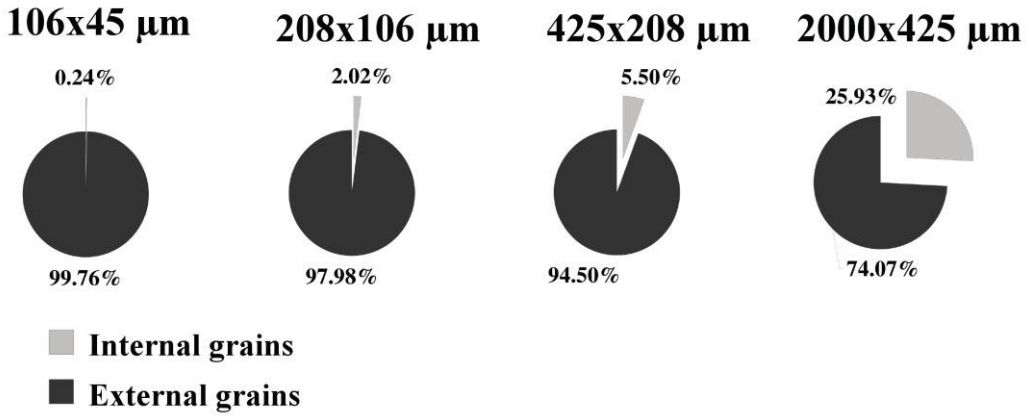

Figure 3.19 Percentage of internal and exposed voxels in feed sample

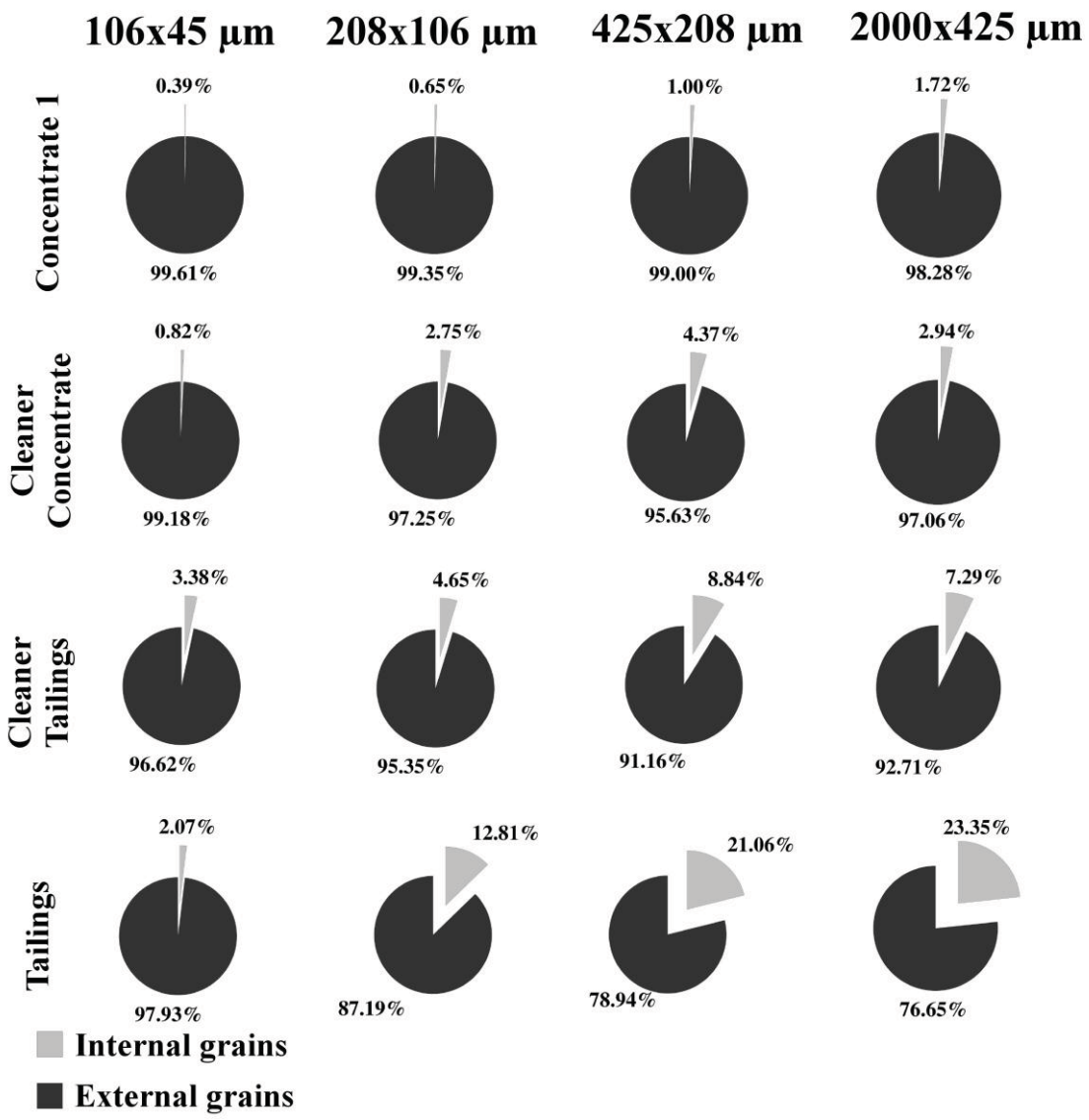

Figure 3.20 Percentage of internal and exposed voxels in products from flotation test # 1 (with cleaner flotation stage)

In general for all the flotation products the smaller the particle size the greater the percentage of exposed grain voxels. There are some exceptions in the cleaner concentrate and the cleaner tailings; in these flotation products the percentage of the exposed grain voxels was lower for the size class 205-425 µm than the percentage in the size class 2000x425 µm.

In concentrate 1 most of the pyrite grains were practically exposed even for the size class 2000x425 µm. The percentage of exposed grain voxels varied from 99.61% to 98.28%.

In the cleaner concentrate the percentage of exposed grain voxels varied from 99.18% to 95.63%. In the cleaner tailings the percentage the exposed grain voxels varied from 96.62% to 91.16%.

The tailings had the lowest values of percentage of exposed grain voxels, the exception was for the size class 106x45 µm. In this size class the lowest percentage of the exposed grain voxels corresponded to the cleaner tailings.

The results of flotation test # 2 (without cleaner flotation stage) are shown in Figure 3.21. In the flotation products of this test the smaller the particle size the greater the percentage of exposed grain voxels. The only exception was for the size classes 425x208 µm and 2000x425 µm. The percentage of exposed grain voxels for the size class 425x208 µm was lower than the percentage in the size class 2000x425 µm. This occurred in concentrate 2, concentrate 3 and tailings.

The percentage of exposed grain voxels was high in concentrate 1 and concentrate 2. For concentrate 1 the percentage of exposed grain voxels varied from 99.60% to 98.37%.

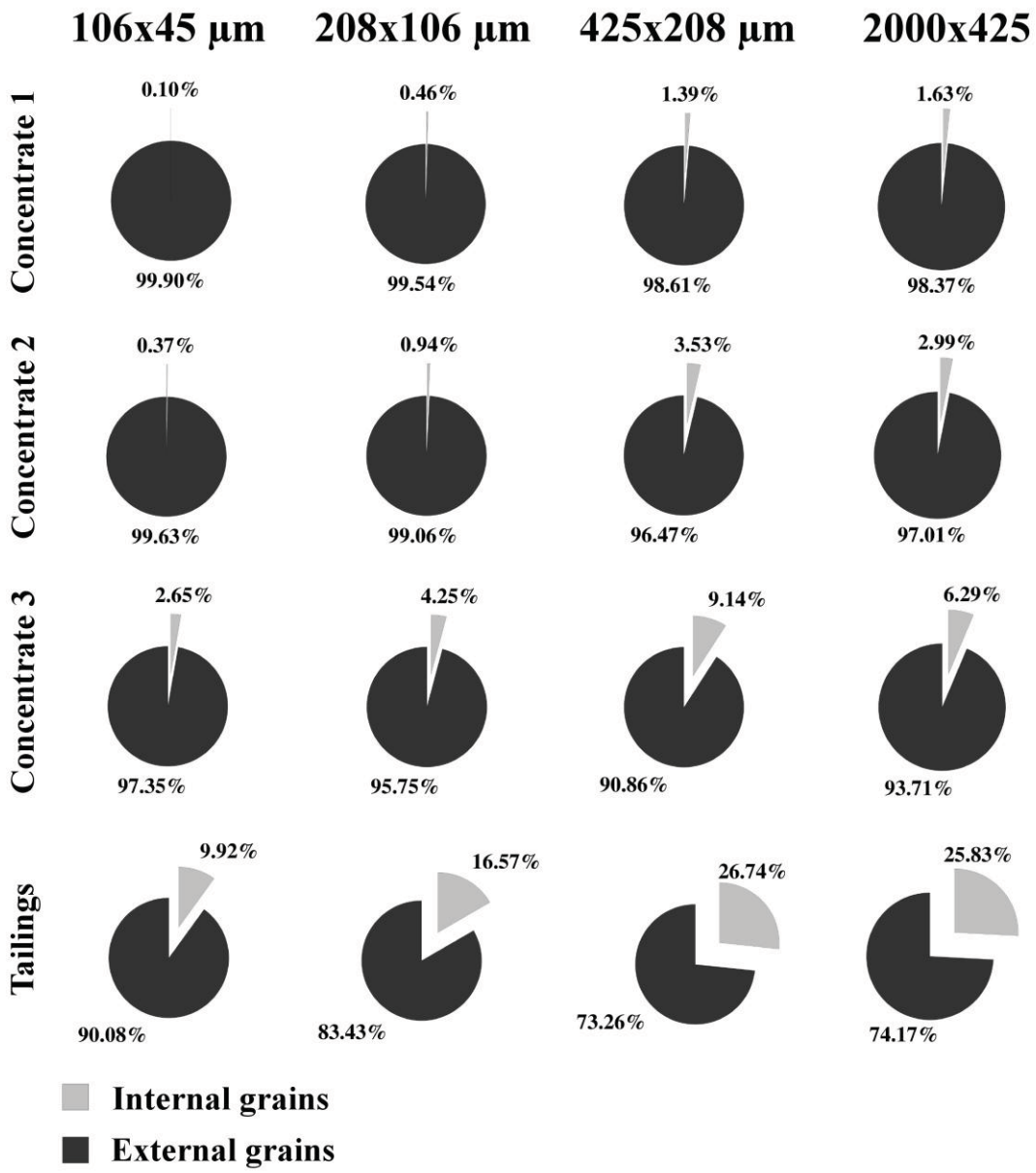

Figure 3.21 Percentage of internal and exposed voxels in products from flotation test # 2 (without cleaner flotation stage)

For concentrate 2 the percentage varied from 99.63% to 96.47%. In concentrate 3 the percentage of exposed grain voxels varied from 97.35% and 90.86%.

The tailings had the lowest percentages of exposed grain voxels in this test, the percentage varied from 90.08% to 73.26%.

The results of flotation test # 3 (high dosage of collectors and low pH) are shown in Figure 3.22. In concentrate 1 and concentrate 2 the highest percentages of exposed grain voxels were found in the size class 208x106 µm. The second best percentage corresponded to the size class 106x45 µm. The other two size classes followed the trend of the smaller the particle size the greater the percentage of exposed grain voxels. In concentrate 1 the percentage of exposed grain voxels varied from 99.68% to 97.03%. The percentage in concentrate 2 varied from 97.29% to 93.84%.

In concentrate 3 and tailings the lowest percentages of exposed grain voxels corresponded to the size class 425x208 µm. The other size classes followed the trend of the smaller the particle size the greater the percentage of exposed grain voxels. The percentage of exposed grain voxels for the concentrate 3 varied from 96.04% to 85.69%. The tailings had the lowest values of percentage of exposed grain voxels of this test, the percentage varied from 95.05% to 69.38%.

The results of flotation test # 4 (Danafloat collector and low pH) are shown in Figure 3.23. For concentrate 1 and concentrate 2 the smaller the particle size the highest the percentage of exposed grain voxels. The percentage of exposed grain voxels in concentrate 1 varied from 99.76% to 97.23%. The percentage of concentrate 2 varied from 99.13% to 93.14%.

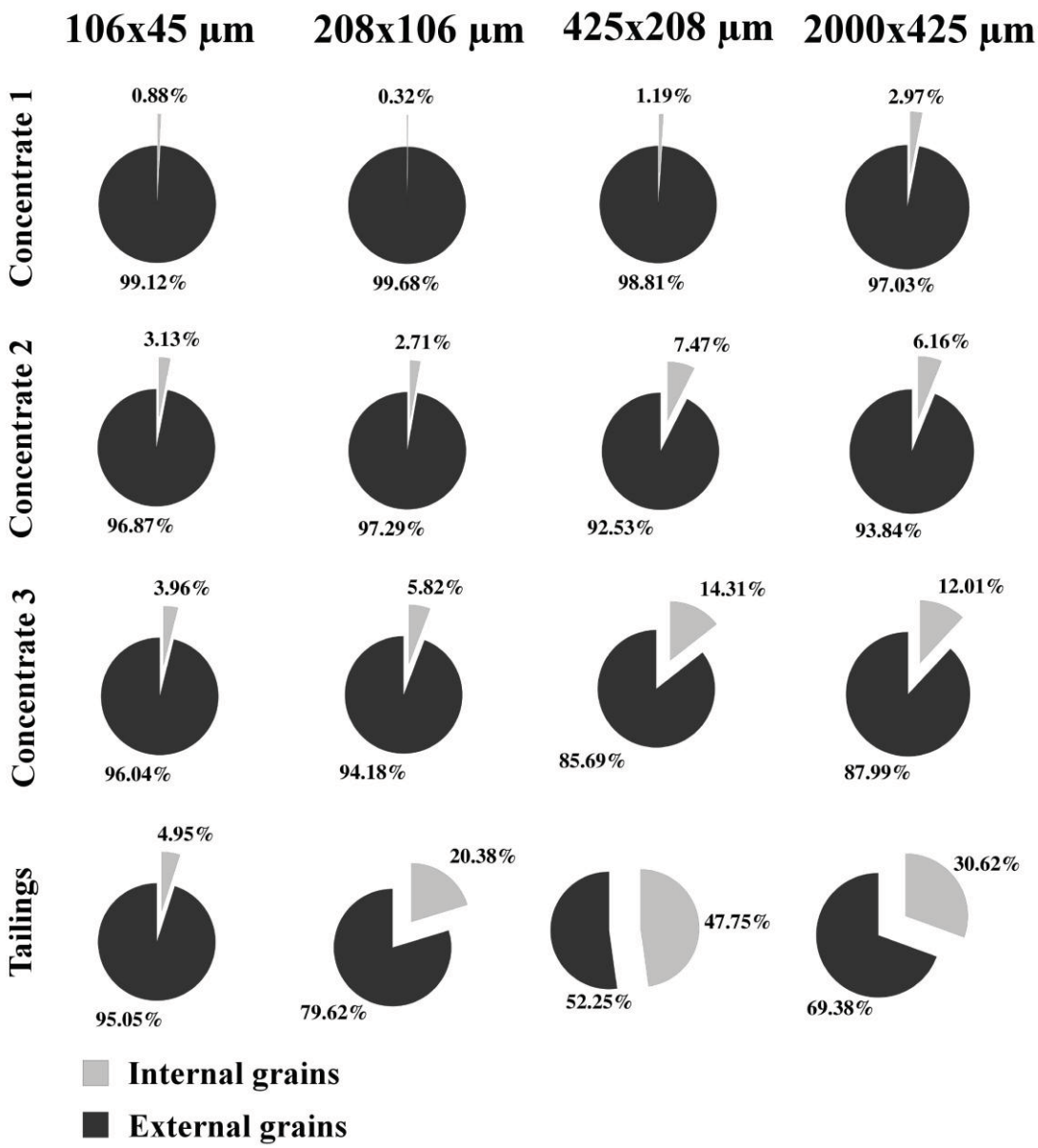

Figure 3.22 Percentage of internal and exposed voxels in products from flotation test # 3 (high dosage of collectors and low pH)

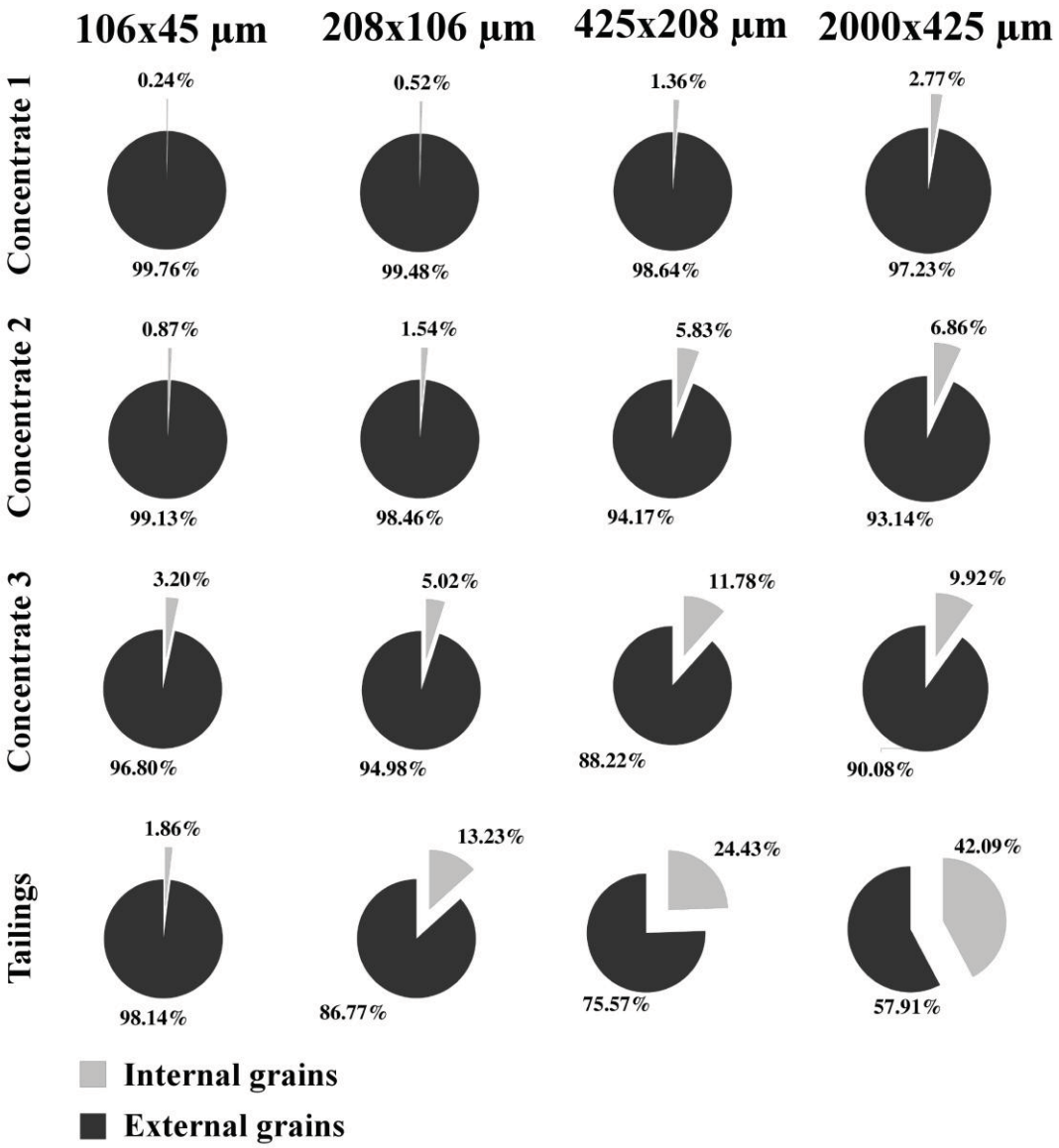

Figure 3.23 Percentage of internal and exposed voxels in products from flotation test # 4 (Danafloat collector and low pH)

In concentrate 3 the size class 425x208 µm had the lowest percentage of exposed grain voxels (88.22%). In the other size classes the smaller the particle size the greater the percentage of exposed grain voxels. In concentrate 3 the percentage of exposed grain voxels varied from 96.80% to 88.22%.

In the tailings the smaller the particle size the greater the percentage of exposed grain voxels. The percentage varied from 98.14% to 57.91%. In this test the percentage of exposed grain voxels (98.14%) was greater than the percentage in concentrate 3 (96.80%).

In general for all the flotation tests the particles with high percentage of exposed grain voxels are recovered in the concentrate 1 in all the size classes. Then the percentage of exposed grain voxels decreased for the particles in concentrate 2. Similar trend occurred in concentrate 3 and tailings. Tailings have the lowest percentage of exposed grain voxels. The pyrite grain exposure is important in the flotation kinetics, the particles with better pyrite exposure are recovered first in concentrate 1.

It can be observed that the variation of the percentages of internal and exposed grain voxels were not significant in the concentrates for all the flotation tests. However, in the tailings the difference between the flotation tests was higher. In flotation test # 3 (high dosage of collectors and low pH), the size classes 208x106 µm and 425x208 µm had a low percentage of exposed grain voxels in comparison with the other flotation tests. In the size classes 208x106 µm and 425x208 µm several internal grains can be found in the tailings of flotation test # 3. In flotation test # 3 particles with low percentage of exposed grain voxels were recovered in the concentrates, this phenomenon did not occurred in the other flotation tests. This is reflected in the tailings of flotation test # 3 which has

particles with lower percentage of exposed grains voxels in comparison with the other flotation tests.

3.6.2.2 Internal and exposed grains of individual particles

The percentage of internal and exposed grain voxels was calculated for individual particles in similar way that the previous section. In some samples thousands of particles were analyzed. Once the percentages of internal and external grains were calculated for each particle in the sample, the particles were classified into the different pyrite volume grade classes: 0-10%, 10-20%, 20-30%, 30-40%, 40-50%, 50-60%, 60-70%, 70%-80%, 80%-90%, 90-100% and 100%. Once the particles were classified into different pyrite volume classes, the particles in each grade class was classified into different classes of percentage of exposed grain voxels: 0%, 0-10%, 10-20%, 20-30%, 30-40%, 40-50%, 50-60%, 60-70%, 70%-80%, 80%-90%, 90-100% and 100%. In total with the combination of grade classes and exposed grain classes the particles were classified into 132 groups. In reality there are 122 groups because a pure pyrite particle can be classified only as 100% exposed grain.

The number voxels of the particles in each group were summed up and the percentage of each group was determined in relation to the total of voxels of the entire sample. The results of the classification of the samples are presented in a 3D plot, for instance the results of the feed sample in the size class 208x106 μm are shown in Figure 3.24. The 3D plots of the feed samples and flotation products for each size class are shown in the Appendix C.

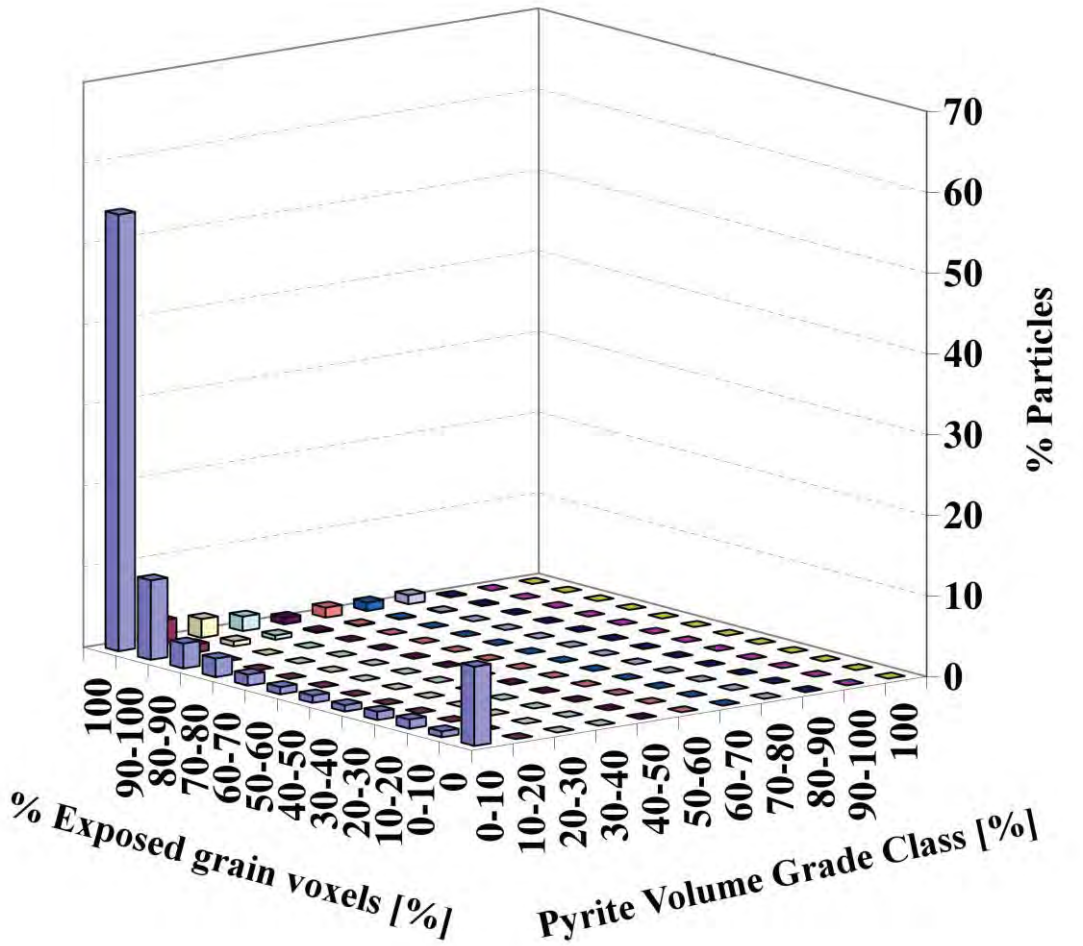

Figure 3.24 Exposure analysis of feed sample of size class 208x106 µm.

3.6.2.2.1 Feed samples. The results of the feed samples of the size classes 106x45 µm, 208x106 µm, 425x208 µm and 2000x425 µm are presented in Appendix B.

In all the size class most of the particles have a pyrite volume grade between 0 and 10%. In the size classes 106x45 µm and 208x106 µm there is a significant amount of particles with high pyrite grade (30-90% pyrite grade). The grains in those particles with a high pyrite grade are exposed or at least most of the grains are exposed. Also, the pyrite

grains in most of the particles in the size classes 106x45 µm and 208x106 µm were classified as 90-100% and 100% exposed grain percentage class.

In the size classes 425x208 µm and 2000x425 µm the pyrite grains had better distribution into the exposed grain percentage classes. The distribution of the size class 2000x425 µm was uniform in the exposed grain classes. In these size classes the particles have a low pyrite volume grade.

3.6.2.2.2 Products of flotation test with cleaner flotation stage (test# 1). The results of flotation test # 1 are presented in Appendix B for concentrate 1, cleaner concentrate, cleaner tailings and tailings.

In concentrate 1 most of the particles had high exposed grain percentage (90-100%) and there was significant amount of particles with a high pyrite volume (30%-90%). In the size classes 106-45 µm and 208x106 µm there were several particles with pyrite grains that were not exposed (0% exposed grains).

In all the size classes of the cleaner concentrate the number particles with a high pyrite grade (30%-90%) decreased in comparison with the concentrate 1. Most of the particles in the cleaner concentrate had a pyrite grade between 0% and 10%. Also, most of the particles had an exposed grain between 70%-100%. In the size classes 106x45 µm and 208x106 µm there were some particles with no exposed grains that were recovered. The size classes 425x208 µm and 2000x425 µm were less affected in the decrement of particles with high pyrite grade. In the size classes 425x208 µm and 2000x425 µm several particles with a pyrite grade between 10% and 70% were collected.

In the cleaner tailings most the particles had a pyrite grade between 0% and 10%. These particles had a high percentage of exposed grains (70%-100%). In the size classes

106x45 µm and 208x106 µm particles with no exposed grains were found. The size class 2000x425 µm was the only size class with certain amount of particles a pyrite grade between 10% and 40%, of course these particles had a exposed grains percentage between 90%-100%.

In the tailings the particles had a pyrite volume grade between 0 and 10%. The pyrite grains in most of the particles in the size classes 106x45 µm and 208x106 µm were classified as 90-100% and 100% exposed grains class. In the size classes 425x208 µm and 2000x425 µm the pyrite grains were well distributed into the exposed grain percentage classes. The distribution of the size class 2000x425 µm was uniform in the exposed grain percentage classes.

3.6.2.2.3 Products of flotation test without cleaner flotation stage (test# 2). The results of flotation test # 2 are presented in Appendix B for concentrate 1, concentrate 2, concentrate 3 and tailings.

In concentrate 1 most of the particles had high exposed grain percentage (90-100%) and there was significant amount of particles with a high pyrite volume (30%-90%). In the size classes 106-45 µm and 208x106 µm there are particles with pyrite grains that were not exposed (0% exposed grains).

In all the size classes of oncentrate 2 the number particles with a high pyrite grade (30%-90%) decreased in comparison with the concentrate 1. Most of the particles in concentrate 2 had a pyrite grade between 0% and 10%. Also, most of the particles had an exposed grain between 70%-100%. In the size classes 106x45 µm and 208x106 µm there were some particles with no exposed grains that were recovered. The size class 2000x425 µm was less affected in the decrement of particles with high pyrite grade.

In concentrate 3 most the particles had a pyrite grade between 0% and 10%. These particles had a high percentage of exposed grains (70%-100%). In the size classes 106x45 µm and 208x106 µm particles with no exposed grains were found. The size class 2000x425 µm was the only size class with certain amount of particles with pyrite grade between 10% and 40%, of course these particles had an exposed grain percentage between 90%-100%.

In the tailings the particles had a pyrite volume grade between 0 and 10%. The pyrite grains in most of the particles in the size classes 106x45 µm and 208x106 µm were classified as 90-100% and 100% exposed grains class. In the size classes 425x208 µm and 2000x425 µm the pyrite grains were well distributed into the exposed grain percentage classes. The distribution of the size class 2000x425 µm was uniform in the exposed grain percentage classes. The tailings in flotation test # 2 had more particles with no exposed grains that the tailings in flotation test # 1 in all the size classes.

3.6.2.2.4 Products of flotation with increment of collector dosage and low pH (test# 3). The results of flotation test # 3 are presented in Appendix B for concentrate 1, concentrate 2, concentrate 3 and tailings.

In concentrate 1 most of the particles had high exposed grain percentage (90-100%) and there was significant amount of particles with a high pyrite volume (30%-90%). The number of particles with high pyrite grade was much higher than the number of particles in the concentrate 1 of flotation test # 1 and # 2. In the size classes 106-45 µm there were particles with pyrite grains that were not exposed (0% exposed grains).

In all the size classes of concentrate 2 the number particles with a high pyrite grade (30%-90%) decreased in comparison with the concentrate 1. Most of the particles in

concentrate 2 had a pyrite grade between 0% and 10%. Most of the particles had an exposed grain between 70%-100%. In the size classes 106x45 µm and 208x106 µm there were some particles with no exposed grains that were recovered, particularly in the size class 106x45 µm. The size class 2000x425 µm was less affected in the decrement of particles with high pyrite grade. This size class had several particles with a pyrite grade between 10%-20%.

In concentrate 3 most the particles had a pyrite grade between 0% and 10%. These particles had a high percentage of exposed grains (70%-100%). In the size classes 106x45 µm and 208x106 µm particles with no exposed grains were found. The size class 2000x425 µm was the only size class with certain amount of particles with pyrite grade between 10% and 50%, these particles had an exposed grain percentage between 90%-100%.

In all the size classes of the tailings the particles had a pyrite volume grade between 0 and 10%. Most of the particles in the size class 106x45 µm were classified as 90-100% and 100% exposed grains class. In the size classes 208x106 µm and 425x208 µm most of the particles were classified as 100% and 0% exposed grain. The distribution of the size class 2000x425 µm was uniform in the exposed grain percentage classes. The tailings in flotation test # 3 had more particles with no exposed grains that the tailings in flotation test # 1, # 2 and # 3, particularly for the size classes 208x106 µm and 425x208 µm.

3.6.2.2.5 Products of flotation with a new collector and low pH (test# 4). The results of flotation test # 4 are presented in Appendix B for concentrate 1, concentrate 2, concentrate 3 and tailings.

In concentrate 1 most of the particles had high exposed grain percentage (90-100%) and there was significant amount of particles with a high pyrite volume (30%-90%). In the size classes 106-45 µm there were particles with pyrite grains that were not exposed (0% exposed grains).

In all the size classes of concentrate 2 the number particles with a high pyrite grade (30%-90%) decreased significantly in comparison with the concentrate 1. Most of the particles in concentrate 2 had a pyrite grade between 0% and 10%. Most of the particles had an exposed grain between 70%-100%. In the size classes 106x45 µm and 208x106 µm there were particles with no exposed grains, particularly in the in the size class 106x45 µm. The size class 2000x425 µm was less affected in the decrement of particles with high pyrite grade. This size class had several particles with a pyrite grade between 10%-50%.

In concentrate 3 most the particles had a pyrite grade between 0% and 10%. These particles had a high percentage of exposed grains (70%-100%), except for the size class 2000x425 µm. In the size classes 106x45 µm, 208x106 µm and 425x208 µm particles with no exposed grains were found. The size class 2000x425 µm was the only size class with particles that had a pyrite grade between 10% and 20%, these particles had an exposed grain percentage between 90%-100%.

In all the size classes of the tailings the particles had a pyrite volume grade between 0 and 10%. Most of the particles in the size classes 106x45 µm, 208x106 µm and 425x208 µm were classified as 90-100% and 100% exposed grains class. The distribution of the size class 2000x425 µm was uniform in the exposed grain percentage classes.

3.6.2.2.6 Summary. In general in concentrate 1 the particles have a high pyrite grade and high percentage of exposed grain voxels. In concentrate 2 the amount of particles with a high pyrite degree decreased. Most of the particles have a pyrite grade between 0% and 10%. However, percentage of exposed grain voxels is high (80%-100%) for the particles. In concentrate 3 practically all the particles have a pyrite grade between 0% and 10%. The percentage of exposed grain voxels varied between 70-100%. Particles with only internal grains were collected in the concentrates.

The particles in the tailings have a pyrite grade between 0% and 10%. In the size classes 425x208 µm, 208x106 µm and 106x45 µm most of the particles have percentage of exposed grain voxels of 100% and 0%. In the size class 2000x425 µm the particles are well distributed in all the exposed grain classes.

In concentrate 1 the particles with a high pyrite grade and high exposure of the pyrite grains were recovered. The high pyrite grade and exposure allows a better interaction between the collectors and the pyrite surface to increased hydrophobicity of the particles.

The particles with a lower pyrite grade are collected in concentrate 2 because the collectors acted on less pyrite surface and the hydrophobicity of these particles is in less proportion. These particles need more time for being collected in the concentrates.

In concentrate 3 the particles have a lower pyrite grade but the pyrite grains are exposed. In these particles the pyrite surface is limited and therefore the interaction between the collectors and the pyrite surface is minimized. These particles are collected at the end in concentrate 3 because they need more time.

Some particles with no exposed grains are collected in the concentrates because they are dragged into concentrate by other hydrophobic particles.

CHAPTER 4

PRODUCTS FROM FLOTATION PLANT OPERATIONS, RESULTS, ANALYSIS, AND DISCUSSION

Results from the analysis of samples collected from the flotation circuit are presented in this chapter. The particle size distributions and pyrite mass percent from the chemical analysis of feed, concentrate and tailings are discussed in Section 4.1. The results from the HRXMT analysis and pyrite volume grade determination are presented in Section 4.2. The correlation of pyrite grade from chemical and HRXMT analysis are presented in Section 4.3. The chemical analysis results were used to calculate the mass balance in the flotation circuit. Flow rates, % solids and pyrite grade in the flotation circuit are presented in Section 4.4 and Appendix D. The liberation-limited grade/recovery curves from the feed samples for different size classes are presented in Section 4.5. The pyrite recovery and pyrite grade of concentrate in the different size classes are compared with the liberation-limited grade/recovery curves in Section 4.6. Next, in Section 4.7 the exposure analysis or texture of samples is presented. Finally, the results from MLA and HRXMT analysis are compared and discussed in Section 4.8.

4.1 Chemical Analysis and Particle Size Distributions of Flotation Products

. Each flotation product was separated into different size classes and representative samples were analyzed for feed, concentrate, and tailings. Also, composite samples were analyzed. The sulfide sulfur was determined in all the samples of feed, concentrate, and tailings . The pyrite mass percent was estimated from the sulfide sulfur using the pyrite formula (FeS_2). It was assumed that all the sulfide sulfur belongs to pyrite. The pyrite mass percent and the pyrite distribution into the size classes for feed, final concentrate and tailings are presented in Tables 4.1 - 4.3. Also, the particle size distributions of feed, final concentrate and tailinsgs are shown in the Tables 4.1 - 4.3.

The P80 values for feed, concentrate and tailings were 136 µm, 68 µm and 161 µm, respectively. In the feed, concentrate, and tailings the -25 µm size class has the greatest mass percent. The particle size distributions for feed and tailings are similar. The particle size distribution (PSD) of the concentrate is finer in comparison with the PSD of the feed and tailings. The particles are of much finer size in the concentrate. The mass percent of the -25 µm and the 45x25 µm size classes is greater than the mass percent of these size classes in the feed and tailings. In the concentrate, particles of the 2000x425 µm size class were not found. It seems that the particles in the fine size classes are easily recovered in the concentrate. Probably this is due to good liberation and exposure of pyrite grains when compared with the coarse particles.

Clearly, the pyrite content in the concentrate is significantly higher than in the feed and tailings. It was expected that the feed sample had a greater pyrite content than the tailings samples. This occurred for the size classes 106x45 µm, 45x25 µm and -25 µm.

Table 4.1

Particle Size Distribution, Pyrite Mass Percent from Chemical Analysis, and Pyrite Distribution in the Flotation Circuit Feed

Size Class [µm]	PSD [%] P80 = 136 µm	Pyrite [%]	Pyrite Distribution [%]
2000x425	0.56	1.74	0.29
425x208	5.65	1.89	3.17
208x106	19.30	3.03	17.35
106x45	20.23	5.29	31.76
45x25	5.65	5.41	9.07
-25	48.60	2.66	38.36
Composite	-	3.18	100.00

Table 4.2

Particle Size Distribution, Pyrite Mass Percent from Chemical Analysis, and Pyrite Distribution in the Flotation Plant Final Concentrate

Size Class [µm]	PSD [%] P80 = 68 µm	Pyrite [%]	Pyrite Distribution [%]
2000x425	0.00	0.00	0.00
425x208	0.13	21.29	0.11
208x106	5.00	33.71	6.88
106x45	18.81	41.61	31.96
45x25	7.59	39.44	12.22
-25	68.47	17.46	48.82
Composite	-	24.98	100.00

Table 4.3

Particle Size Distribution, Pyrite Mass Percent from Chemical Analysis, and Pyrite Distribution in the Flotation Plant Tailings

Size Class [µm]	PSD [%] P80 = 161 µm	Pyrite [%]	Pyrite Distribution [%]
2000x425	1.04	1.93	0.91
425x208	7.78	2.04	7.20
208x106	21.60	3.01	29.50
106x45	19.99	3.22	29.21
45x25	5.28	2.86	6.85
-25	44.30	1.31	26.33
Composite	-	1.98	100.00

However in the size classes 2000x425 µm, 425x208 µm and 208x106 µm the pyrite percent in the tailings was slightly greater that the feed. The method and procedure for sampling of the plant products are unknown, the sample was done by plant personnel. The 1 kg samples from the flotation circuit were received after the samples were prepared in the metallurgy laboratory at plant operations. The error from the sampling method, procedure, and sample preparation may decrease the accuracy of the chemical analysis, especially in the coarse size classes. This may account for the pyrite grade in the tailings for some size classes having a greater value than the feed.

It can be observed in Tables 4.1 – 4.3 that the pyrite content of the size class 2000x425 µm is very small in comparison with the other size classes as expected for P80 of 136 µm.

In the feed and tailings the pyrite is contained principally in the size classes 208x106 µm, 106x45 µm and -25 µm. In the concentrate the pyrite is contained in the size classes below 106 µm. The percentage mass percent of the size class 45x25 µm in the feed, final

concentrate and tailings is small. Thus pyrite contribution from size class 45x25 µm is not significant as the pyrite contribution from size class -25 µm.

4.2 HRXMT Analysis of Flotation Products

Representative samples of different size classes from feed, concentrate and tailings were analyzed by HRXMT. Representative samples of the size classes 2000x425 µm, 425x208 µm, 208x106 µm, 106x45 µm, 45x25 µm were prepared and analyzed by HRXMT. The size class -25 µm was not analyzed because of resolution limitations and the partial volume effect. Section images of the reconstructed particles for the feed, concentrate, and tailings are shown in Figure 4.1. The images correspond to the size class 208x106 µm, the black color corresponds to the air void between the particles, the dark gray color corresponds to the gangue minerals, most of the bright grains are pyrite. Only a few of the bright grains are higher density minerals such as chalcopyrite and gold.

It can be observed that there is a notorious difference between the concentrate and the other two samples (feed and tailings) in terms of pyrite-containing particles. The concentrate has lot of pyrite-containing particles (bright grains). In the feed the amount of pyrite-containing particles is much less than in the concentrate. In the tailings apparently the number of pyrite-containing particles is less than the number of pyrite-containing particles in the feed.

The pyrite grains in the concentrate appear to have a higher degree of liberation than the pyrite grains in the feed and tailings. This makes sense because in the concentrate the pyrite grains with a better exposure and liberation are recovered. The pyrite grains with a better exposure have more change of being recovered in the concentrate.

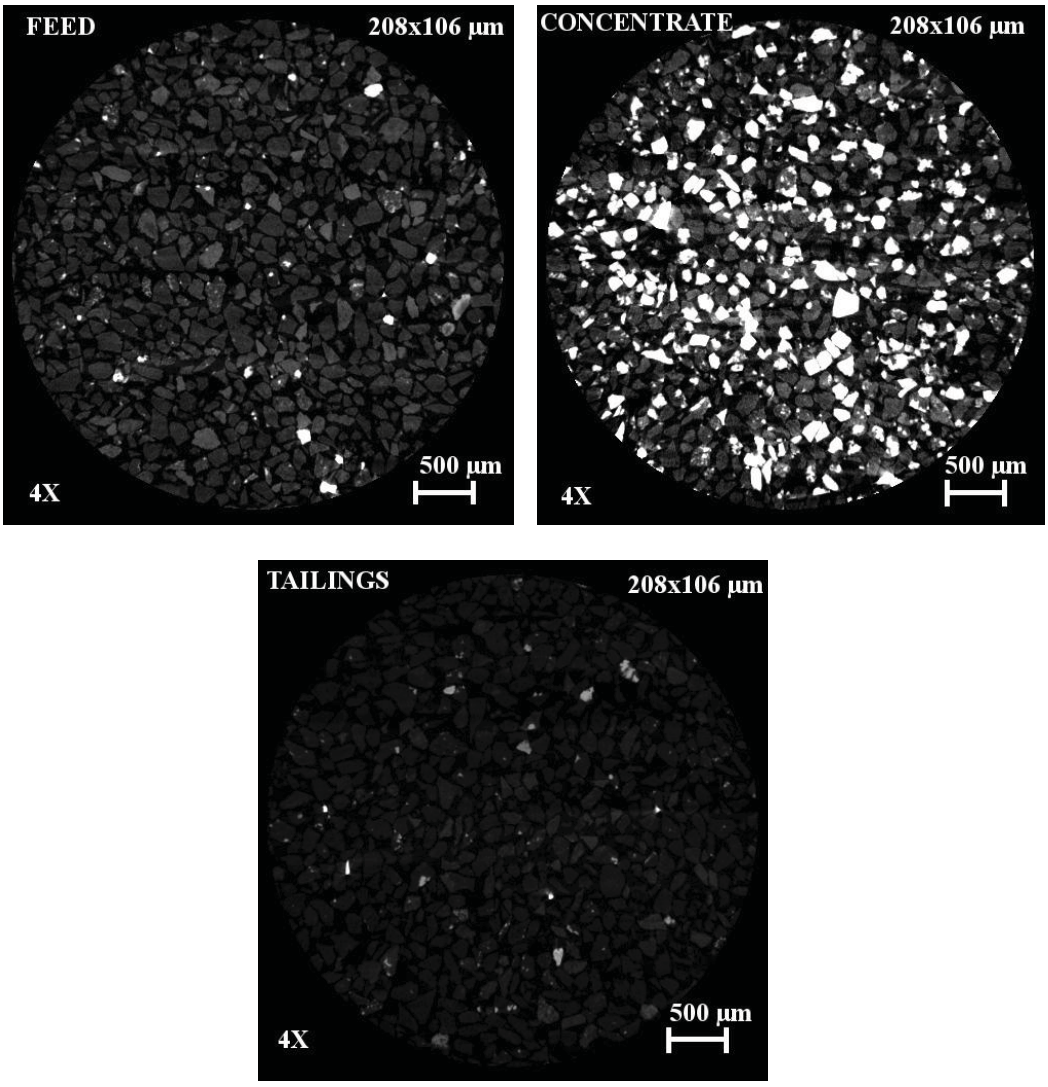

Figure 4.1 Section images of feed, concentrate and tailings for size class 208x106 µm.

In the feed and tailings most of the pyrite grains are locked in the section images. The pyrite volume grade of each sample was calculated from the HRXMT analysis. The pyrite volume grade is based on the number of voxels corresponding to pyrite and the total number of voxels of each sample. The pyrite volume grade results from the HRXMT analysis are shown in Table 4.4. The concentrate does not have particles in the size class 2000x425 µm.

Table 4.4

Pyrite Volume Grade from HRXMT Analysis for Flotation Circuit Samples

	Pyrite volume grade [%]		
Size Class [µm]	Feed	Concentrate	Tailings
2000x425	0.56	-	0.90
425x208	0.85	16.96	0.86
208x106	2.29	22.29	1.49
106x45	3.51	25.12	2.87
45x25	4.90	21.39	4.24

For the size classes 2000x425 µm and 208- 425 µm the pyrite volume grade of the tailings and the volume grade of pyrite in the feed are small. Similar tendency was found in the chemical analysis results of pyrite.

4.3 Correlation of HRXMT Data and Chemical Analysis

The correlation between pyrite volume grade from HRXMT analysis and the pyrite mass grade from chemical analysis is shown in Figure 4.2. The data presented in Figure 4.2 correspond to samples from the feed, concentrate, and tailings for different size classes. In total 14 samples were compared. The relation predicted from Equation 3.1 (Section 3.3) was calculated using a pyrite density of 5.09 g/cm^3 and a density for the gangue minerals of 2.87 g/cm^3. The solid gray line corresponds to the values predicted from Equation 3.1. There is a good correlation between the pyrite volume grade from HRXMT analysis and the pyrite mass percent from the chemical analysis.

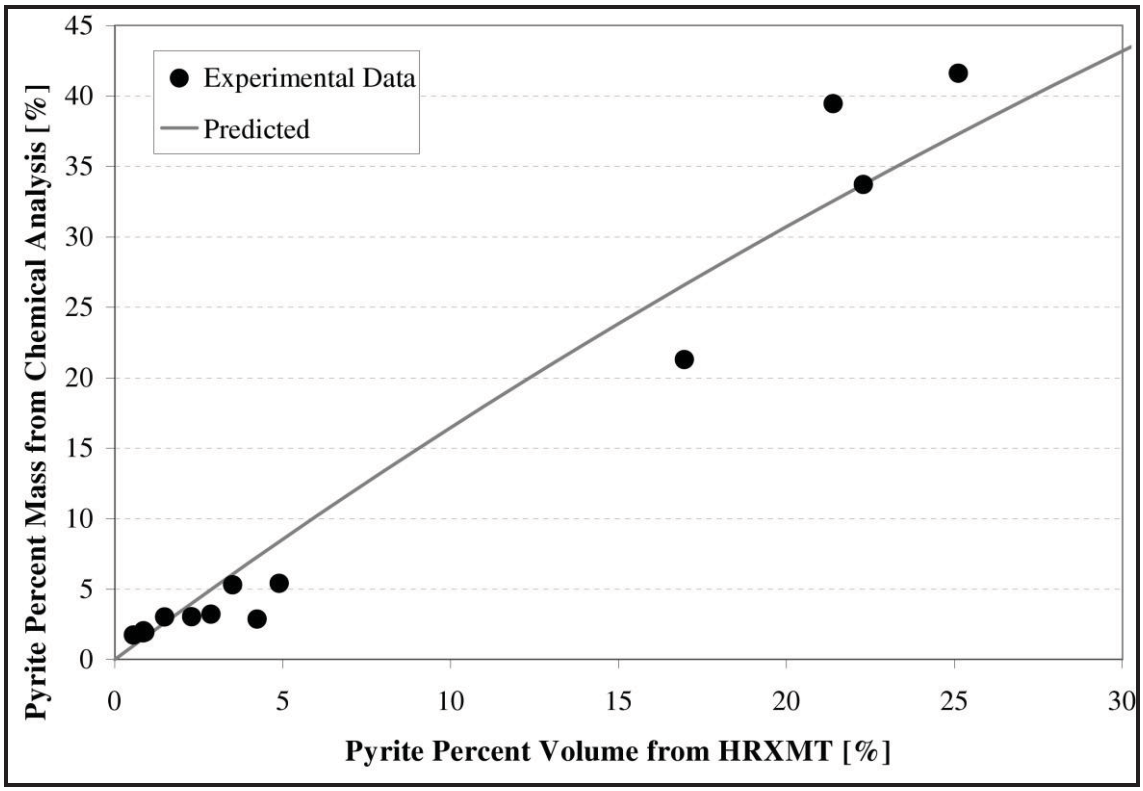

Figure 4.2 Correlation between pyrite volume grade from HRXMT analysis and pyrite mass grade from chemical analysis. The predicted line is calculated from the Equation 3.1 with a density of gangue minerals = 2.87 g/cm^3 and pyrite density = 5.09 g/cm^3.

4.4 Mass Balance of Flotation Circuit from Chemical Analysis

Details of the design of the plant flotation circuit were not provided, as it was explained that samples were taken from the feed to the flotation circuit, final tailings and final concentrate. The solids flow rates for the flotation circuit are unknown for this study. Therefore the flotation circuit is considered as a system with one input (feed) and two outputs (final concentrate and tailings). In this flotation circuit the slurry flow rate and the % solids of the feed are known, also the density of the concentrate slurry is known. A schematic of the flotation circuit and the known variables are illustrated in Figure 4.3. The pyrite grades (mass percent calculated from chemical assays of composite samples) were used to determine the pyrite recovery from the two-product formula

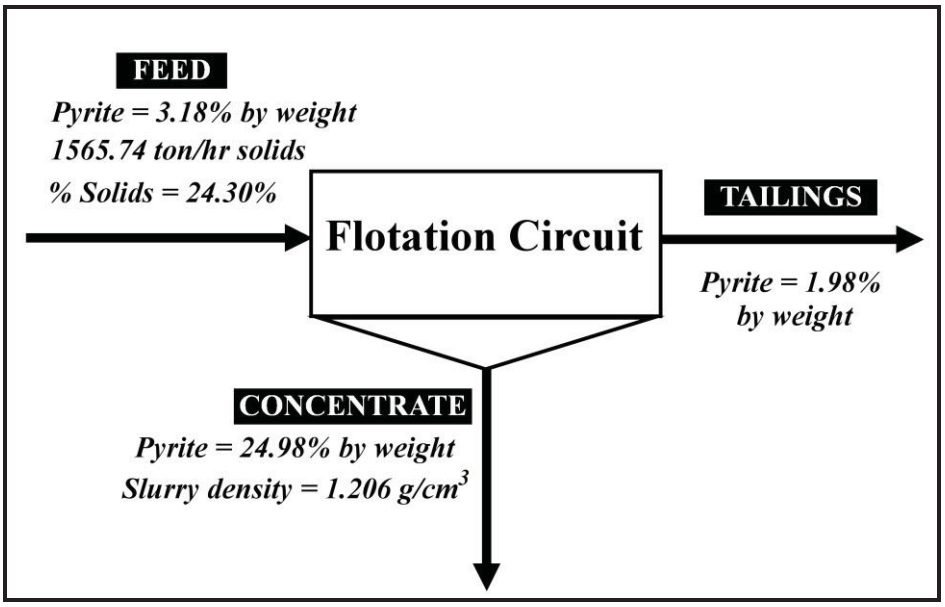

Figure 4.3 Schematic flotation circuit and known variables for flotation circuit ore.

(Equation 4.1). The ratio of concentration was calculated using Equation 4.2. The flow rate of the concentrate slurry was calculated from the ratio of concentration. Finally, the flow rate of the tailings slurry was estimated by subtraction of the concentrate slurry flow rate from the feed flow rate (Equation 4.3). The % solids in the concentrate slurry was calculated from the density of the concentrate slurry using the Equation 4.4. The density of the concentrate was calculated from Equation 4.5, the densities for the pyrite and gangue minerals used in Equation 4.4 were 5.09 g/cm^3 and 2.87 g/cm^3, respectively. The flow rate of solids in each stream was calculated from the flow rate of the slurries and the % solids.

The results of pyrite recovery and the mass balance for solids in the flotation circuit are shown in Table 4.5. A diagram with the mass balance for the solids and water are given in Appendix D.

Table 4.5

Pyrite Recovery, Flowrates and % Solids in Flotation Circuit

	Slurry flowrate [ton/hr]	% Solids	Solids flow rate [ton/hr]	Pyrite Recovery [%]	Pyrite Grade Mass percent [%]
Feed	1565.74	24.30	380.47	-	3.18
Concentrate	79.98	24.77	19.81	40.89	24.98
Tailings	1485.76	24.27	360.66	59.11	1.98

Based on the characteristics of the samples taken from the plant flotation circuit the pyrite recovery was calculated to be 40.39%. It has been reported from plant operations that on a regular basis a pyrite recovery is expected to be 70%. The pyrite recovery is low and suggests that the separation efficiency of pyrite in the flotation circuit could be improved.

$$R = \frac{c(f-t)}{f(c-t)} \cdot 100 \tag{4.1}$$

$$\frac{F}{C} = \frac{(c-t)}{(f-t)} \tag{4.2}$$

$$T = F - C \tag{4.3}$$

$$X = \left[\frac{1}{\rho_{SlurryC}} - \frac{y}{\rho_{Water}} \right] \cdot \rho_C \cdot 100 \tag{4.4}$$

$$\frac{1}{\rho_C} = \frac{m_{py}}{100 \cdot \rho_{Py}} + \frac{(100 - m_{Py})}{100 \cdot \rho_G} \tag{4.5}$$

where,

R = Pyrite recovery from flotation circuit [%]

f = Pyrite grade of feed [%]

c = Pyrite grade of concentrate [%]

t = Pyrite grade of tailings [%]

F = Flow rate of feed [ton/hr]

C = Flow rate of concentrate [ton/hr]

T = Flow rate of tailings [ton/hr]

m_{Py} = Pyrite percent by mass [%]

ρ_G = density of gangue minerals [g/cm^3]

ρ_C = density of concentrate [g/cm^3]

X = percent solids of concentrate

$\rho_{SlurryC}$ = Density of concentrate slurry [g/cm^3]

y = water fraction in the concentrate slurry

ρ_{Water} = density of water [g/cm^3]

4.5 Liberation-Limited Grade/Recovery Curves for Flotation Products

As it was explained previously the liberation-limited grade/recovery curves represent the boundary for separation efficiency for each feed particle size class. The curves predict

the maximum pyrite recovery and concentrate grade for each particle size class that can be achieved in the flotation process considering pyrite liberation as the only limitation.

The liberation-limited grade/recovery curves were calculated for the size classes 45x25 µm, 106x45 µm, 208x106 µm and 425x208 µm. The liberation-limited grade/recovery curve for the size class 2000x425 µm was not calculated because of the limited number of particles. Most of the sample in this size class was used for chemical analysis and only 115 particles were analyzed by HRXMT. The liberation-limited grade/recovery curves of the size classes 45x25 µm, 106x45 µm, 208x106 µm and 425x208 µm are shown in Figure 4.4.

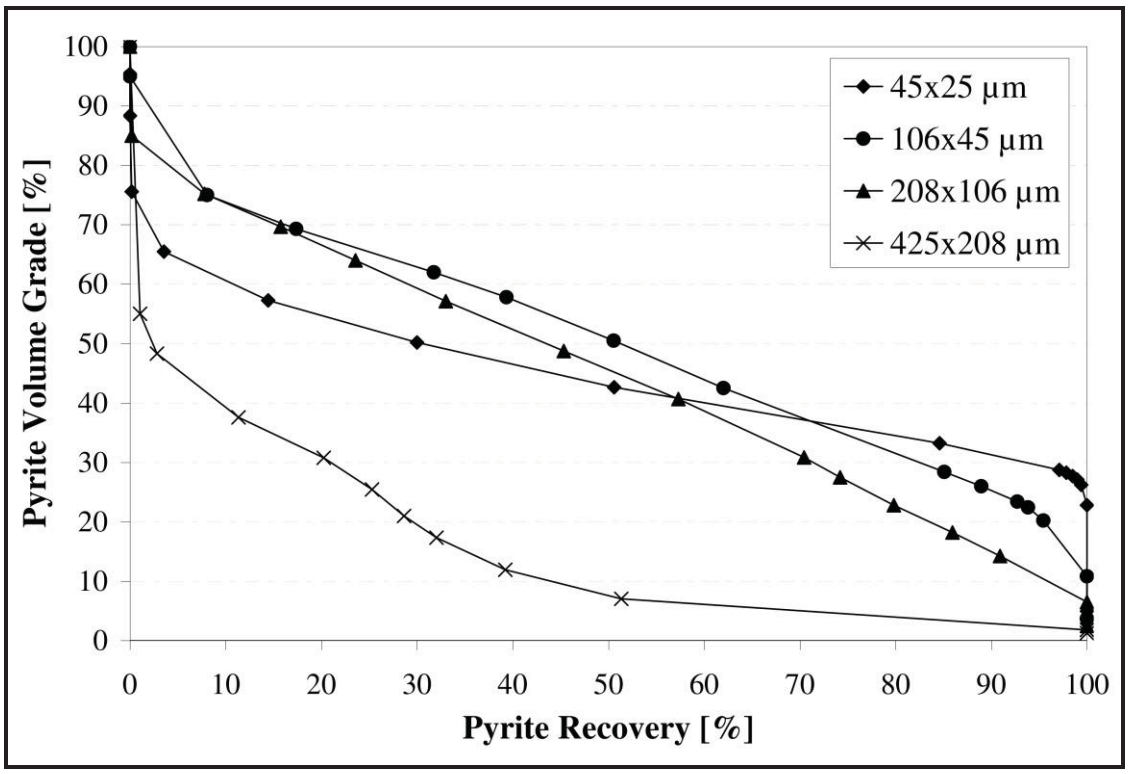

Figure 4.4 Liberation-limited grade/recovery curves from HRXMT analysis feed samples for flotation circuit ore.

From these results it is evident that when the particle size is reduced better pyrite liberation is achieved and a higher pyrite grade can be obtained. The liberation-limited grade/recovery curve for the size class 45x25 μm is above the curve for the size classes 106x45 μm and 208x106 μm in the region of high pyrite recovery (70-100%). However liberation-limited grade/recovery curve for the size class 45x25 μm is below the curves for the size classes 106x45 μm and 208x106 μm when the pyrite recovery lower than 70%. This unexpected behavior of the liberation-limited grade/recovery curve for the size class 45x25 μm is caused by the resolution limitation and the partial volume effect. For the liberated grains and high pyrite grade particles the degree of liberation is reduced due to the partial voxel effect. The small particles are described by a reduced number of voxels therefore the influence of the partial volume effect is more significant in the case of small particles. In the future a non local mean filter will be included in the particle segmentation process. The non local mean filter will smooth the noise preserving the edges of the particles and it will reduce significantly the partial volume effect that decreases mineral liberation of the fine particles (Buades et al. 2005) This filter has been tested successfully for 2D images. A 3D algorithm for the non local mean is still in the development stage.

4.6 Discussion of Results from HRXMT Analysis for Flotation Products

Pyrite recovery in the concentrate for each size class was calculated as was done for mine site ore (Section 3.4.2) using Equations 3.2-3.6. In this case the particle size distribution, densities of pyrite and gangue material, and mass balance of the flotation

circuit (Section 4.4) were used to determine the volumetric rate (m^3/hr) of each size class for each product. The pyrite volume grade of the feed was calculated for each size class from the pyrite volume grade of the tailings and concentrate. The pyrite volume grade used for these calculations was determined from HRXMT analysis. The calculated pyrite volume grade of the feed and the pyrite recovery are shown in the Table 4.6. The calculated pyrite volume grade of feed was greater than the pyrite volume grade from HRXMT analysis probably except in the size class 208x106 µm. The difference in the calculated pyrite grade of the feed and the pyrite grade from HRXMT analysis is due to the sampling and analysis errors.

The liberation-liberation grade/recovery curves of each size class were compared with the pyrite recovery and pyrite volume grade of the concentrate. The pyrite recovery and pyrite volume grade of the concentrates for each size class are shown in Table 4.7.

Table 4.6

Comparison of Pyrite Volume Grade of Flotation Feed from HRXMT Analysis and Calculated Pyrite Volume Grade

	Pyrite volume grade of flotation feed [%]	
Size Class [µm]	HRXMT analysis	Calculated
2000x425	0.56	1.57
425x208	0.85	1.14
208x106	2.29	1.85
106x45	3.51	3.75
45x25	4.90	5.11

Table 4.7

Pyrite Recovery and Pyrite Volume Grade of Concentrate

for each Size Class in flotation circuit ore

Size Class [µm]	Mass Percent [%]	Pyrite Recovery [%]	Concentrate Pyrite volume grade [%]
2000x425	0.00	-	-
425x208	0.41	1.59	16.96
208x106	15.86	14.10	22.29
106x45	59.66	27.91	25.12
45x25	24.07	26.07	21.39

The results for pyrite recovery and pyrite volume grade of the concentrate from HRXMT analysis are plotted with the corresponding liberation-limited grade/recovery curves for each size class to determine if the separation efficiency is limited only by the pyrite liberation. The liberation-limited grade/recovery curves with the corresponding pyrite recovery and pyrite volume grade of concentrate for the size classes 45x25 µm, 106x45 µm, 208x106 µm and 425x208 µm are shown in Figures 4.5 - 4.8, respectively.

The pyrite recovery and pyrite volume grade of the concentrate for all the size classes are below the liberation-limited grade/recovery curves. The results suggest that the separation efficiency of all size classes for the flotation circuit ore is limited by other factors in addition to liberation.

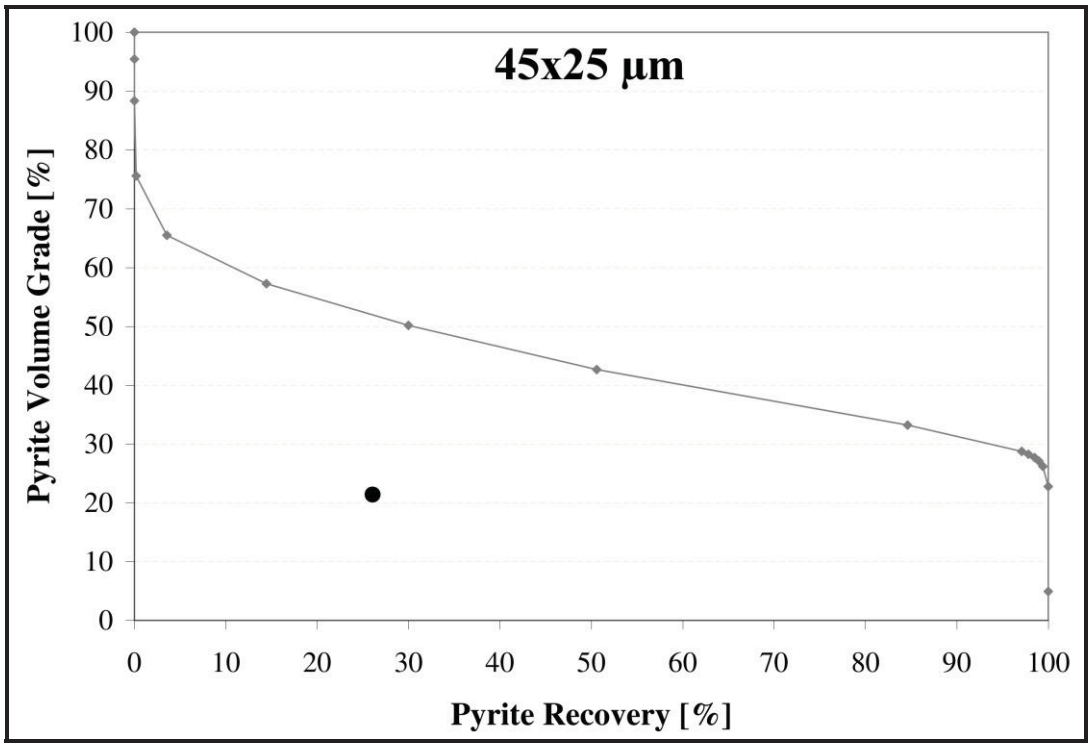

Figure 4.5 Pyrite recovery and pyrite volume grade of concentrate with the corresponding liberation-limited grade/recovery curve for size class 45x25 µm.

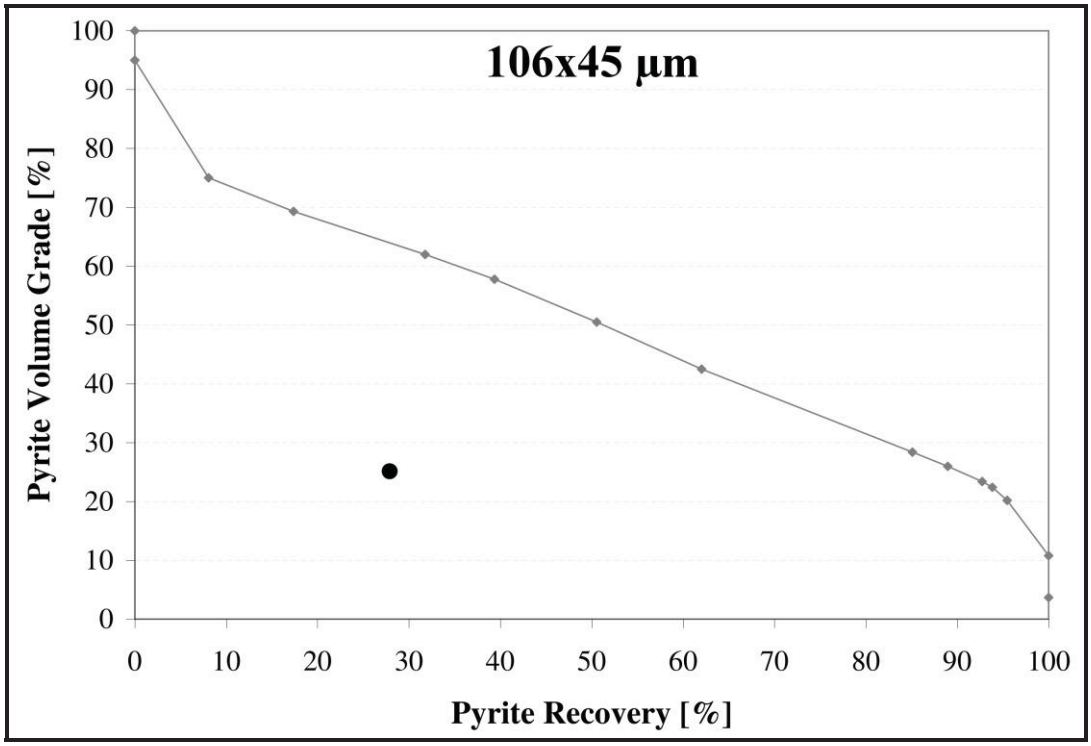

Figure 4.6 Pyrite recovery and pyrite volume grade of concentrate with the corresponding liberation-limited grade/recovery curve for size class 106x45 µm.

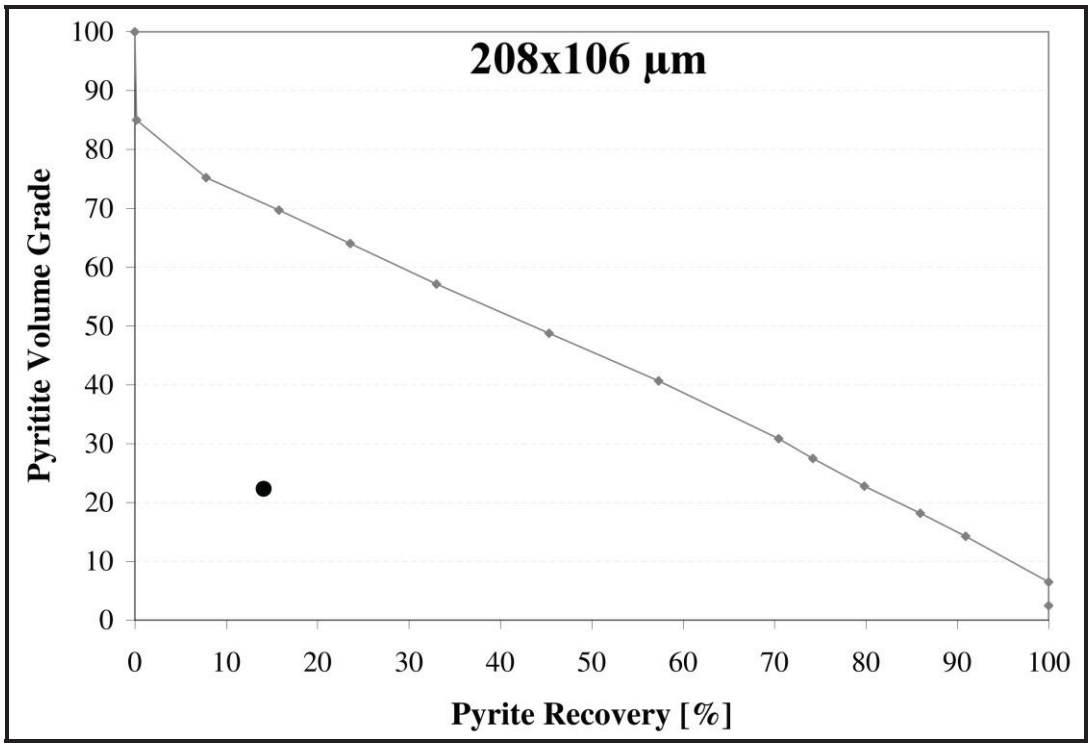

Figure 4.7 Pyrite recovery and pyrite volume grade of concentrate with the corresponding liberation-limited grade/recovery curve for size class 208x106 µm.

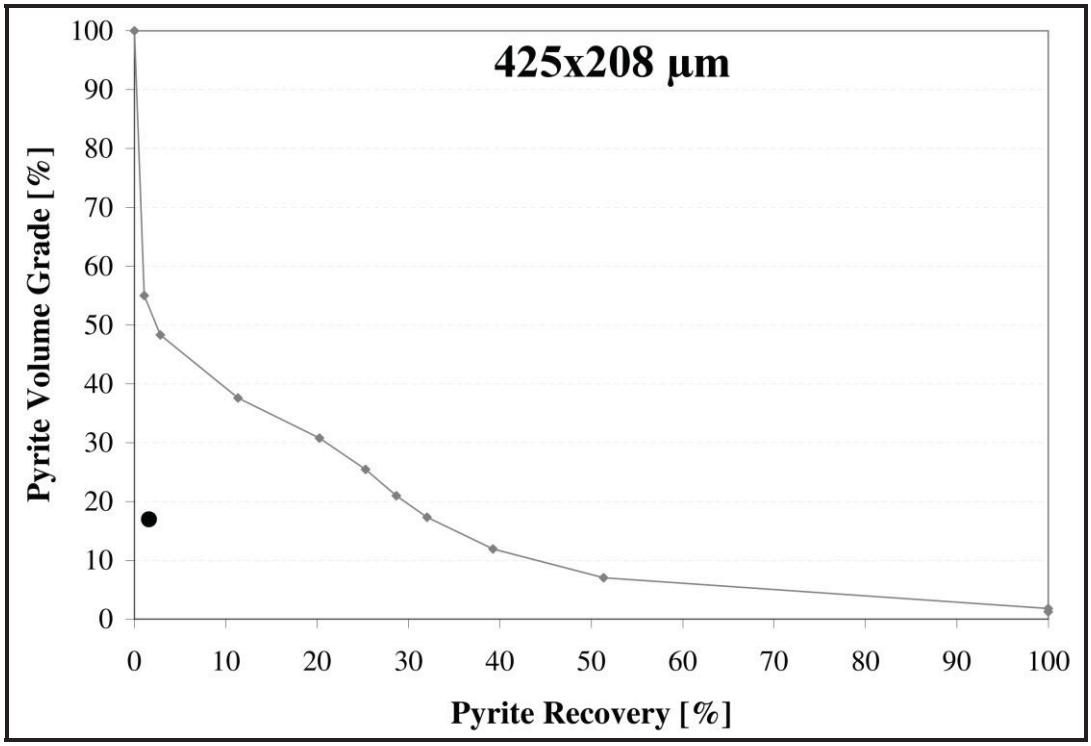

Figure 4.8 Pyrite recovery and pyrite volume grade of concentrate with the corresponding liberation-limited grade/recovery curve for size class 425x208 µm.

4.7 Exposure Analysis of Flotation Products

The exposure analysis of flotation circuit samples from the HRXMT analysis was completed to determine the percentage of voxels for internal and exposed grains of pyrite for the entire sample and the percentage of voxels for exposed and internal grains of pyrite for individual particles in the samples. The exposure analysis calculations were done in similar way to the exposure analysis for mine site ore. The samples of feed, concentrate, and tailings for the different size classes were analyzed.

4.7.1 Internal and Exposed Grains of Entire Samples

The percentage of exposed and internal grain voxels was determined for the pyrite-containing particles in the entire samples. The percentages of internal and exposed pyrite grain voxels are shown in Figure 4.9.

In general the percentage of exposed grain voxels is high for most of the samples. The percentage is greater than 90% for the particles below the size class 2000x425 µm. Most of the pyrite grains are exposed particularly for the fines particles.

The feed the size class 2000x425 µm has the lowest percentage of exposed grain voxels (75.81%). The size class 425x208 µm has a percentage of exposed grain voxels of 93.34%. The percentage of exposed grain voxels for the size classes 208x106 µm, 106x45 µm and 45x25 µm was greater than 98%.

In the concentrate all the size classes have a percentage of exposed grain voxels greater than 99%, practically all the pyrite grains are exposed in the concentrate.

In the tailings the size class 2000x425 µm has the lowest percentage of exposed grain voxels with a value of 85.05%. The size class 425x208 µm has a percentage of exposed

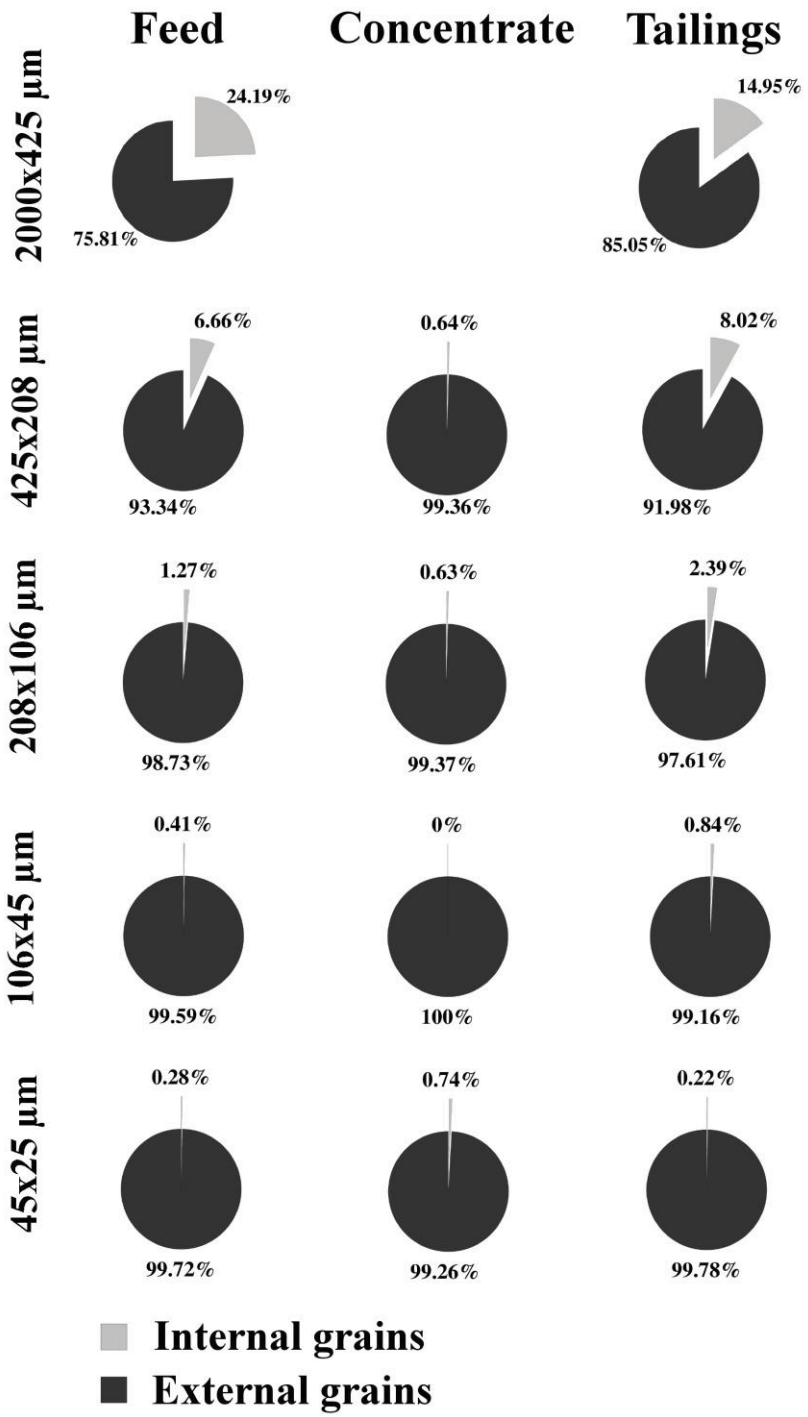

Figure 4.9 Percentage of internal and exposed grain voxels for Flotation circuit samples

grain voxels of 91.98%. The size classes 208x106 µm, 106x45 µm and 45x25 µm have a percentage of exposed grain voxels greater than 97.50%.

As it was expected the tailings samples have a lower percentage of exposed grain voxels than the feed samples. The only exception occurred for the size classes 2000x425 µm and 45x25 µm which have a lower percentage of exposed grain voxels in the feed. In the case of the size class 45x25 µm the difference is very small. In the feed, concentrate and tailings practically all the pyrite grains are exposed for particles below 208 µm in size. In the size classes 2000x425 µm and 425x208 µm, the amount of internal grains in the particles is significant.

4.7.2 Internal and Exposed Grains of Individual Particles

The percentage of exposed and internal voxels was determined for individual particles in all the samples of flotation circuit ore. The particles were classified into 122 groups with different pyrite volume grade and percentage of exposed voxels as explained in the Section 3.6.2.2. The results for the different size classes of the feed, concentrate and tailings are presented in 3D plots in Appendix E.

The 3D plots for the feed to the flotation circuit for the different size classes are shown in Appendix D. In the size class 45x25 µm most of the particles have a pyrite grade between 0 and 60%. Most of the particles have a high percentage of exposed grain voxels (90-100%). In the pyrite grade class 0-10% there is a small percentage of particles with only internal grains (0% exposed grains).

In the size class 106x45 µm most of the particles have a pyrite grade between 0 and 10%. There are a lot of particles with a pyrite grade between 10% and 70%, but those

particles with a high pyrite grade decrease in comparison with size class 45x25 µm. Also, there is an increment of the particles with only internal grains (0% exposed grains).

In the size class 208x106 µm, most of the particles have a pyrite grade between 0% and 10%. And most the particles in this pyrite grade class are classified in the exposed grain voxel classes 0%, 90-100% and 100%. Particles with a pyrite grade between 10% and 70% are present in this size class but in less proportion. These particles with a high pyrite grade were classified in the exposed grain classes 90-100% and 100%.

In the size class 425x208 µm practically all the particles have a pyrite grade between 0% and 10%. Most of the particles have a percentage of exposed grain voxels between 80%-100%. The amount of particles with only internal grains (0% exposed grains) is similar to the size class 208x106 µm.

In the size class 2000x425 µm again most of the particles have a pyrite grade between 0% and 10% similar to the size class 425x208 µm but in this case the particles have a better distribution in all the exposed grain classes.

The exposure results of the concentrate from the plant flotation circuit are shown in Appendix D. In the size class 45x25 µm the particles have pyrite grade between 0% and 60% and the most of the particles are classified with a percentage of exposed grain voxels between 80%-100%.

In the size class 106x45 µm all the pyrite grains are exposed (100%) and the pyrite grade varied between 0% and 70%.

In the size class 208x106 µm the particles have pyrite grade that varied between 0% and 80%, the pyrite grade classes have similar values. Most of the particles were

classified in the exposed grain voxel classes 90%-100% and 100%. There is a significant amount of particles with only internal pyrite grains (0% exposed grains).

In the size class 425x208 µm most of the particles have a pyrite grade between 0% and 70%. Most of these particles are classified in the exposed grain voxel classes 90-100% and 100%, particularly in the class 90-100%.

The exposure results of the tailings from the plant flotation circuit are shown in Appendix D. In the size class 45x25 µm most of the particles have pyrite grade between 0% and 60%. These particles have a percentage of exposed grain voxels between 90%-100%. Most of particles in the size class have a high pyrite grade and are exposed but they were not recovered in the concentrate.

In the size class 106x45 µm most of the particles have a pyrite grade between 0% and 10%. There are particles with a pyrite grade between 10% and 70% but in less proportion in comparison with the size class 45x25 µm. Most of the particles were classified in the exposed grain voxel classes 0%, 90%-100% and 100%.

In the size class 208x106 µm most of the particles have a pyrite grade between 0% and 10%. The amount of particles with a pyrite grade between 0% and 70% was decreased significantly in comparison with the particles in the size class 106x45 µm. Most of the particles have a percentage of exposed grain voxels between 80%-100%, the other classes have a lower percentage. There is a significant amount of particles with only internal pyrite grains (0% exposed grains).

In the size class 425x208 µm practically all the particles have a pyrite grade between 0% and 10%. Most of the particles were classified in the exposed grain voxel classes 0%, 90%-100% and 100%, the other classes have a lower percentage.

In the size class 2000x425 µm the particles have a pyrite grade between 0% and 10%. Most of the particles have a percentage of exposed grain voxels between 40% and 100%, the other classes have a lower percentage.

The particles with a high pyrite grade and high exposure are recovered in the concentrate. The high pyrite grade and pyrite exposure enhances the recovery of these particles in the concentrate. The interaction of the collector with the pyrite surface is better and these particles have greater possibility to be floated.

In the tailings particles with a high pyrite grade and exposure of pyrite grains are found, especially in the size classes 106x45 µm and 45x25 µm. These particles are lost in the tailings because other factors in addition to the liberation and exposure of pyrite are affecting the recovery of these particles in the concentrate.

4.8 Comparison of Pyrite Grade from MLA and HRXMT Analysis

Samples from feed, concentrate and tailings of flotation circuit ore were separated into different size classes and representative samples were analyzed by MLA. In the concentrate the size class 425x208 µm was not analyzed by MLA because the weight in this size class was limited and the entire sample was used for the chemical analysis. The size class 2000x425 µm was not analyzed because no particles were found in this size class.

MLA analysis provided information for individual particles. The pyrite area grade of each particle was estimated for all the samples. The particles in each sample were classified into 11 pyrite grade classes based on the area occupied by pyrite in each particle. The pyrite grade classes are: 0-10%, 10-20%, 20-30%, 30-40%, 40-50%, 50-

60%, 60-70%, 70-80%, 80-90%, 90-100% and 100%. The percentage of particles in each pyrite grade class was calculated. Based on the individual pyrite grade from MLA analysis the pyrite grade of the entire sample was calculated for each sample.

Similar analysis was elaborated from the HRXMT data of the particles in the samples. The particles were classified according to the pyrite volume grade. In the HRXMT results the same pyrite grade classes were used. The percentage of particles in each pyrite grade class was calculated.

In the Section 4.2 the pyrite volume grade from HRXMT analysis of each sample were presented. The pyrite areal grade from MLA analysis and pyrite volume grade from HRXMT analysis are compared in Table 4.8.

The difference between the pyrite grade from MLA and HRXMT analysis is evident. There is not a clear tendency in the difference between the pyrite grade results of the two methods. However it seems that the difference between the results in the coarse particles (425x208 µm and 2000x425 µm) is smaller than the difference between the results for the fine particles (45x25 µm, 106x45 µm and 208x106 µm).

The results of pyrite grade from MLA analysis and HRXMT analysis are presented in Appendix F. The percentage of particles in each pyrite grade class from MLA and HRXMT results are compared.

In the feed, concentrate and tailings it is evident that there is overestimation of the pyrite grade from the MLA results in comparison with HRXMT results. The amount of particles in the high pyrite grade classes (>50%) was greater in the MLA analysis. The overestimation of the pyrite grade is more accentuated in the fine particles (45x25 µm, 106x45 µm and 208x106 µm).

The pyrite grade from the MLA analysis is overestimated because the sectioned particles on the polished sections appear to be fully liberated. On the other hand in the HRXMT analysis the total volume of the particles is used for the pyrite grade calculations. Of course it should be considered that in the HRXMT analysis the voxel resolution limitation and the partial volume effect can reduce the pyrite volume grade, particularly in the fine particles.

Table 4.8

Comparison of Pyrite Grade from MLA and HRXMT Analysis

	Pyrite Grade [%]					
	Feed		Concentrate		Tailings	
Size Class [µm]	MLA (area)	HRXMT (volume)	MLA (area)	HRXMT (volume)	MLA (area)	HRXMT (volume)
2000x425	0.66	0.56	-	-	0.69	0.90
425x208	1.02	0.85	-	16.96	1.04	0.86
208x106	1.48	2.29	27.59	22.29	1.46	1.49
106x45	4.67	3.51	46.66	25.12	1.84	2.87
45x25	2.73	4.90	26.86	21.39	1.24	4.24

CHAPTER 5

SUMMARY AND CONCLUSIONS

5.1 Batch Flotation Experiments

The HRXMT analysis of pyrite ore revealed that in the particle size classes 2000x425 μm and 425x208 μm the pyrite grains are locked. For the particle size classes 208x106 μm and 106x45 μm, the pyrite grains appear have a high degree of liberation. It was found that reliable results can be obtained by HRXMT for mine site ore, including sample preparation, sample scanning and data processing. The size limitation for the HRXMT analysis of mine site ore was demonstrated for samples having a particle size small as 45 μm. At this particle size the results are affected by the partial voxel effect and limited by voxel resolution. In the future the non local mean filter will be implemented in the segmentation process and the partial volume effect will be reduced.

Of course, an overestimation of pyrite liberation for the two-dimensional analysis was expected. The analysis by HRXMT had a good correlation with chemical assays, and provides for a reliable quantitative analysis.

In general the best results were obtained in the flotation test # 3 and test # 5 in terms of pyrite recovery and grade of the overall concentrate. In test # 3 the collectors Cytec 208 and potassium amyl xanthate (PAX) were added in high dosage and the pH was ~5. In the test # 5, the flotation conditions were the same as in test # 3, the only difference

was the P80 of the feed. The test # 3 had a P80 of 262 µm and test # 5 had a P80 of 150 µm. In flotation test # 3 the excess of collector addition and the low pH improved the recovery and pyrite grade of the size classes 425x208 µm and 2000x425 µm. The improvement in these size classes has an important impact on the pyrite recovery and grade of the overall concentrate. In flotation test # 5 the P80 of the feed sample was 150 µm, the mass of the size class 106x45 µm was increased in comparison to the particle size distribution with a P80 of 262 µm. In general for all the flotation tests the size class 106x45 µm had the best results for pyrite recovery and concentrate grade. The size reduction increased the mass for the size class 106x45 µm and this mass increment of the size class 106x45 µm affected positively the pyrite recovery and grade of the overall concentrate for flotation test # 5.

The flotation results and the liberation-limited grade/recovery curves for the size class 2000x425 µm suggest that the pyrite recovery and pyrite grade in flotation test # 1 and flotation test # 2 are limited by factors other than liberation. On the other hand, flotation test # 3 and flotation test # 4 the pyrite recovery and pyrite grade are limited only by liberation.

The pyrite recovery and pyrite grade in the size class 425x208 µm for all the flotation tests are limited by liberation. Therefore the results of the flotation tests can be improved by a further size reduction of the feed sample.

In flotation test # 2 and flotation test # 3, the pyrite recovery and grade of the size class 208x106 µm can be improved only by further liberation. In flotation tests #1 - #4 the pyrite recovery and grade of the size class 208x106 µm are limited by factors other than liberation.

In the size class 106x45 µm the pyrite recovery and pyrite grade of flotation test # 1, flotation test # 3 and flotation test # 4 are limited by factors other than liberation. The pyrite recovery and pyrite grade in flotation test # 3 are limited by liberation. The pyrite recovery and grade of flotation test # 3 can be improved only by reducing the particle size of the feed sample.

It was found that the collector Cytec 208 had a better performance for mine site ore in comparison with the Danafloat 571. The excess of collectors (Cytec 208 and PAX) and adjustment of the pH value to pH 5 improved the pyrite recovery of the concentrate for the size classes 425x208 µm and 2000x425 µm.

It was found that the particles of size class 2000x425 µm had the best recovery in concentrate 3 when compared to other size classes. It seems that the large particles have a slower kinetics probably to their relatively large size. These particles have more probability to come out of the cell into the concentrate when they are not competing with particles which are more hydrophobic and smaller.

The negative effect of the fine particles fraction (-45 µm) was not significant when the collectors were added in excess. The pyrite recovery and grade of the concentrates of the flotation test with individual size classes were lower than the pyrite recovery and grade of most of the flotation tests, especially in that flotation test with excess of collectors. The negative effect of the fine particles was slightly evident in the size classes 208x106 µm and 106x45 µm.

In general the texture analysis revealed that the pyrite-containing particles with a high pyrite grade and with high percentage of exposed pyrite grains are recovered faster in concentrate 1. The particles recovered in concentrate 2 had a lower pyrite grade and a

lower percentage of exposed pyrite grains than concentrate 1. The particles collected in the in concentrate 3 had a pyrite grade between 0% and 10%, these particles had a high percentage of exposed pyrite grains. Finally in the tailing the pyrite-containing particles had a pyrite grade between 0% and 10% and high percentage of exposed pyrite grains, similar to the particles in the concentrate 3 however these particles are lost in the tailings. Probably, these pyrite-containing particles are lost in the tailings because the pyrite grains are disseminated in the particles and the collector is acting only on small pyrite surfaces. The hydrophobic state of the surface for these particles is not sufficient to cause a strong attachment to the bubble and collection in the froth phase. Examples of particles collected in each concentrate and tailings product are illustrated in Figure 5.1.

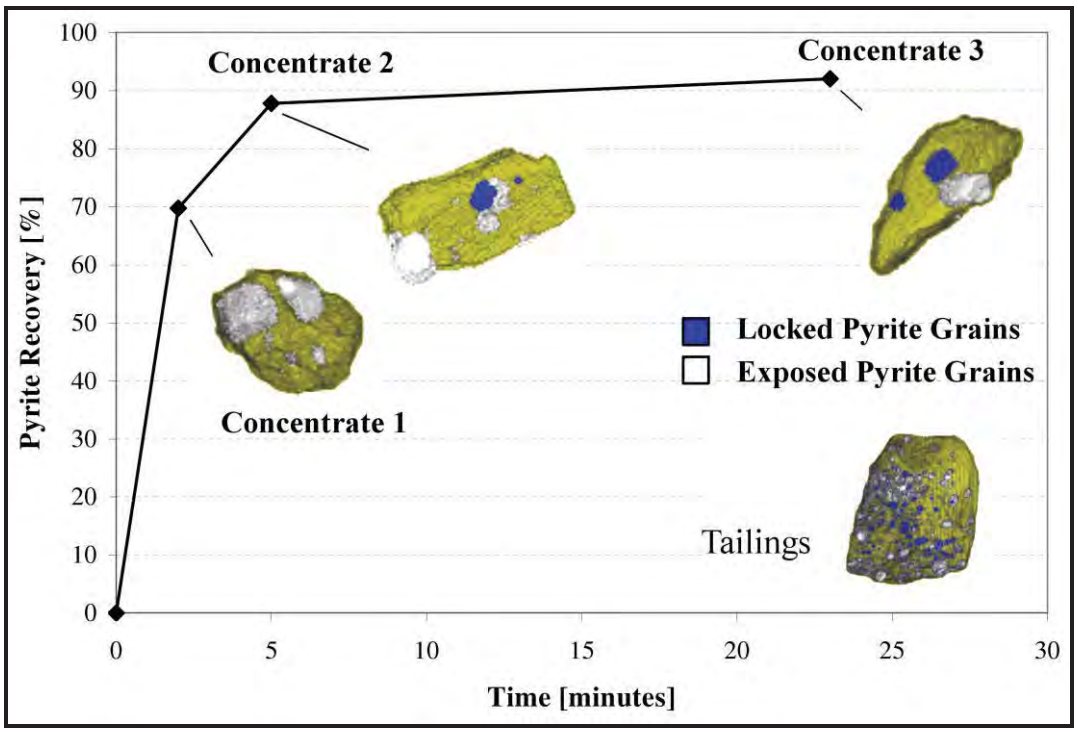

Figure 5.1 Schematic illustration of pyrite-containing particles collected in the concentrates and tailings of the flotation test based on texture analysis.

HRXMT offers a great opportunity to study the texture of the mineral particles. Since the texture analysis is done in 3D reconstructed images from HRXMT, stereological models are not required to simulate the actual texture of the individual particles. In addition, the samples do not require any preparation such as mounting the sample in epoxy plugs which is required for the analysis of polished surfaces.

In the future, research of the texture analysis will focus on the measurement of exposed surface area instead of percentage of exposed grains voxels. The exposed surface area will used as parameter to evaluate the flotation performance.

5.2 Flotation Plant Operation

It was found that there is a good correlation between the pyrite grade from HRXMT and Chemical Analysis for plant flotation circuit ore. Reliable quantitative and qualitative analysis can be obtained from HRXMT analysis of samples from plant flotation circuit.

Based on the chemical analysis and mass balance the pyrite recovery was calculated. It was found that the pyrite recovery is very low for plant operations because the samples collected were not representative statistically for the process in the plant. Also, for some size classes the feed samples had a lower pyrite grade than the pyrite grade of the tailings. The same trend was found in the chemical and HRXMT analysis.

In the liberation-limited grade/recovery curves it was evident that when the particle size is reduced the pyrite grains have better liberation, the size reduction also improves the pyrite grade of the concentrates. The size limitation for the HRXMT analysis of flotation circuit ore was found to be 45 μm. In the size class 45x25 μm the voxel resolution limitation and partial volume effect decreased the apparent pyrite grade and

liberation of the individual particles. This caused the liberation-limited grade/recovery curve the size class 45x25 µm to be below liberation-limited grade/recovery curves of the size classes 106x45 µm and 208x106 µm in the low pyrite recovery region.

It was found that the separation efficiency in all the size classes for the flotation circuit ore is limited by factors other than liberation. The separation efficiency can be improved by changing the flotation conditions using similar particle size distribution of the feed to the flotation circuit.

From texture analysis it was found that the percentage of exposed pyrite grains was greater than 90% for feed, concentrate and tailings below 425 µm in particle size. The pyrite grains practically are exposed at a particle size of 425 µm.

From the textural analysis it can be concluded that the pyrite-containing particles with a high pyrite grade and high percentage of exposed pyrite grains are recovered in the concentrate in all size classes.

In the tailings for size classes 45x25 µm, 106x45 µm and 208x106 µm most of the pyrite grains are exposed, however these particles are not recovered in the concentrate. In the size classes 425x208 µm and 2000x425 µm all the particles had a pyrite grade between 0% and 10% and most of the particles had a percentage of exposed pyrite grains greater than 50%. Also in the tailings the percentage of particles with only internal pyrite grains is significant, especially for the size classes 106x45 µm, 208x106 µm and 425x208 µm.

The flotation separation efficiency of the flotation circuit ore can be improved modifying the flotation strategy in order to recover those particles with a high pyrite grade that are lost in the tailings. It seems that the pyrite grains are exposed in the

particles but the hydrophobic state of the particles is compromised by other factors and flotation conditions.

As it was expected the pyrite grade was overestimated in the MLA analysis of individual particles in comparison with HRXMT analysis. The MLA analysis was done on 2D polished surfaces and only a partial section of the particles were considered for the analysis. Locked pyrite grains may appear to be fully liberated in the partial section. In the HRXMT analysis of pyrite grade the entire particle is interrogated considering the total volume of the particle therefore the pyrite grade results are more reliable.

APPENDIX A

EXAMPLE OF CALCULATION OF LIBERATION-LIMITED GRADE/RECOVERY CURVES

A.1 Example of calculation of liberation-limited grade/recovery curves

A sample of 208x106 µm is used in this example. The grade class distribution was estimated from data obtained by HRXMT analysis. The 16 grade classes with the corresponding percentage are presented in Figure A.1. Also, grade class distribution is shown in a histogram plot (Figure A.1).

Feed 208x106 µm

Grade Class [%]	Percentage [%]
0	58.95
1	30.70
3	2.26
5	1.18
7	0.55
9	0.36
15	1.45
25	1.38
35	0.98
45	0.47
55	0.63
65	0.53
75	0.44
85	0.11
95	0.00
100	0.00

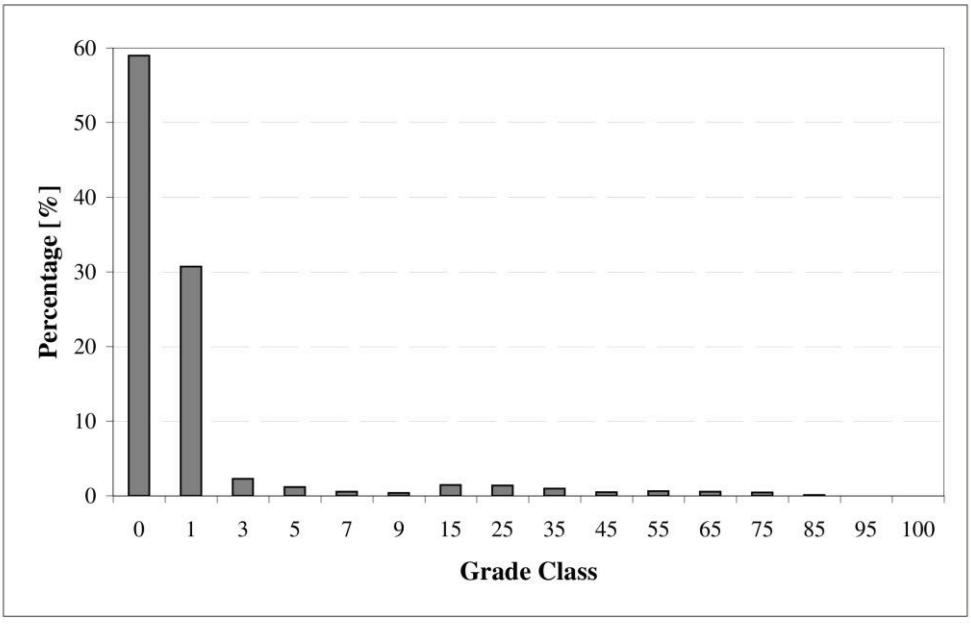

Figure A.1 Grade class distribution for 208x106 µm sample

The pyrite content in each grade class is calculated, the formulas (Column C) and results (Column D) are presented in Table A.1. The total pyrite content in the sample is calculated in row 19.

The formulas and results for the calculation of pyrite distribution (Column B and C) and the cumulative pyrite recovery (Column D and E) are presented in the Table A.2. The formulas and results for the calculation of the cumulative pyrite grade are presented in Table A.3 (Column C and D). The cumulative pyrite grade is calculated from the grade class distribution.

Table A.1

Calculation of Pyrite Content in each Grade Class

	A	B	C	D
1	**Grade Class [%]**	**Percentage [%]**	**Pyrite content [%]**	**Pyrite content [%]**
2	0	58.95	=(A2*B2)/100	0.0000
3	1	30.70	=(A3*B3)/100	0.3070
4	3	2.26	=(A4*B4)/100	0.0679
5	5	1.18	=(A5*B5)/100	0.0591
6	7	0.55	=(A6*B6)/100	0.0385
7	9	0.36	=(A7*B7)/100	0.0327
8	15	1.45	=(A8*B8)/100	0.2176
9	25	1.38	=(A9*B9)/100	0.3444
10	35	0.98	=(A10*B10)/100	0.3414
11	45	0.47	=(A11*B11)/100	0.2129
12	55	0.63	=(A12*B12)/100	0.3455
13	65	0.53	=(A13*B13)/100	0.3476
14	75	0.44	=(A14*B14)/100	0.3313
15	85	0.11	=(A15*B15)/100	0.0930
16	95	0.00	=(A16*B16)/100	0.0000
17	100	0.00	=(A17*B17)/100	0.0000
18				
19			=C1+C2+C3+…+C17	2.7390

Table A.2

Calculation of Pyrite Distribution

	A	B	C	D	E
	Pyrite content	**Pyrite Distribution**	**Pyrite Distribution**	**Pyrite Recovery**	**Pyrite Recovery**
1	**[%]**	**[%]**	**[%]**	**[%]**	**[%]**
2	0.0000	=A2*100/A19	0.00	=D3+C2	100.00
3	0.3070	=A3*100/A19	11.21	=D4+C3	100.00
4	0.0679	=A4*100/A19	2.48	=D5+C4	88.79
5	0.0591	=A5*100/A19	2.16	=D6+C5	86.31
6	0.0385	=A6*100/A19	1.41	=D7+C6	84.15
7	0.0327	=A7*100/A19	1.19	=D8+C7	82.75
8	0.2176	=A8*100/A19	7.94	=D9+C8	81.55
9	0.3444	=A9*100/A19	12.57	=D10+C9	73.61
10	0.3414	=A10*100/A19	12.47	=D11+C10	61.04
11	0.2129	=A11*100/A19	7.77	=D12+C11	48.57
12	0.3455	=A12*100/A19	12.62	=D13+C12	40.80
13	0.3476	=A13*100/A19	12.69	=D14+C13	28.18
14	0.3313	=A14*100/A19	12.09	=D15+C14	15.49
15	0.0930	=A15*100/A19	3.39	=D16+C15	3.40
16	0.0000	=A16*100/A19	0.00	=D17+C16	0.00
17	0.0000	=A17*100/A19	0.00	=C17	0.00
18					
19	2.7390				

Table A.3

Calculation of Cumulative Pyrite Grade

	A	B	C	D
	Grade Class	**Percentage**	**Pyrite Grade**	**Pyrite Grade**
1	**[%]**	**[%]**	**[%]**	**[%]**
2	0	58.95	=(B17*A17+B16*A16+...+B3*A3+B2*A2)/(B17+B16+…+B3+B2)	2.74
3	1	30.70	=(B17*A17+B16*A16+…+B4*A4+B3*A3)/(B17+B16+…+B4+B3)	6.67
4	3	2.26	=(B17*A17+B16*A16+…+B5*A5+B4*A4)/(B17+B16+…+B5+B4)	23.50
5	5	1.18	=(B17*A17+B16*A16+...+B6*A6+B5*A5)/(B17+B16+...+B6+B5)	29.24
6	7	0.55	=(B17*A17+B16*A16+...+B7*A7+B6*A6)/(B17+B16+...+B7+B6)	33.38
7	9	0.36	=(B17*A17+B16*A16+...+B8*A8+B7*A7)/(B17+B16+...+B8+B7)	35.67
8	15	1.45	=(B17*A17+B16*A16+...+B9*A9+B8*A8)/(B17+B16+...+B9+B8)	37.29
9	25	1.38	=(B17*A17+B16*A16+...+B10*A10+B9*A9)/(B17+B16+...+B10+B9)	44.40
10	35	0.98	=(B17*A17+B16*A16+...+B11*A11+B10*A10)/(B17+B16+…+B11+B10)	52.86
11	45	0.47	=(B17*A17+B16*A16+...+B12*A12+B11*A11)/(B17+B16+...+B12+B11)	60.82
12	55	0.63	=(B17*A17+B16*A16+...+B13*A13+B12*A12)/(B17+B16+...+B13+B12)	65.19
13	65	0.53	=(B17*A17+B16*A16+...+B14*A14+B13*A13)/(B17+B16+...+B14+B13)	71.08
14	75	0.44	=(B17*A17+B16*A16+B15*A15+B14*A14)/(B17+B16+B15+B14)	76.99
15	85	0.11	=(B17*A17+B16*A16+B15*A15)/(B17+B16+B15)	85.00
16	95	0.00	=(B17*A17+B16*A16)/(B17+B16)	100.00
17	100	0.00	=(B17*A17/B17)	100.00

The pyrite recovery and pyrite recovery for liberation-limited grade/recovery curve are presented in Figure A.2.

Pyrite Recovery [%]	Pyrite Grade [%]
100.00	2.74
100.00	6.67
88.79	23.50
86.31	29.24
84.15	33.38
82.75	35.67
81.55	37.29
73.61	44.40
61.04	52.86
48.57	60.82
40.80	65.19
28.18	71.08
15.49	76.99
3.40	85.00
0.00	100.00
0.00	100.00

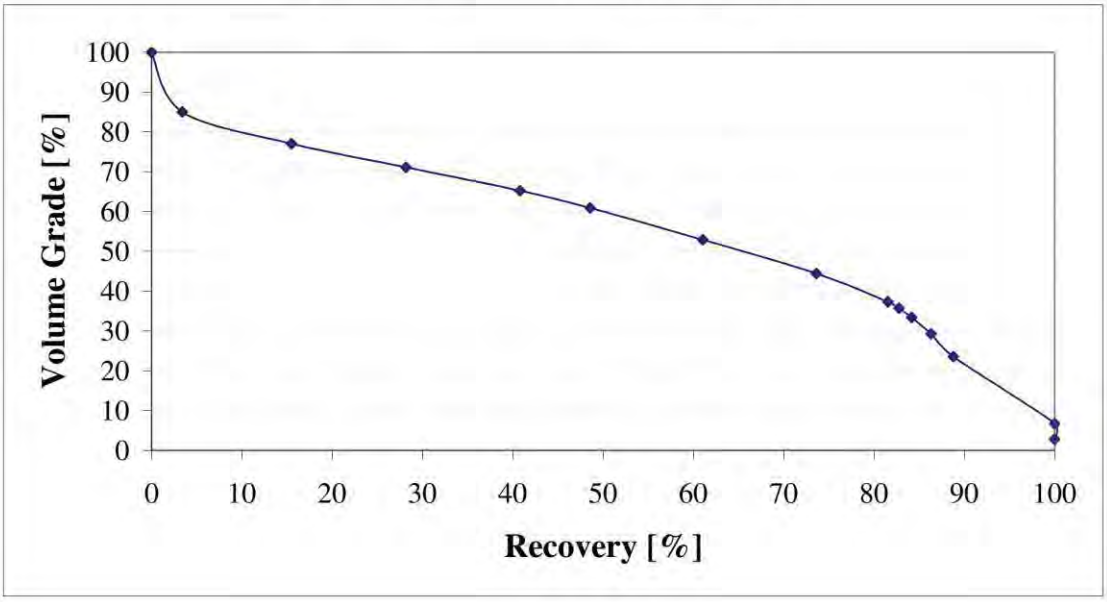

Figure A.2 Liberation-limited grade/recovery curve calculated from HRXMT data.

APPENDIX B

DETERMINATION OF MINIMUM SAMPLE WEIGHT

Table B.1

Factors and Parameters Used for the Determination of the Minimum Sample Weight for Feed

Factors and Parameters	Size Class [μm]				
	-45	106x45	208x106	425x208	2000x425
d [cm]	0.0045	0.0106	0.0208	0.0425	0.2000
d'[cm]	0.0001	0.0045	0.0106	0.0208	0.0425
s^2	0.0225	0.0225	0.0225	0.0225	0.0225
f_S	0.5	0.5	0.5	0.5	0.5
E	0.25	0.5	0.75	0.5	0.25
L_S [cm]	0.0075	0.0075	0.0075	0.0075	0.0075
ℓ	1.2910	0.8412	0.6005	0.4201	0.1936
A	0.0301	0.0436	0.0301	0.0200	0.0196
ω [g/cm^3]	5.01	5.01	5.01	5.01	5.01
τ [g/cm^3]	2.74	2.74	2.74	2.74	2.74
β [g/cm^3]	159.13	107.75	159.13	243.05	247.81
C_S [g/cm^3]	25.68	22.66	35.83	25.52	6.00
M [g]	0.00023	0.00270	0.03224	0.19595	4.79891

B.1 Example of minimum sample weight calculation using Gy's Equation

The calculations presented in this section were done for the size class 208x106 µm of Hope Bay ore feed. The pyrite mass percent from the chemical analysis is 3.01 %. The relative variance is assumed to be 0.01. The liberation size for pyrite is estimated to be 75 µm. The densities for pyrite and gangue minerals were 5.01 g/cm^3 and 2.74 g/cm^3, respectively.

The value of β (mineral composition) is estimated from Equation 2.9, using pyrite and gangue mineral densities, and the pyrite mass percent of the size class 208x106 µm.
The largest size of the sized sample is 208 µm (d). The shape factor f_S is equal to 0.5 for non-gold ores.

$$\beta = \frac{1-\alpha}{\alpha}\left[(1-\alpha)\omega + \alpha\,\tau\right] = \frac{1-0.0301}{0.0301}\left[(1-0.0301)(5.01\,\text{g/cm}^3) + (0.0301)\,(2.74\,\text{g/cm}^3)\right]$$

$$\beta = 159.13\,\text{g/cm}^3$$

The value of ε was determined from the Table 2.16. The value of d was 208 µm and the value of d' was 106 µm. The value of d/d' is equal to 1.96 therefore ε is equal to 0.75.

The liberation factor was calculated from Equation 2.8. L_S has a value of 75 µm.

$$\ell = \sqrt{\frac{L_S}{d}} = \sqrt{\frac{75\mu\text{m}}{208\,\mu\text{m}}} = 0.6004$$

The sampling constant C_S was calculated from the Equation 2.7.

$$C_S = f\,\varepsilon\,\ell\,\beta = (0.5)(0.75)(0.6004)(159.13\,g/cm^3) = 35.83\,g/cm^3$$

The relative standard deviation is calculated from the relative variance using the following equation:

$$s = \sqrt{\sigma} = \sqrt{0.01} = 0.1$$

Finally, the minimum weight sample of the size class 208x106 μm is calculated from Equation 2.6.

$$M = \frac{C_S d^3}{s^2} = \frac{(35.83\,g/cm^3)(0.0208\,cm)^3}{(0.1)^2} = 0.03224\,g$$

APPENDIX C

EXPOSURE ANALYSIS OF INDIVIDUAL PARTICLES OF FEED AND FLOTATION PRODUCTS

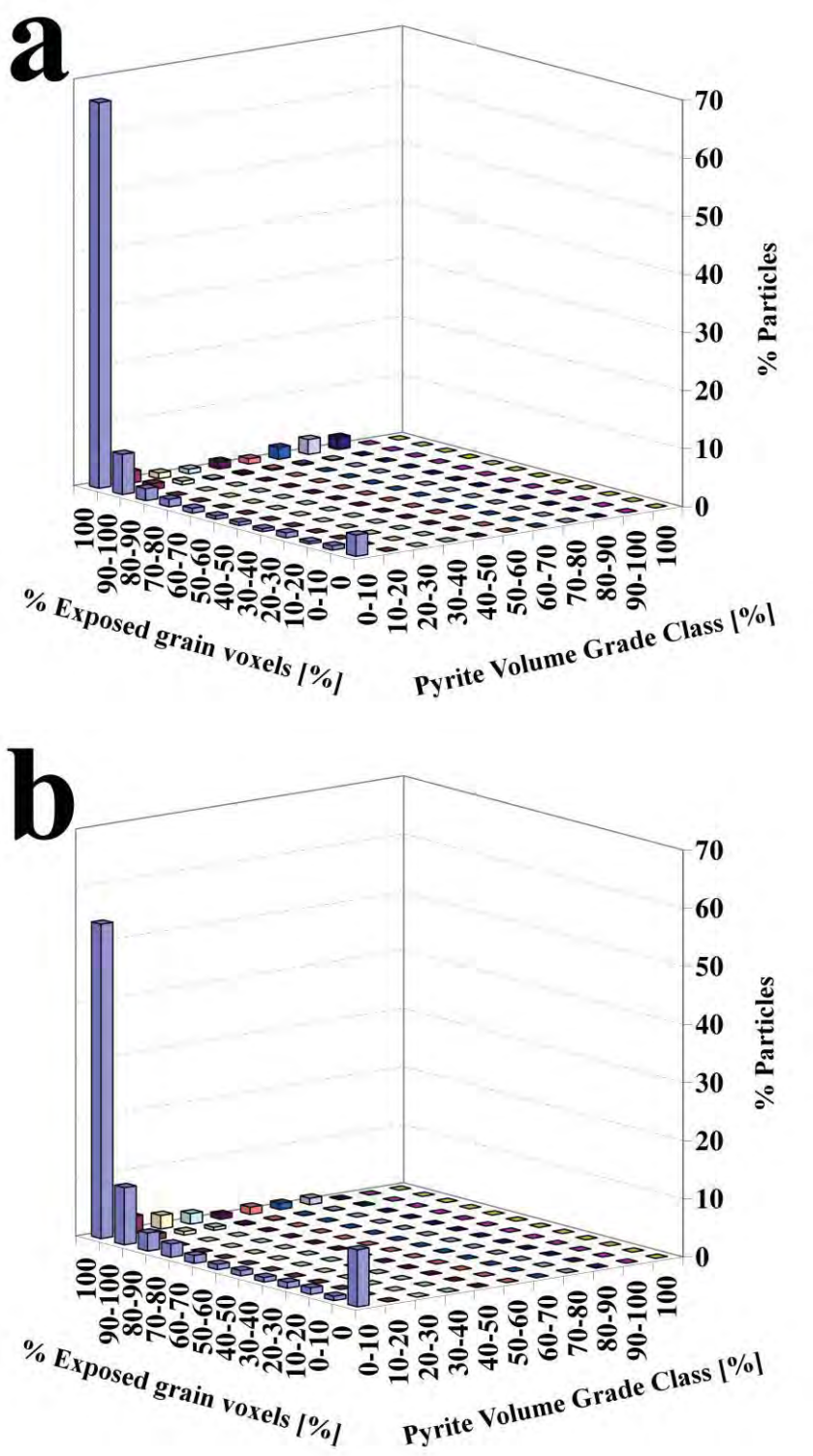

Figure C.1 Exposure results of feed samples. a) 106x45 µm, b) 208x106 µm, 425x208 µm and d) 2000x425 µm.

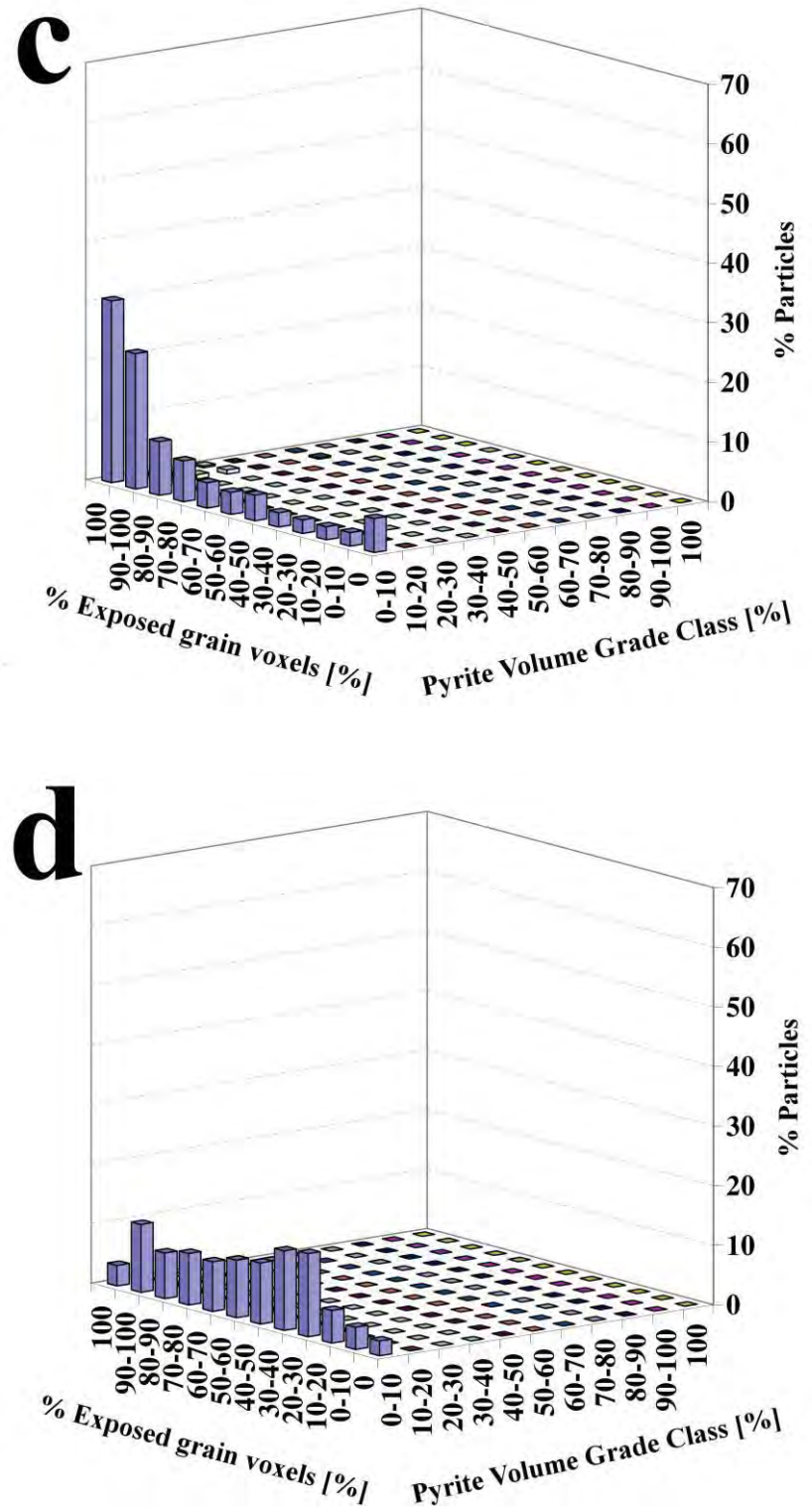

Figure C.1 Continued

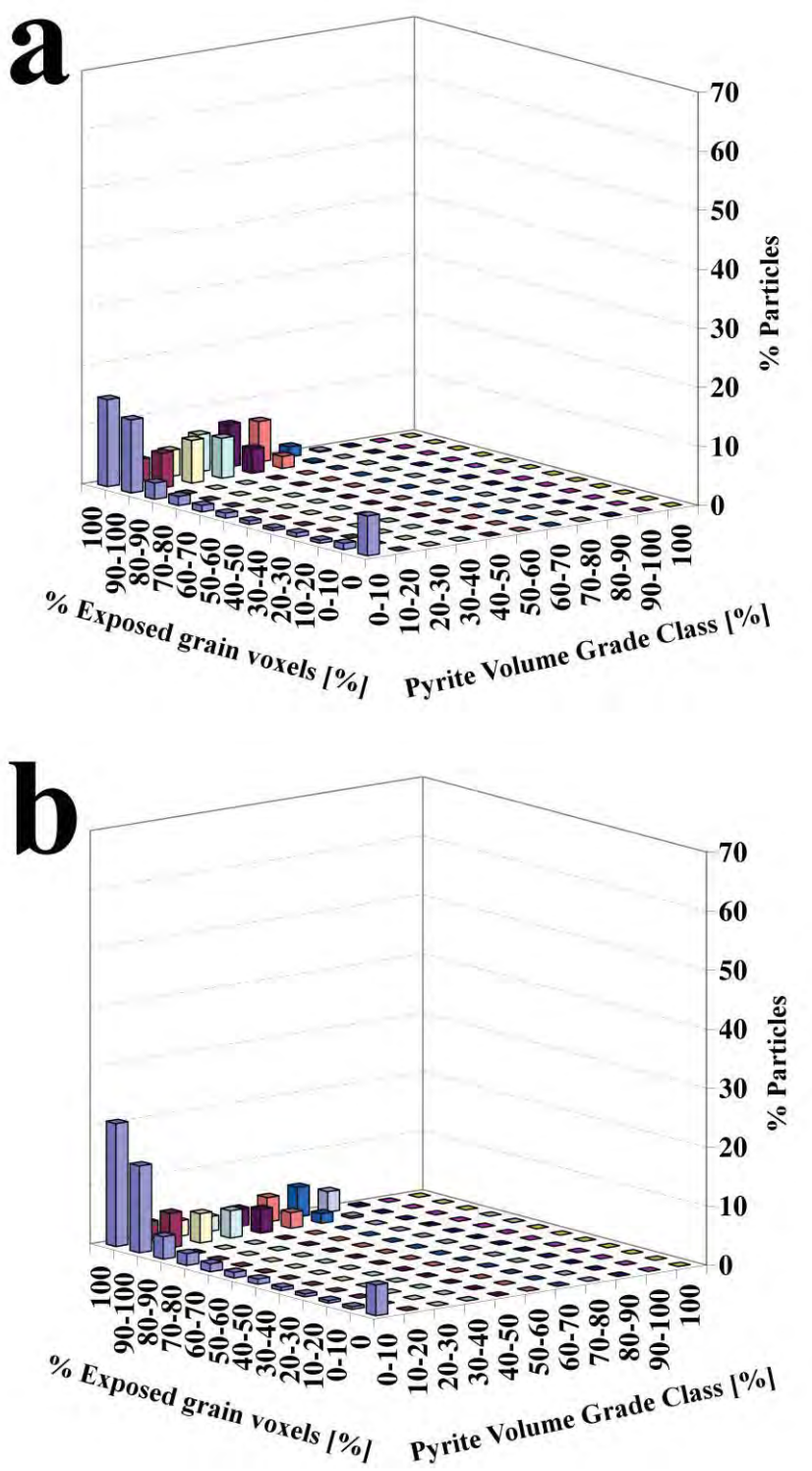

Figure C.2 Exposure results for concentrate 1 of flotation test # 1. a) 106x45 µm, b) 208x106 µm, c) 425x208 µm and d) 2000x425 µm.

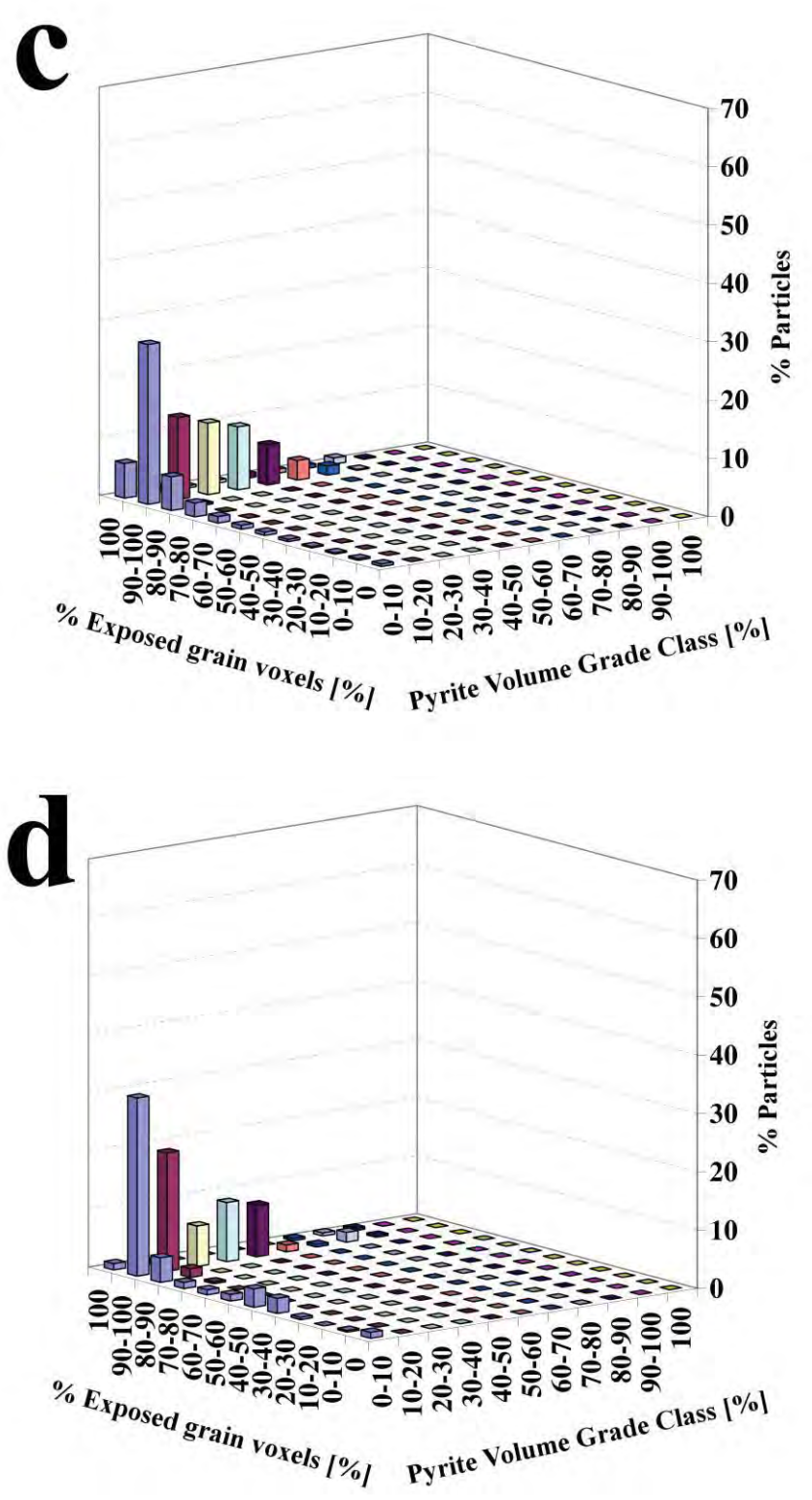

Figure C.2 Continued

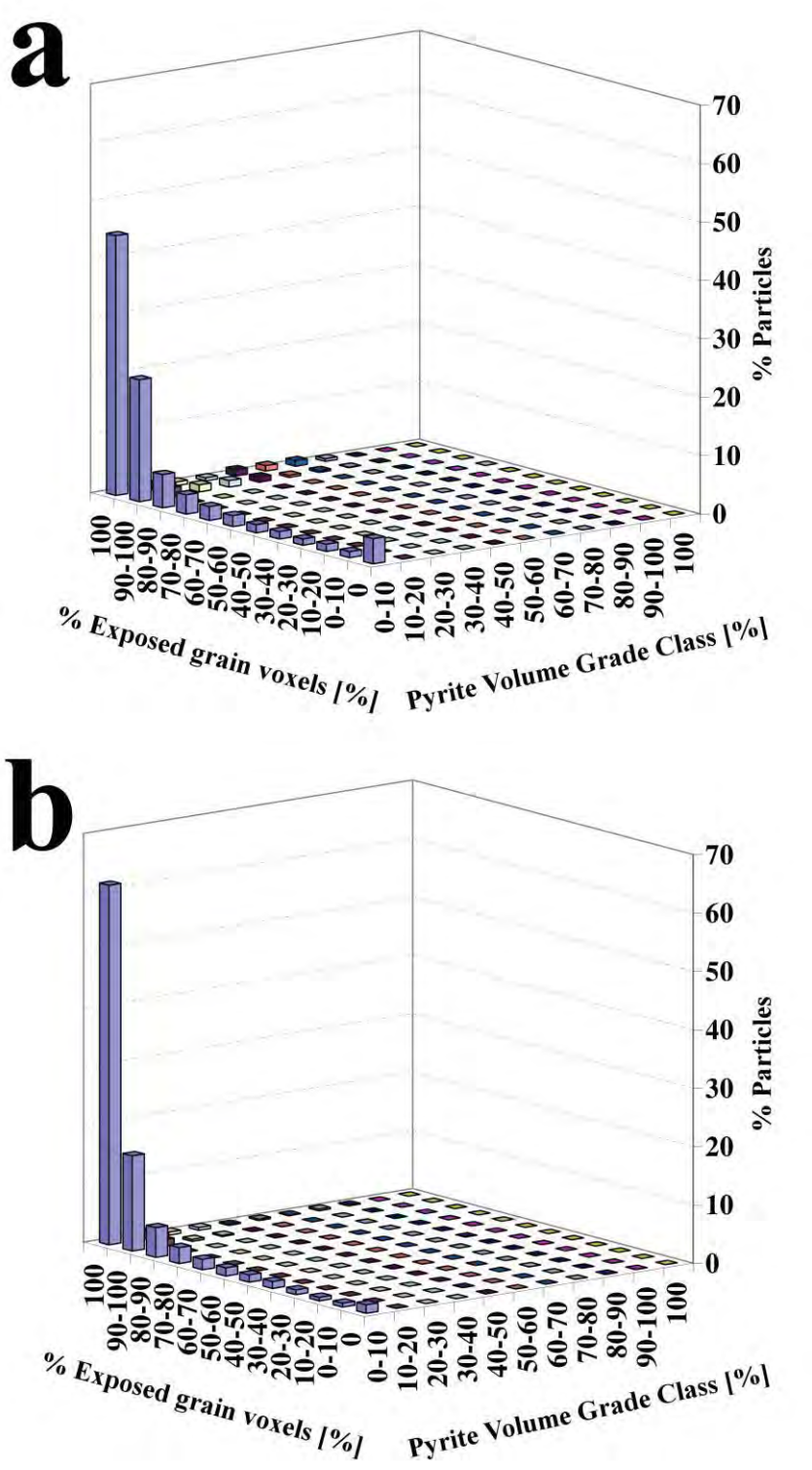

Figure C.3 Exposure results for cleaner concentrate of flotation test # 1. a) 106x45 µm, b) 208x106 µm, c) 425x208 µm and d) 2000x425 µm.

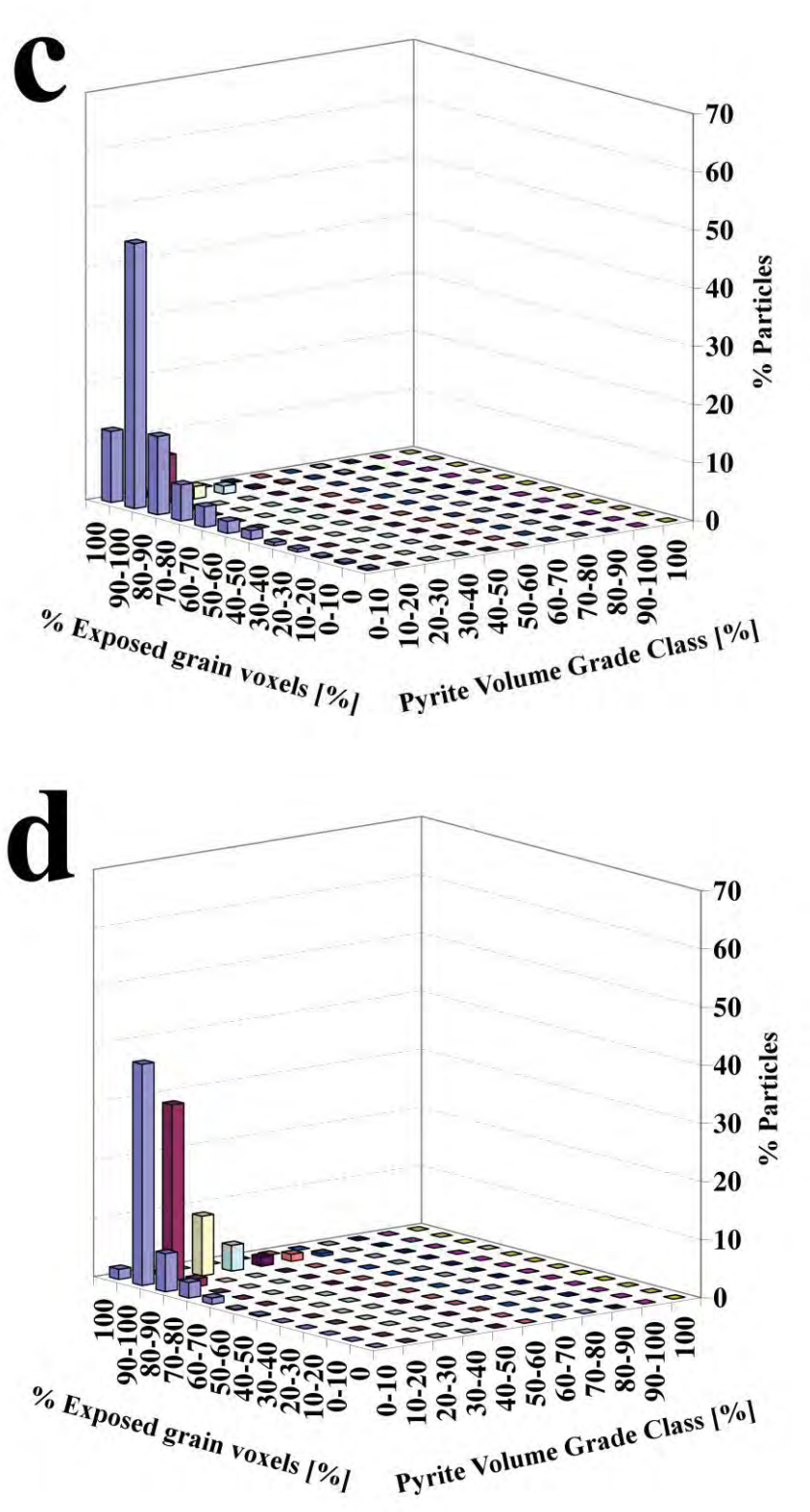

Figure C.3 Continued

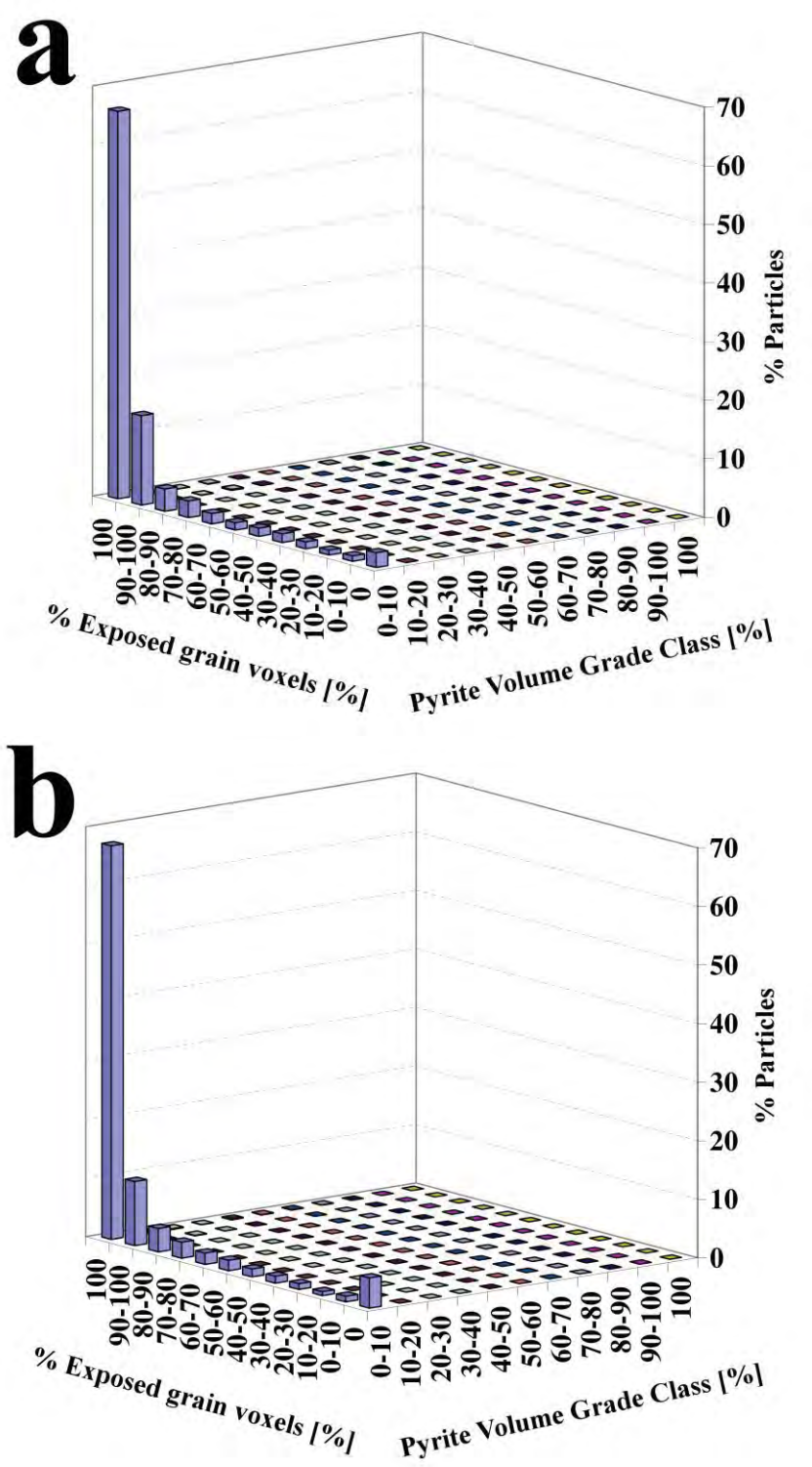

Figure C.4 Exposure results for cleaner tailings of flotation test # 1. a) 106x45 µm, b) 208x106 µm, c) 425x208 µm and d) 2000x425 µm.

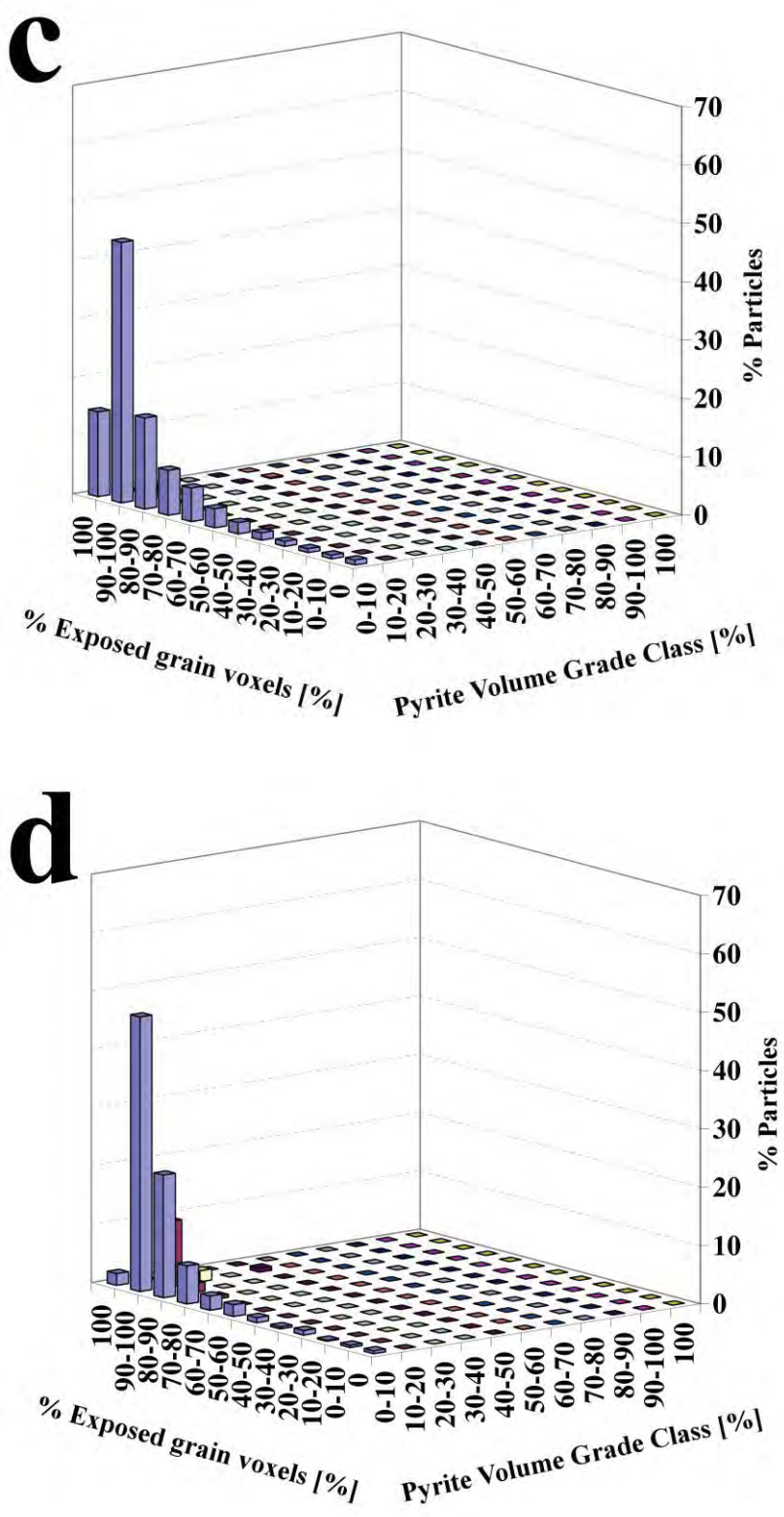

Figure C.4 Continued

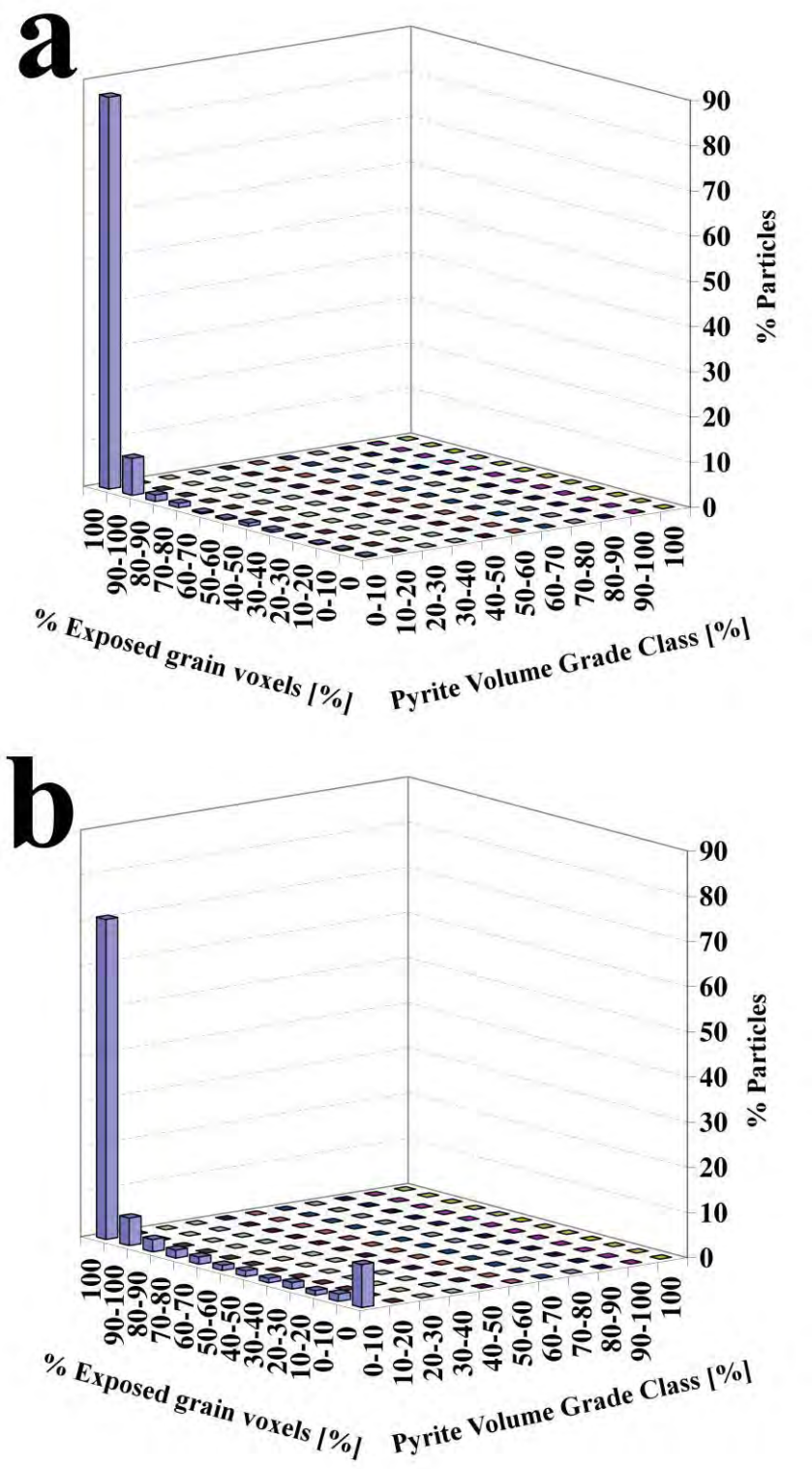

Figure C.5 Exposure results for tailings of flotation test # 1. a) 106x45 µm, b) 208x106 µm, c) 425x208 µm and d) 2000x425 µm.

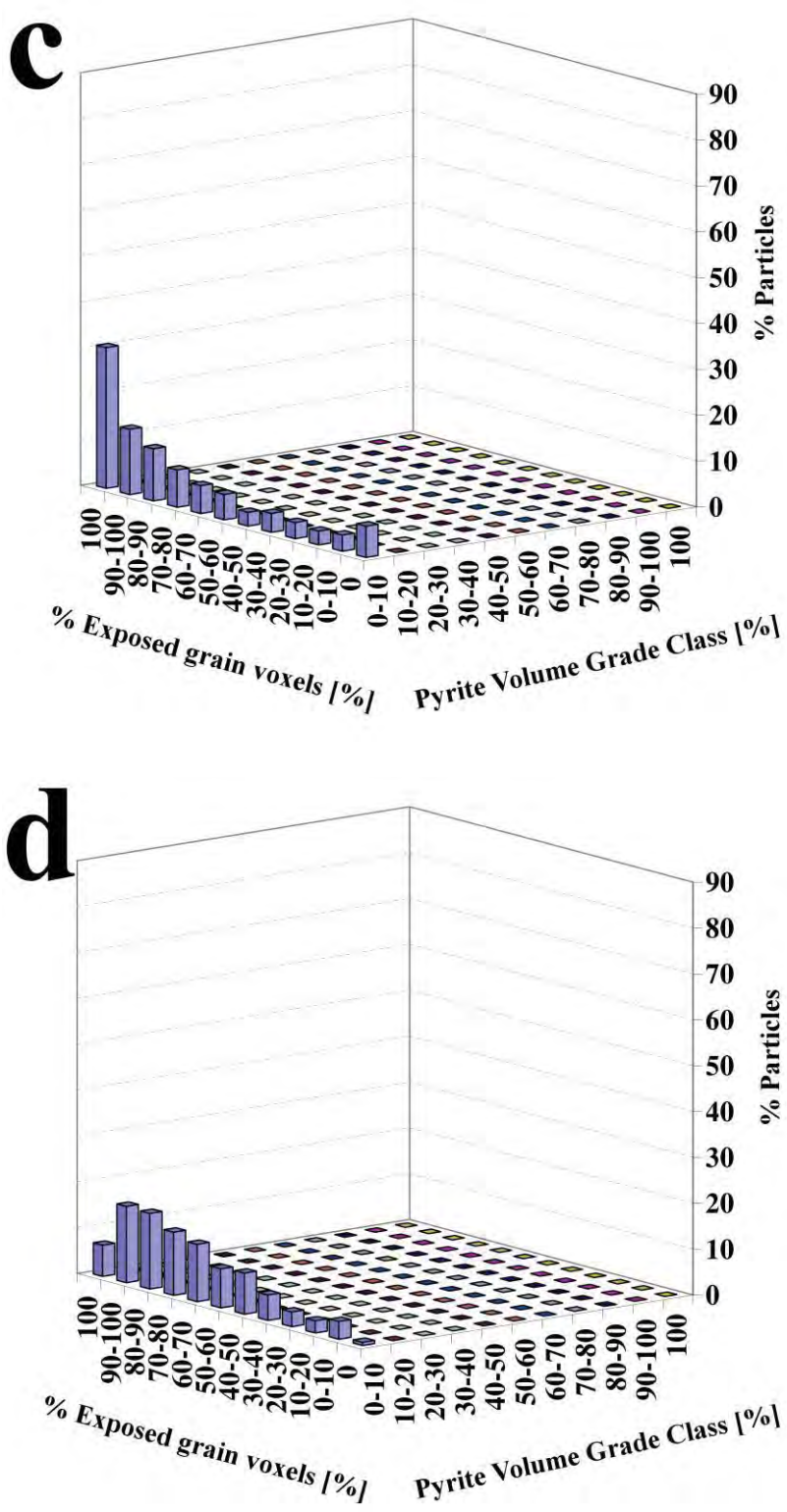

Figure C.5 Continued

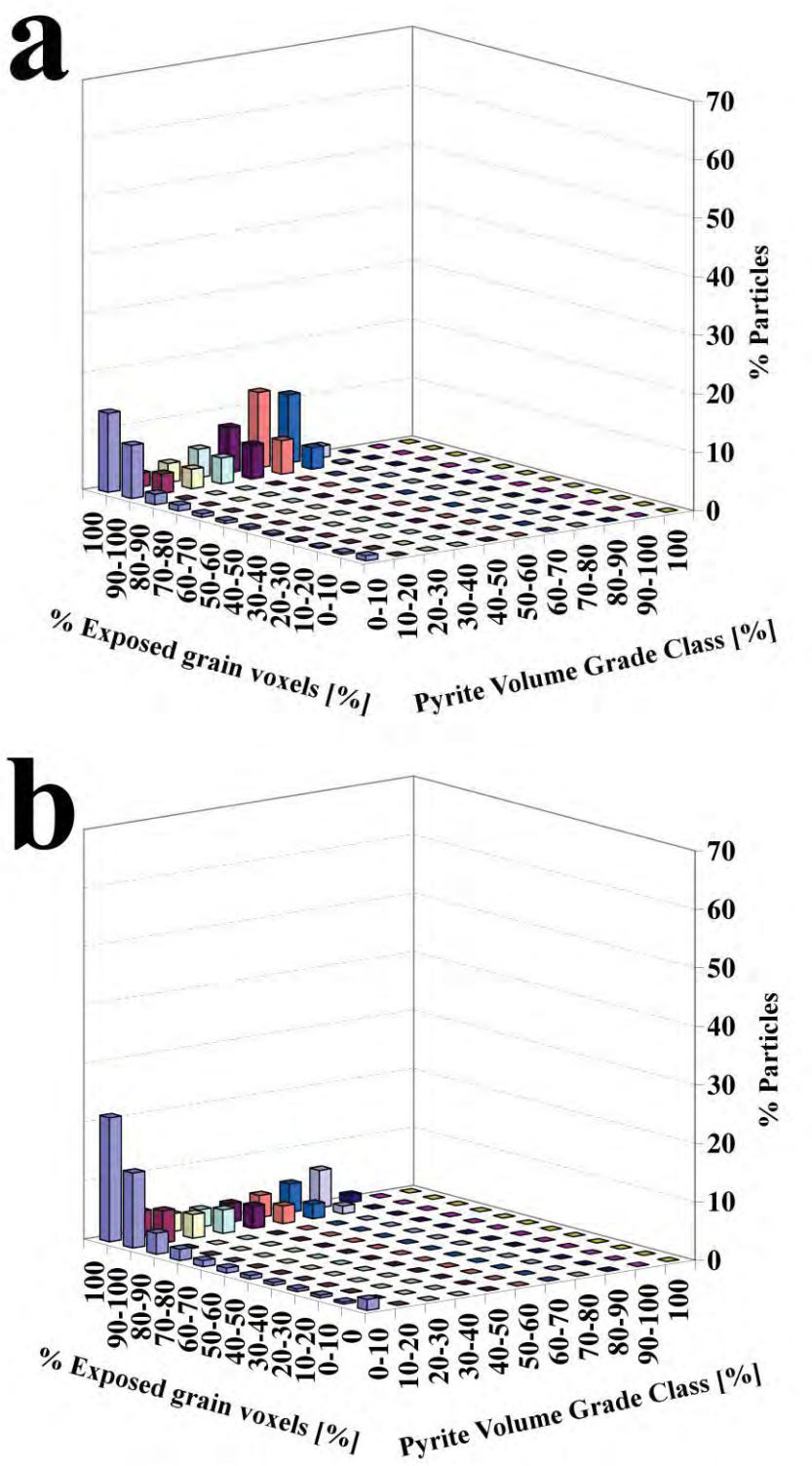

Figure C.6 Exposure results for concentrate 1 of flotation test # 2. a) 106x45 µm, b) 208x106 µm, c) 425x208 µm and d) 2000x425 µm.

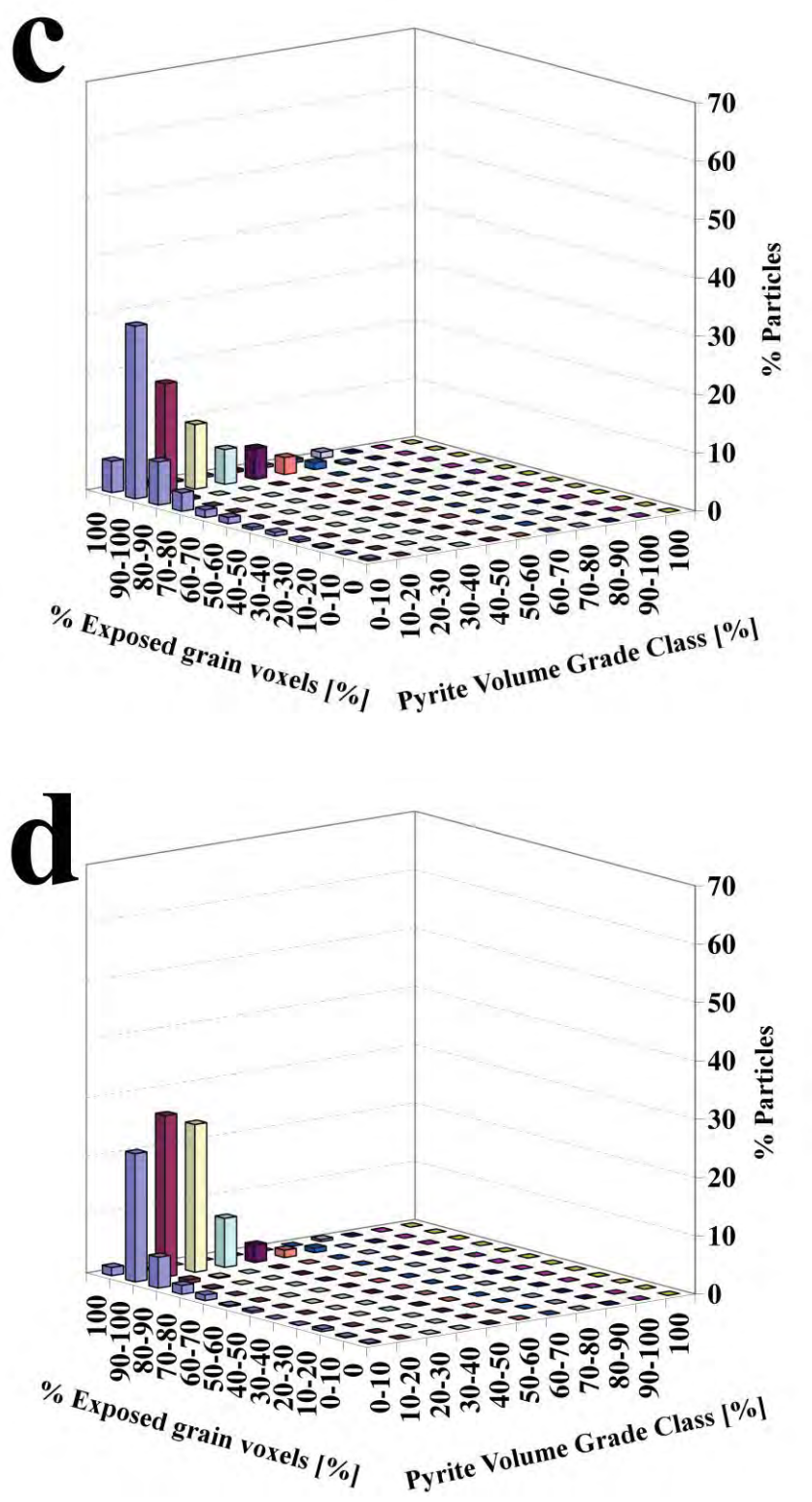

Figure C.6 Continued

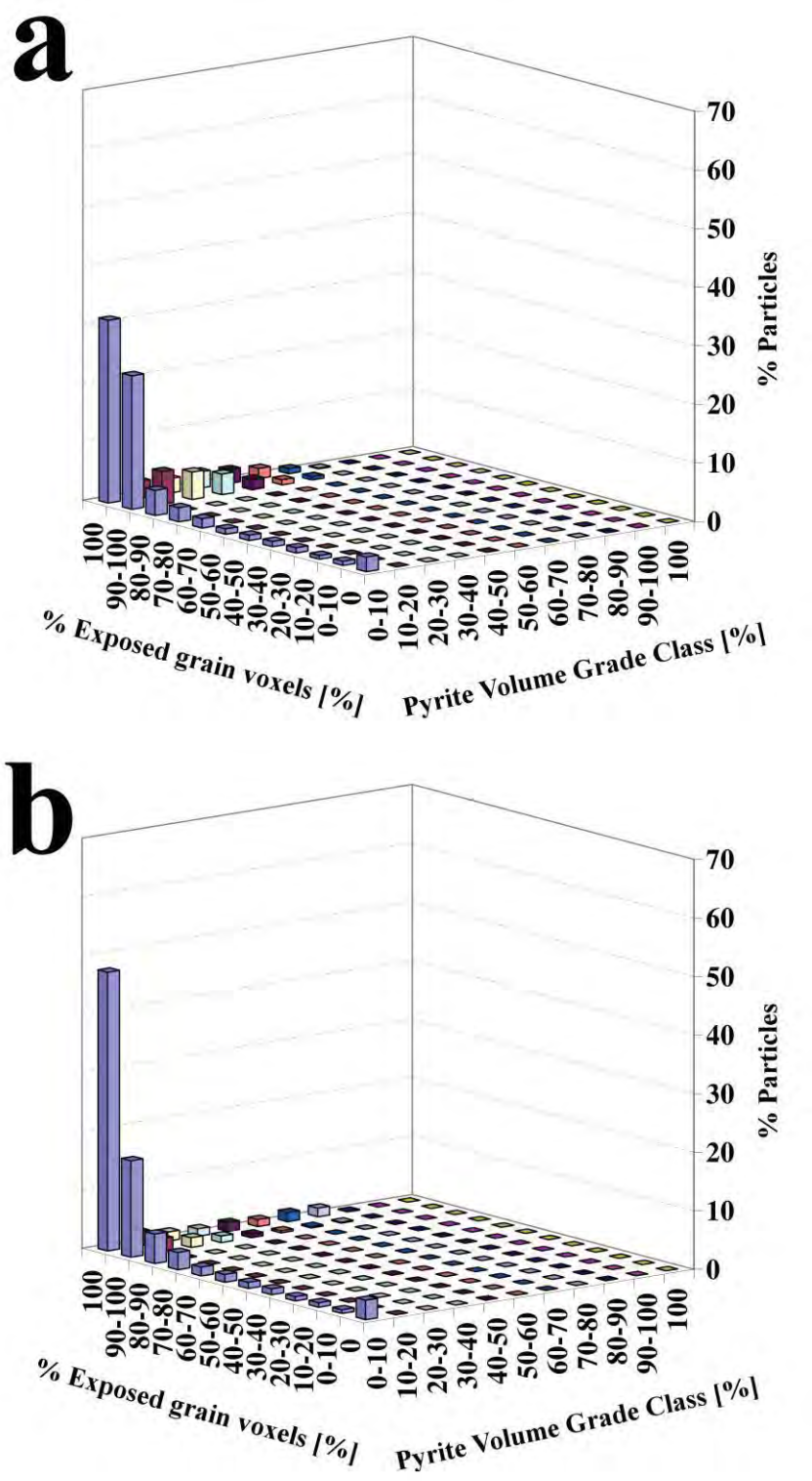

Figure C.7 Exposure results for concentrate 2 of flotation test # 2. a) 106x45 µm, b) 208x106 µm, c) 425x208 µm and d) 2000x425 µm.

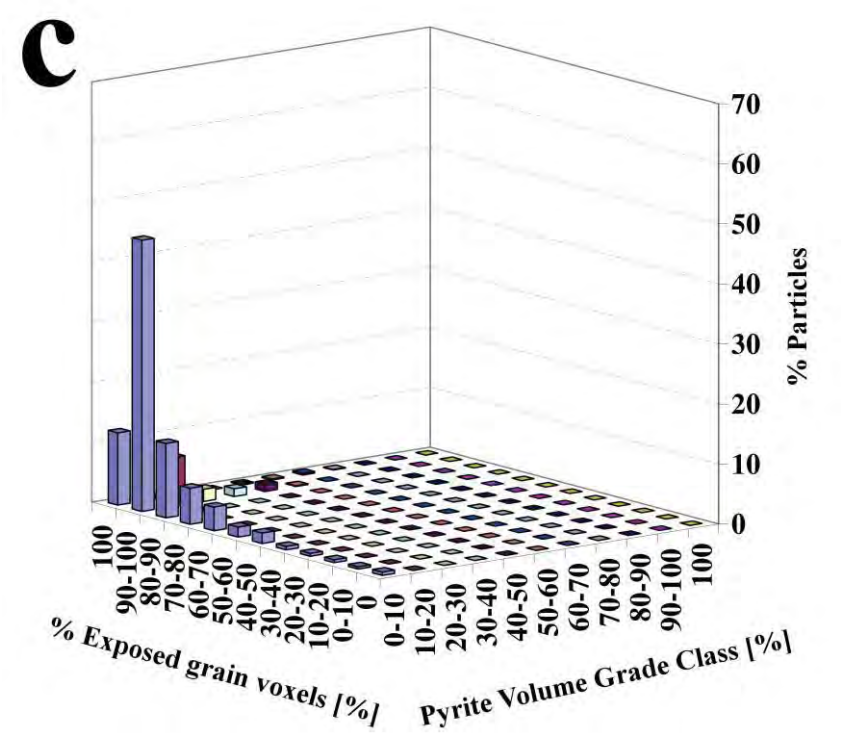

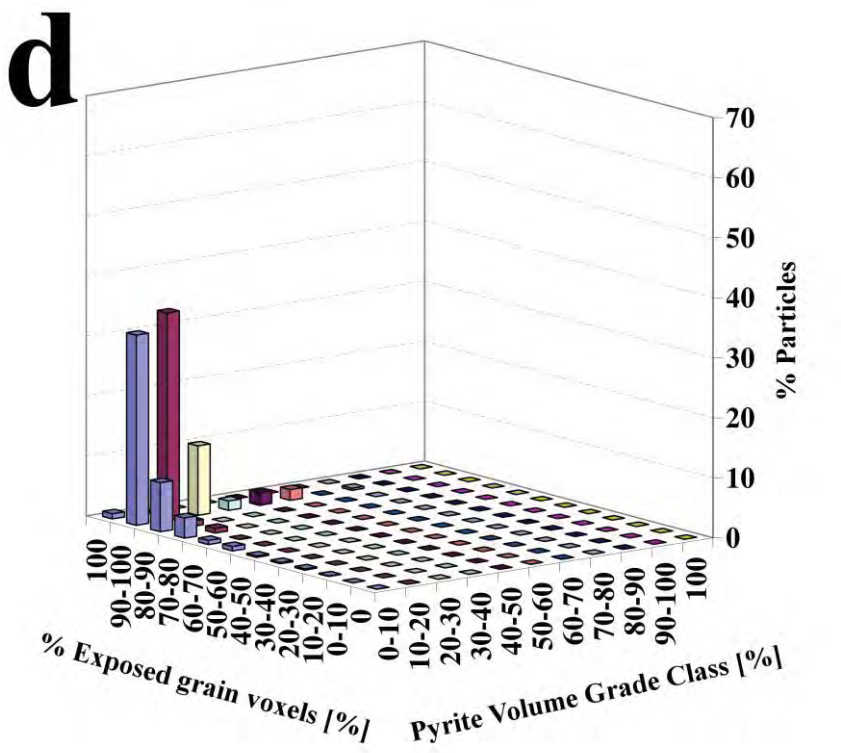

Figure C.7 Continued

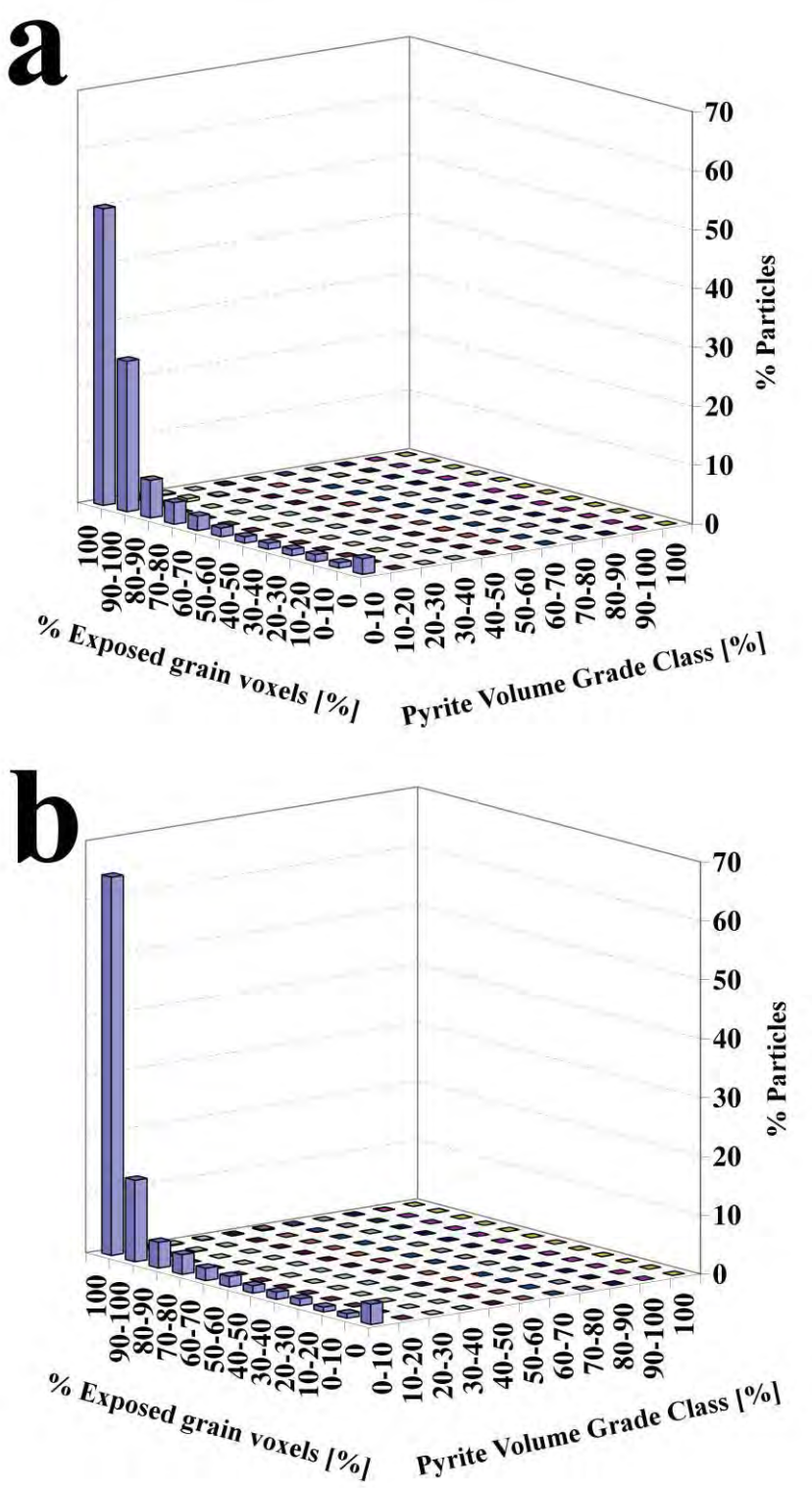

Figure C.8 Exposure results for concentrate 3 for flotation test # 2. a) 106x45 µm, b) 208x106 µm, c) 425x208 µm and d) 2000x425 µm.

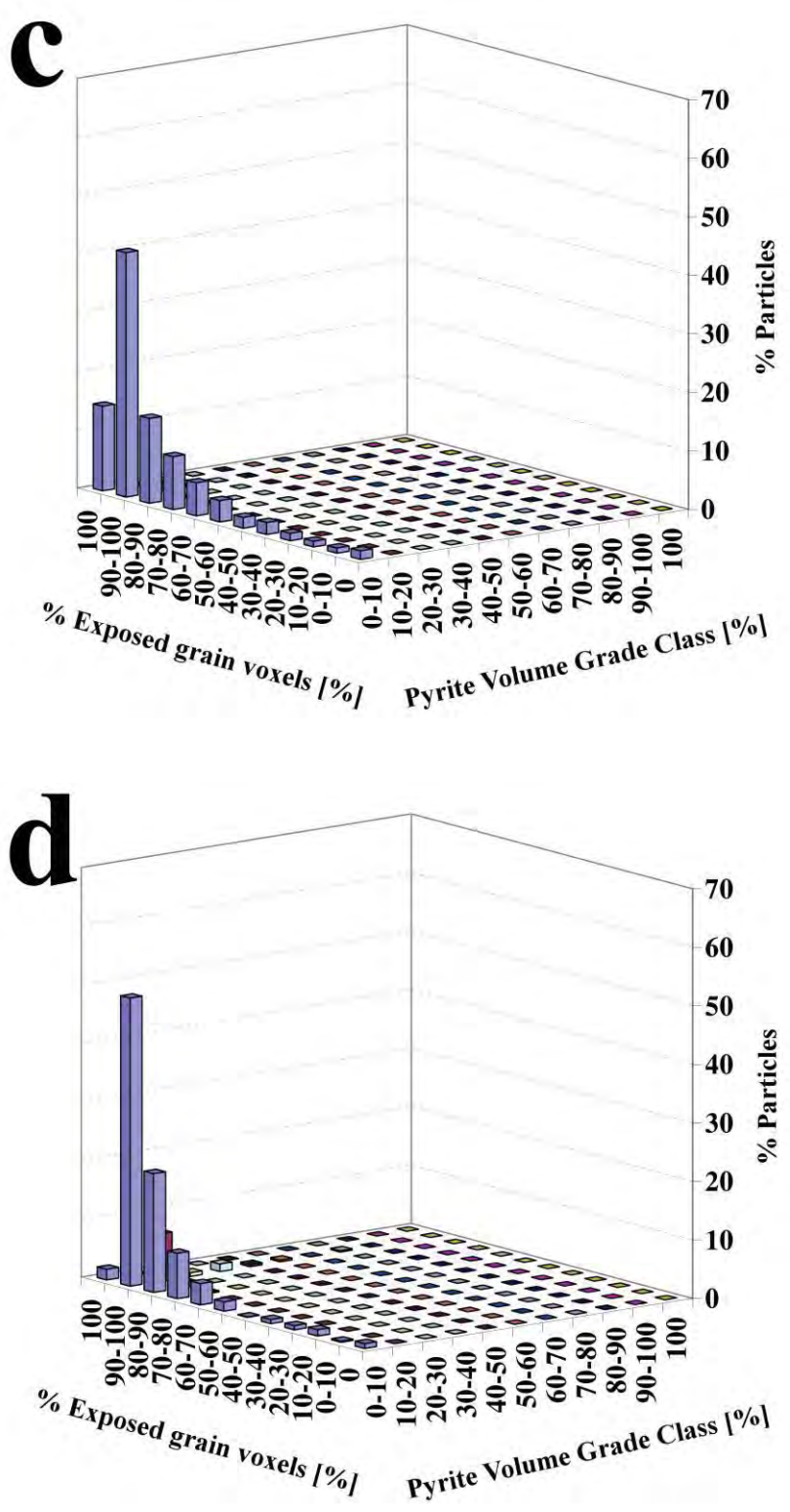

Figure C.8 Continued

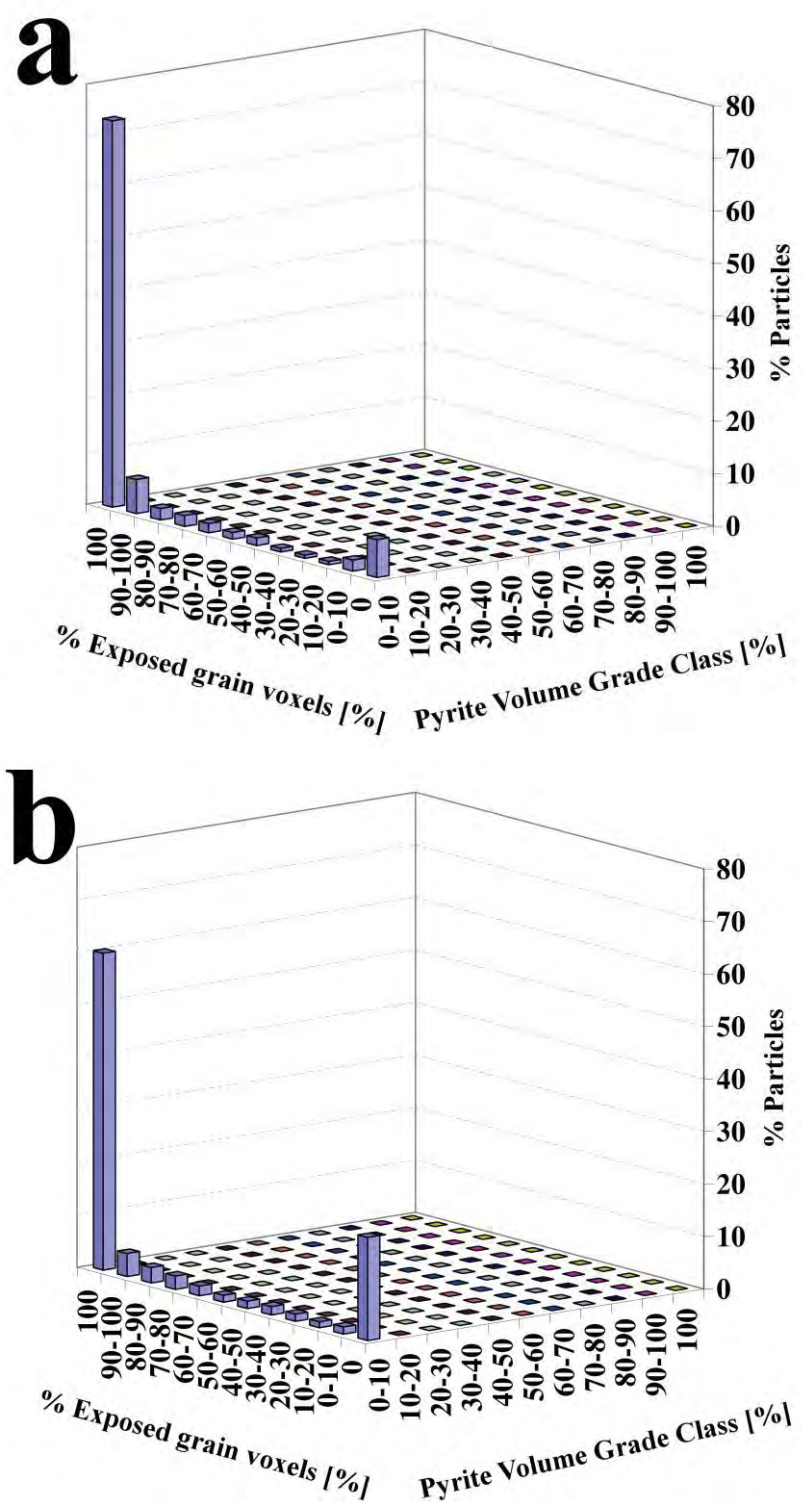

Figure C.9 Exposure results for tailings of flotation test # 2. a) 106x45 µm, b) 208x106 µm, c) 425x208 µm and d) 2000x425 µm.

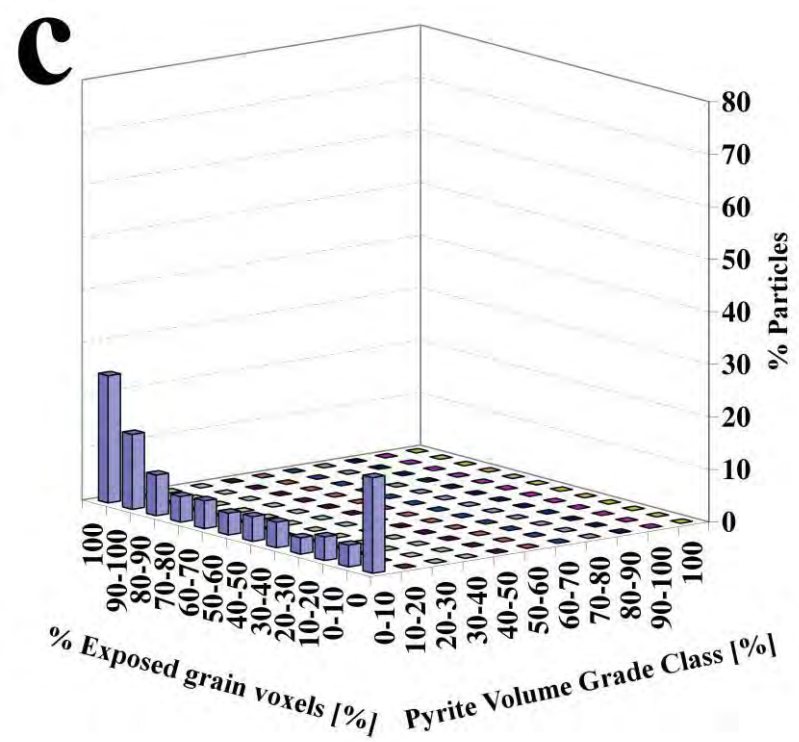

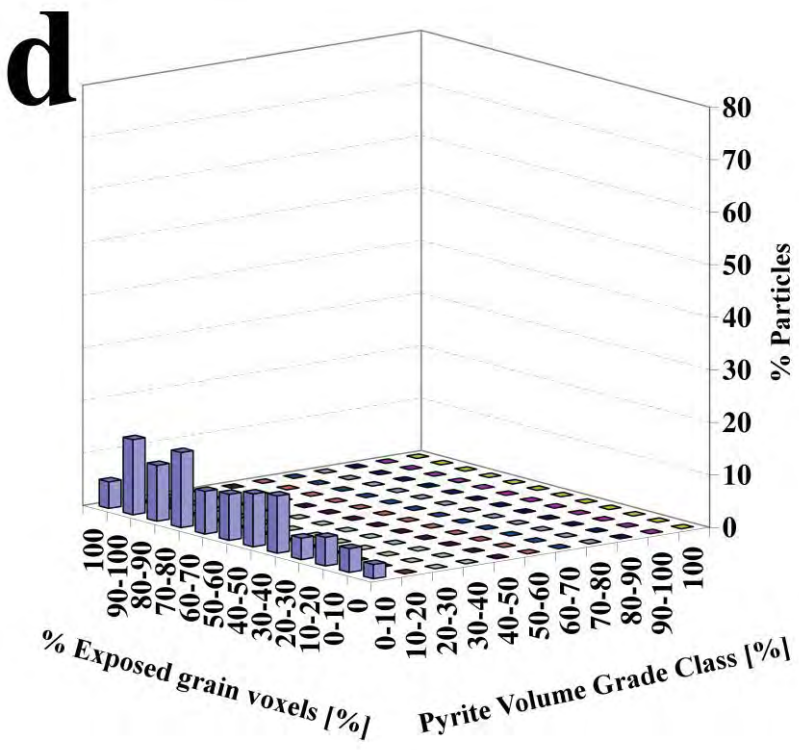

Figure C.9 Continued

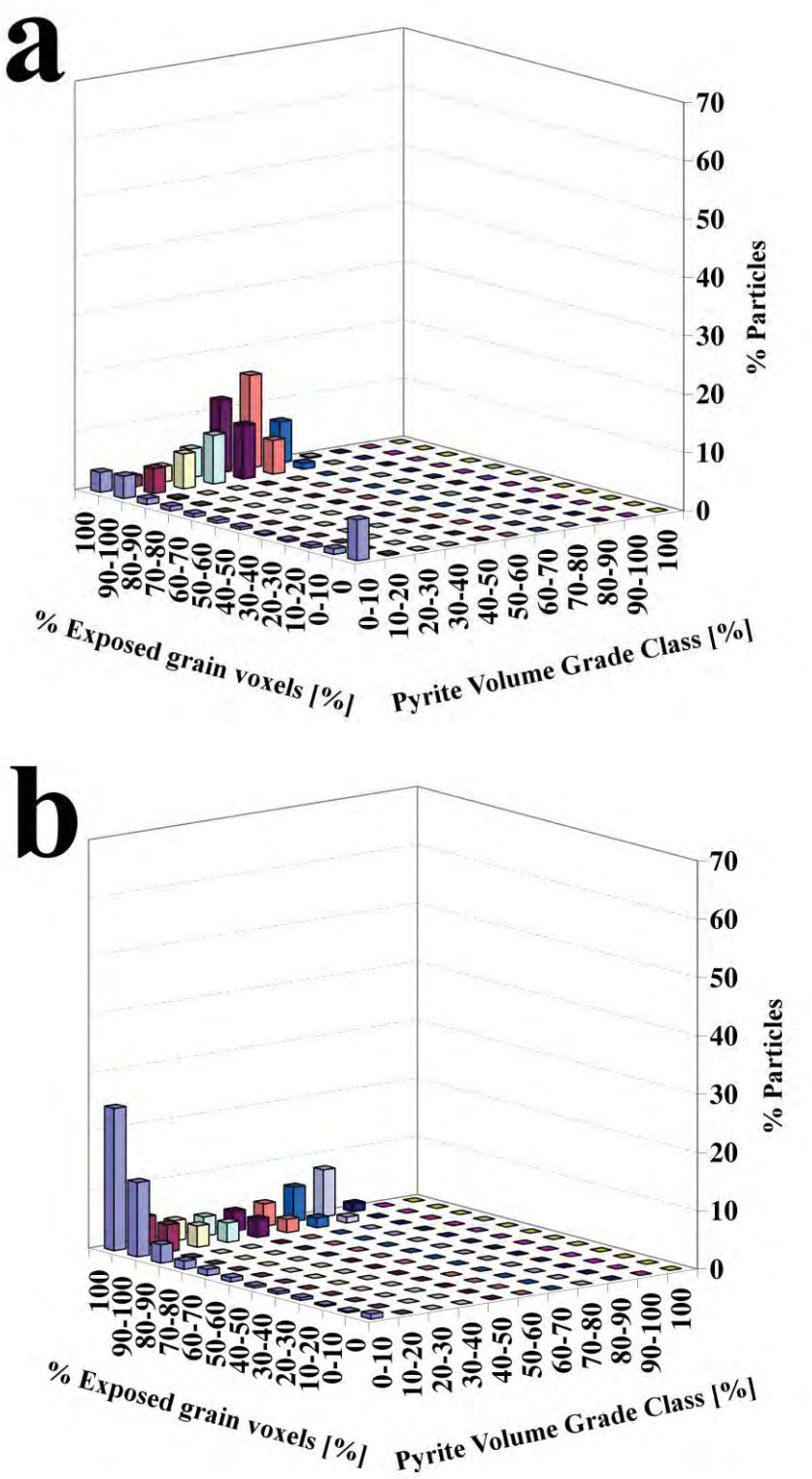

Figure C.10 Exposure results for concentrate 1 of flotation test # 3. a) 106x45 µm, b) 208x106 µm, c) 425x208 µm and d) 2000x425 µm.

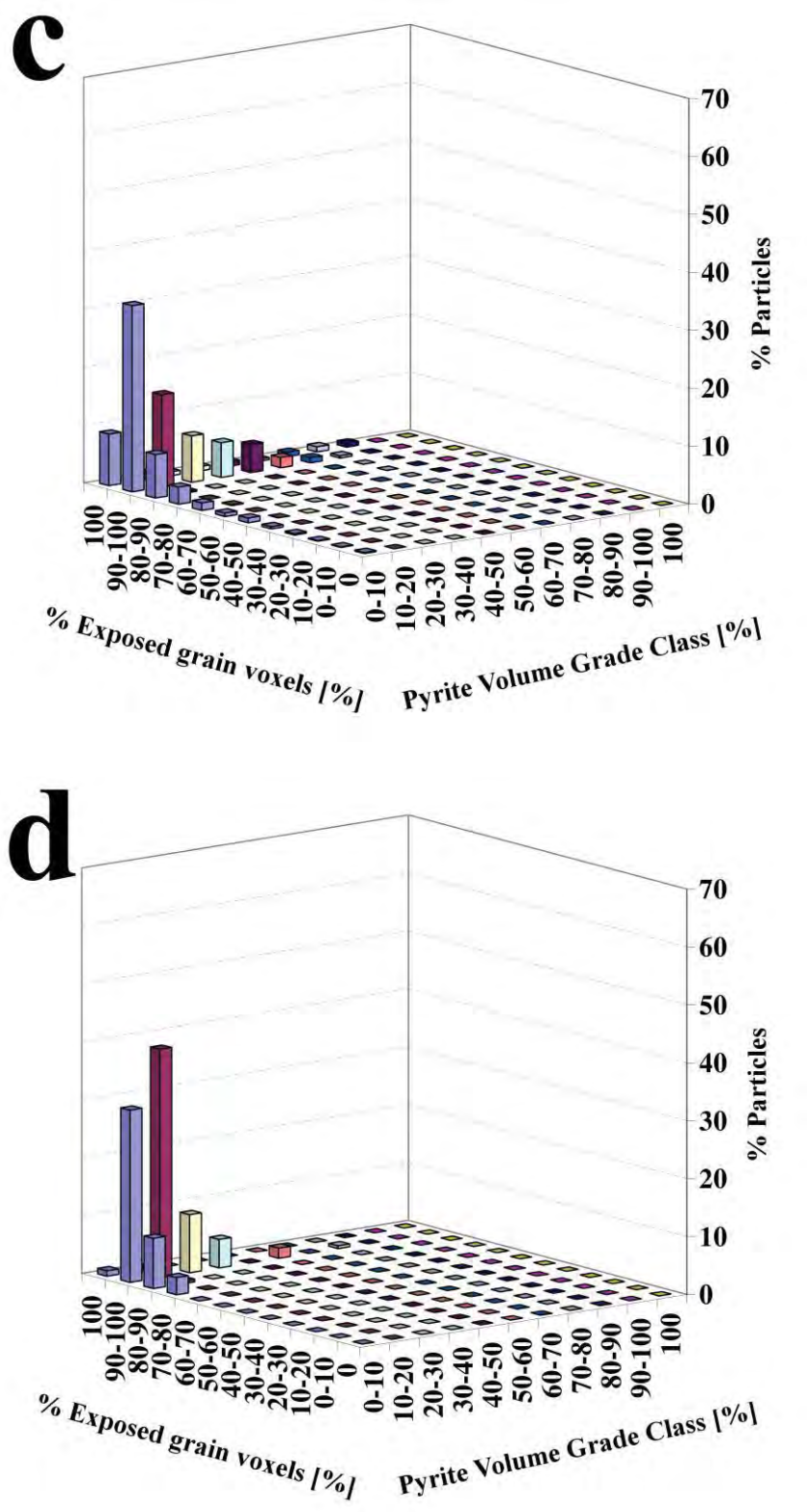

Figure C.10 Continued

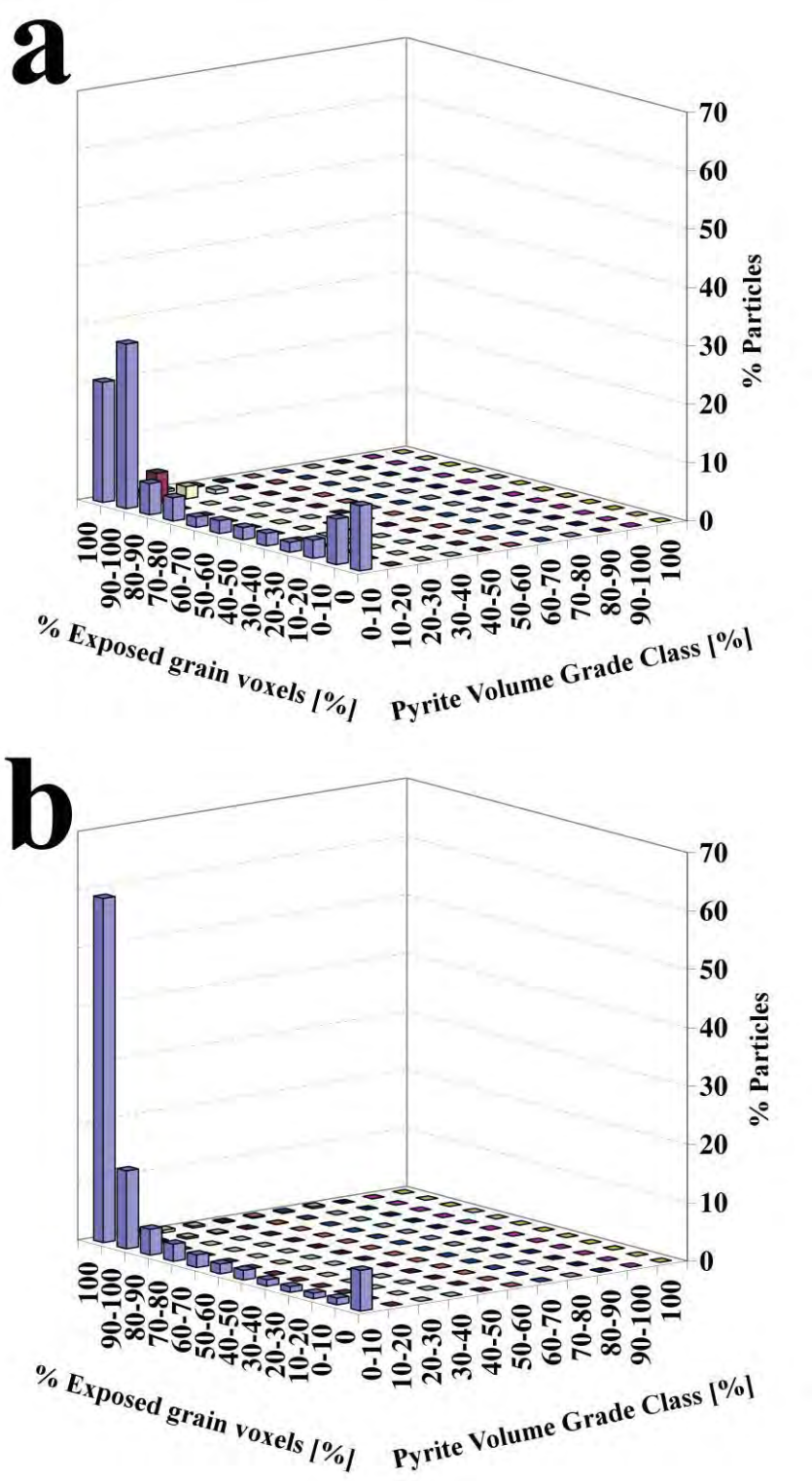

Figure C.11 Exposure results for concentrate 2 of flotation test # 3. a) 106x45 µm, b) 208x106 µm, c) 425x208 µm and d) 2000x425 µm.

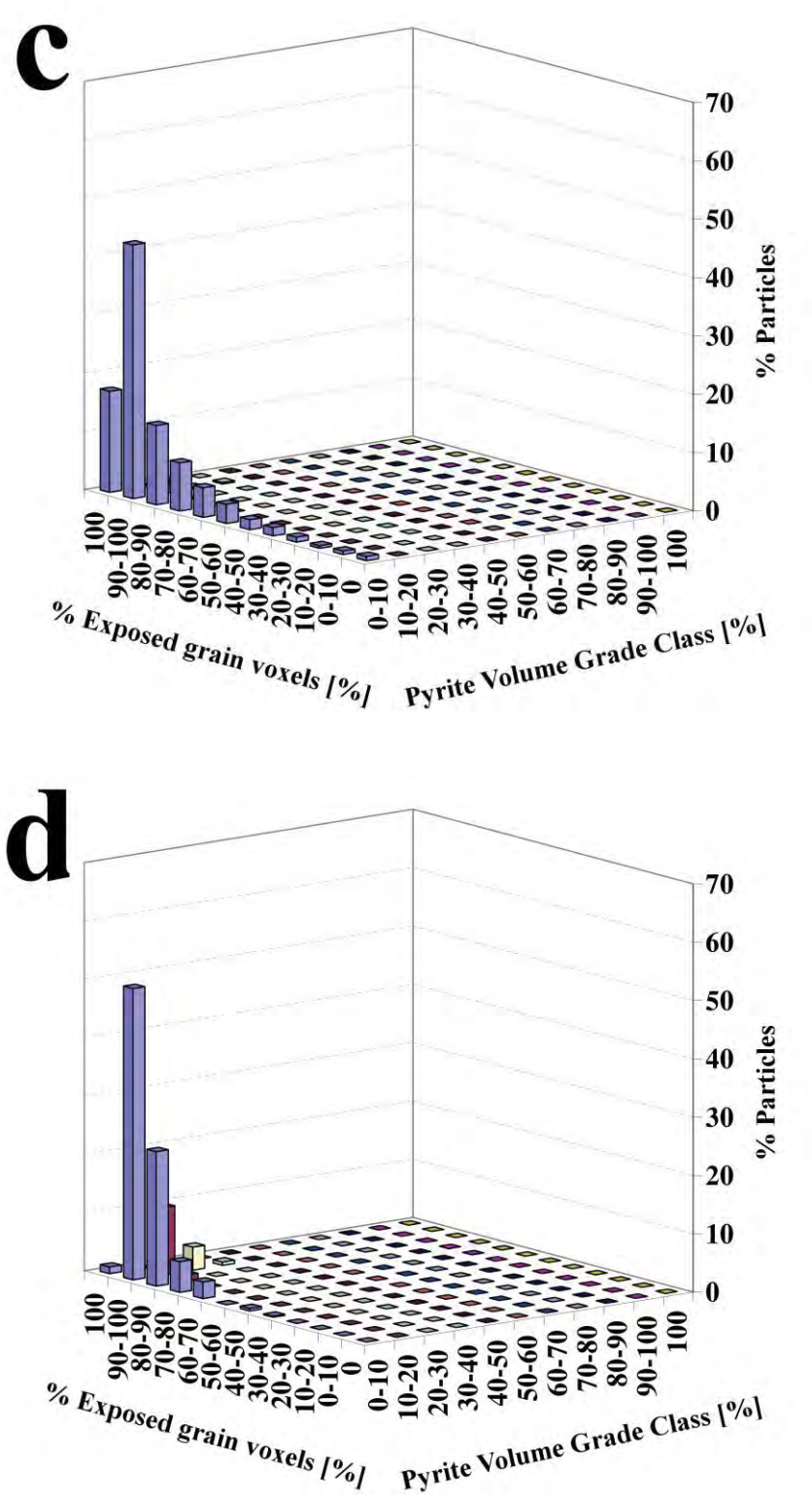

Figure C.11 Continued

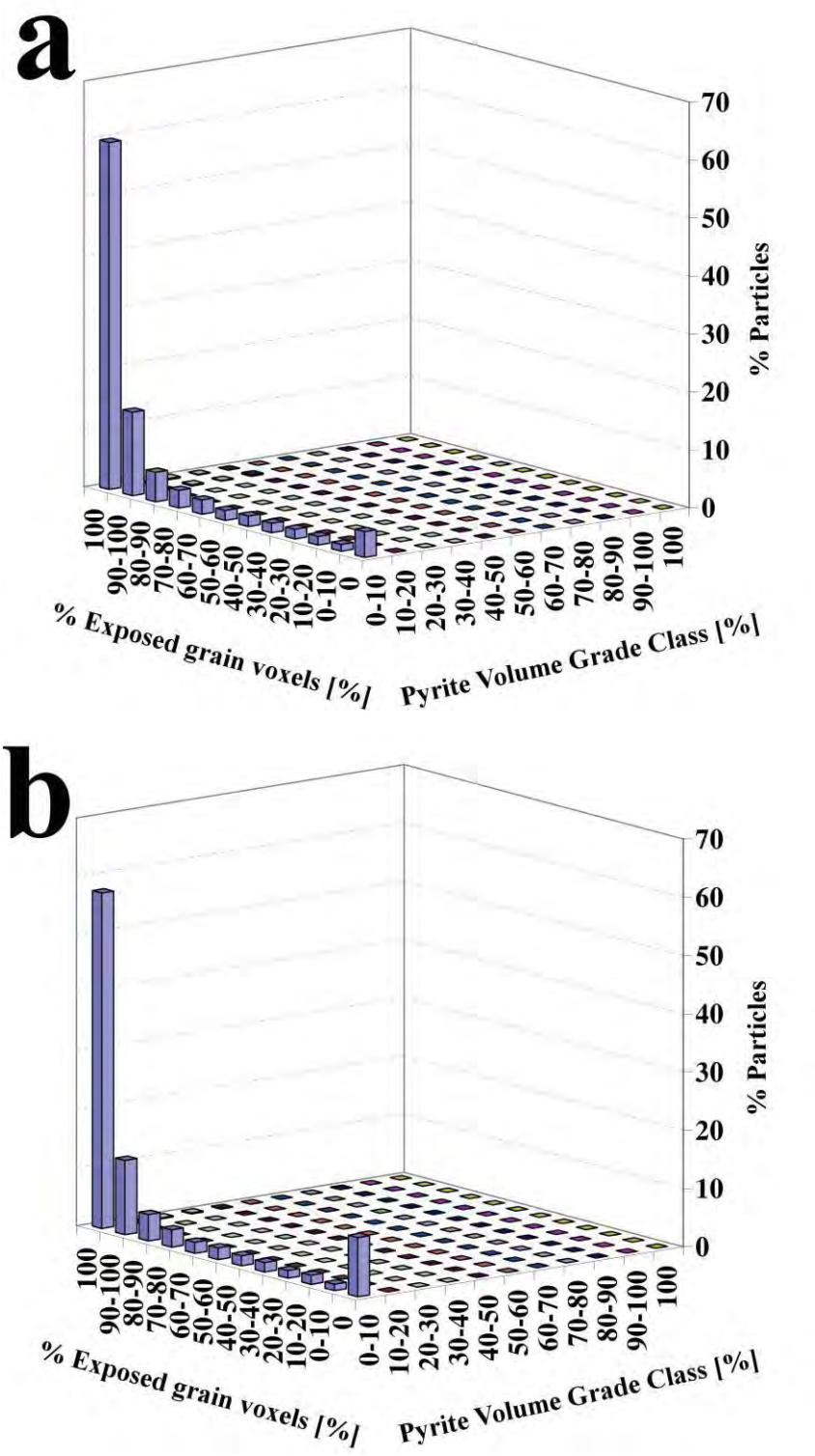

Figure C.12 Exposure results for concentrate 3 of flotation test # 3. a) 106x45 µm, b) 208x106 µm, c) 425x208 µm and d) 2000x425 µm.

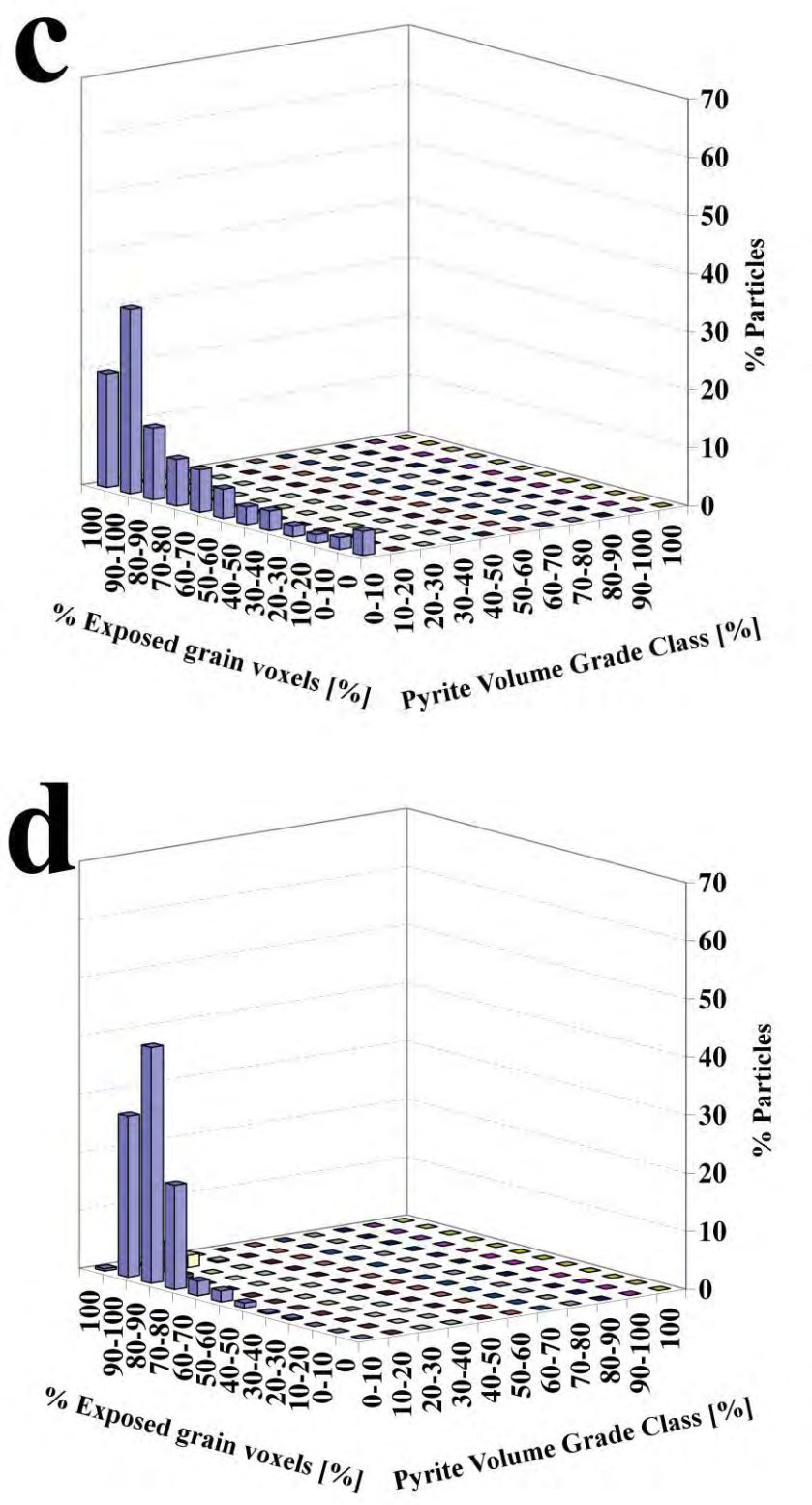

Figure C.12 Continued

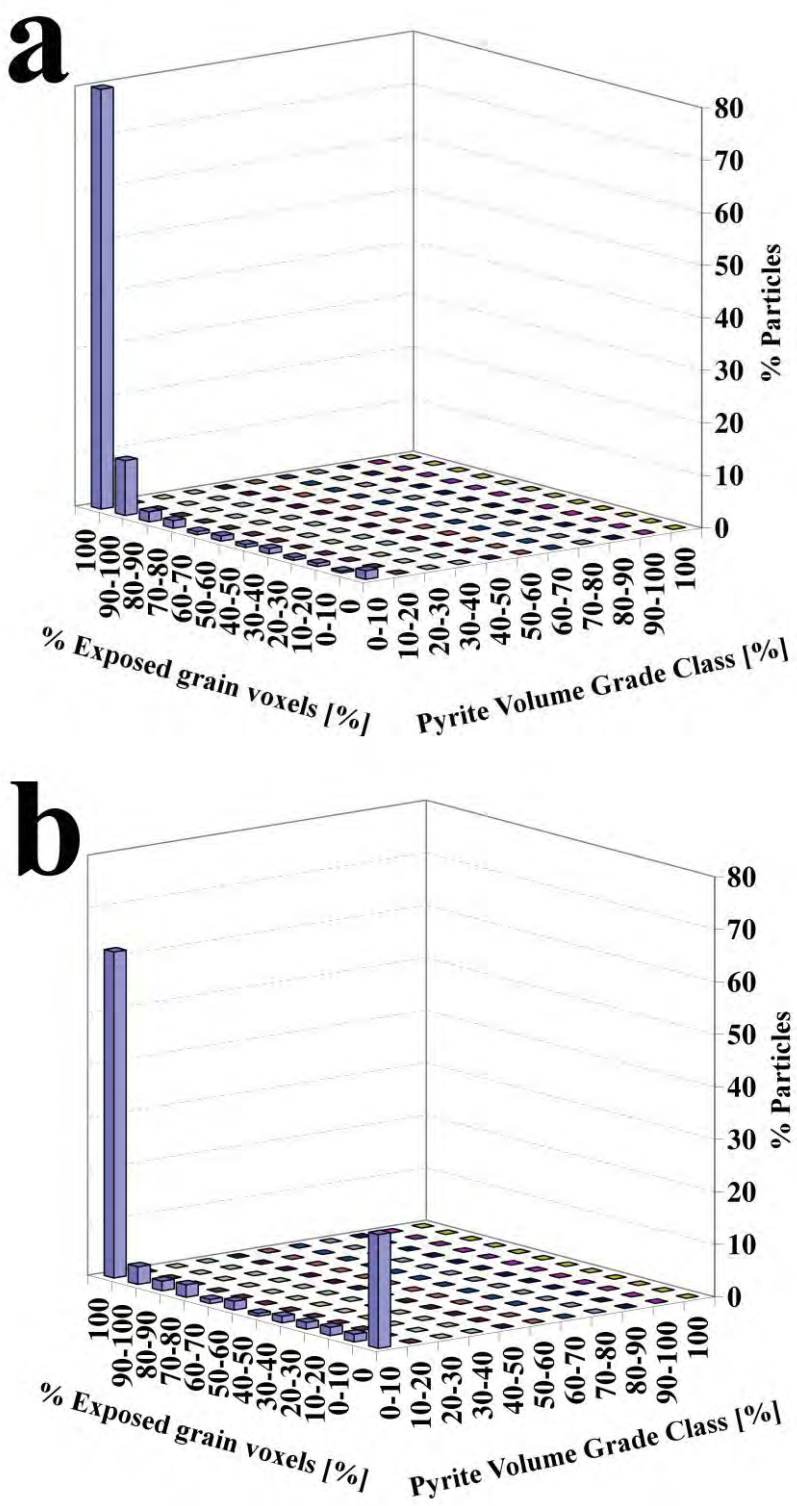

Figure C.13 Exposure results for tailings of flotation test # 3. a) 106x45 µm, b) 208x106 µm, c) 425x208 µm and d) 2000x425 µm.

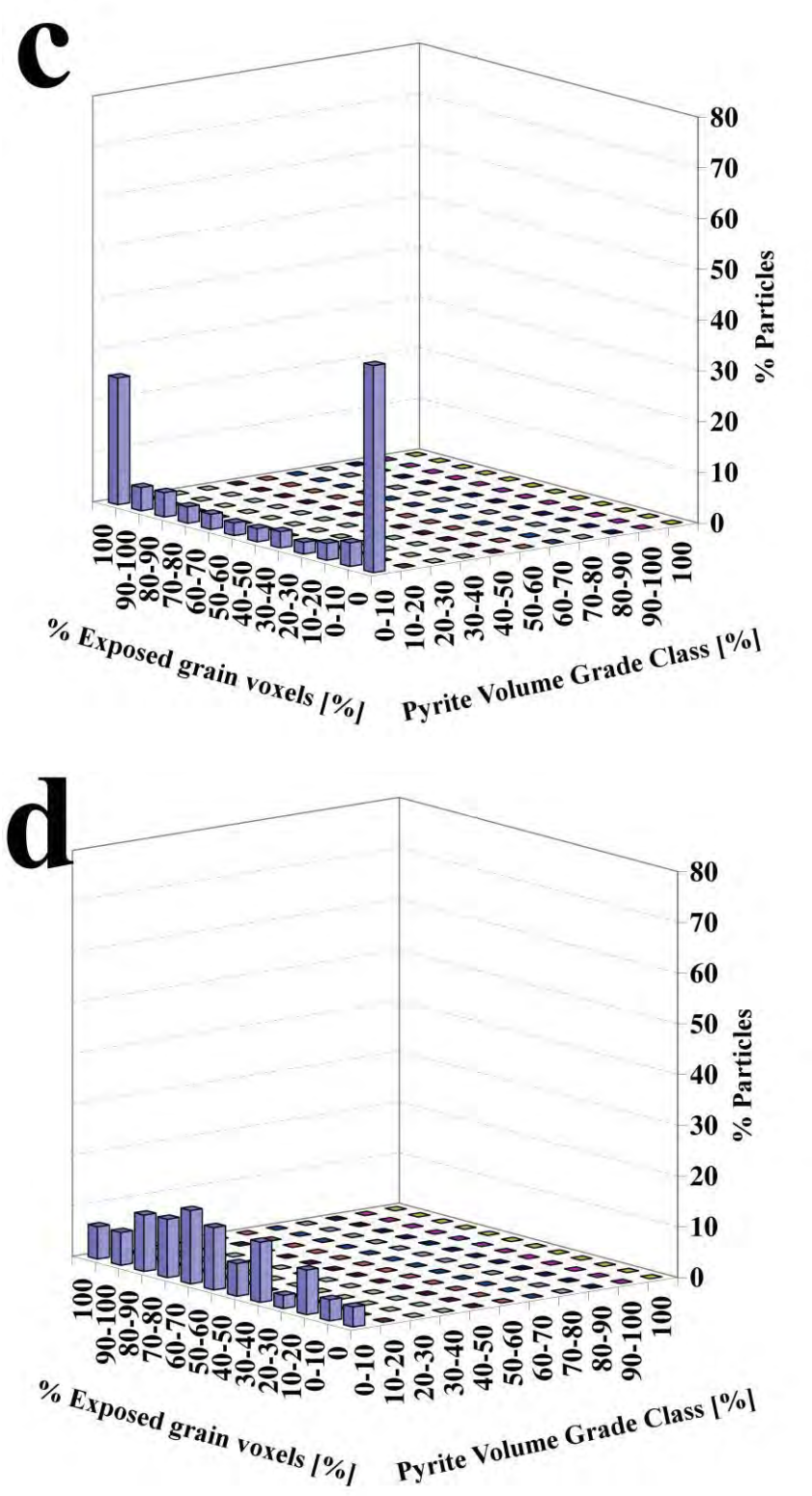

Figure C.13 Continued

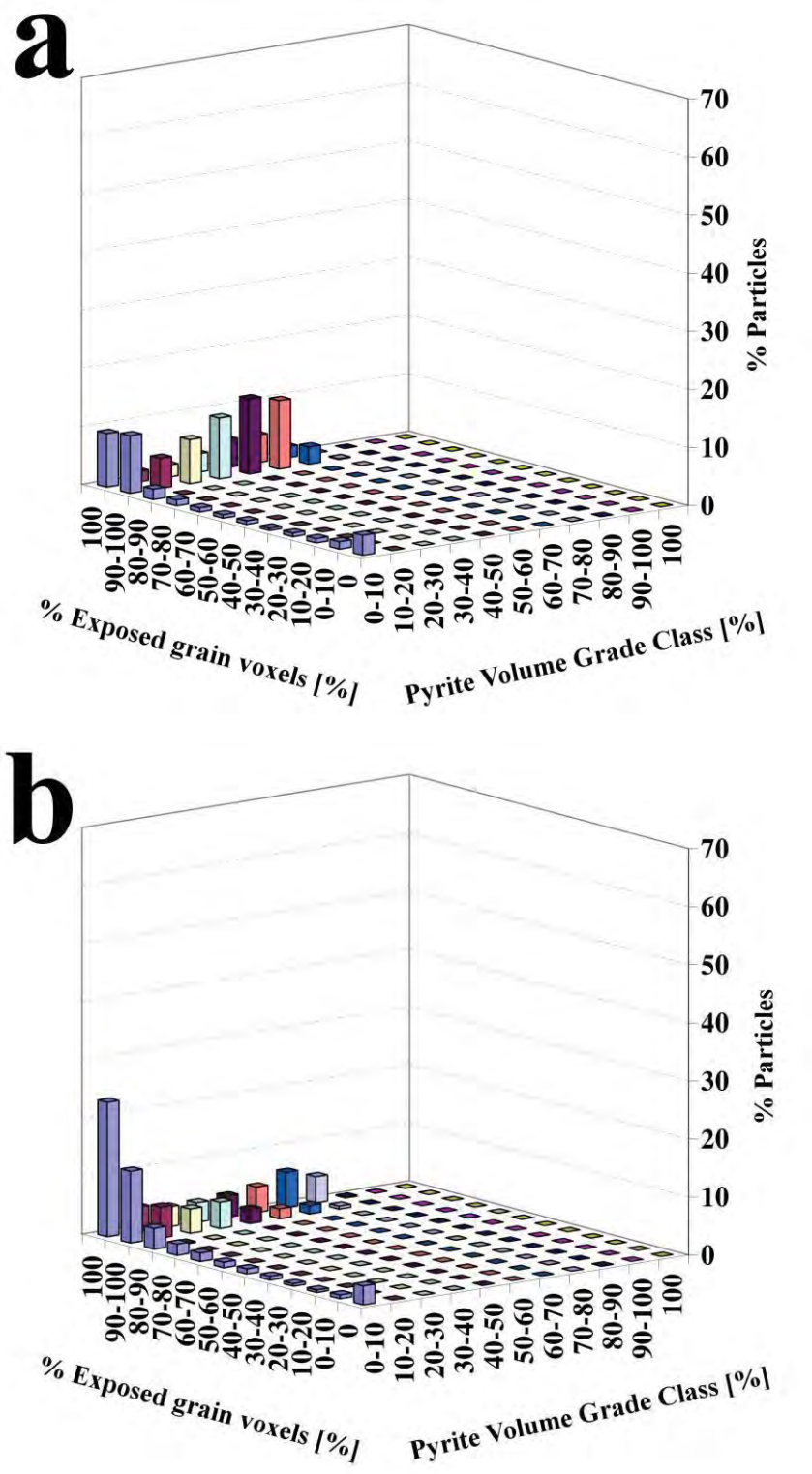

Figure C.14 Exposure results for concentrate 1of flotation test # 4. a) 106x45 µm, b) 208x106 µm, c) 425x208 µm and d) 2000x425 µm.

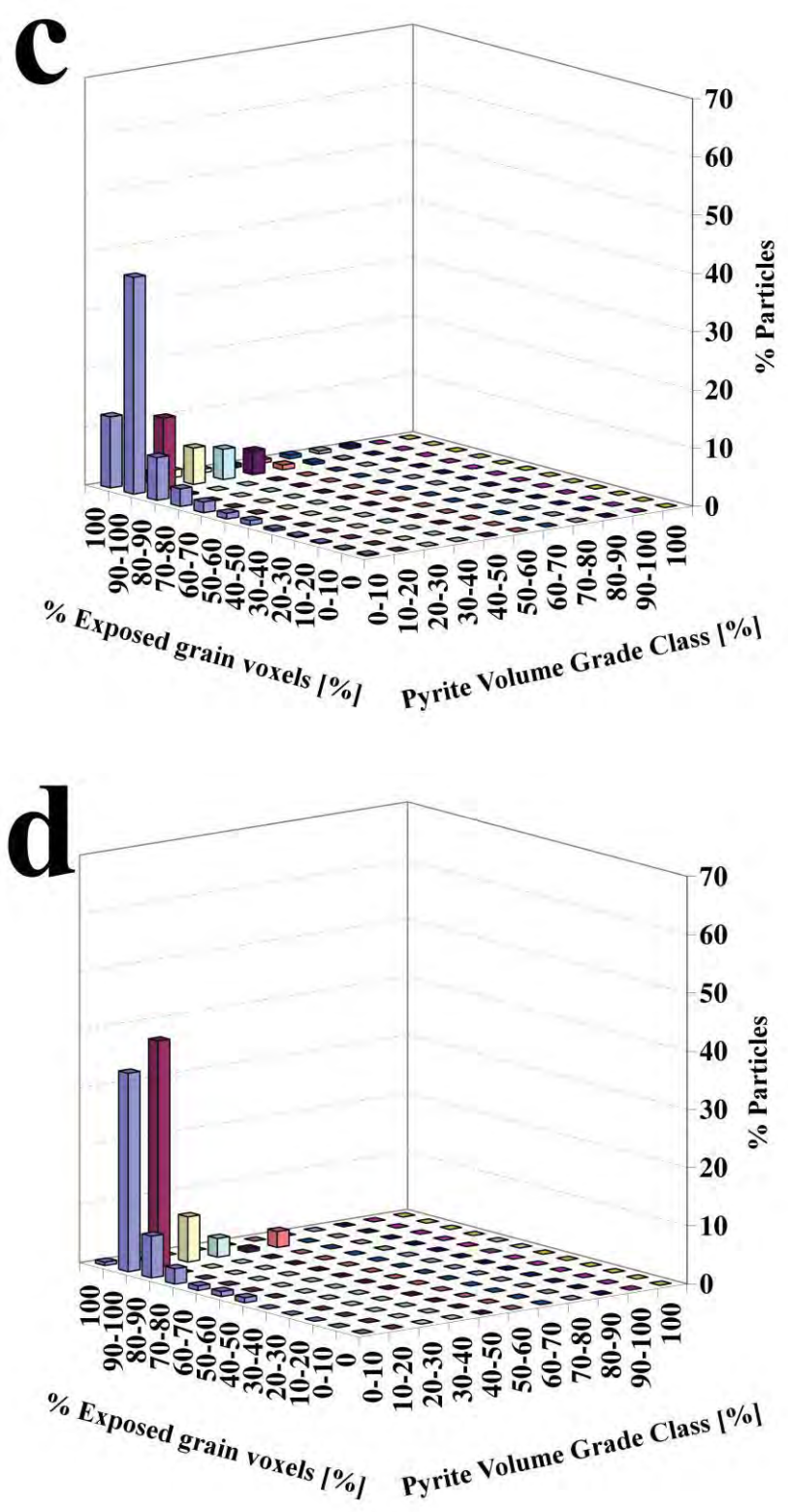

Figure C.14 Continued

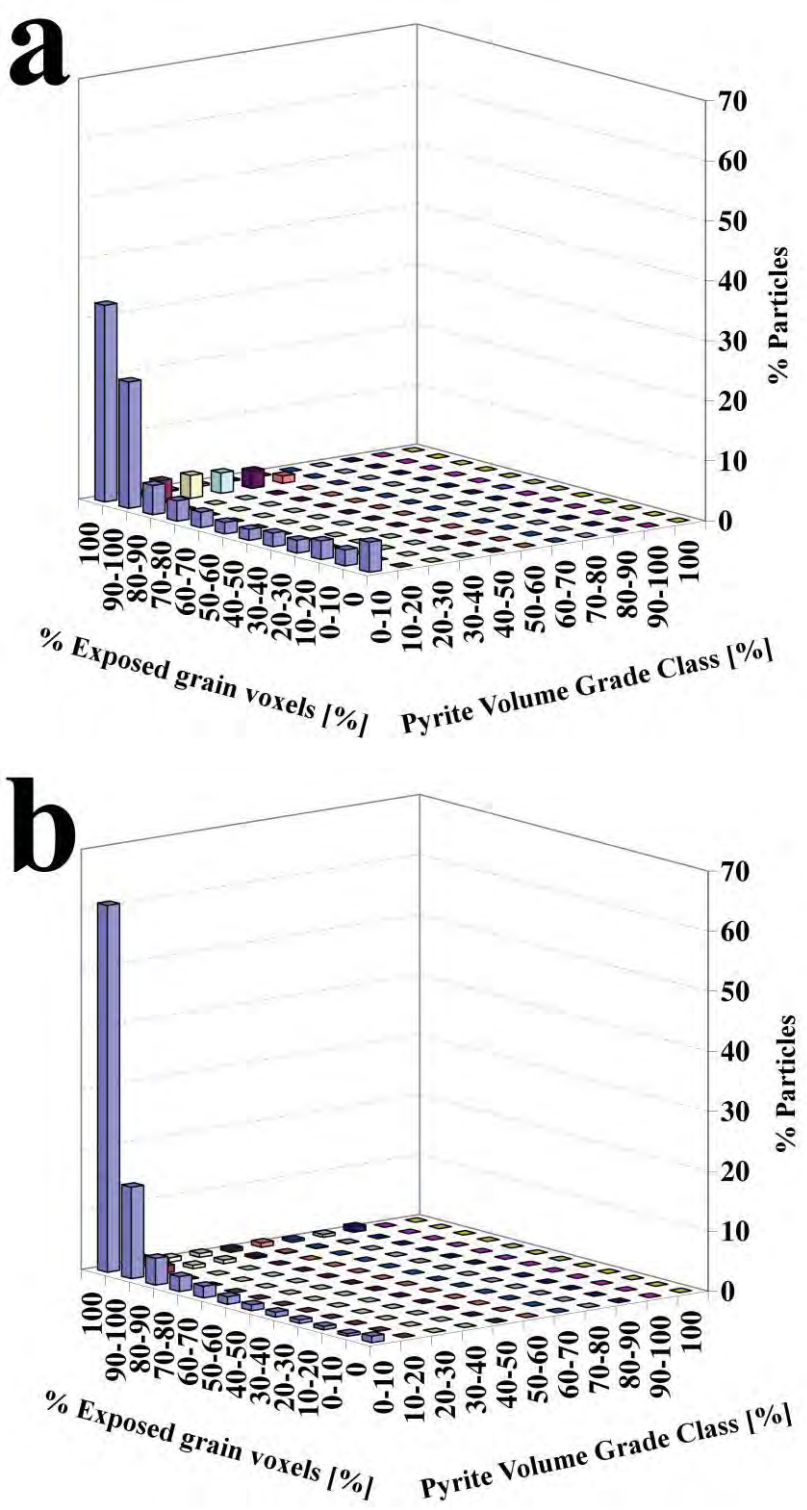

Figure C.15 Exposure results for concentrate 2 of flotation test # 4. a) 106x45 µm, b) 208x106 µm, c) 425x208 µm and d) 2000x425 µm.

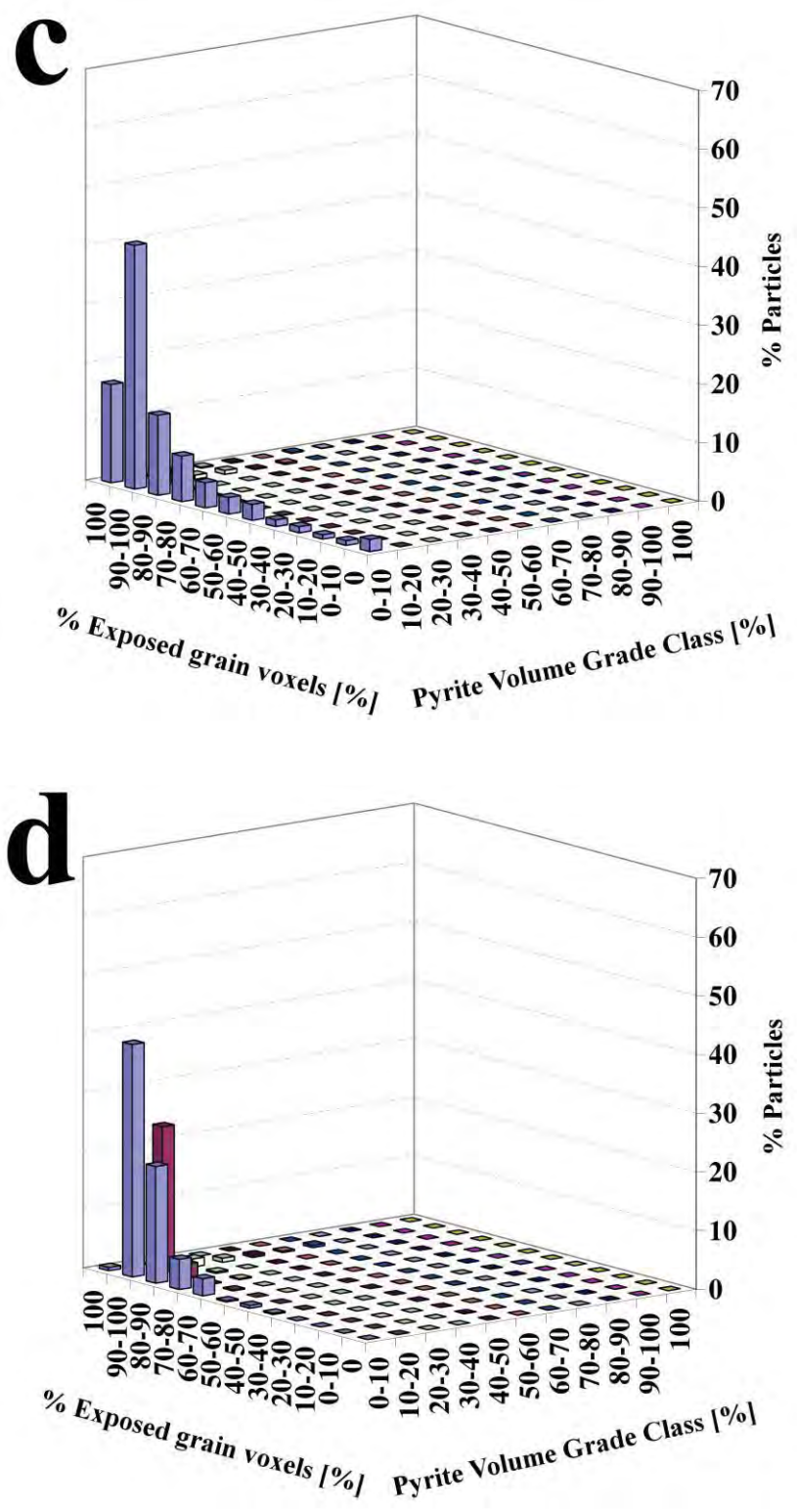

Figure C.15 Continued

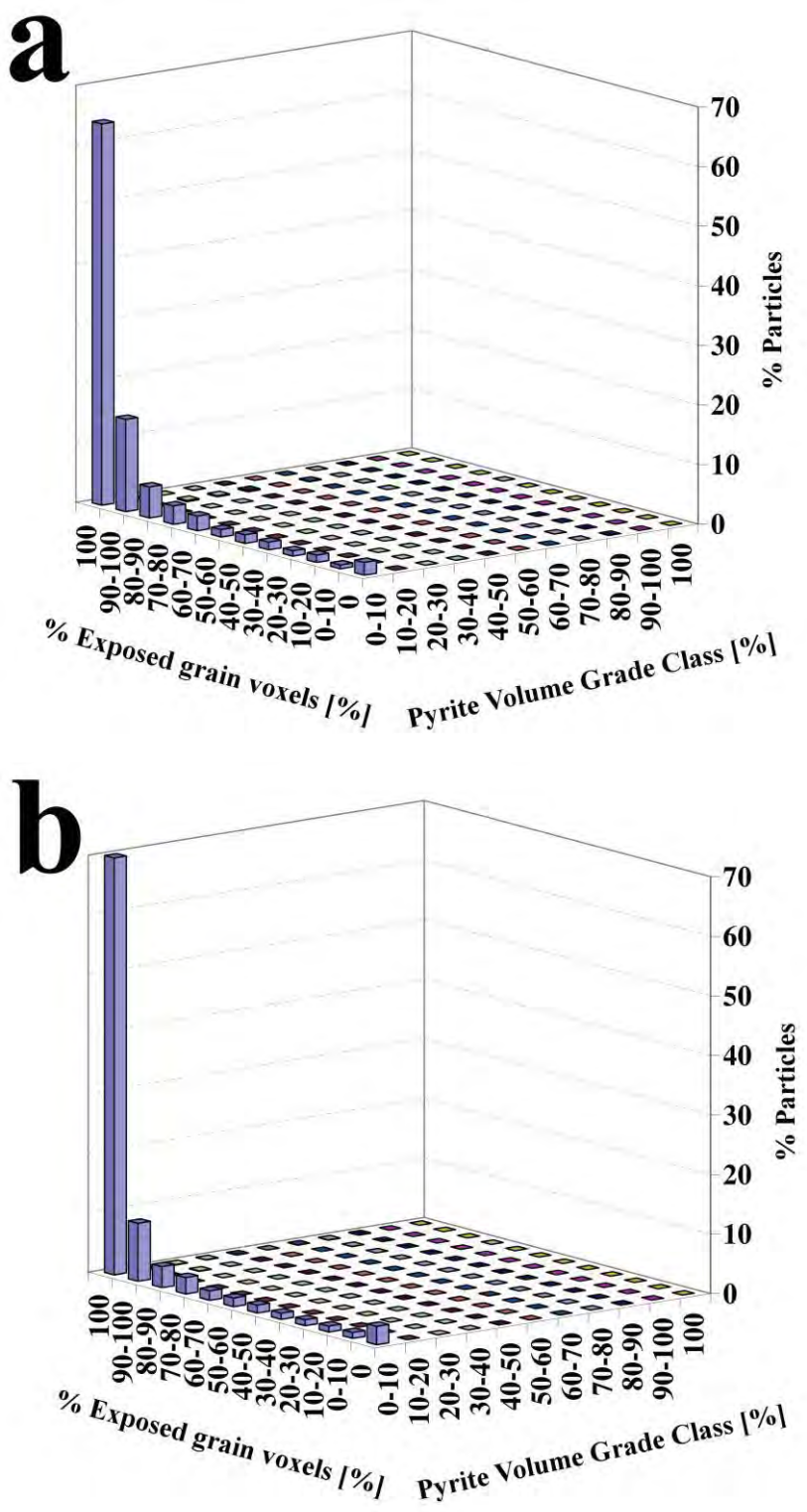

Figure C.16 Exposure results for concentrate 3 of flotation test # 4. a) 106x45 µm, b) 208x106 µm, c) 425x208 µm and d) 2000x425 µm.

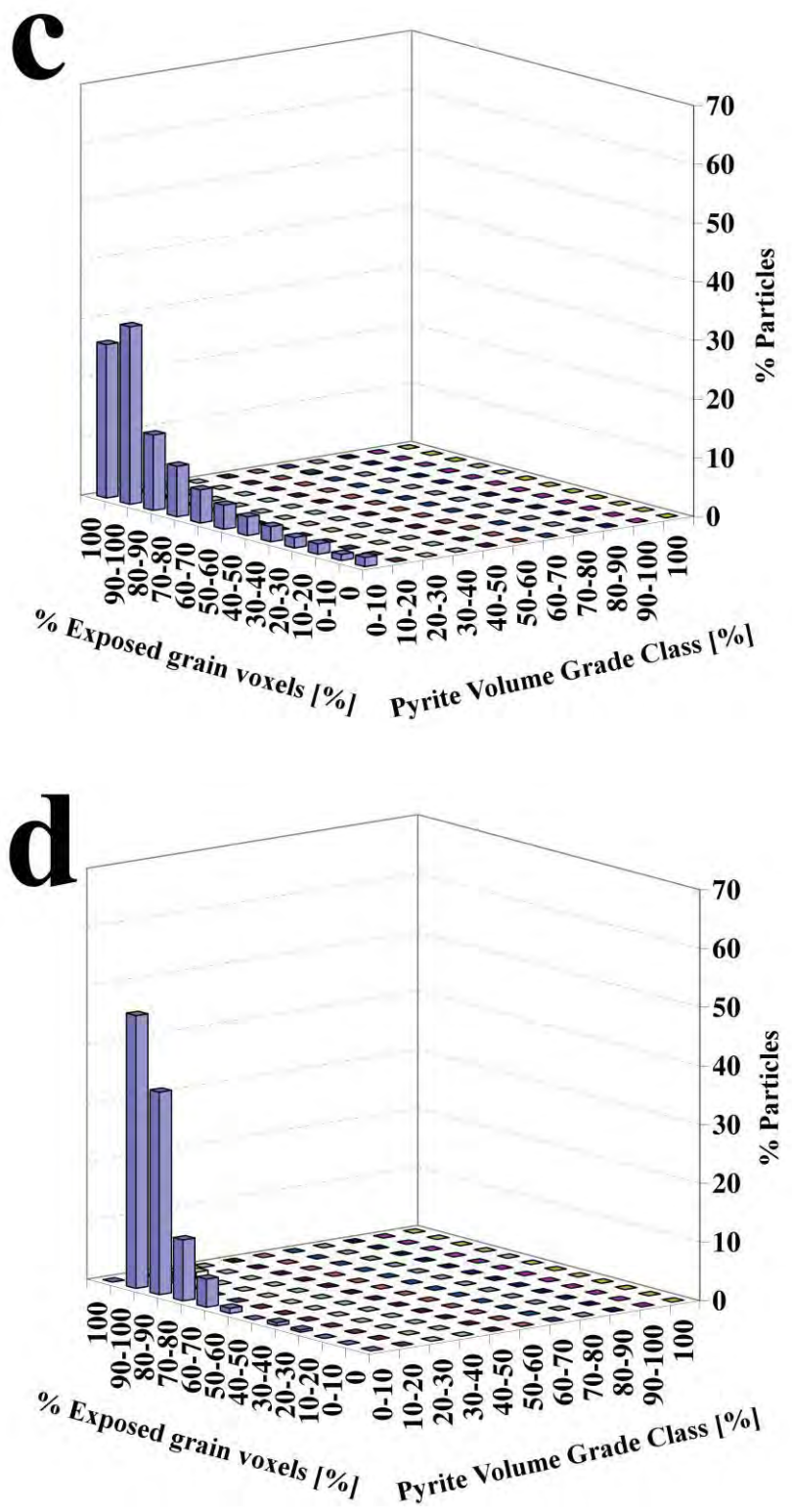

Figure C.16 Continued

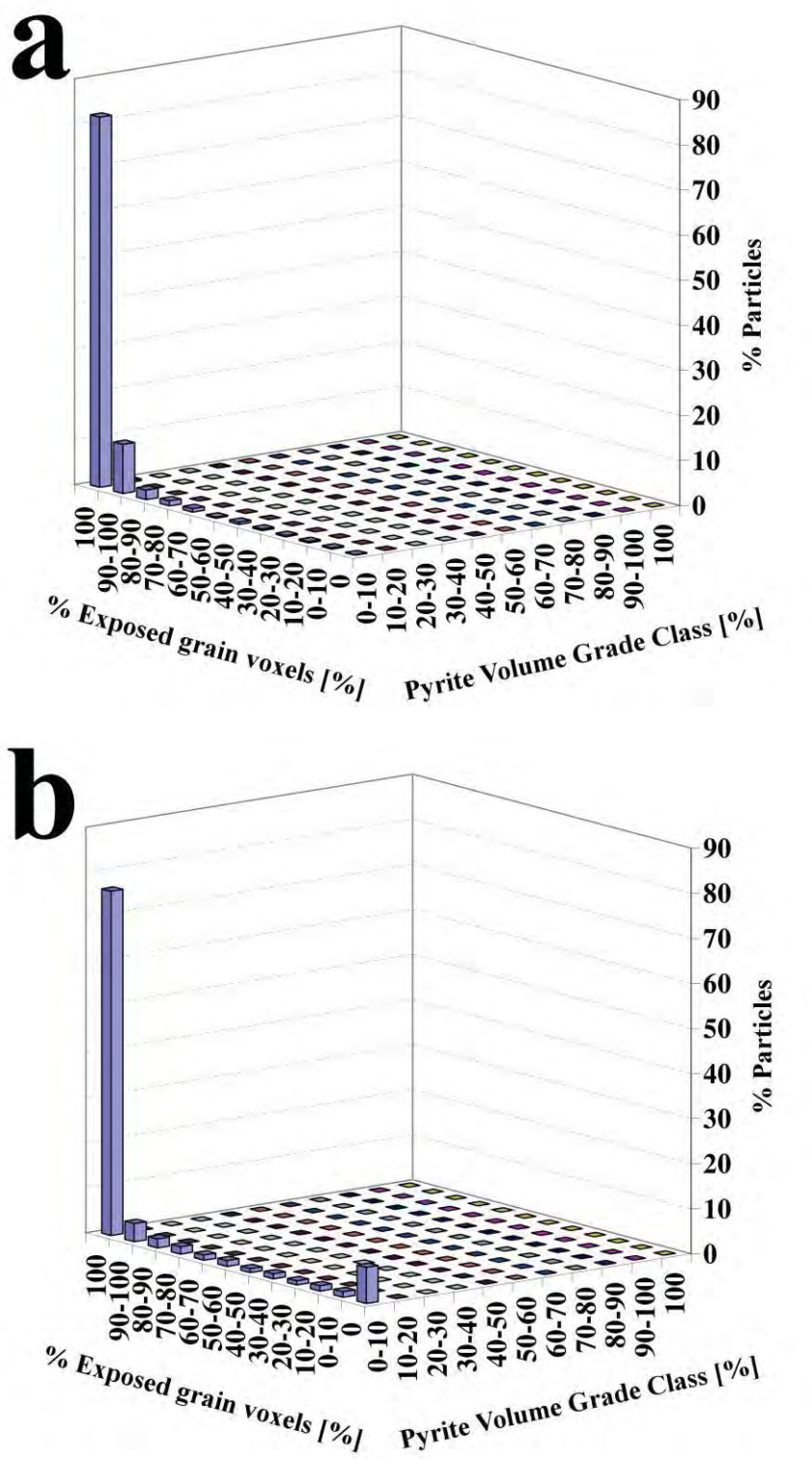

Figure C.17 Exposure results for tailings of flotation test # 4. a) 106x45 µm, b) 208x106 µm, c) 425x208 µm and d) 2000x425 µm.

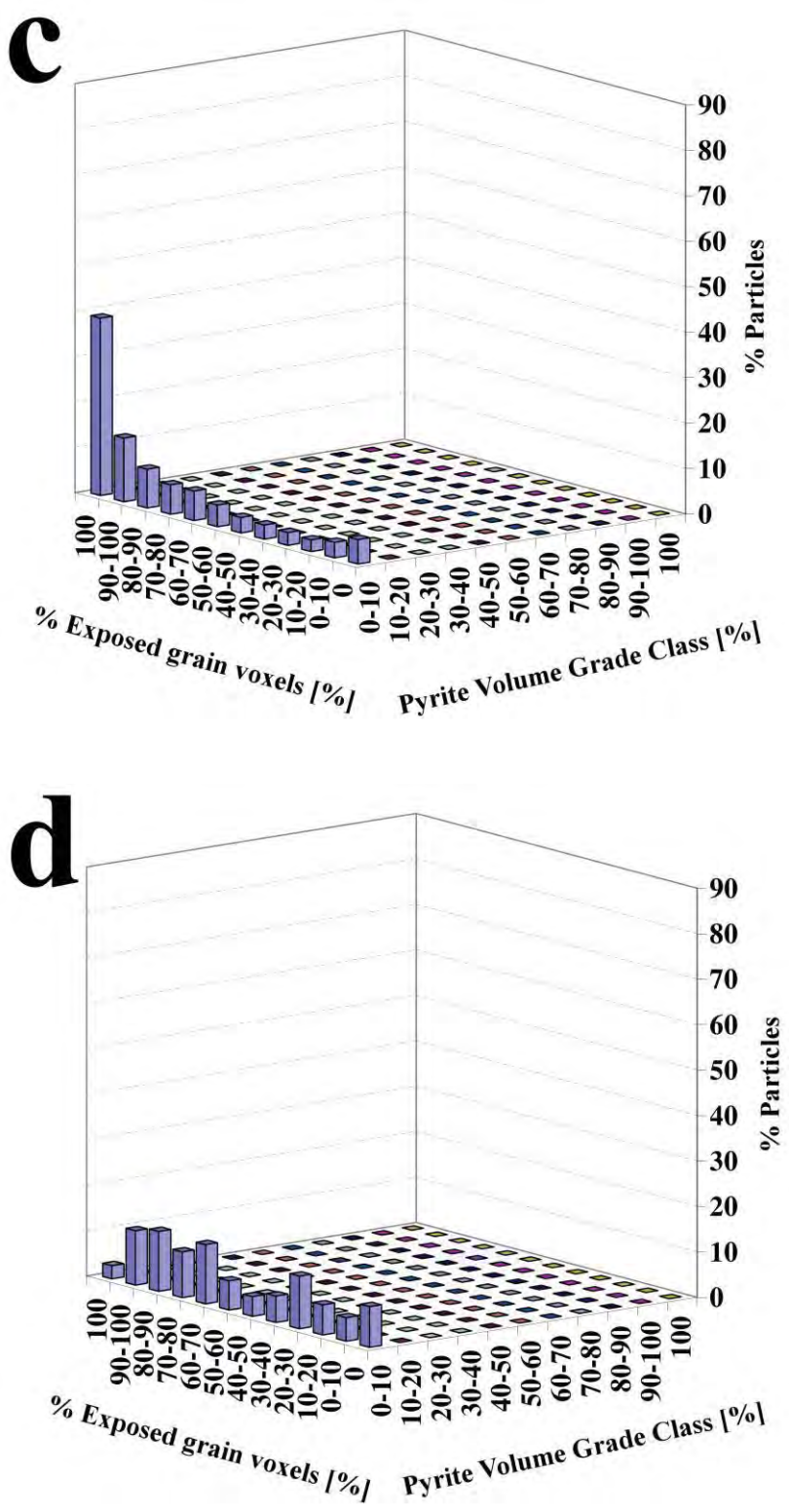

Figure C.17 Continued

APPENDIX D

MASS BALANCE OF PLANT FLOTATION CIRCUIT

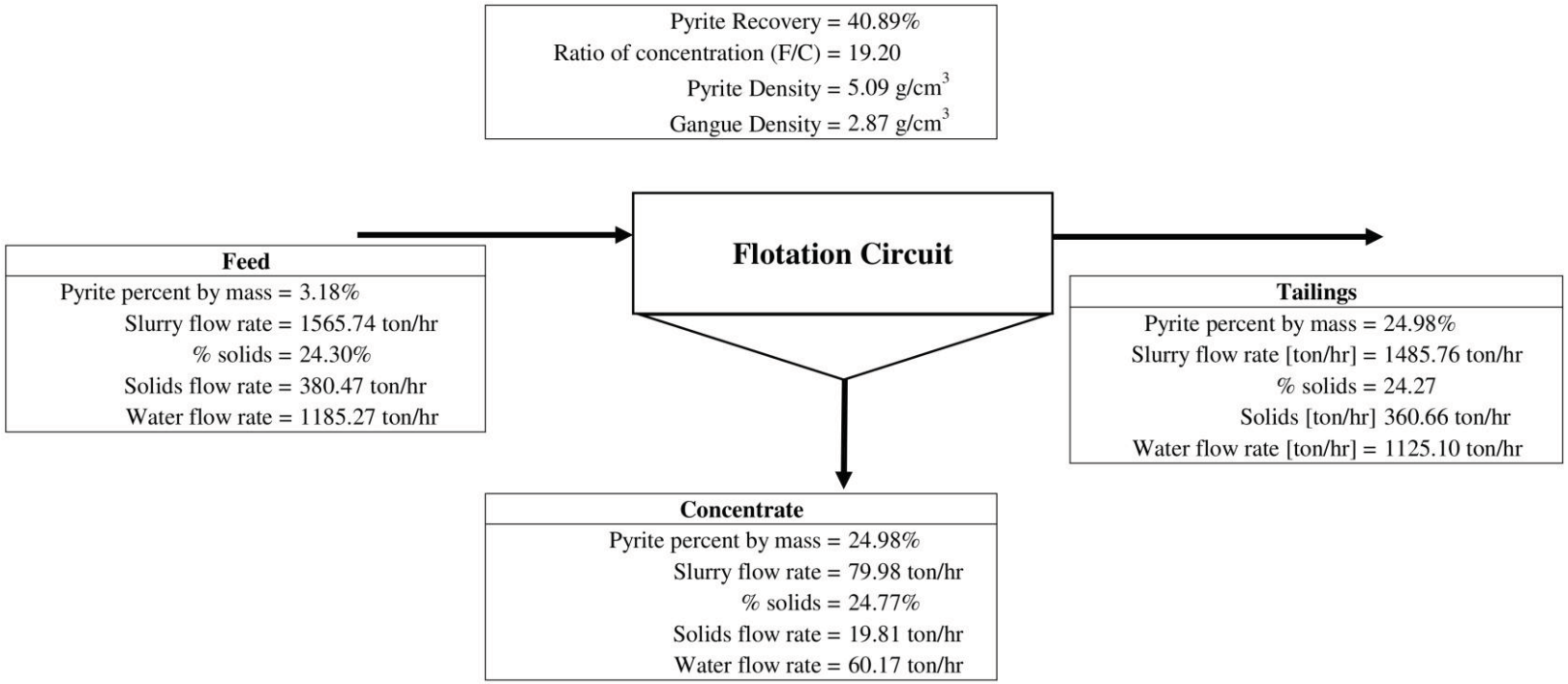

Figure D.1 Mass balance of solids and water for flotation circuit.

APPENDIX E

EXPOSURE ANALYSIS OF INDIVIDUAL PARTICLES OF SAMPLES FROM PLANT FLOTATION CIRCUIT

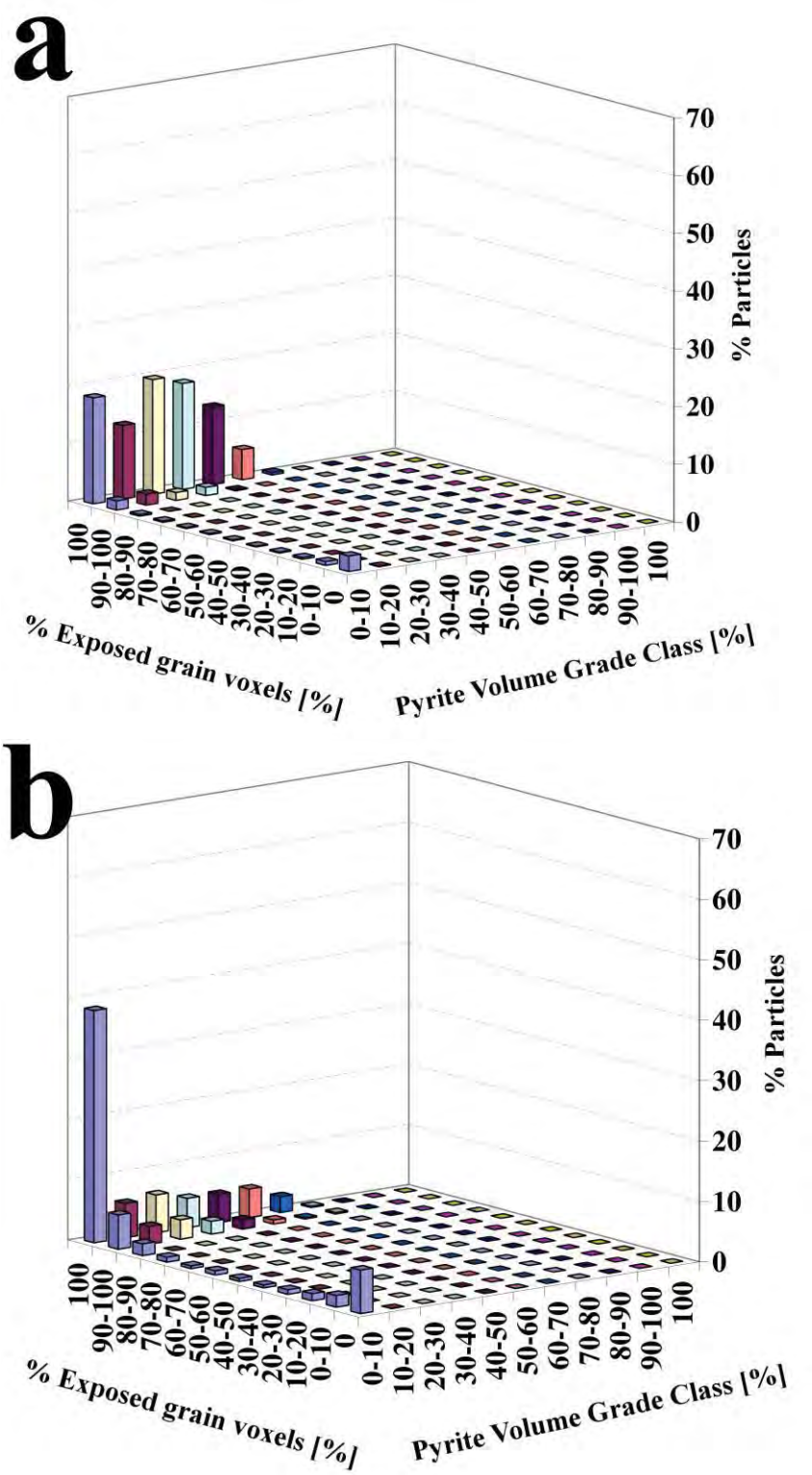

Figure E.1 Exposure results of feed from flotation circuit. a) 45x25 µm, b) 106x45 µm, c) 208x106 µm, d) 425x208 µm and e) 2000x425 µm.

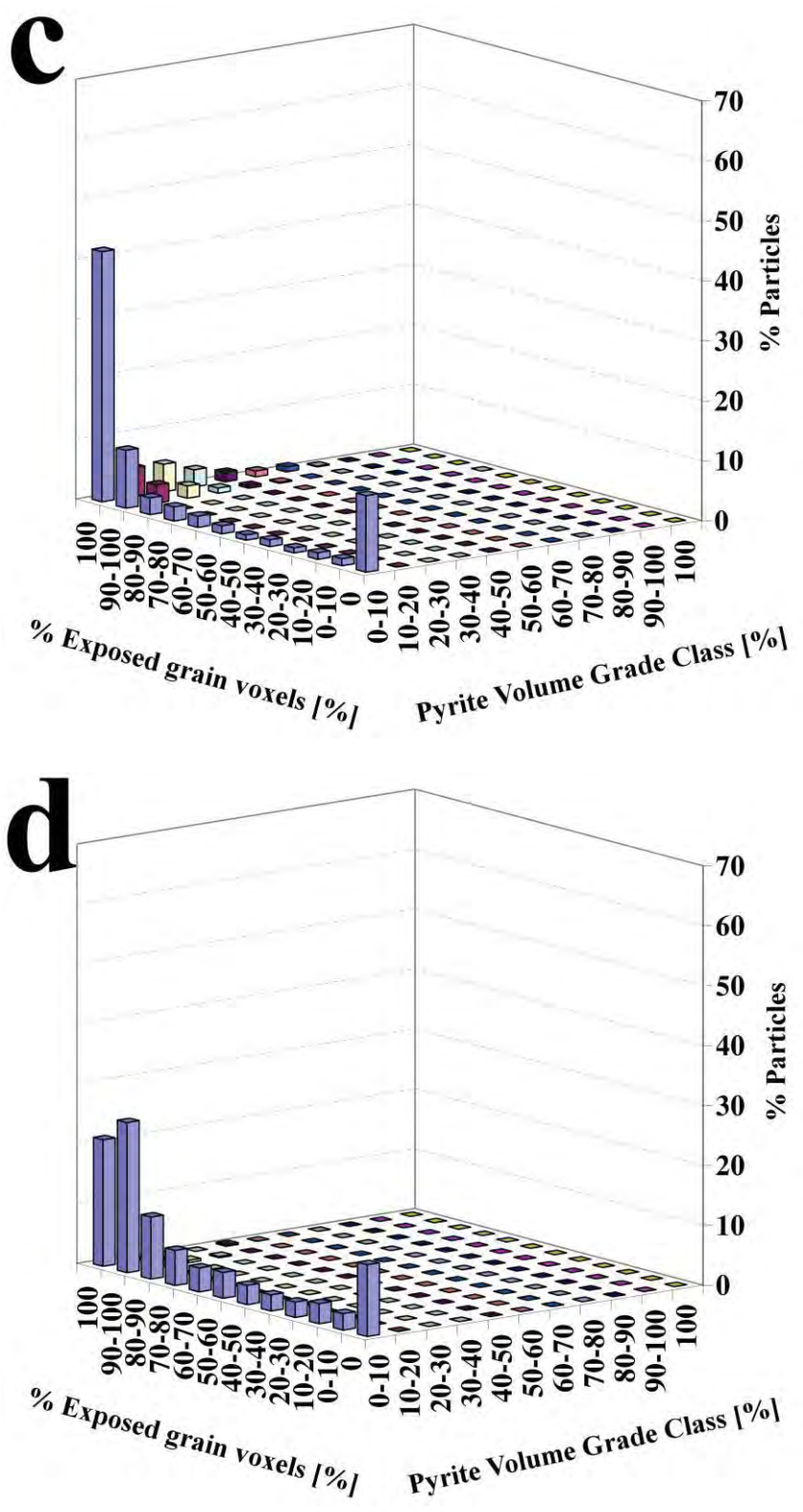

Figure E.1 Continued

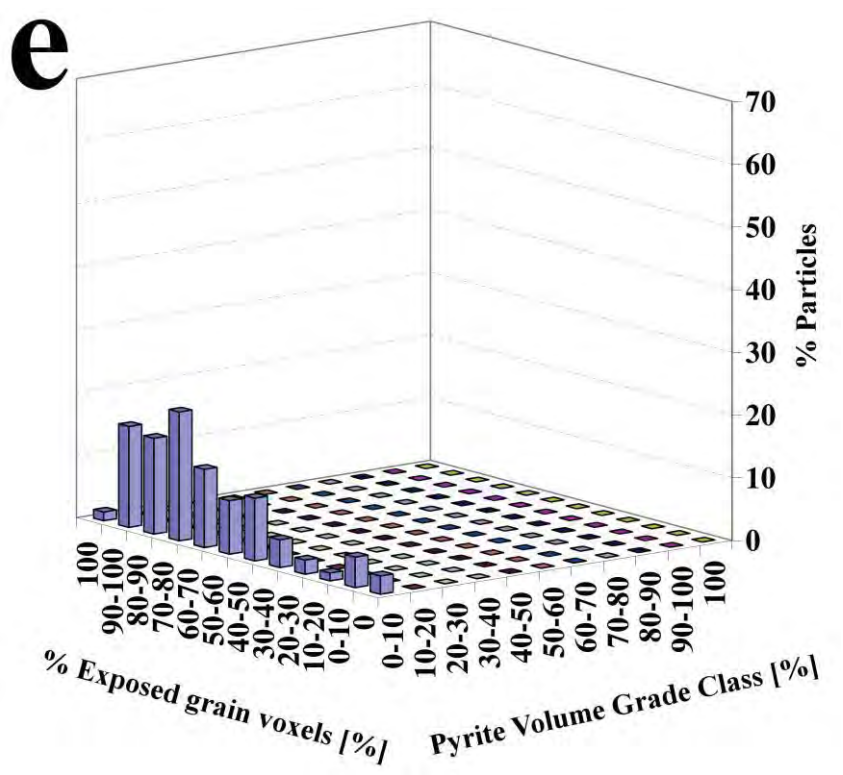

Figure E.1 Continued

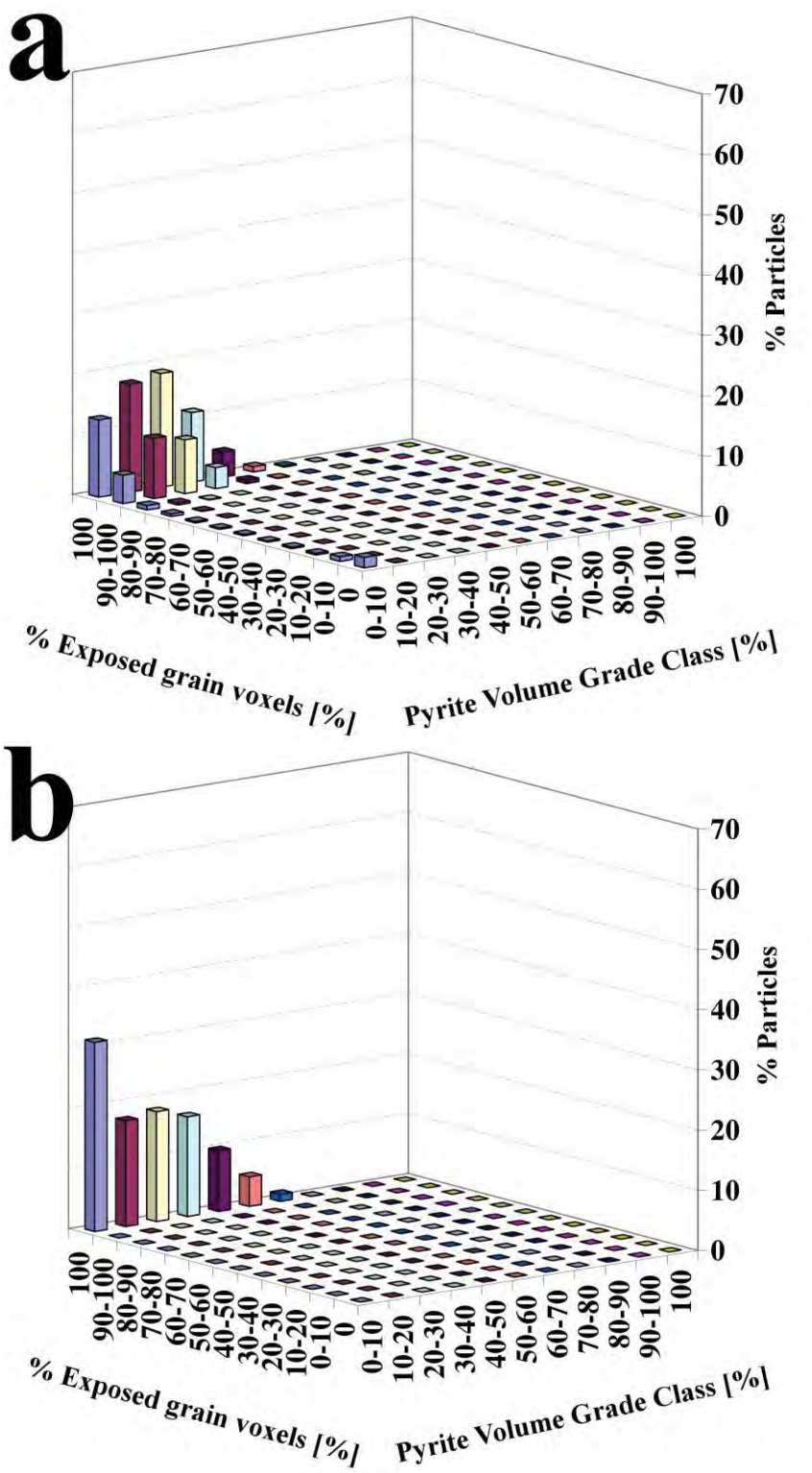

Figure E.2 Exposure results of concentrate from flotation circuit. a) 45x25 µm, b) 106x45 µm, c) 208x106 µma and d) 425x208 µm

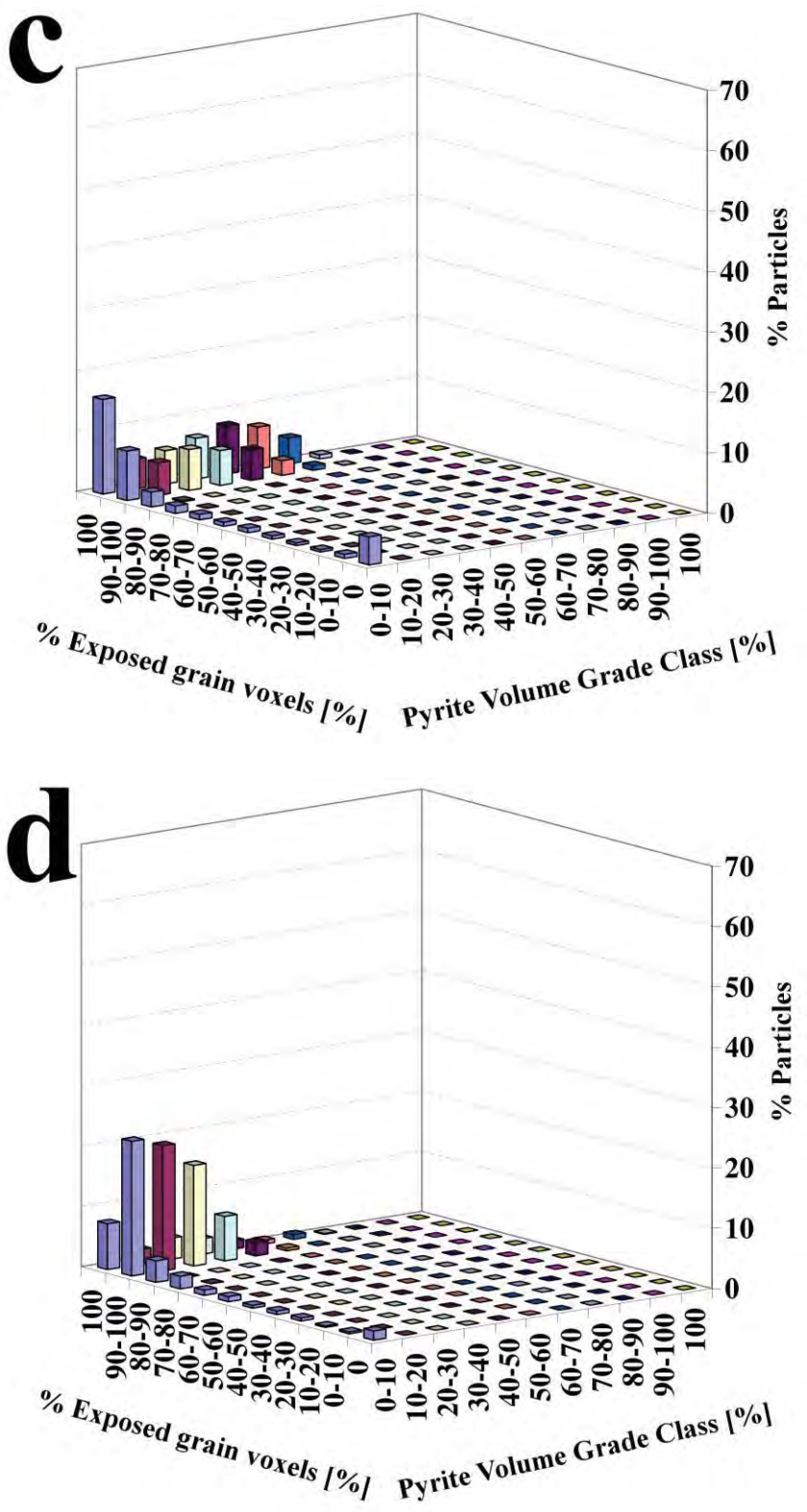

Figure E.2 Continued

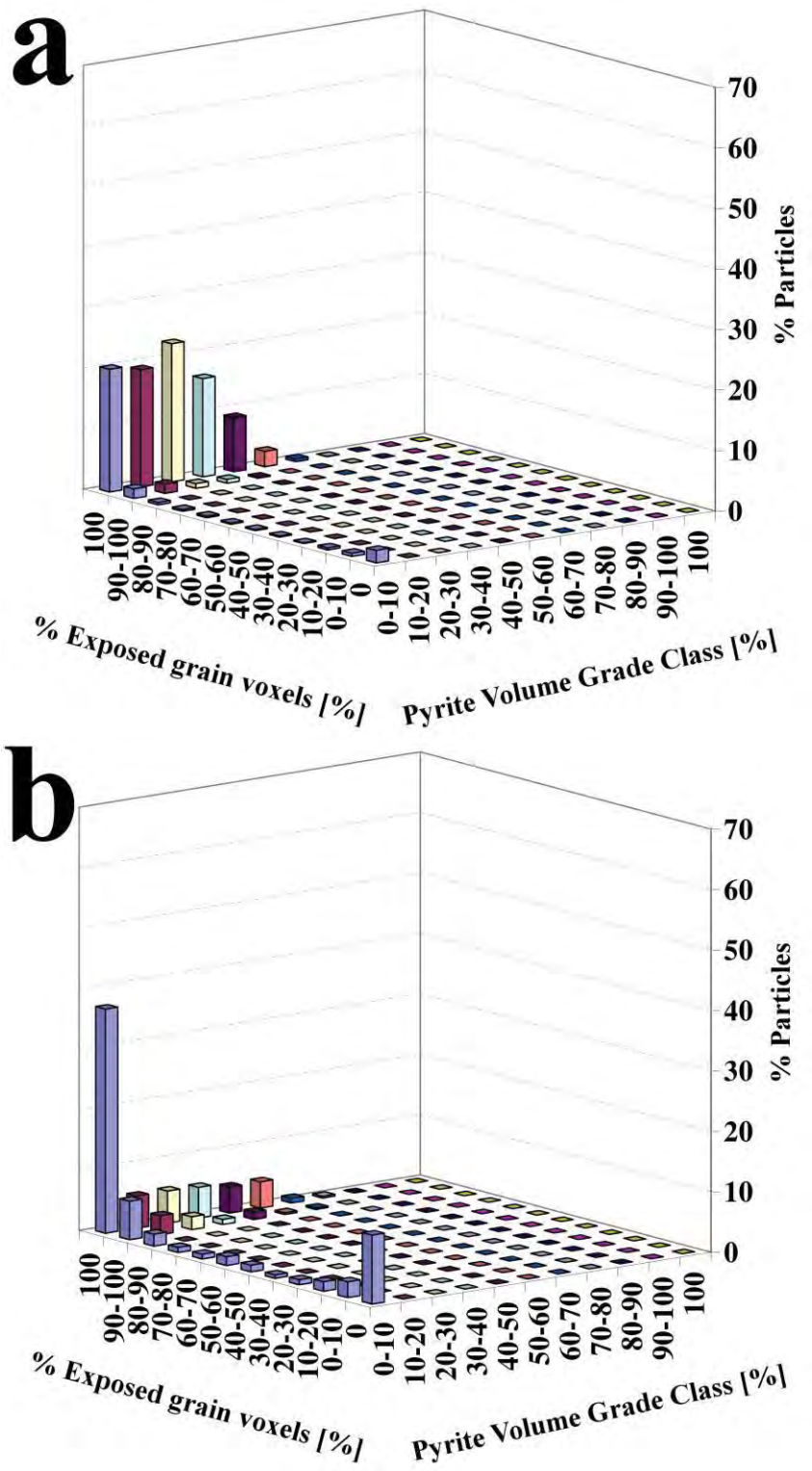

Figure E.3 Exposure results of tailings from flotation circuit. a) 45x25 µm, b) 106x45 µm, b) 208x106 µm, c) 425x208 µm and e) 2000x425 µm.

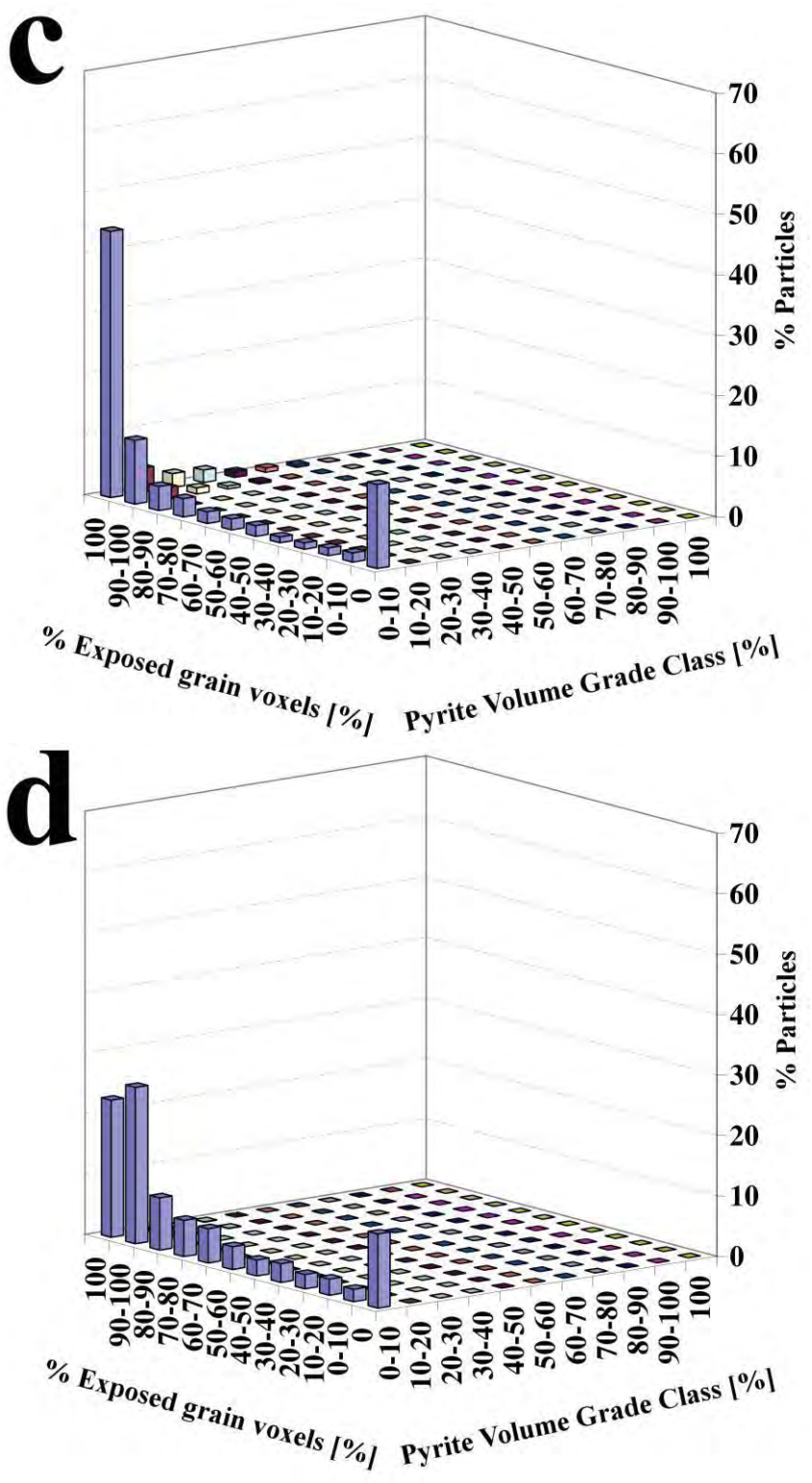

Figure E.3 Continued

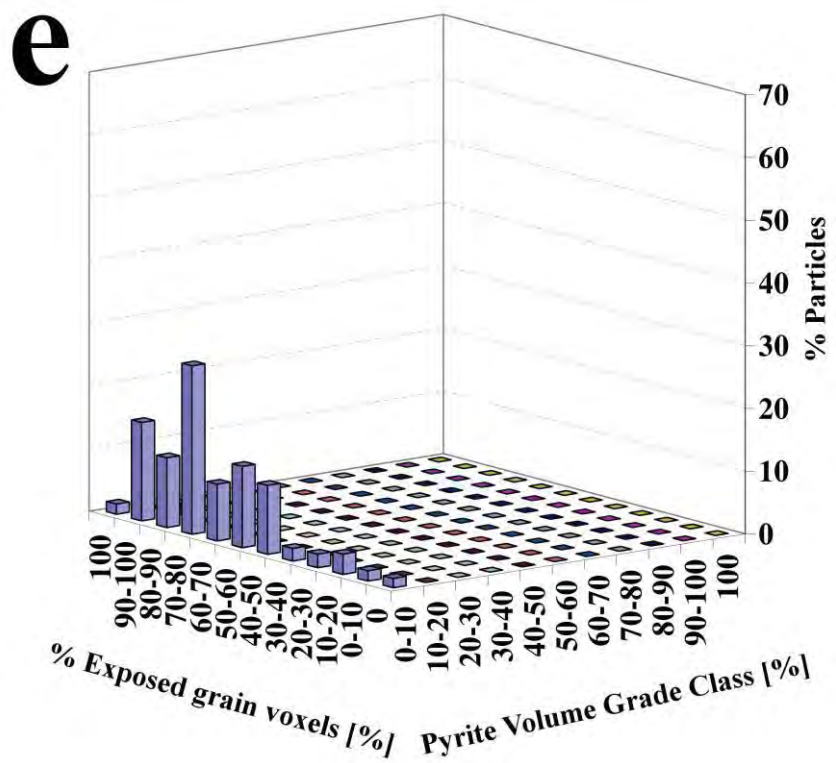

Figure E.3 Continued

APPENDIX F

PYRITE GRADE RESULTS OF MLA AND HRXMT ANALYSIS

OF FLOTATION CIRCUIT SAMPLES

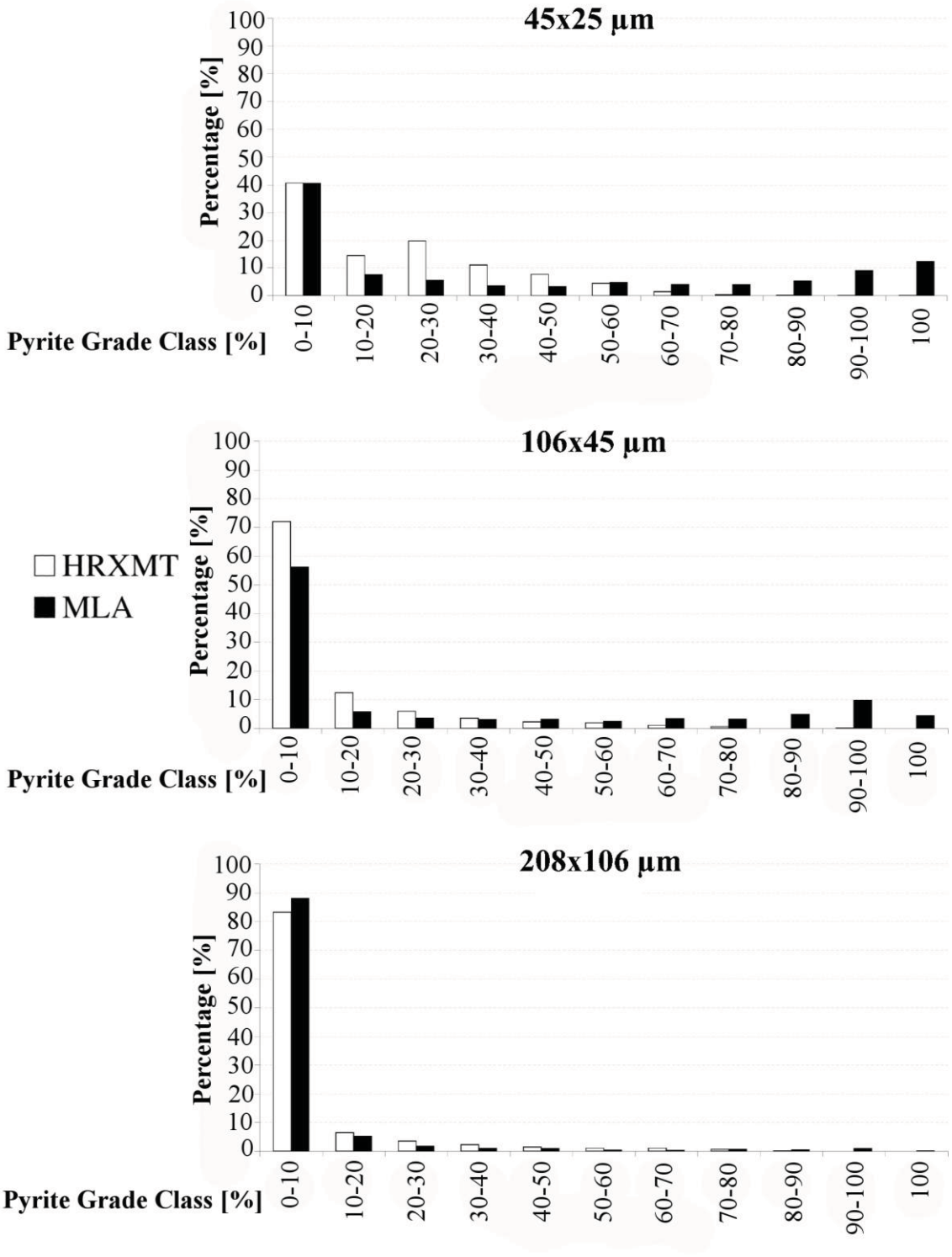

Figure F.1 Comparison of pyrite grade results of feed from flotation circuit for size classes 45x25 µm, 106x45 µm and 208x106 µm.

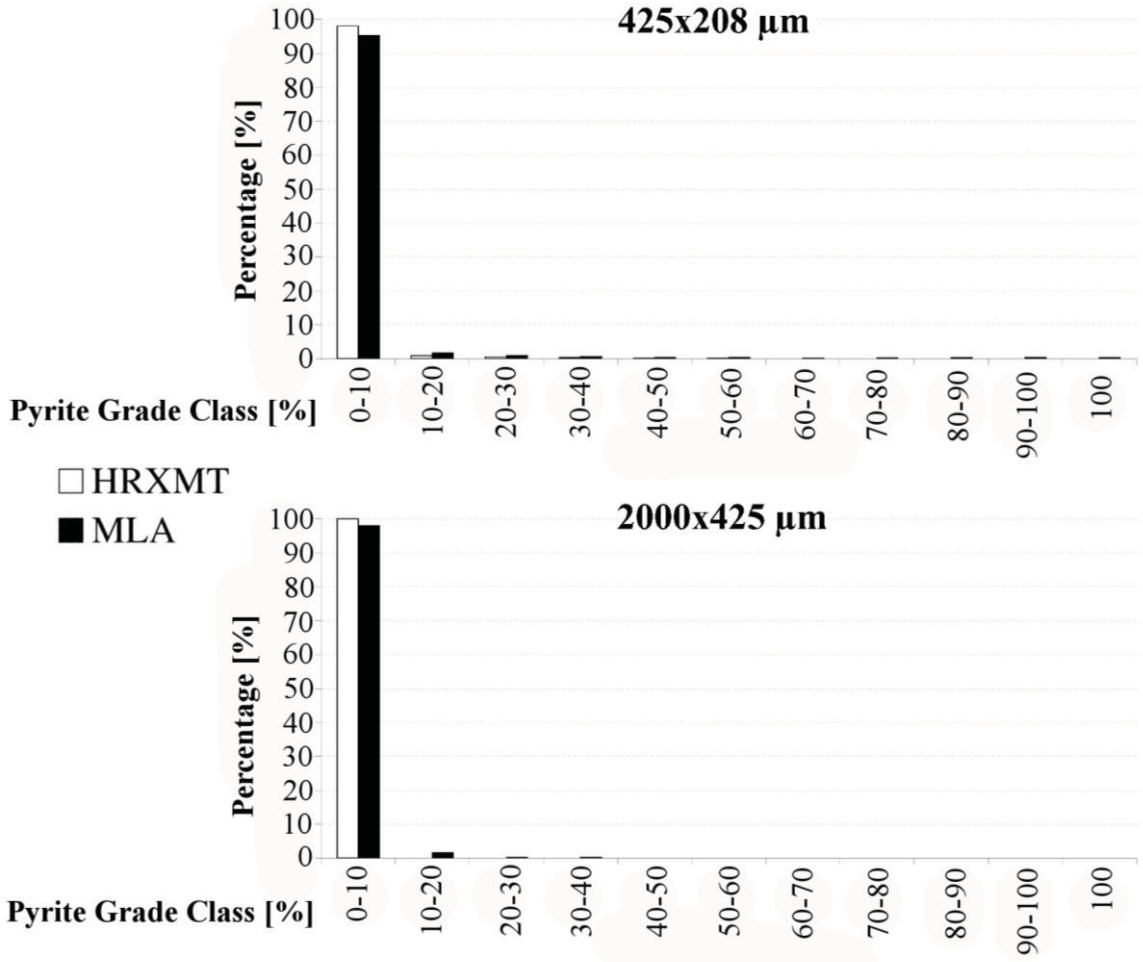

Figure F.2 Comparison of pyrite grade results of feed from flotation circuit for size classes 425x208 µm and 2000x425 µm.

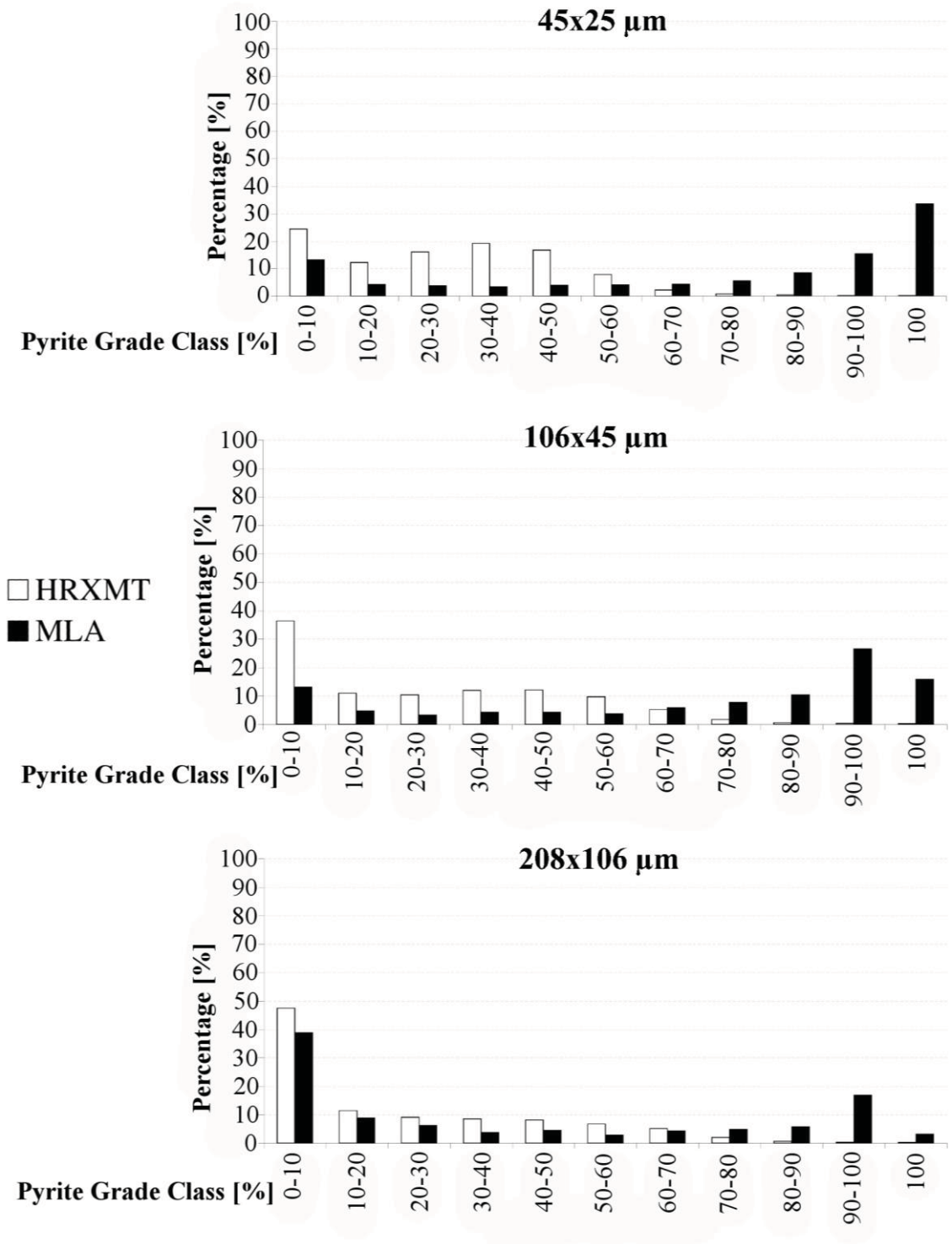

Figure F.3 Comparison of pyrite grade results of concentrate from flotation circuit for size classes 45x25 µm, 106x45 µm and 208x106 µm.

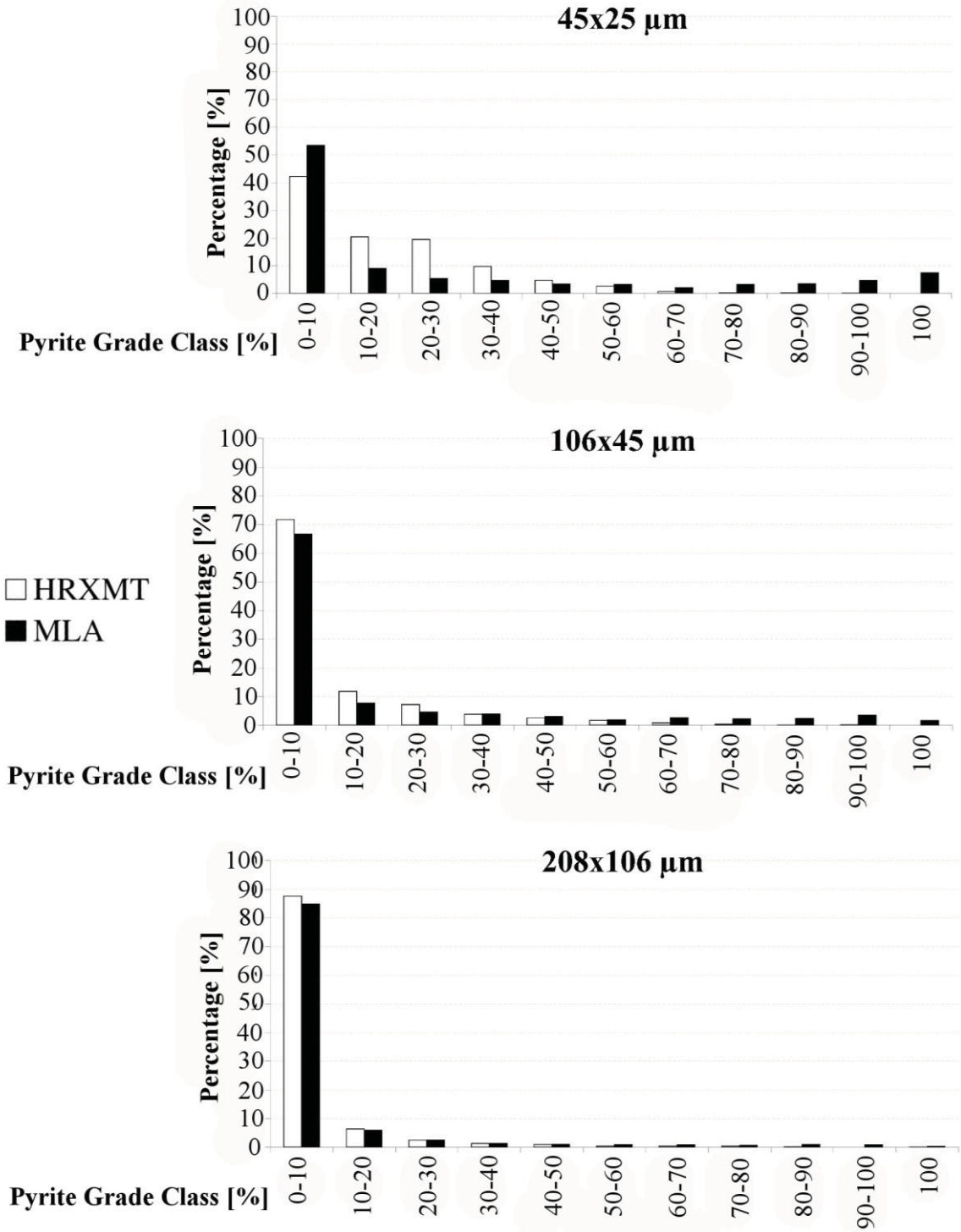

Figure F.4 Comparison of pyrite grade results of tailings from flotation circuit for size classes 45x25 µm, 106x45 µm and 208x106 µm.

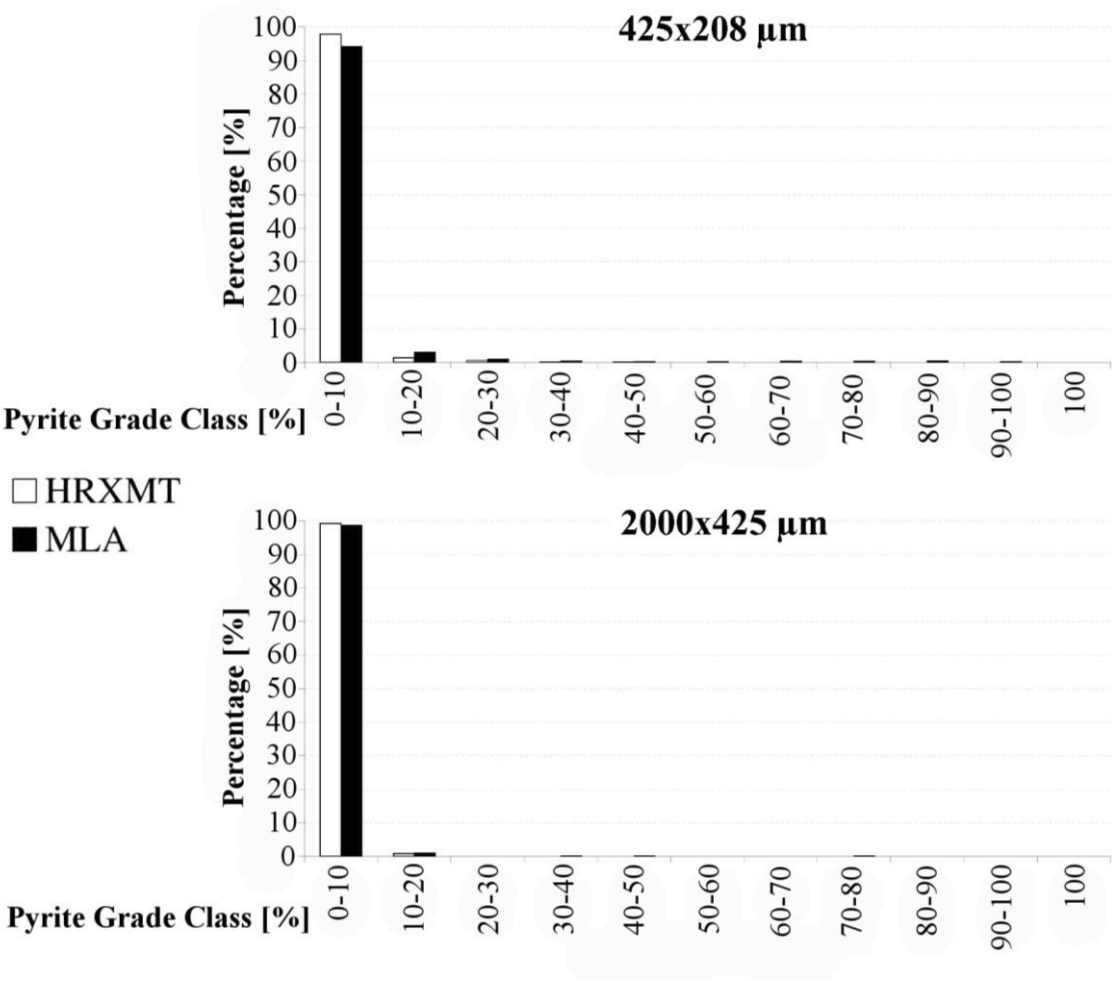

Figure F.5 Comparison of pyrite grade results of tailings from flotation circuit for size classes 425x208 µm and 2000x425 µm.

REFERENCES

Adams, M.D. 2005. Advances in gold ore processing. Developments in Mineral Processing, Vol. 15. Elsevier, Burlington.

Azenkeng, A., Eylands K. and Kleven, P. 2010. A Fast Approach to Quantitative Evaluation of Minerals by Scanning Electron Microscopy – Application to Diverse Natural Materials and Metallurgy. *Microscopy and Microanalysis*, 16(2):1528-1529.

Barbery, G. 1991. *Mineral liberation. Measurement, simulation and practical use in mineral processing*. Les Editions GB, Quebec.

Bryant, J.A., Drage, N.A., and Richmond, S. 2012. CT number definition. *Radiation Physics and Chemistry*, 81:358-361.

Buades, A., Coll, B. and Morel, J. M. 2005. A review of image denoising algoritms, with a new one. *Multiscale Model. Simul.,* 4(2):490-530.

Davy, P. J. 1984. Probability for liberation. *Journal of Applied Probability,* 21(2):260-269.

Dominy, S.C., Johansen, G. F. and Annels, A. E. 2001. Bulk sampling as a tool for the grade evaluation of gold-quartz reefs. *Trans. Instn. Min. Metall (Sect. B: Appl. earth sci.),* 110:176-191.

Donskoi, E., Suthers, S. P., Fradd, S. B., Young, J. M., Campbell, J. J., Raynlyn, T.D. and Clout, J. F. M. 2007. Utilization of optical image analysis and automatic texture classification for iron ore particle characterisation. *Minerals Engineering*, 20: 461-471.

Fandrich, R., Gu, Y., Burrows, D., and Moeller, K. 2007. Modern SEM-based mineral liberation analysis. *Int. J. Miner. Process.,* 84:310-320.

Garcia, D., Lin, C. L., Miller, J. D. 2009. Quantitative analysis of grain boundary fracture in the breakage of single multiphase particles using x-ray microtomography procedures, *Minerals Engineering*, 22:236-243.

Gaudin, A. M. 1939. *Principles of mineral dressing.* McGraw-Hill Book Company, Inc., New York.

Gay, S. L. 1999. Numerical verification of a non-preferential-breakage liberation model. *Int. J. Miner. Process.,* 57: 125-134.

Gay, S. L. 2004a. A liberation model for comminution based on probability theory. *Minerals Engineering*, 17: 525-534.

———.2004b. Simple texture-based liberation modeling of ores. *Minerals Engineering*, 17: 1209-1216.

Goodall, W.R. 2008. Characterisation of mineralogy and gold deportment for complex tailings deposit using QEMSCAN. *Minerals Engineering,* 21:518-523.

Gottlieb, P., Wilkie, G., Sutherland, D., Ho-Tun, E., Suthers, S., Perera, K., Jenkins, B., Spencer, S. And Butcher, A. 2000. Using quantitative electron microscopy for process mineralogy applications. *JOM*. 4:24-25.

Gu, Y. 2003. Automated scanning electron microscope based mineral liberation analysis. *Journal of Minerals & Materials Characterization & Engineering,* 2(1):33-41.

Gu, Y. and Napier-Munn, T. 1997. JK/Phillips mineral liberation analyzer – an introduction. *Minerals Processing Conference*, Cape Town, South Africa, 2.

Kelly, E. G. 1982. *Introduction to mineral processing.* John Wiley & Sons, New York.

King, R.P. 1982. Prediction of mineral liberation from mineralogical textures. *XIV International Mineral Processing Congress*, paper VIII-1, CIM, 17-23 October, Toronto, Canada.

King, R. P. 2001. *Modeling and simulation of mineral processing systems,* Butterworth-Heinemann, Oxford.

King, R.P. and Schneider C.L. 1998. Stereological correction of linear grade distributions for mineral liberation. *Powder Technology*, 98: 21-37.

Lastra, R. 2007. Seven practical cases of liberation analysis. Int. J. Miner. Process., 84:337-347.

Lin, C. L. 1986. Measurement and prediction of mineral liberation during grinding. Ph.D. dissertation. University of Utah.

Lin, C. L. and Miller, J. D. 2005. 3D characterization and analysis of particle shape using x-ray microtomography (XMT), *Powder Technology*, 154:61-69.

Miller, J. D. 2010. Characterization, analysis, and simulation of multiphase particulate systems using high resolution x-ray micro tomography (HRXMT). In *Proceedings for XXV International Mineral Processing Congress.* CD-ROM. Brisbane, Australia, September 6-10.

Miller, J. D. and Lin, C. L. 1988. Treatment of polished section data for detailed liberation analysis, *Int. J. Miner. Process*., 22:41-58.

———.2004. Three-dimensional analysis of particulates in mineral processing systems by cone beam x-ray microtomography, *Mineral & Metallurgical Processing*, 21(3):113-124.

Miller, J. D., Lin, C. L., Garcia, C., Arias, H. 2003. Ultimate recovery in heap leaching operations as established from mineral exposure by X-ray microtomography, *Int. J. Miner. Process.*, 72:331-340.

Miller, J. D., Lin, C. L., Hupka, L., Al-Wakeel, M. I. 2009. Liberation-limited grade/recovery curves from x-ray micro CT analysis of feed material for the evaluation of separation efficiency, *Int. J. Miner. Process.* 93:48-53.

Pirard, E., Lebichot, S. and Krier, W. 2007. Particle texture analysis using polarized light imaging and gray level intercepts. *Int. J. Miner. Process*., 84:299-309.

Pitard, F. F. 2002. Practical and theoretical difficulties when sampling gold in *Mineral processing plant design, practice, and control: proceedings* edited by Mular, A. L., Halbe, D. N. and Barrat, D. J. Society of Mining, Metallurgy, and Exploration, Inc. Littleton.

Schneider, C. L. 1995. Measurement and calculation of liberation in continuous milling circuits. Ph.D. dissertation. University of Utah.

Schneider, C.L., Neumann, R., King, R. P. 2003. Prediction of liberation from unbroken 3-phase texture: a case study on cial sample. *XXII International Mineral Processing Congress,* 29 September – 3 October, Cape Town, South Africa, 363-369.

Smart, R. St. C., Skinner, W. M., Gerson, A. R., Mielczarski, J., Chryssoulis, S., Pratt, A. R., Lastra, R., Hope, G. A., Wang, X., Fa, K. and Miller, J. D. 2007. Surface characterization and new tools for research in *Froth Flotation: a century of innovation* edited by Fuerstenau, M. C., Jameson, G. and Yoon, R. Society of Mining, Metallurgy, and Exploration, Inc. Littleton.

Videla, A. 2006. Development of three-dimensional image computer tools for x-ray computed tomography analysis of multiphase particulate systems. M.S. thesis. University of Utah.

Videla, A., Lin, C. L., Miller, J. D. 2006. Watershed functions applied to 3D image segmentation problem for the analysis of packed particle beds, *Part. Part. Syst. Charact*., 23:237-245.

———. 2007. 3D characterization of individual multiphase particles in packed particle beds by X-ray microtomography (XMT), *Int. J. Miner. Process.*, 84:321-326.

Wiegel, R. L. 1976. Integrated size reduction-mineral liberation model, *Trans. AIME*, 260: 179-189.

Wills, B. A. 2006. *Mineral processing technology. An introduction to the practical treatment and mineral recovery.* Seventh edition, Butterworth-Heinemann, Oxford.

Xu, W. 2010. Breakage of multiphase particles and analysis of fragmentation in three dimensions. M. S. thesis. University of Utah.